2020

Novel Insights Into The Cellular Basis Of Pigmentation Using Mouse Models Of Albinism

Linh Le
University of Pennsylvania

Novel Insights Into The Cellular Basis Of Pigmentation Using Mouse Models Of Albinism

Abstract

Melanin synthesis is required for proper development and function of the visual system and for protection against ultraviolet radiation. Defects in melanin synthesis result in albinism, which is characterized by visual defects and increased skin cancer risk. Melanin is synthesized in pigment cells within specialized subcellular organelles called melanosomes. Some forms of albinism result from defects in melanosome maturation, but the underlying molecular mechanisms are incompletely understood. Melanosome maturation requires the trafficking of melanogenic cargoes to melanosome precursors and an increase in melanosome pH, thereby supporting activity of the enzyme tyrosinase to promote melanin synthesis. In this work, we investigate melanosome biogenesis and maturation in melanocytes derived from mouse models of two forms of albinism, (1) oculocutaneous albinism type 4 (OCA4) due to loss of function of SLC45A2, and (2) the Hermansky-Pudlak syndrome mouse model buff that has a missense mutation in VPS33A. (1) Here we show that SLC45A2, a putative sugar/proton symporter, localizes to melanosomes and increases organellar pH at its sites of localization. Further, we show that SLC45A2 likely functions at a later stage of melanosome maturation than the ion channel OCA2, which is also necessary to raise melanosomal pH and is defective in another subtype of OCA. Additionally, we show that a common SLC45A2-L374F variant associated with lighter pigmentation in humans is degraded more rapidly than the dark skin-associated L374 variant, indicating that decreased pigmentation reflects reduced proton export from melanosomes. (2) VPS33A, an SM protein that mediates fusion, is required in the endolysosomal and autophagosomal pathways, but whether it plays a direct role in melanosomal trafficking is unknown. Contrary to a previous report, we show that a VPS33A-D251E mutation in melan-bf cells does not prohibit pigmentation; instead, buff melanocytes cells contain enlarged, mature melanosomes despite partial mistrafficking of the mature melanosomal marker TYRP1. Replacement of wild-type VPS33A in wild-type melanocytes by VPS33A-D251E does not phenocopy buff melanocytes, suggesting that an additional mutation may be responsible for our observed buff phenotype. Our analyses of mouse albinism models have thus yielded significant insights into mechanisms of melanosome maturation.

Degree Type

Dissertation

Degree Name

Doctor of Philosophy (PhD)

Graduate Group

Cell & Molecular Biology

First Advisor

Michael S. Marks

Subject Categories

Biology | Cell Biology | Molecular Biology

NOVEL INSIGHTS INTO THE CELLULAR BASIS OF PIGMENTATION USING MOUSE MODELS OF ALBINISM

Linh Le

A DISSERTATION

in

Cell and Molecular Biology

Presented to the Faculties of the University of Pennsylvania

in

Partial Fulfillment of the Requirements for the

Degree of Doctor of Philosophy

2020

Supervisor of Dissertation

_____

Michael S. Marks, Ph.D., Professor of Pathology and Laboratory Medicine, Professor of Physiology

Graduate Group Chairperson

_____

Daniel S. Kessler, Ph.D., Associate Professor of Cell and Developmental Biology

Dissertation Committee

Sarah E. Millar, Ph.D., Director of the Black Family Stem Cell Institute, Professor of Cell, Developmental & Regenerative Biology, Professor of Dermatology, Professor of Oncological Sciences

Margaret M. Chou, Ph.D., Associate Professor of Pathology and Laboratory Medicine, Associate Professor of Cell and Developmental Biology

Melike Lakadamyali, Ph.D., Assistant Professor of Physiology

Matthew D. Weitzman, Ph.D., Professor of Microbiology, Professor of Pathology and Laboratory Medicine

For my grandmother.

I love you Bà Nội and I miss you every day. I hope I make you proud.

ACKNOWLEDGMENTS

First, I would like to thank the University of Pennsylvania and Children's Hospital of Philadelphia for providing brilliant communities and resources that allowed me to grow as a scientist. Many thanks to everyone who participates in the Cell Biology Joint Lab Meeting, the Electron Microscopy Resource Lab at PSOM (especially Dr. Biao Zuo for being a joy to work with), and the Flow Cytometry Core Laboratory at CHOP. A huge thank you to Chris Davis, our office administrator, for always having the answers to my questions and for always offering a quick word of encouragement. Thank you to the members of the Cell and Molecular Biology graduate group, especially Dr. Craig Bassing for his thoughtful advice and support when I started the program and when I chose thesis labs and also our CAMB office coordinator Kathy O'Connor-Cooley for all of her help and kindness.

My sincerest gratitude goes to Dr. Michael S. Marks for being the most incredible, most supportive, and most brilliant mentor anyone could ever ask for. Ever since I met him my freshman year of college, Mickey has been unwavering in his support. Thank you, Mickey, for always believing in me, for caring so deeply about my academic growth and my mental wellbeing, and for being an excellent example of how to be not only an intelligent scientist but also a truly good human being. Thank you for our long discussions on science and on life; thank you for the corny jokes (they might always make me roll my eyes but they make me laugh too); and thank you for being a pillar of strength and support. Mickey - I am so grateful that you are a part of my life and I hope that one day I can make a difference in someone's life the way that you have made a difference in mine.

I would also like to thank my thesis committee – Dr. Sarah E. Millar, Dr. Margaret M. Chou, Dr. Melike Lakadamyali, and Dr. Matthew D. Weitzman – for your thoughtful

advice and your kind encouragement. Thank you for helping to keep me focused as my projects took twists and turns. I truly appreciate your time and your mentorship.

Thank you to the members of the Marks lab, both past and present, for being wonderful colleagues and friends. Jing, Dawn, Yueyao, Adriana, Cynthia, Xing, Anand, Preethi, and Shanna – thank you for the scientific discussions and for the laughter. Thank you for listening to me vent about experiments gone wrong and thank you for the advice, help, and encouragement. I am so glad to be a part of this lab with you all. Thank you especially to Anand who was my very smart, very patient graduate student mentor when I worked in Mickey's lab as an undergraduate student.

I also want to thank the scientific community at Haverford College for instilling in me a love for science and for being the most incredible, fun, and stimulating place to have spent four years. Thank you especially to my mentors Dr. Andrea Morris and Dr. Rachel Hoang for being wonderful examples of strong, brilliant, and caring women scientists.

I am so lucky to have wonderful friends who are smart, funny, and kind. Thank you to everyone who has been a part of this journey, especially Peter (thank you for being my wisest friend who is also the most willing to share blocks of cheese with me) and Liz, Clark and Tahi, Emily, Tori, Giff, and Jesse – your joy and laughter keep me going and I always have so much fun with you all. A huge, heartfelt thank you to Sagal and Becky for being the best friends I could ever ask for. Thank you for the movie nights, the weekend visits, uno games, brunches, and fits of laughter. Becky, you're the Paris to my Nicole and the Nicole to my Paris. Sagal, the best thing to ever happen to me was Haverford deciding to put us in neighboring cinderblock rooms. You have no idea how much I treasure your friendship and not only because you share your lovely family with me. I love you guys.

Finally, none of this would be possible without the love and support of my family. To my aunts Co Thu, Co Hoa, and Co Thuan – thank you for always believing in me; thank you always being so positive; and thank you for all the food. Thank you to my grandmother who is no longer with us but who took care of me every day after school and during the summers so my parents could work and provide for us. My favorite childhood memories are watching The Price is Right, Jeopardy, and The Wheel of Fortune with my grandmother every day wile eating her incredible food. To Khang, my not-so-little little brother who is the smartest person I know – thank you for your love and support. I am so proud of you for figuring out what you love and pursuing your dreams. Your students are lucky to have you. You truly inspire me. The biggest thank you goes to my parents who have always put my needs and my education first. I love you guys so much. Thank you for always believing in me; thank you for your love; thank you for working so hard to give Khang and me a wonderful home to grow in; thank you for making my favorite foods every time I come home; and thank you for feeding me even now even though I live hundreds of miles away. I love you, Mom and Dad. Thank you also, Mom, for always setting an incredible example for me. I remember being a toddler and going with Dad to pick you up from school. You were able to do it all – be a wife, be a loving and attentive mother, work full-time, and finish a graduate program. You succeed at everything you do and you do it all with so much grace, patience, and love. You are an inspiration. Last but certainly not least, thank you to Ron, my partner and my favorite person in the world, for being my rock. Thank you for your encouragement and your love. Thank you for always making me laugh and making every day better. My favorite part of every day is you. I love you and I'm so excited we get to go on this adventure together. I can't wait to see what's next for us.

ABSTRACT

NOVEL INSIGHTS INTO THE CELLULAR BASIS OF PIGMENTATION USING MOUSE MODELS OF ALBINISM

Linh Le

Michael S. Marks

Melanin synthesis is required for proper development and function of the visual system and for protection against ultraviolet radiation. Defects in melanin synthesis result in albinism, which is characterized by visual defects and increased skin cancer risk. Melanin is synthesized in pigment cells within specialized subcellular organelles called melanosomes. Some forms of albinism result from defects in melanosome maturation, but the underlying molecular mechanisms are incompletely understood. Melanosome maturation requires the trafficking of melanogenic cargoes to melanosome precursors and an increase in melanosome pH, thereby supporting activity of the enzyme tyrosinase to promote melanin synthesis. In this work, we investigate melanosome biogenesis and maturation in melanocytes derived from mouse models of two forms of albinism, (1) oculocutaneous albinism type 4 (OCA4) due to loss of function of SLC45A2, and (2) the Hermansky-Pudlak syndrome mouse model *buff* that has a missense mutation in VPS33A. (1) Here we show that SLC45A2, a putative sugar/proton symporter, localizes to melanosomes and increases organellar pH at its sites of localization. Further, we show that SLC45A2 likely functions at a later stage of melanosome maturation than the ion channel OCA2, which is also necessary to raise melanosomal pH and is defective in another subtype of OCA. Additionally, we show that a common SLC45A2-L374F variant

associated with lighter pigmentation in humans is degraded more rapidly than the dark skin-associated L374 variant, indicating that decreased pigmentation reflects reduced proton export from melanosomes. (2) VPS33A, an SM protein that mediates fusion, is required in the endolysosomal and autophagosomal pathways, but whether it plays a direct role in melanosomal trafficking is unknown. Contrary to a previous report, we show that a VPS33A-D251E mutation in melan-bf cells does not prohibit pigmentation; instead, *buff* melanocytes cells contain enlarged, mature melanosomes despite partial mistrafficking of the mature melanosomal marker TYRP1. Replacement of wild-type VPS33A in wild-type melanocytes by VPS33A-D251E does not phenocopy *buff* melanocytes, suggesting that an additional mutation may be responsible for our observed *buff* phenotype. Our analyses of mouse albinism models have thus yielded significant insights into mechanisms of melanosome maturation.

TABLE OF CONTENTS

ACKNOWLEDGMENTS ..... **III**

ABSTRACT ..... **VI**

LIST OF FIGURES ..... **XII**

LIST OF TABLES ..... **XIV**

CHAPTER 1: INTRODUCTION **1**

1.1. Specialized cells generate melanin: Epidermal, follicular, and uveal melanocytes and pigmented epithelial cells 1

1.1.1. Epidermal melanocytes 2

1.1.2. Follicular melanocytes 3

1.1.3. Uveal melanocytes 4

1.1.4. Pigmented epithelial cells 5

1.2. Evolution of human pigmentation diversity 7

1.2.1. UVR effects on metabolism 7

1.2.2. Melanin as a defense against UVR 9

1.3. Melanin synthesis 12

1.3.1. The TYR family of proteins 15

1.3.2. Melanin subtypes: Eumelanin and pheomelanin 19

1.3.3. The melanocortin-1 receptor 21

1.4. Melanosomes serve as the site for melanin synthesis and storage 24

1.5. pH regulation of melanosomes 29

1.6. Cargo delivery: Trafficking to and from melanosomes.....36

1.6.1. Function of AP-1 and AP-3 in sorting melanosomal cargo 38

1.6.2. BLOC function in the tubulovesicular pathway 39

1.6.3. Fusion of transport intermediates with melanosomes.....40

1.6.4. HOPS, VPS33A, and the *buff* mouse 42

1.7. Molecular basis of albinism 45

1.7.1. Non-syndromic albinism.....47

1.7.2. Syndromic albinism.....50

1.8. Dissertation Aims.....54

CHAPTER 2.....57

2.1. Abstract 58

2.2. Introduction.....58

2.3. Results.....63

2.3.1. Functionality of HA-SLC45A2.....63

2.3.2. HA-SLC45A2 localizes to the limiting membrane of pigmented melanosomes and is partially enriched in a membrane subdomain.....65

2.3.3. SLC45A2 localizes to lysosomes and regulates lysosomal pH when ectopically expressed in HeLa cells. 67

2.3.4. SLC45A2 and OCA2 function at distinct stages of melanosome maturation.....69

2.3.5. OCA2 overexpression partially compensates for loss of SLC45A2 expression. 74

2.3.6. The light skin-associated SLC45A2-F374 variant protein is expressed at lower levels than the dark skin-associated SLC45A2-L374 variant. 76

2.4. Discussion 81

2.5. Acknowledgements....86

2.6. Materials and Methods....87

CHAPTER 3....97

3.1. Abstract....98

3.2. Introduction....99

3.3. Results....103

3.3.1. Homozygous *Vps33a*^{bf} allele in melan-bf cells. 103

3.3.2. Melan-bf cells are hyperpigmented and contain enlarged, mature melanosomes. 106

3.3.3. Melan-bf melanosomes have an increase in intralumenal vesicles that correlates with their increased size. 109

3.3.4. Melanosomal genes and proteins are decreased in melan-bf cells....111

3.3.5. Pigment granules contain TYRP1 but a proportion of TYRP1 is present in a distinct compartment in melan-bf cells....113

3.3.6. The endocytic pathway is normally segregated from melanosomes in melan-bf cells. 117

3.3.7. Knockdown of endogenous VPS33A and overexpression of human VPS33A does not replicate the melan-bf phenotype. 119

3.4. Discussion 126

3.5. Materials and Methods....136

CHAPTER 4: DISCUSSION....147

4.1. Data Summary....147

4.2. Future Directions 150

4.2.1. Is there a functional role for SLC45A2 punctate structures?....150

4.2.2. How does SLC45A2 traffic to melanosomes? 153
4.2.3. What is the role of sugar in the melanosome? 158
4.2.4. How to further investigate the differences between SLC45A2 localization and OCA2 localization on melanosomes? 160
4.2.5. How to measure melanosomal pH? 163
4.2.6. How do other ion transport proteins regulate melanosome pH and melanogenesis?.....166
4.2.7. How to investigate VPS33A functions in the melanosomal pathway?....170
4.2.8. How to assess GPR143 pathway in melan-bf cells? 173
4.3. Concluding remarks.....174

APPENDIX.....176

Appendix A: VPS33A.....176

Appendix B: MELOPS 180

BIBLIOGRAPHY.....186

LIST OF FIGURES

Figure 1.1: Melanin synthesis pathway. 13
Figure 1.2: Ion transport channels in melanosome biogenesis 31
Figure 1.3: Trafficking pathways to melanosomes. 38
Figure 2.1: HA-SLC45A2 functionally restores pigmentation in Slc45a2-deficient underwhite melanocytes. 64
Figure 2.2: HA-SLC45A2 localizes to melanosomes when expressed in SLC45A2-deficient melan-uw melanocytes. 66
Figure 2.3: HA-SLC45A2 localizes to melanosomes upon transient transfection in WT melanocytes. 67
Figure 2.4: HA-SLC45A2 expressed in HeLa cells localizes to lysosomes and neutralizes lysosomal pH. 68
Figure 2.5: SLC45A2 and OCA2 occupy partially distinct melanosome subsets. 71
Figure 2.6: SLC45A2 is required for melanosomes to progress from stage III to stage IV 73
Figure 2.7: OCA2 overexpression compensates for loss of SLC45A2-dependent melanosome neutralization in melanocyte pigmentation. 75
Figure 2.8: The human light skin-associated SLC45A2-F374 variant is expressed in melanosomes at lower levels than the dark variant. 77
Figure 2.9: The F374 variant is less stable than the L374 variant and is degraded by a proteasome-dependent endolysosomal pathway. 79
Figure 2.10: Early phase of rapid SLC45A2-F374 degradation is blocked by vATPase inhibition. 80
Figure 3.1: Melan-bf cells are homozygous for Vps33abf allele 105
Figure 3.2: Melan-bf cells are hypopigmented and contain enlarged, mature melanosomes 109
Figure 3.3: Melan-bf cells contain increased ILVs per melanosome due to increased melanosome area 111
Figure 3.4: TYRP1 and VPS33A protein expression is decreased in melan-bf cells 113
Figure 3.5: Most pigment granules contain TYRP1 but a majority of TYRP1 does not localize to pigment granules 116

Figure 3.6: The endocytic pathway is segregated from melanosomes in melan-bf cells 119
Figure 3.7: Expression of VPS33A variants in Vps33a knockdown cells does not phenocopy melan-bf cells 125
Figure 4.1. Model of SLC45A2 function in melanosome pH regulation 149
Figure 4.2: Annotated human SLC45A2 amino acid sequence and aligned sequence 155
Appendix Figure 1: Decreased expression of melanosomal genes and Vps33a in melan-bf cells 176
Appendix Figure 2: Low levels of LAMP2 colocalize to pigment granules 177
Appendix Figure 3: Overexpression of human VPS33A and knockdown of endogenous Vps33a does not phenocopy melan-bf cells at 14 days post-selection 178
Appendix Figure 4: Overexpression of human WT VPS33A or variants does not phenocopy melan-bf cells 179
Appendix Figure 5: MELOPS localizes to TYRP1-containing melanosomes.....181
Appendix Figure 6: MELOPS indicates a low melanosome pH 182
Appendix Figure 7: pH curve in LAMP1-GFP/MELOPS-expressing HeLa cells 183
Appendix Figure 8: MELOPS measurements of HA-OCA2 and HA-SLC45A2 effects on late-endosomal/lysosomal pH in HeLa cells.....185

LIST OF TABLES

Table 1.1: Selected Ion transporters with known or putative effects on melanogenesis 35
Table 1.2: Non-syndromic Albinism 50
Table 1.3: Syndromic Albinism 53

CHAPTER 1: INTRODUCTION

Humans display a broad spectrum of pigmentation in the skin, hair, and eyes. Melanin, the major determinant of human pigmentation, serves a variety of purposes, including protection from DNA damage, protection from folate degradation, and a role in retinal development. Melanin is synthesized in melanosomes, specialized organelles generated in melanocytes and pigmented epithelial cells, primarily in the skin, hair and eyes. A complex network of genes and proteins coordinates melanin synthesis, storage, transport, transfer, and degradation, all of which influence the degree of pigmentation. Much of our understanding of these processes has come from studying pigmentation variants and defects in animal models, particularly in mice, rats, zebrafish, and drosophila. Approximately 130 genes have been identified that influence hair color in mice (Bennett and Lamoreux, 2003; Steingrimsson et al., 2006), making the mouse model system critically important for the identification and study of pigmentation genes. Despite this, our understanding of how many of these genes function in the establishment and maintenance of human pigmentation is relatively limited. Further investigation is required to better understand the basic cellular mechanisms underlying human pigmentation in both normal and disease states.

1.1. Specialized cells generate melanin: Epidermal, follicular, and uveal melanocytes and pigmented epithelial cells

In humans, melanin is produced by epidermal, follicular, and uveal melanocytes and pigmented epithelial cells. Melanoblasts, the undifferentiated precursor of melanocytes, arise from the neural crest and migrate to the epidermis and hair follicles,

where they give rise to epidermal melanocytes in the skin, melanocyte stem cells in the hair follicle bulge, and follicular melanocytes in the hair follicle (Vandamme and Berx, 2019). Melanoblasts also migrate into the uvea, where they differentiate into uveal melanocytes of the choroid, the iris, and the ciliary body at 7-8 months gestation (Hu et al., 2008; Nickla and Wallman, 2010). Pigmented epithelial cells arise from the optic neuroepithelium and migrate to the posterior eye to form the retinal pigment epithelium (RPE), the iridial pigment epithelium, and the ciliary pigment epithelium, of which the RPE has been the most well studied (Hu et al., 2002). Both epidermal and follicular melanocytes transfer their melanosomes, the organelles that make and store melanin, to neighboring keratinocytes, thereby providing pigment to skin and hair. On the other hand, uveal melanocytes and pigmented epithelial cells retain their melanosomes.

1.1.1. Epidermal melanocytes

Epidermal melanocytes, sometimes called interfollicular melanocytes, are located at the basal layer of the epidermis adjacent to the basement membrane. Although melanocytes are relatively rare in the epidermis compared to other cells, primarily keratinocytes, they are the source of all pigmentation in the epidermis. Melanocytes accomplish this through their dendritic shape. Each melanocyte is estimated to contact and transfer melanin to 36 keratinocytes on average, forming the epidermal-melanin unit. While melanocytes remain on the basal layer of the epidermis, keratinocytes migrate upwards over the course of their lifetime, transporting pigment to the upper layers of the skin, where it can provide protection from ultraviolet radiation (UVR). Crosstalk between keratinocytes and melanocytes stimulates melanocyte proliferation, survival, melanogenesis, and melanin secretion (Weiner et al., 2014).

Diversity in human pigmentation is most apparent in human skin, which evidence suggests was under strong natural selection during human evolution and migration (Jablonski and Chaplin, 2017). In comparison, pigmentation in the eyes and hair do not seem to have been under natural selection in humans. The factors influencing skin pigmentation, particularly UVR, and the role of melanin in modulating UVR's effect on skin and human health will be discussed in a later section.

1.1.2. Follicular melanocytes

In humans, hair growth occurs in an asynchronous and stochastic life cycle that can be categorized into four phases: anagen, the active growth phase of hair within a follicle; catagen, a transition phase during which time cells of the hair bulb undergo apoptosis and hair growth stops; telogen, when the hair shaft prepares to be shed; and neogen, when the dermal papilla reconnects with stem cells to generate a new hair and a new cycle can begin (Koch et al., 2020; Stenn and Paus, 2001). The timing of the hair cycle depends on the type and length of hair. Human scalp hairs are longer and thus have extended anagen phases that can last for years (Park et al., 2018). In contrast, shorter hairs such as eyelashes have short anagen phases that last only days (Paus et al., 2016).

During anagen, melanocytes reside at the base of the hair follicle in the hair bulb where they can transfer melanosomes to keratinocytes that generate the hair shaft, providing pigment to the hair as it grows (Koch et al., 2020). During catagen, the follicular melanocytes undergo apoptosis; however, their population is replenished by the melanocyte stem cells in the hair bulge (Lin and Fisher, 2007; Vandamme and Berx, 2019). Differentiated melanocytes migrate from the hair bulge to the hair bulb adjacent to the dermal papilla, a region of densely packed fibroblasts that determines hair shaft

diameter and length and anagen duration (Schneider et al., 2009). Thus, another round of pigmented hair growth can occur.

A similar hair cycle occurs in other mammals, but the timing varies depending on the animal. In mice, for example, the hair cycles over weeks not years (Muller-Rover et al., 2001). Interestingly, the backs of mice do not contain epidermal melanocytes and the pigmentation of these regions of their skin is dependent on follicular melanocytes (Nishimura, 2011; Stenn and Paus, 2001). However, the hairless regions of mice, particularly the ears and tail, contain epidermal melanocytes that are often cultured and used in studies. Analyses of these melanocytes translate well to human epidermal melanocytes, making the obvious diversity in mouse coat colors and easily cultured immortalized mouse melanocytes a powerful system for studying pigmentation genes.

1.1.3. Uveal melanocytes

Whereas epidermal and follicular melanocytes have been studied extensively both in situ and in culture, the pigment producing cells of the eye, the biogenesis and turnover of their melanosomes, and the roles of ocular melanin are less well understood. The uvea is a layer of the eye that consists of the iris, the ciliary body, and the choroid (Hu et al., 2008). The iris is the colored part of the eye and helps regulate the amount of light entering the eye. Melanocytes comprise about 65% of the iris stroma, and iris color is determined by the structure of melanosomes in the stroma, the quantity of melanin synthesized, and the ratio of eumelanin to pheomelanin (two types on melanin that will be discussed in Chapter 1.3) (Eagle, 1988; Hu et al., 2008; Wakamatsu et al., 2008; Wilkerson et al., 1996). Melanin in the iris and RPE plays a role in photoprotection, protecting the retina from excess light and from light reflection (d'Ischia et al., 2015). Uveal melanoma and age-

related macular degeneration are both correlated with lower pigmentation of the iris, which is likely due to decreased UVR protection and potentially increased oxidative stress in the cases of high pheomelanin levels (Wakamatsu et al., 2008). The ciliary body is a structure containing melanocytes, muscle, connective tissue, and blood vessels and arteries and is located behind the iris. The ciliary body produces the aqueous humor and contracts to change the shape of the lens when the eye focuses (Delamere, 2005). Melanin generated by melanocytes in this tissue likely contributes to photoprotection but other roles have not been identified (Hu et al., 2008). The choroid is a vascular structure containing a network of arteries, veins, and capillaries, which serves this tissue's primary function of supplying blood and oxygen to the outer retina (Nickla and Wallman, 2010). Surrounding this network are various cell types, including melanocytes, that comprise the stroma. Adjacent to this vascular layer of the choroid is the lamina fusca, which is composed of layers of compacted melanocytes and fibroblast-like cells (Nickla and Wallman, 2010). The role of melanocytes in the choroid is thought to be in light absorption and reactive oxygen species (ROS) scavenging to protect the vasculature (Nickla and Wallman, 2010; Peters et al., 2006). While uveal melanocytes are not directly involved with vision, they are critically important for supporting and maintaining the ocular tissues that receive and transmit visual information; therefore, uveal melanocytes are necessary for normal vision.

1.1.4. Pigmented epithelial cells

The ocular pigment epithelium is comprised of the iris pigment epithelium, the ciliary pigment epithelium, and the RPE (Hu et al., 2002). Retinal pigment epithelial cells generate the retinal pigment epithelium, a monolayer adjacent to the photoreceptor layer in the eye (Hu et al., 2002). The RPE is important for ocular homeostasis and its functions

include phagocytosis of shed photoreceptors, operating as a blood-retinal barrier, and producing cytokines and growth factors (Hu et al., 2002). The RPE is densely pigmented and contains mostly eumelanin (Hu et al., 2002; Hu et al., 2008; Istrate et al., 2020). Melanogenesis in the RPE is mostly inactive after gestation, with the majority of melanin synthesis occurring early in fetal development and little to no melanin synthesis occurring in adult RPE cells (d'Ischia et al., 2015; Hu et al., 2008; Istrate et al., 2020).

While retinal melanin is photoprotective and can absorb stray light, the RPE's location at the posterior region of the eye suggests that this is a minor role. Likely a more important role for retinal melanin is in its antioxidant effects in reducing ROS and scavenging free radicals. The RPE accumulates lipofuscin over time, which is autofluorescent material associated with high oxidative stress that, in RPE cells, is thought to be a product of incomplete lysosomal digestion of shed photoreceptor fragments. Lipofuscin can generate ROS and free radicals which can be counterbalanced by melanin. Melanosomes in RPE cells may also closely interact with phagocytosed photoreceptors and lipofuscin-containing compartments. There is evidence that phagosomes and lipofuscin fuse with melanosomes (Kayatz et al., 2001; Schraermeyer and Heimann, 1999; Schraermeyer et al., 1999), and although the function of this process is unclear, it has been speculated that these fusion events occur in RPE in response to high oxidative stress of the cellular environment.

Over time, the melanin content of RPE cells decreases and lipofuscin accumulates (Weiter et al., 1986), which may play a role in age-related macular degeneration (d'Ischia et al., 2015). While the RPE has been the most well studied tissues of the ocular pigment epithelium, it is likely that the iris pigment epithelium and ciliary pigment epithelium play similar roles in blocking stray light and UV and in antioxidant responses. Similar to uveal

melanocytes, ocular pigment epithelial cells are necessary for normal vision due to their protective effects on other ocular tissues.

1.2. Evolution of human pigmentation diversity

Human evolution from primates is marked by loss of the primate hair coat, which is hypothesized to occur due to natural selection to improve thermoregulation in the high temperature conditions in equatorial Africa (Jablonski and Chaplin, 2017). This loss of body hair left the exposed skin vulnerable to UVR. Genomic evidence indicates that the loss of body hair in humans coincided with a gain of dark, melanin-rich skin, which is thought to be a protective, adaptive response to high UVR (Jablonski, 2012; Jablonski and Chaplin, 2017, 2018; Lucock et al., 2017; Lucock et al., 2018b).

1.2.1. UVR effects on metabolism

UVR is comprised of UVA radiation (320-400 nm) and UVB radiation (290-320 nm) (Diffey, 2002). While UVA radiation is constant globally, UVB radiation varies according to latitude, season, and time of day; therefore, total UVR is highest at the equator and UVR is generally lower and seasonal outside of the equator due to decreased UVB radiation (Jablonski and Chaplin, 2010). UVR has both beneficial and harmful effects on human health.

UVB radiation stimulates the synthesis of vitamin D, a fat-soluble compound that is necessary for human reproduction and life (Jablonski and Chaplin, 2018). UVB initiates the conversion of 7-dehydrocholesterol (7-DHC) in the skin into pre-vitamin D_3 which is subsequently converted to vitamin D_3. Vitamin D_3 enters the circulation and subsequently undergoes a series of hydroxylation reactions in the liver and kidney to form 1α,25-

dihydroxyvitamin D_3 (calcitriol), a hormone that binds to vitamin D receptors on many tissues to promote pleiotropic effects and that has an essential role in calcium absorption and skeletal health (Lips, 2006; Norman, 2008). Although vitamin D_3 can be obtained through some dietary sources, the major source of vitamin D_3 in most humans is through UVB-mediated synthesis in the skin. This can be a concern in certain regions or populations as evidence indicates that the presence of melanin in skin reduces vitamin D synthesis (Armas et al., 2007; Enechukwu et al., 2019; Harris and Dawson-Hughes, 1998; Young et al., 2020), likely due to melanin's role in preventing UV penetration through the skin.

Conversely, both UVA and UVB promote folate degradation (Branda and Eaton, 1978; Lucock et al., 2017) and depletion (Lucock et al., 2018a) in the skin and blood stream. Folates are a large group of vitamins that function as coenzymes or cosubstrates in reactions that transfer one-carbon units into biosynthetic pathways, including for nucleic acid and protein synthesis; thus, low folate levels are associated with neural tube defects and other developmental and degenerative disorders and have major impacts on human reproductive health and life (Lucock, 2000). Folate is photolabile and UVR is able to cleave folate between its C9 and N10 bond, resulting in irreversible loss of bioactivity, and to generate ROS that oxidize and inactivate folate derivatives (Off et al., 2005; Williams et al., 2012). UVR-induced DNA damage also depletes folate levels due to the need for nucleotide biosynthesis for DNA repair (Lucock, 2000).

Exposure to UVR is the most significant environmental risk factor for the development of skin cancers – i.e. squamous cell carcinoma, basal cell carcinoma, and melanoma (Narayanan et al., 2010). UVR stimulation induces DNA damage in all cells of the epidermis both directly through pyrimidine dimer formation upon DNA absorption of

UVR and indirectly through the generation of ROS (Narayanan et al., 2010; Valejo Coelho et al., 2016). Unrepaired DNA damage can be mutagenic, and mutations arising from pyrimidine dimer formation and other nucleotide changes that are hallmarks of UV-induced DNA damage can be found in several genes commonly mutated in skin cancers (Valejo Coelho et al., 2016). These include the tumor suppressor gene *p53*, genes encoding proteins in the Hedgehog signaling pathway, and *PTEN*, *CDKN2A*, and *BRAF* genes (Valejo Coelho et al., 2016).

1.2.2. Melanin as a defense against UVR

Melanin, a ubiquitous biological polymer that is the major determinant of pigmentation in humans, serves as the skin's first line of defense against the harmful effects of UVR. There is a drastically lower incidence of skin cancer in darkly pigmented skin compared to lightly pigmented skin (Agbai et al., 2014; Gloster and Neal, 2006). Melanin protects its surrounding tissues by absorbing and scattering UVR, which limits UVR penetrance into the skin (Kaidbey et al., 1979). Melanin also acts as a ROS scavenger and decreases the indirect DNA damage done by UVA. Therefore, melanin acts as a natural sunscreen, and the photoprotective effects of melanin account for the different tolerances to sun exposure in lightly pigmented versus darkly pigmented humans.

Skin color is highly correlated with UVR (Chaplin, 2004; Roberts and Kahlon, 1976). It is hypothesized that positive selective pressures resulted in the initial gain in pigmentation after the loss of body hair and that negative selective pressures resulted in decreasing pigmentation as humans migrated away from Africa (Jablonski and Chaplin, 2000). Regions along the equator, which have the highest UV index in the world, have the highest population of darkly pigmented humans, corresponding to the protective nature of

pigmentation against UV-induced folate degradation and DNA damage (Chaplin, 2004). As humans migrated from Africa and the high UV index along the equator, UVB availability decreased and individuals with darkly pigmented skin had reduced capacity to synthesize vitamin D; this therefore served as a positive selective pressure for decreased skin pigmentation in order to increase vitamin D photosynthesis. Conversely, hair color and eye color do not seem to be under strong natural selection but rather may have been influenced by sexual selection (Jablonski and Chaplin, 2017).

Human skin color is a polygenic trait and is determined by a complex architecture of genetic loci; however, some gene variants are strongly associated with changes in skin pigmentation and several genes seem to have played major roles in the evolution of human skin pigmentation (Quillen et al., 2019). Genomic evidence indicates that the acquisition of dark, melanin rich skin correlated with functional constraints at the melanocortin 1 receptor (*MC1R*) locus, with an increase in synonymous variants compared to the nonsynonymous variants found in primates (Quillen et al., 2019). Outside of equatorial Africa, non-synonymous *MC1R* polymorphisms can be found throughout Europe and East Asia with differing frequencies of variant alleles in the two regions (Quillen et al., 2019), indicating that the requirement for MC1R signaling (which is a critical regulator of melanocyte biology and melanin synthesis and will be discussed in Chapter 1.3.3) was relaxed outside of high UVR regions. There is evidence that depigmented skin evolved independently multiple times in human history, presumably to increase vitamin D synthesis capabilities. Many of the polymorphisms associated with lighter skin in Europe are distinct from those associated with lighter skin in East Asia (Hider et al., 2013; Izagirre et al., 2006; Lao et al., 2007; McEvoy et al., 2006; Myles et al., 2007; Norton et al., 2007). Genes that are associated with selection in European populations include *SLC24A5*,

SLC45A2, and tyrosinase (*TYR*), and genes associated with selection in East Asian populations include dopachrome tautomerase (*DCT*), *ADAM17*, *ADAMT20*, and tyrosinase-related protein 1 (*TYRP1*). Polymorphisms in *OCA2* correlating with lighter skin pigmentation have been observed in both populations. Although these handful of genes have been identified in multiple studies as being important for the adaptive transition from darkly pigmented skin to lightly pigmented skin in European and East Asian populations, there is also much evidence that many other genes play roles in human pigmentation variation within populations (Crawford et al., 2017; Martin et al., 2017).

The genetic regulation of pigmentation in African populations has been severely understudied. The majority of large analyses of pigmentation genetics have, until recently, focused on European and European-derived populations. Many older studies of human pigmentation used genetic analyses of Black Americans or Black Europeans to make broad claims about Africa. However, Africa is a diverse continent with both genetic and pigmentation diversity. Recent data suggest that regions of Africa also underwent depigmentation while others acquired increased pigmentation and identified the *SLC24A5, SLC45A2, TYRP1, KITLG, and SNX13* loci (Martin et al., 2017) and *MFSD12*, *TMEM138*, and *DDB1* (Crawford et al., 2017) as correlating with these changes in skin color. These identified genes only explained a small portion of the phenotypic variance observed in African regions and populations, indicating that much more work needs to be done.

The study of human pigmentation is a multidisciplinary field involving the study of human evolution, genomes, and cell biology. Although many genes have been correlated with human pigmentation, their functional relevance is unclear and more work needs to be done to identify: (1) whether the proteins encoded by these genes influence pigmentation

or whether the correlation is merely due to gene linkage; (2) how these proteins influence pigmentation; and (3) how they coordinate with other proteins to accomplish this. The mouse model and its derived cells have proved useful tools for dissecting these questions. Indeed, studying coat color mutations in mice has yielded many insights into the genes that have roles in pigmentation, how those genes function, and how their variants modulate pigmentation (Bennett and Lamoreux, 2003; Nakamura et al., 2002; Steingrimsson et al., 2006). In the Marks lab, we use mouse models to study the function of proteins that influence human pigmentation and that cause pathogenic changes when mutated.

1.3. Melanin synthesis

There are two types of melanins in humans – eumelanin and pheomelanin. Eumelanin comprises brown and black pigments and is composed of crosslinked 5,6-dihydroxyindole (DHI), 5,6-dihydroxyindole-2-carboxylic acid (DHICA), and their oxidized forms (D'Alba and Shawkey, 2019) (**Figure 1.1**). The structure of eumelanin has not been completely resolved due to its insolubility. Attempts to study eumelanin structure have been made using synthetic melanin but the structures of the product vary because they are strongly dependent on reaction conditions and starting materials (D'Alba and Shawkey, 2019). Based on experiments using X-ray diffraction, atomic force microscopy, and scanning tunneling microscopy, the favored model of eumelanin structure proposes that four monomers comprising any combination of DHI, DHICA, or their oxidized forms are covalently linked to form a planar unit or protomolecule. These protomolecules are stacked vertically via noncovalent interactions to make eumelanin (Cheng et al., 1994a;

Cheng et al., 1994b; Clancy and Simon, 2001; Diaz et al., 2005; Gallas et al., 1999; Kaxiras et al., 2006; Liu and Simon, 2003a, b; Meng and Kaxiras, 2008a, b; Mondal et al., 2018; Thathachari and Blois, 1969; Zajac et al., 1994). Pheomelanin comprises red and yellow pigments and is composed of benzothiazine intermediates (Ito and Wakamatsu, 2003, 2008). Pheomelanin has been understudied compared to eumelanin. Currently, the only way to reliably quantify pheomelanin content in samples is by high-performance liquid chromatography (HPLC), which is done by Shosuke Ito, PhD and Kazumasa Wakamatsu, PhD at Fujita Health University in Japan (Ito and Wakamatsu, 2003; Wakamatsu and Ito, 2002).

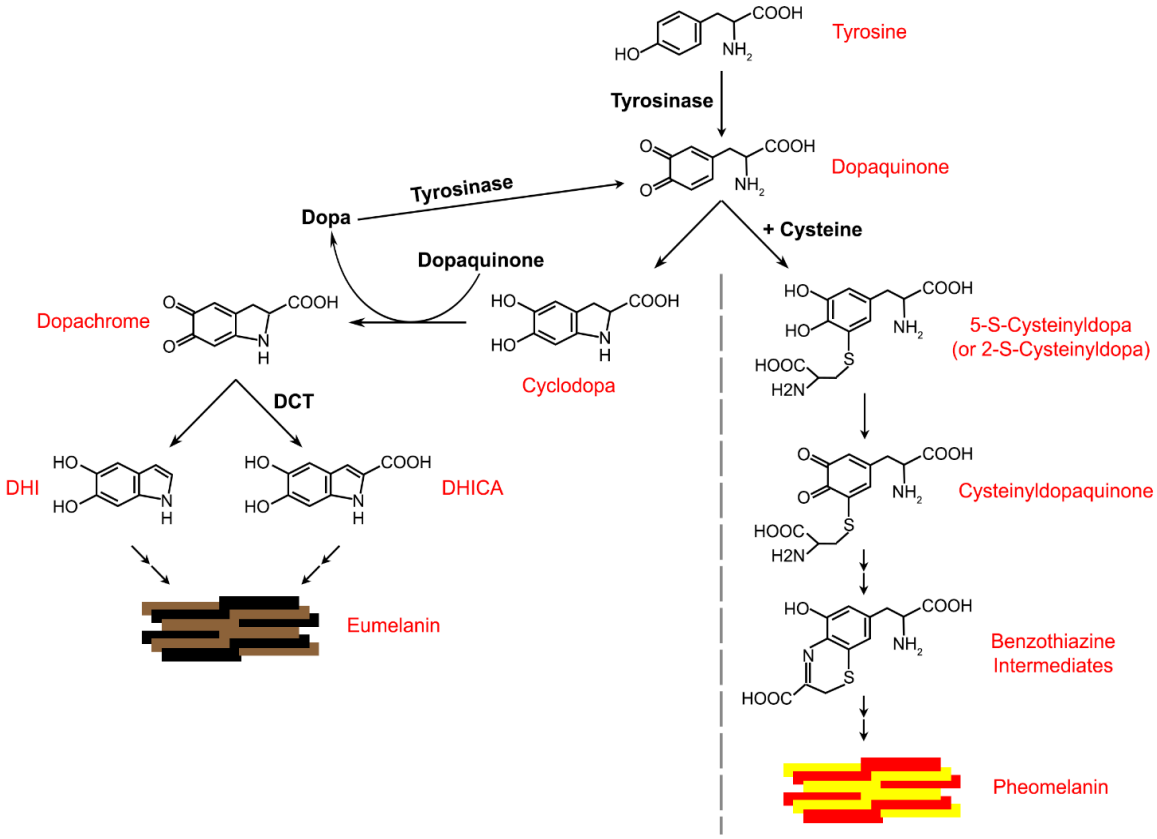

Figure 1.1: Melanin synthesis pathway. Tyrosinase (TYR) oxidizes tyrosine directly to dopaquinone. (Right) Dopaquinone in the presence of cysteine preferentially is converted to 5-S-cysteinyldopa or 2-S-cysteinyldopa which undergo spontaneous rearrangements to forms cysteinyldopaquinone. Cysteinyldopaquinone undergoes a series of rearrangements to form benzothiazine intermediates and pheomelanin, which are red and yellow pigments. (Left) In

the absence of cysteine, dopaquinone spontaneously forms cyclodopa. Cyclodopa reacts with dopaquinone to form dopachrome. 3,4-dihydroxyphenylalanine (dopa) is a byproduct of this reaction and can be converted to dopaquinone by TYR. Dopachrome can spontaneously rearrange to form 5,6-dihydroxyindole (DHI) or can be oxidized by DCT to form 5,6-dihydroxyindole-2-carboxylic acid (DHICA). DHI, DHICA, and their oxidized forms can crosslink to form eumelanin, which are black and brown pigments. TYR is the only enzyme in this pathway that is required for melanin synthesis. DCT modulates but is not required for eumelanin synthesis. The role of TYRP1 (not shown in the schematic) in the eumelanin synthesis pathway is unknown. Adapted from (Ito and Wakamatsu, 2008) .

Aside from color and composition, a major difference between eumelanin and pheomelanin is in their reactions to UV radiation. While melanin as a whole is considered photoprotective, these properties can be attributed to eumelanin specifically, not pheomelanin. Eumelanin functions as a barrier against UVR to block its surrounding tissues (e.g. keratinocytes in the skin or ocular tissues in the eye) from UV penetration and it also actively scavenges free radicals to reduce ROS (Bustamante et al., 1993; Cesarini, 1988; Kobayashi et al., 1998a). Conversely, UV stimulation of pheomelanin generates ROS. UVR results in photolysis of pheomelanin to produce hydroxyl radicals and superoxide anions, which can cause DNA breaks (Cesarini, 1988; Chedekel et al., 1980; Chedekel et al., 1978).

Both eumelanin and pheomelanin require the enzyme tyrosinase (TYR) for the initial step of melanin synthesis (**Fig 1.1**) (Evans and Raper, 1937; Mason, 1948; Raper, 1926, 1927; Raper and Speakman, 1926; Raper and Wormall, 1923; Solano, 2018). TYR catalyzes the oxidation of tyrosine to dopaquinone (Cooksey et al., 1997; Evans and Raper, 1937; Mason, 1948; Ramsden and Riley, 2014; Raper, 1926, 1927; Raper and Speakman, 1926; Raper and Wormall, 1923). Dopaquinone serves as the branch point for synthesis of either eumelanin or pheomelanin. In the presence of high amounts of cysteine, cysteinyldopaquinones, precursors to pheomelanin, are formed; in the absence

of excess cysteine, eumelanin is synthesized (**Figure 1.1**). All subsequent reactions from dopaquinone to eumelanin or from dopaquinone to pheomelanin can occur spontaneously. However, although other enzymes are not required for eumelanin synthesis, they may play roles in either stabilizing tyrosine or influencing the composition or chemical structure of eumelanin.

Pathogenic mutations that prevent proper melanin synthesis cause albinism (discussed in more detail in Chapter 1.7), which is characterized by decreased pigmentation in skin, hair, and eyes and is associated with visual defects and increased risk for skin cancers (Montoliu et al., 2014). By genetic analysis of individuals with albinism and by studying coat color mutations in mice, some of which are bona fide models of albinism, genes with proven and putative roles in the melanin synthesis pathway have been identified.

1.3.1. The TYR family of proteins

TYR, tyrosinase-related protein 1 (TYRP1), and dopachrome tautomerase (DCT a.k.a. TYRP2) comprise the tyrosinase family of enzymes, which all feature a cysteine-rich domain, two metal-binding sites, a single transmembrane domain, and a short cytosolic C-terminal tail (Solano, 2018). TYR is the most well-characterized member of the family. It is a copper-binding enzyme, and binding two Cu^{2+} ions and an oxygen molecule allows it to function as an oxidative enzyme to convert tyrosine to dopaquinone (Ramsden and Riley, 2014; Solano, 2018). Mutations in any one member of the tyrosinase family of enzymes results in oculocutaneous albinism (OCA), a group of autosomal recessive disorders characterized by decreased melanin in the skin, hair, and eyes. Loss of TYR function in OCA type 1A results in severe hypopigmentation due its requirement for the

synthesis of both eumelanin and pheomelanin. Mutations in *TYRP1* and *DCT* cause milder forms of OCA, suggesting that although they are not required for melanin synthesis, they have a role in modulating the pigmentary system (Boissy et al., 1996; Oetting and King, 1994a, b; Pennamen et al., 2020b; Tomita et al., 1992).

DCT is a zinc ion-binding enzyme and catalyzes the isomerization of dopachrome to DHICA. Its activity is therefore responsible for determining the ratio of DHICA to DHI, the latter of which is spontaneously formed from the decarboxylation of dopachrome (Olivares and Solano, 2009; Solano et al., 1996; Tsukamoto et al., 1992) (**Fig 1.1**). Experiments comparing eumelanin formed solely by DHI monomers and melanin formed solely by DHICA monomers determined that the antioxidant properties of eumelanin were due solely to the scavenging capabilities of DHICA; DHI is pro-oxidant alone but is neutralized when mixed with DHICA (Jiang et al., 2010). The authors also show that in *Dct*$^{-/-}$ mice, which have mild hypopigmentation compared to wild-type (WT) mice, chronic exposure to UVA resulted in increased ROS, sunburn, and cell death (Guyonneau et al., 2004; Jiang et al., 2010). These data suggest that, while DCT is not required for eumelanin synthesis, it is important for determining the composition and antioxidant properties of the final eumelanin product.

The role of TYRP1 is controversial and has been difficult to determine, potentially because of differing roles in humans and mice. Mice with loss-of-function mutations in *Tyrp1* have a brown coat color as opposed to a black coat color, suggesting that TYRP1 contributes to full and proper eumelanin synthesis. In mice, TYRP1 has been shown to catalyze the oxidation of DHICA, although TYRP1 in humans does not appear to have this function (Boissy et al., 1998; Jimenez-Cervantes et al., 1994; Kobayashi et al., 1994). Early studies of TYRP1 have also indicated that it may have tyrosine hydroxylase activity,

dopa oxidase activity, or hydroperoxidase activity; however, none of these results have been substantiated, which are possibly due to artifacts from TYR copurifying with TYRP1, and they would need to be repeated with purified human TYRP1 (Boissy et al., 1998; Halaban and Moellmann, 1990; Jimenez-Cervantes et al., 1993; Jimenez et al., 1991). The crystal structure of the intralumenal domain of human TYRP1 has recently been described and sheds some light on possible TYRP1 functions (Lai et al., 2017). While there has been controversy about whether TYRP1 binds copper, zinc, or iron, the crystal structure shows that human TYRP1's metal binding site contains zinc ions, which lack redox activity, further supporting the model that human TYRP1 cannot function as an oxidative enzyme (Furumura et al., 1998; Lai et al., 2017; McCall et al., 2000; Williams, 1987). Studies have also suggested that the main function of TYRP1 is to chaperone TYR. Orlow et al. showed by gel-filtration HPLC that a proportion of TYRP1, DCT, and TYR could be found in a high-molecular weight complex and confirmed this by immunoprecipitating TYRP1 or DCT and assaying the bound fraction for TYR activity (Orlow et al., 1994). Their data also show that TYR activity in the high molecular weight complex was decreased compared to monomeric TYR, suggesting a role for TYRP1 and DCT in regulating TYR activity (Orlow et al., 1994). Another group showed that in mouse cells lacking TYRP1, TYR was degraded more quickly than in WT cells and that this was rescued by expression of WT TYRP1 (Kobayashi et al., 1998b). Taken together, these data suggest a model where TYRP1 could form a complex with TYR and DCT to both regulate TYR activity and to protect TYR from degradation. However, the accuracy of this model has not been tested and several questions remain. (1) These studies were performed in mouse melanocytes with mouse TYRP1 and TYR, so are these results applicable to the human forms of the proteins? (2) Some evidence suggests that, whereas

TYRP1 is primarily localized to the limiting membrane (Raposo et al., 2001), TYR is partially localized to internal membranes (Theos et al., 2005). If this is the case, only the cohort of TYR at the membrane would interact with TYRP1, so what are the different functions, if any, of these two cohorts of TYR? (3) Additionally, is TYR degradation in the absence of TYRP1 due to loss of a specific interaction between the two proteins or is it because the system is not functional? For example, TYR is also less stable in several models where proteins in the pigmentary pathway are mutated (Chintala et al., 2005; Costin et al., 2003; Toyofuku et al., 2002). Researchers then concluded that these proteins have a direct role in TYR stabilization; however, further studies have failed to uncover direct interactions between these proteins and TYR. Rather, it is possible that these findings reflect sensitivity of TYR to degradation in the absence of melanin. Two groups have independently shown that loss of TYRP1 in human and mouse melanocytes causes cell death and that this was dependent on pigment production, suggesting that the synthesis of melanin itself in the absence of TYRP1 is cytotoxic (Johnson and Jackson, 1992; Luo et al., 1994; Rad et al., 2004). Considering that DHI-melanin has prooxidant properties and that DHICA-melanin is an effective ROS scavenger, it is possible that TYRP1 plays a similar role as DCT and functions in the synthesis of DHICA or its downstream intermediates to prevent the formation of a toxic form of eumelanin. Although the role of TYRP1 is unclear, the fact that pathological mutations in the enzyme cause OCA3 in humans and coat color phenotypes in mice indicates that it modulates eumelanin synthesis in some way.

1.3.2. Melanin subtypes: Eumelanin and pheomelanin

While eumelanin and pheomelanin are typically considered separately, overall human pigmentation is determined by the ratio of eumelanin to pheomelanin. In almost all humans, pigmentation is a product of mixed melanins consisting of both eumelanin and pheomelanin (Ito and Wakamatsu, 2003). Shosuke Ito and his colleagues have been at the forefront of pheomelanin research and have greatly contributed to our understanding of the synthesis of pheomelanin and its physiological relationship to eumelanin. Using HPLC, they analyze the degradation products of melanin and can therefore differentiate between and estimate eumelanin and pheomelanin in their samples (Prota, 1995; Wakamatsu and Ito, 2002). Specifically, they measure pyrrole-2,3,5-tricarboxylic acid (PTCA) and aminohydroxyphenylalanine (AHP), which are degraded from DHICA-derived eumelanin and from pheomelanin, respectively (Wakamatsu and Ito, 2002). Using this method, they and their colleagues have shown that human skin and hair contain both eumelanin and pheomelanin at various ratios, but that eumelanin is the predominant melanin type in human skin in most cases (Ito and Wakamatsu, 2003; Wakamatsu et al., 2006).

Studies of cultured human melanocytes show that, although both eumelanin and pheomelanin are present, eumelanin is more closely correlated with visible pigmentation. In one study rigorously comparing the visual phenotype (the observed pigmentation of the skin or of cultured cells by light microscopy), melanin content, and eumelanin and pheomelanin content of human skin and primary human melanocytes, the authors show that the ratio of eumelanin to pheomelanin widely varied in their samples and that eumelanin content correlated more with visual pigmentation (Wakamatsu et al., 2006). For example, skin and cultured melanocytes with a higher ratio of pheomelanin to eumelanin

could be more darkly pigmented than other samples if they contained more total eumelanin. If pheomelanin is toxic and only a determinant of pigmentation in rare cases (i.e. red hair), then why is it always present? The intrinsic reactive properties of dopaquinone, which can be converted to either a pheomelanin precursor or a eumelanin precursor, partially explain why eumelanin and pheomelanin are always found together. Dopaquinone is highly reactive and will preferentially form cysteinyldopa in the presence of cysteine, a reaction that occurs rapidly (Ito and Wakamatsu, 2008). Conversely, the conversion of dopaquinone to cyclodopa is much slower. Based on this, a model for mixed melanogenesis has been proposed: (1) dopaquinone is rapidly and preferentially converted to cysteinyldopa in the presence of cysteine and pheomelanin production occurs; (2) upon cysteine depletion, dopaquinone undergoes the relatively slower cyclization to cyclodopa and eumelanin production occurs (Ito and Wakamatsu, 2008; Wakamatsu et al., 2006). Additionally, the conversion rate of dopaquinone to cyclodopa is reduced in acidic pH; cyclodopa formation is reduced 100-fold when the pH decreases from 8.6 to 5.6 (Ito and Wakamatsu, 2008; Thompson et al., 1985). This means that, in acidic pH, dopaquinone is much less likely to form cyclodopa before cysteine can accumulate and react with dopaquinone to form cysteinyldopa. A low pH would also decrease TYR activity and therefore dopaquinone production, increasing the likelihood that pheomelanin would be synthesized in excess of eumelanin due to preferential conversion of dopaquinone to cysteinyldopa in the presence of cysteine (Ito and Wakamatsu, 2008). Indeed, increasing pH in melanocytes preferentially increases the production of eumelanin (Ancans et al., 2001b).

Thus, the amounts of pheomelanin and eumelanin synthesized are dependent on cysteine availability for the preferential generation of pheomelanin and on pH for its effect

on (1) TYR activity and the generation of dopaquinone and (2) the rate of dopaquinone to cyclodopa conversion. If there is low TYR activity, low pH, and high cysteine availability, pheomelanin is likely to be the major melanin produced. If there is high TYR activity, high pH, and low cysteine availability, eumelanin is likely to be the major melanin produced. It is postulated that this stepwise generation of pheomelanin and eumelanin allows eumelanin to surround pheomelanin as it is being produced, creating a pheomelanin core encased by eumelanin and sequestering the prooxidant effects of pheomelanin (Ito and Wakamatsu, 2008).

1.3.3. The melanocortin-1 receptor

The melanocortin-1 receptor (MC1R) plays a major role in regulating eumelanin and pheomelanin synthesis and is a central component of the crosstalk between epidermal melanocytes and keratinocytes. Activation of this pathway stimulates eumelanogenesis while inhibition of this pathway stimulates pheomelanogenesis (Robbins et al., 1993). MC1R is a G_s-protein coupled receptor (GPCR) expressed on the surface of pigment producing cells (melanocytes and pigmented epithelial cells) (Chhajlani and Wikberg, 1992; Mountjoy et al., 1992). α-melanocortin stimulating hormone (α-MSH) and adrenocorticotropic hormone (ACTH) are MC1R agonists and are secreted by both melanocytes and keratinocytes for autocrine and paracrine signaling (De Luca et al., 1993; Donatien et al., 1992; Slominski et al., 2004). Activation of MC1R results in pleiotropic effects due to powerful downstream regulators and pathway crosstalk (Hemesath et al., 1998; Herraiz et al., 2017). The major downstream pathway that mediates the most well-characterized effects of MC1R activation involves classical GPCR signaling.

Ligand binding to MC1R induces a conformational change that induces the alpha subunit ($G_{\alpha s}$) of its associated heterotrimeric G-protein to exchange GDP for GTP, resulting in the dissociation of both $G_{\alpha s}$ and the beta/gamma dimeric subunits from MC1R (Wolf Horrell et al., 2016b). Dissociated $G_{\alpha s}$ stimulates adenylyl cyclase activity to increase cyclic AMP (cAMP) synthesis. Increased cAMP levels can stimulate multiple downstream signaling pathways, including a major pathway initiated by protein kinase A (PKA) activation. Activated PKA phosphorylates and activates multiple proteins, including the transcription factor cAMP responsive-element-binding protein (CREB). CREB in turn promotes transcription of microphthalmia-associated transcription factor (MITF), a master regulator of melanocyte and pigmented epithelial cell biology. MITF belongs to the MITF-TFE family of basic helix-loop-helix-leucine zipper (bHLH-Zip) transcription factors, and it upregulates expression of a network of melanogenic genes, including *TYR*, *TYRP1*, and *DCT*, to promote eumelanogenesis (Aksan and Goding, 1998; Bentley et al., 1994; Bertolotto et al., 1996; Fang and Setaluri, 1999; Opdecamp et al., 1997; Yasumoto et al., 1995; Yasumoto et al., 1994). MITF also increases the expression of Rab27a (Chiaverini et al., 2008; Hoek et al., 2008), a small G-protein that is required for the transport of mature melanosomes to the cell periphery to position melanosomes for transfer to keratinocytes.

Both keratinocytes and melanocytes secrete α-MSH and ACTH upon UVR as a cellular response to DNA damage (Chakraborty et al., 1996; Rousseau et al., 2007; Schauer et al., 1994). This UV-stimulated signaling to MC1R and the subsequent increase in eumelanin is, at least in keratinocytes, dependent on functional P53 (Cui et al., 2007). P53 is stabilized upon UVR and transcribes the *proopiomelanocortin* (*POMC*) gene, encoding the precursor to α-MSH and ACTH. Thus, the tanning response to UV is a

crosstalk between keratinocytes and melanocytes and is likely a protective mechanism against further UVR-induced damage. Downstream of MC1R, MITF also upregulates the expression of genes involved in reducing oxidative stress and in the DNA damage response pathway (Kadekaro et al., 2012; Swope et al., 2014). Therefore, activation of MC1R stimulates a broad host of protective effects that are both dependent on and independent of pigment production. Conversely, binding of agouti signaling protein (ASIP), an MC1R antagonist, decreases melanogenic enzyme expression and total melanin synthesis and shifts the ratio of melanin towards pheomelanin (Miller et al., 1993; Suzuki et al., 1997). Several SNPs in *ASIP* are associated with increased risk of skin cancers (Gudbjartsson et al., 2008; Helsing et al., 2012; Lin et al., 2011; Maccioni et al., 2013). There is some evidence that MC1R has ligand-independent basal activity (Bennett and Lamoreux, 2003; Sanchez-Mas et al., 2004), suggesting a model in which MC1R maintains basal levels of melanogenesis but, that upon stimulation (e.g. UVR), binds available ligand and increases signaling as a protective response.

MC1R is highly polymorphic, with >200 nonsynonymous variants reported (Garcia-Borron et al., 2014). Many variants are associated with skin and hair color phenotypes and thus are a major contributor to the normal variation of human pigmentation (Rees, 2003). Additionally, MC1R is dimeric and evidence suggests that dimerization occurs in the endoplasmic reticulum (ER) before MC1R can traffic to the plasma membrane (Wolf Horrell et al., 2016a). This adds an additional layer of complexity to MC1R regulation and signaling because (1) dominant negative alleles can sequester WT MC1R in the ER or inhibit signal transduction at the plasma membrane, and (2) heterozygous mutations can modulate signaling of the WT protein.

Loss-of-function, hypomorphic, and dominant negative MC1R variants result in increased pheomelanin synthesis and many of these variant alleles are associated with red hair, fair skin, and freckles (Duffy et al., 2004; Frandberg et al., 1998; Herraiz et al., 2009; Newton et al., 2005; Ringholm et al., 2004; Sanchez-Laorden et al., 2009; Sanchez-Laorden et al., 2006; Schioth et al., 1999; Valverde et al., 1995). Individuals with MC1R variants display increased sun sensitivity, resulting in increased risk for sun damage and skin cancers. This is likely a consequence of decreased eumelanin, increased pheomelanin, an inefficient tanning response, and a decrease in the MITF-mediated expression of antioxidant and DNA damage response genes (Bastiaens et al., 2001; Raimondi et al., 2008; Scherer and Kumar, 2010; Williams et al., 2011).

Studying the coordination of eumelanogenesis and pheomelanogenesis is critically important for understanding human health and disease. Questions remain about whether pheomelanin is synthesized in the same melanosome as eumelanin, whether a separate pheomelanosome exists, or a combination of both. Unfortunately, few tools exist to study pheomelanin synthesis and there are no markers specific for this pathway. Most cell biology studies, including this work, center on eumelanin biology. In the rest of this work, melanin refers specifically to eumelanin, unless stated otherwise.

1.4. Melanosomes serve as the site for melanin synthesis and storage

Melanin synthesis occurs in melanosomes, specialized organelles that are found in melanocytes and pigmented epithelial cells. The term melanosome was coined in 1961 after work involving fractionation experiments and electron microscopy (EM) determined that TYR activity and melanin synthesis took place in a so-called “ultramicroscopic

compartment" (Lerner et al., 1949; Seiji et al., 1961). Researchers were able to isolate these compartments biochemically and, by EM, could visualize membrane-bound structures that contained lamellae or that were filled with dense particles. They proposed that melanin synthesis in these compartments was a gradual process with melanin depositing on the lamellae until they could no longer be seen (Barnicot and Birbeck, 1958; Birbeck et al., 1956). These works served as the basis for the study of melanosome biogenesis and maturation.

Melanosomes mature in four morphologically distinct stages from stage I to stage IV (Seiji et al., 1961). Stage I melanosomes derive from early endosomes, are unpigmented, and resemble maturing multivesicular bodies (MVBs) which have intralumenal vesicles (ILVs) and PMEL fibrils. Stage II melanosomes contain organized fibrillar sheets. In stage III, melanin is synthesized and deposited onto the PMEL fibrils, and by stage IV, the melanosome is completely dark and filled with melanin.

Stage I melanosomes are maturing early endosomes that are accessible to endocytic cargo and harbor known early endosomal constituents such as EEA1 but, in addition, contain the melanosomal protein PMEL. PMEL is an integral membrane glycoprotein that can be observed both on the limiting membrane and on ILVs by immunogold-labeled EM (Berson et al., 2001; Hurbain et al., 2008; Kikuchi et al., 1996; Raposo et al., 2001). Few other melanosomal proteins are present, with only a negligible number of TYRP1 gold-labeled particles at this stage, suggesting that other melanosomal proteins are transported to maturing melanosomes (Raposo et al., 2001).

Although they remain unpigmented, stage II melanosomes can be clearly identified in electron micrographs by the presence of long internal striations, which are composed of lumenal fragments of PMEL (Berson et al., 2001; Berson et al., 2003; Raposo et al.,

2001; Seiji et al., 1961; Seiji et al., 1963; Theos et al., 2006a). PMEL is composed of a long lumenal N-terminal domain, a single transmembrane domain, and a short cytoplasmic C-terminal domain (Adema et al., 1994; Kwon et al., 1987; Maresh et al., 1994a). The lumenal domain of PMEL is cleaved in stage I melanosomes to generate a soluble Mα form and a membrane-bound Mβ form (Berson et al., 2001; Berson et al., 2003; Maresh et al., 1994b). The Mα form is amyloidogenic and, after further cleavage and processing steps, assembles into the fibrillar structure necessary for proper melanosome formation (Berson et al., 2003; Fowler et al., 2006; Hee et al., 2017; Hurbain et al., 2008; Leonhardt et al., 2013; Rochin et al., 2013). Loss of PMEL fibril formation results in a disorganized melanosomal matrix, uneven melanin deposition, and a circular rather than ovoid melanosome shape (Berson et al., 2003; Hellström et al., 2011; Theos et al., 2006a; Theos et al., 2006b). Thus, PMEL fibril formation is initiated in stage I and completion of the PMEL melanosomal matrix marks the transition of the melanosome to stage II. Antibodies to full-length and the various PMEL fragments can be used to visualize stage I and II melanosomes by immunofluorescence microscopy (IFM); although the cleaved, fibrillar Mα fragments exist in stage III and IV melanosomes, their epitopes become buried by melanin and are inaccessible (Donatien and Orlow, 1995; Raposo et al., 2001). Stage II melanosomes also contain low levels of TYR, TYRP1, and DCT (Kushimoto et al., 2001; Raposo et al., 2001), but because melanosome maturation and cargo trafficking to melanosomes are dynamic processes, these markers cannot be used to reliably differentiate between stage I and stage II melanosomes. The most reliable method for distinguishing between stages is by EM, by which the fibrillar matrix of stage II melanosomes is easily seen. Additionally, stage II melanosomes are fully segregated from

early endosomes, so unlike stage I melanosomes, stage II melanosomes do not accumulate endocytosed cargo (Raposo et al., 2001).

In stage III melanosomes, melanin is synthesized and deposited onto PMEL fibrils. TYRP1, TYR, and DCT continue to accumulate and are most prevalent in these maturing melanosomes (Kushimoto et al., 2001; Raposo et al., 2001). Antibodies to TYRP1 or TYR are commonly used to visualize stage III and IV melanosomes by IFM as the majority of TYRP1-positive or TYR-positive structures are pigmented (Benito-Martinez et al., 2020). As melanin accumulates, the PMEL fibrils become obscured until only pigment can be seen, generating a stage IV melanosome.

ILVs, formed by the invagination of the limiting membrane, within melanosomes are important for melanosome maturation. In stage I melanosomes, ILVs serve as the site of PMEL fibril initiation and growing fibrils can be found adjacent to ILVs (Berson et al., 2001; Hurbain et al., 2008). Indeed, PMEL sorting to ILVs is required for fibril formation (Theos et al., 2006b). Additionally, evidence suggests TYR is present both on limiting membranes of stage III and IV melanosomes and on ILVs of stage III melanosomes (Theos et al., 2005). This may allow increased coverage of the enzyme throughout the melanosome for even melanin synthesis; however, this has not been tested. Protein localization to ILVs may also be a mechanism to regulate protein activity. For example, the GPCR GPR143 localizes to melanosomes and can be found on the limiting membrane and sometimes on ILVs (Samaraweera et al., 2001; Schiaffino et al., 1996), likely as a regulatory mechanism to sequester GPR143 from its downstream effectors.

The fate of a stage IV melanosome depends on the cell type in which it resides. In epidermal and follicular melanocytes of the skin and hair, respectively, the mature melanosome is transported to the cell periphery where it is secreted to be taken up by

keratinocytes (Bahadoran et al., 2001; Hume et al., 2001; Koch et al., 2020; Wilson et al., 2000). This requires the small GTPase Rab27a, the adaptor protein melanophilin, and the actin-based motor myosin Va. The mechanism of melanosome transfer is a topic of debate and four possible modes of transfer have been posited: cytophagocytosis, membrane fusion, shedding-phagocytosis, and exocytosis-endocytosis (Van Den Bossche et al., 2006; Wu and Hammer, 2014). In the cytophagocytosis model, melanosomes are transported to the dendritic tips of melanocytes where keratinocytes can reach out and pinch off the tip to phagocytose the mature melanosomes (Birbeck et al., 1956; Cohen and Szabo, 1968; Cruickshank and Harcourt, 1964; Mottaz and Zelickson, 1967; Okazaki et al., 1976). The membrane fusion model proposes that melanocytes and keratinocytes undergo localized membrane fusion to generate a pore or channel through which melanosomes can travel (Scott et al., 2002). The shedding-phagocytosis model suggests that melanosomes are packaged into vesicles, which are exocytosed by the melanocyte and phagocytosed by a neighboring keratinocyte (Ando et al., 2012; Ando et al., 2011; Aspengren et al., 2006; Cerdan et al., 1992; Singh et al., 2010; Wu et al., 2012). In the exocytosis-endocytosis model, the melanosomal membrane fuses with the plasma membrane of melanocytes to exocytose naked melanin, which is then endocytosed by keratinocytes (Quast et al., 2003; Swift, 1964; Tarafder et al., 2014; Virador et al., 2002). There is little current evidence to indicate that melanosome transfer occurs via cytophagocytosis or membrane fusion. It is more likely that the mechanism of melanosome transfer involves shedding-phagocytosis, exocytosis-endocytosis, or both. While debate exists about how melanosomes are transferred to keratinocytes, the field agrees that transfer involves close contact between melanocytes and keratinocytes, at

sites similar to an immunological synapse, and that protease-activated receptor-2 (PAR-2), a GPCR on the plasma membrane of keratinocytes, is required (Seiberg et al., 2000).

1.5. pH regulation of melanosomes

The regulation of pH in melanosomes is critically important for proper melanosome biogenesis and maturation. Vacuolar-type H(+)-ATPase (V-ATPase) localizes to the plasma membrane, trans Golgi network, and all endosomal organelles, including melanosomes, where it uses energy from ATP hydrolysis to drive proton transport into the lumen of their resident organelle, resulting in acidification (Bhatnagar and Ramalah, 1998; Cotter et al., 2015; Tabata et al., 2008). An acidic pH is required in stage I and II melanosomes for PMEL processing into Mα and Mβ forms by a proprotein convertase (Berson et al., 2001; Berson et al., 2003). However, Mα remains linked to Mβ via disulfide bond (Berson et al., 2001) until cleavage by beta site APP cleaving enzyme-2 (BACE2) releases Mα to allow its oligomerization into fibrils (Rochin et al., 2013). BACE2 activity is pH-dependent, with maximal activity at low pH and decreasing activity as the pH approaches 6 (Abdul-Hay et al., 2012). Loss of BACE2 activity results in a disorganized melanosomal matrix and mild hypopigmentation due to lack of PMEL processing (Rochin et al., 2013). Therefore, an acidic pH is required for the proper formation of stage I and II melanosomes; however, as melanosomes mature, neutralization of the melanosome must occur.

The enzymatic activity of TYR is related to pH, with maximal TYR activity at neutral pH and decreased activity at acidic pH (Ancans et al., 2001b; Fuller et al., 2001; Saeki and Oikawa, 1985). Consequently, treatment with V-ATPase inhibitors (e.g. bafilomycin

A1 and concanamycin A1), membrane-permeant basic molecules (e.g chloroquine and ammonium chloride), or ionophores (e.g. monensin) to inhibit or reverse acidification results in increased TYR activity and melanin content (Ancans and Thody, 2000; Oikawa et al., 1987; Saeki and Oikawa, 1983, 1985). These data directly disproved the hypothesis that melanosomes became more acidic as they matured (Bhatnagar et al., 1993; Puri et al., 2000).

Studies to identify the cellular mechanisms underlying human pigmentation variances have focused on TYR because it is the rate-limiting enzyme for melanin synthesis. In melanocytes derived from lightly pigmented Caucasian skin and from darkly pigmented Black skin, TYR protein and mRNA levels did not correlate well with skin color but TYR activity did (Iozumi et al., 1993). Incubating these melanocytes in ammonium chloride to increase pH resulted in a 5-20-fold increase in TYR activity in Caucasian melanocyte cell lines but not in Black melanocyte cell lines, indicating that the melanosomes in Caucasian melanocytes are more acidic and prevent maximal TYR activity and melanin synthesis (Ancans et al., 2001b; Fuller et al., 2001). Therefore, a shift from acidic pH to neutral pH promotes the transition from PMEL fibril formation in stage I and II melanosomes to melanin synthesis in stage III and IV melanosomes. This was confirmed using the acidotropic pH indicator, N[3-[(2,4-dinitrophenyl)amino]propyl]-N-(3-aminopropyl)methylamine dihydrochloride (DAMP), which selectively accumulates in acidic compartments by becoming protonated and thus no longer able to cross the lipid bilayer. Assessing DAMP accumulation in melanosomes using immunogold-labeled EM showed that DAMP accumulated to a much higher degree in stage I and II melanosomes than in stage III and IV melanosomes (Raposo et al., 2001).

The regulation of pH in the melanosome is an intriguing topic of investigation. Currently, only a few proteins involved in ion transport in melanosomes have been characterized. However, it is likely that the ion transport system in melanosomes is complex and highly coordinated, so there is much more to learn about how pH is regulated in this system (**Figure 1.2**). Ion transport proteins include ion pumps, channels, and transporters, and they function relative to the electrochemical gradient. Whereas ion channels allow passive diffusion of an ion or substrate along its concentration gradient, ion pumps and transporters use energy from ATP hydrolysis or from the electrochemical gradient to drive transport against an ion or substrate's concentration gradient (Alberts et al., 2002). While V-ATPase mediates H^+ influx in melanosomes to generate an acidic lumen in early stage melanosomes, it is unclear how this is counteracted in maturing melanosomes to generate a neutral environment.

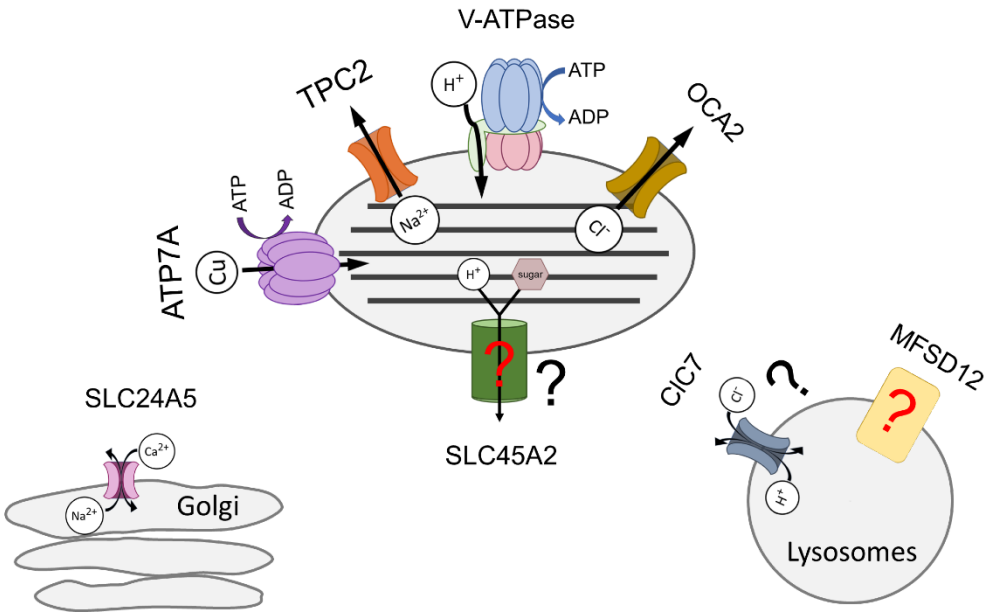

Figure 1.2: Ion transport channels in melanosome biogenesis. A schematic of ion transport proteins that affect pigmentation. ATP7A is an ATP-dependent copper transporter on melanosomes, the Golgi, and endosomes. Its activity is required to provide copper for TYR function.

V-ATPase on melanosomes uses ATP hydrolysis to pump protons into the lumen to acidify the melanosome. TPC2 is a cation channel on melanosomes that allows sodium and/or calcium cation efflux and promotes melanosome acidification by increasing membrane potential, which would putatively increase V-ATPase actiivty. OCA2 is a chloride-selective anion channel on melanosomes that allows chloride efflux from the melanosomes and promotes melanosome deacidification by decreasing membrane potential, which would putatively decrease V-ATPase activity. SLC45A2 functions as a proton/sugar co-transporter and it is hypothesized to localize to melanosomes but this is unclear. SLC24A5 localizes primarily to the Golgi and is a calcium/sodium antiporter. The function of MFSD12 is unknown but it localizes to lysosomes in melanocytes and its knockdown results in increased pigmentation. ClC7 is a proton/chloride antiporter that localizes to lysosomes in non-pigmented cells but its localization in pigmented cells has not been shown. Black question marks signify proteins with unknown localization. Red question marks signify proteins with unknown function.

The protein oculocutaneous albinism type 2 (OCA2 a.k.a. p-protein) is a chloride-selective anion channel localized to melanosomes that allows Cl^- ions to flow from the melanosomal lumen to the cytoplasm (Bellono et al., 2014; Sitaram et al., 2009). Loss-of-function mutations in *OCA2* in humans result in OCA type 2 (OCA2), characterized by moderate-to-severe hypopigmentation of the skin, hair, and eyes (Brilliant, 2001; Getting and King, 1994; Manga and Orlow, 1999). Mice with loss-of-function mutations in the *Oca2* gene (*pink-eyed dilution* mice) or melanocytes cultured from those mice (melan-p1 cells) are also hypopigmented (Sviderskaya et al., 1997). Treatment of melan-p1 cells with bafilomycin A1, monensin, or ammonium chloride resulted in a 4-5-fold increase in melanin content, indicating that loss of OCA2 results in an aberrantly acidic organelle (Ancans et al., 2001a). Indeed, OCA2 expressed in AD-293 cells, derivatives of the HEK293 cell line, localizes to late endosomes/lysosomes and increases pH in the organelles to which they localize (Bellono et al., 2014). This is dependent on OCA2's Cl^- transport function as a mutation that inhibits Cl^- transport does not change the pH in these organelles (Bellono et al., 2014). One model for how OCA2 neutralizes pH is that Cl^- efflux reduces melanosome membrane potential, resulting in decreased V-ATPase activity and fewer or no protons being pumped into the melanosomal lumen (Bellono et al., 2014).

Additionally, Cl^- efflux may be necessary for the action of one or multiple transporters that actively pumps protons out of the melanosome; however, if this is the case, the transporter(s) has not yet been identified.

Two-pore channel 2 (TPC2) is a voltage-independent cation channel localized to melanosomes where, upon binding its ligand phosphatidylinositol 3,5-bisphosphate (PtdIns(3,5)P2), a pore opens to allow Na^{2+} efflux from the melanosomal lumen (Ambrosio et al., 2016; Bellono et al., 2016; Wang et al., 2012). While it has been proposed that nicotinic acid adenine dinucleotide phosphate (NAADP) is a TPC2 ligand and that Ca^{2+} transport is also mediated by TPC2 (Ambrosio et al., 2016; Lin-Moshier et al., 2014), patch clamp data indicate otherwise (Bellono et al., 2016; Wang et al., 2012). Overexpression of TPC2 results in decreased melanosomal pH and hypopigmentation, which is dependent on TPC2 channel activity (Ambrosio et al., 2016; Bellono et al., 2016; Lin-Moshier et al., 2014). Conversely, knockdown of TPC2 results in increased pH and increased melanin content (Ambrosio et al., 2016; Bellono et al., 2016). Therefore, TPC2 promotes acidic melanosomal pH and is a negative regulator of melanin production. Current clamp recordings of melanosomes show that TPC2 activity increases melanosome membrane potential (Bellono et al., 2016). Therefore, a model for how TPC2 activity achieves an acidic pH is that the increase in membrane potential from TPC2 activity increases V-ATPase activity and proton influx. In this model, TPC2 and OCA2 would counterbalance each other to alter membrane potential. Understanding how each protein localizes to and is active within each melanosome maturation stage will provide important insight into one mechanism of how pH regulation is coordinated in melanosomes.

A major question remains: if OCA2 activity decreases membrane potential and V-ATPase activity, how are protons removed from the lumen to deacidify melanosomes?

One candidate protein is solute carrier family 45 member 2 (SLC45A2 a.k.a. MATP, AIM1, OCA4). Pathologic mutations in *SLC45A2* result in OCA type 4 (OCA4), characterized by moderate-to-severe hypopigmentation of the skin, hair, and eyes (Gronskov et al., 2007; Marcon and Maia, 2019; Martinez-Garcia and Montoliu, 2013; Montoliu et al., 2014). When expressed in yeast cells, mouse SLC45A2 functions as a sugar/proton-symporter that imports protons into the cytosol (Bartolke et al 2014), indicating that it could mediate proton transport out of the melanosome. However, while it has been proposed to reside on melanosomes (Bin et al 2015), its localization and function in mammalian cells has not been clearly defined. This is the focus of Chapter 2.

Many other ion transport proteins play a role in melanosome pH regulation (**Table 1.1**). RNA-sequencing data of human epidermal melanocytes from Haltaufderhyde and Oancea (2014) list numerous abundantly expressed ion transport proteins (Haltaufderhyde and Oancea, 2014). Among them are OCA2, TPC2, and SLC45A2; they also include members of the TRPM family of cation channels, members of the chloride intracellular channel (CLIC) family, and members of the chloride channel voltage-sensitive (CLCN) family (Haltaufderhyde and Oancea, 2014). This is a wide field of study as it is necessary to identify not only the localization and function of each of these proteins in melanocytes but also how they crosstalk with each other and with the other ion transport proteins in melanosomes and elsewhere in the cell.

Table 1.1: Selected ion transporters with known or putative effects on melanogenesis			
Protein	**Localization in Pigmented Cells**	**Function**	**Selected References**
V-ATPase	PM, TGN, endosomal pathway, melanosomes	ATP-dependent proton pump	(Tabata et al., 2008)
OCA2 (P protein)	Melanosomes	Chloride-selective ion channel	(Bellono et al., 2014; Sitaram et al., 2009)
SLC45A2 (MATP; AIM-1; OCA4)	Melanosomes (putative)	Sugar/proton symporter	(Bartolke et al., 2014; Bin et al., 2015)
Two-pore channel 2 (TPC2)	Melanosomes	Sodium-selective ion channel	(Ambrosio et al., 2016; Bellono et al., 2016; Wang et al., 2012)
ATP7A	Melanosomes	Copper transporting ATPase	(Setty et al., 2008)
SLC24A5 (NCKX5)	TGN; mitochondria	Potassium-dependent sodium/calcium exchanger	(Ginger et al., 2008; Rogasevskaia et al., 2019; Zhang et al., 2019)
MFSD12	Lysosomes	Unknown	(Crawford et al., 2017)
Chloride channel, voltage-sensitive 7 (CLCN7; CLC7)	Lysosomes (non-pigmented cells)	Chloride/proton antiporter	(Graves et al., 2008; Weinert et al., 2014)
TRP cation channel, subfamily M, member 1 (TRPM1)	Non-melanosomal compartment; PM (putative)	Calcium channel	(Oancea et al., 2009)
TRP cation channel, subfamily M, member 7 (TRPM7)	Plasma membrane (putative)	Cation non-selective, calcium permeant ion channel	(McNeill et al., 2007; Monteilh-Zoller et al., 2003)
Mucolipin 3 (MCOLN3; TRPML3)	Unknown	Cation non-selective, calcium permeant ion channel	(Xu et al., 2007)

Abbreviations: PM, plasma membrane; TGN, trans Golgi network; ATP, adenosine triphosphate

1.6. Cargo delivery: Trafficking to and from melanosomes

Melanosomes are a type of lysosome-related organelle (LRO), a class of cell type-specific subcellular organelles that are often distinct from lysosomes but derive from the endosomal pathway and share some features including acidic pH and certain lysosomal proteins at some point in their maturation (Bowman et al., 2019; Raposo and Marks, 2002; Raposo and Marks, 2007; Raposo et al., 2007). LROs play specialized roles that confer unique properties to their resident cell type (e.g. melanosomes generating pigment in melanocytes and pigmented epithelial cells; platelet dense granules as the storage site for small molecule mediators in platelets; lamellar bodies synthesizing pulmonary surfactant in alveolar type II (AT2) cells; etc.) (Bowman et al., 2019). An organizational problem for all organelle biogenesis and maturation, but especially for cells that contain LROs, is how to maintain organelle identity. After synthesis, folding, and modifications in the ribosome, ER and Golgi, proteins must be accurately directed to their final destinations. Therefore, trafficking needs to be tightly spatiotemporally regulated. A dedicated system of proteins exists for cargo protein trafficking to LROs. Mutations in the gene encoding some of these proteins result in Hermansky-Pudlak syndrome (HPS), which is a group of autosomal recessive diseases with pleiotropic effects due to defective LRO biogenesis (Bowman et al., 2019). Hypopigmentation of the skin, hair, and eyes is always associated with HPS, reflecting the requirement for these proteins for melanosome maturation. Therefore, melanosomes serve as a model system for studying LRO trafficking mechanisms and have provided much insight into how cells accurately transport cargo proteins.

In previous sections, the functions of melanosomal cargo proteins have been discussed but not how they are transported to melanosomes. All known melanosomal

proteins are integral membrane glycoproteins and are synthesized in the endoplasmic reticulum (ER) and modified by glycosidases and glycotransferases in the Golgi. They then are transported to melanosomes either directly from the Golgi or via endosomal intermediates, in some cases after delivery to and internalization from the plasma membrane. As discussed earlier, PMEL-containing stage II melanosomes diverge from maturing vacuolar early endosomes by mechanisms that are not understood (Raposo et al, 2001). Once they are segregated, they then mature to stage III and IV by the delivery of additional cargos – including TYR, TYRP1, DCT, and transporters such as OCA2 and ATP7A – by membrane trafficking pathways (Delevoye et al 2019; Bowman et al 2019).

There are three known pathways for cargo transport to maturing melanosomes: the aforementioned pathway from the trans Golgi network, which utilizes vesicle-mediated trafficking; a vesicular pathway from early endosomes; and a tubulovesicular pathway from early endosomes (**Figure 1.3**) (Bowman et al., 2019). Currently, it is known that two proteins (DCT and MART-1 a.k.a. melan-a) are transported to maturing melanosomes directly from the Golgi (Patwardhan et al., 2017); one, TYR, is transported via vesicles from endosomes (Theos et al., 2005); and three, TYRP1, OCA2, and APT7A, are transported via tubules from endosomes (Setty et al., 2008; Setty et al., 2007; Sitaram et al., 2012). The two pathways from the early endosome to melanosomes utilize multimeric protein complexes that are targeted by mutations in HPS variants. Many melanosomal cargo proteins contain either dileucine-based or tyrosine-based sorting sequences in their cytoplasmic domains that allow them to be targeted for sorting and transport (Blagoveshchenskaya et al., 1999; Calvo et al., 1999; Robila et al., 2008; Simmen et al., 1999; Sitaram et al., 2009; Theos et al., 2005; Theos et al., 2006b; Vijayasaradhi et al., 1995).

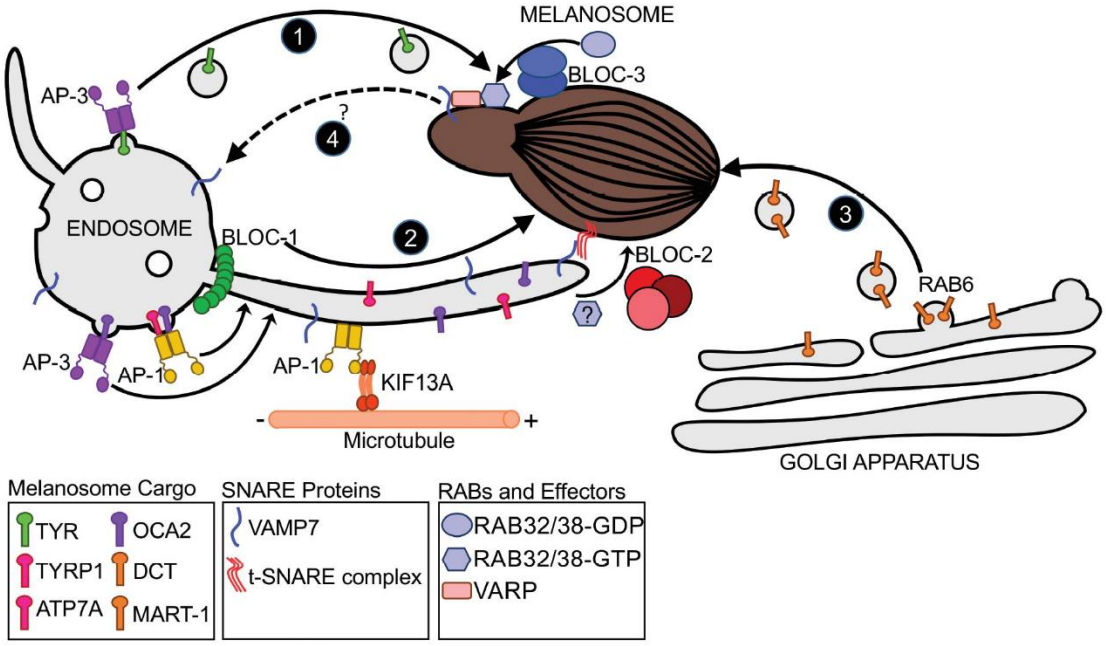

Figure 1.3: Trafficking pathways to melanosomes. Cargo of mature melanosomes traffic to melanosomes in one of three pathways. (1) Melanosomal proteins (e.g. TYR) on endosomes can be sorted by the coat protein AP-3 and transported to melanosomes via vesicles. (2) Melanosomal proteins (e.g. TYRP1 and ATP7A) on endosomes can be sorted by AP-1 or AP-3 into tubules which transport cargo to melanosomes. These tubules require BLOC-1 for initiation and elongation by coupling tubules to the microtubule motor protein KIF13A via AP-1 and they require BLOC-2 for engagement with melanosomal membranes. The v-SNARE VAMP7 engages unknown t-SNAREs at the melanosome to drive membrane fusion, allowing for cargo transfer. (3) Melanosomal proteins (e.g. DCT and MART-1) can also be transported to melanosomes directly from the Golgi via RAB6-mediated vesicles. (4) Non-resident proteins (e.g. VAMP7) are recycled from melanosomes through a retrograde pathway that requires BLOC-3 – a GEF for RAB32/28 – and VARP – an effector for RAB32/38. Figure copied with permission from (Bowman et al., 2019).

1.6.1. Function of AP-1 and AP-3 in sorting melanosomal cargo

Adaptor proteins 1 and 3 (AP-1 and AP-3) are heterotetrameric cytoplasmic complexes that bind to either dileucine-based or tyrosine-based sorting sequences and that function as coat proteins primarily from early endosomes through their interactions with early endosomal markers (Robinson and Bonifacino, 2001). Whereas AP-1 appears to function only in the tubulovesicular pathway to melanosomes by recruiting the

microtubule motor KIF13A (Delevoye et al 2009), AP-3 can mediate sorting into both vesicles and tubules. TYR contains a dileucine-based motif that preferentially binds AP-3 but can also bind AP-1 (Theos et al., 2005); therefore, TYR is transported from the early endosome primarily via vesicle-mediated trafficking but also a minor cohort can be transported via tubules. Conversely, TYRP1 contains a dileucine sorting signal that interacts only with AP-1 (Theos et al., 2005), which packages TYRP1 into tubules that extend from the early endosome to the melanosome (Delevoye et al., 2009a; Dennis et al., 2016; Dennis et al., 2015; Raposo et al., 2001). OCA2 can interact with both AP-1 and AP-3 through its dileucine-based sorting signal, but uses solely the tubulovesicular pathway to traffic to melanosomes (Sitaram et al., 2012; Sitaram et al., 2009). ATP7A interacts with AP-1 to enter the tubulovesicular pathway to melanosomes (Alsaif et al., 2019; Hartwig et al., 2019; Holloway et al., 2013; Setty et al., 2008; Yi and Kaler, 2015). Thus, AP-1 and AP-3 are critical mediators of melanosomal cargo sorting.

1.6.2. BLOC function in the tubulovesicular pathway

Central to the proper function of the tubulovesicular pathway to melanosomes are the biogenesis of lysosome-related organelles complex-1, -2, and -3 (BLOC-1, BLOC-2, and BLOC-3) (**Fig 1.3**). These multisubunit protein complexes coordinate tubule initiation and elongation, membrane engagement, and recycling (Bowman et al., 2019). BLOC-1 promotes the extension of tubules at least in part by coordinating the function of the kinesin motor protein KIF13A to pull tubules along microtubule motors (Delevoye et al., 2016; Delevoye et al., 2009a). Additionally, negative stain EM of recombinant BLOC-1 shows that the complex adopts a flexible linear shape, often curved (Lee et al., 2012). BLOC-1 associates with tubulovesicular regions (Di Pietro et al., 2006), which contain highly curved

membrane, and knockdown of BLOC-1 results in loss of tubule formation despite the emergence of buds at endosomes (Delevoye et al., 2016). Together, these data suggest that BLOC-1 may also be involved in the initiation of tubules, potentially by promoting membrane curvature.

BLOC-2 functions downstream of BLOC-1 and facilitates stable contacts between tubules and the melanosome; however, the mechanism by which BLOC-2 accomplishes this is unclear (Dennis et al., 2015; Di Pietro et al., 2006). BLOC-3 is a guanine nucleotide exchange factor (GEF) for RAB32 and RAB38 and functions in a retrograde transport pathway from melanosomes, which is required to ensure that proteins that mediate trafficking are recycled to the endosome and available for another round of anterograde transport (Dennis et al., 2016). BLOC-3, RAB32 and RAB38 might also function in anterograde transport (Bultema et al., 2012; Ohishi et al., 2019; Wasmeier et al., 2006).

1.6.3. Fusion of transport intermediates with melanosomes

Both vesicles and tubules must undergo membrane fusion to transport cargo, but how are docking and fusion coordinated to occur at the appropriate target? Membrane fusion specificity is dictated by soluble *N*-ethylmaleimide-sensitive factor attachment protein receptors (SNARE) proteins and by small GTPases that signal to effector proteins. Effectors include Sec1/Munc18 (SM) family members and tethering proteins (Ohbayashi and Fukuda, 2018; Stenmark, 2009).

SNARE proteins function essentially as molecular zippers to facilitate membrane fusion. In order to drive fusion, SNARE proteins on opposite membranes assemble into a coiled-coil four-helix bundle called a SNARE complex, which generates enough force to overcome the energy barrier to membrane fusion (Sudhof and Rothman, 2009). SNARE

proteins can be subdivided into R-SNAREs, or Qa-, Qb, or Qc-SNAREs. This designation is given by the amino acid (either an arginine or a glutamine) at the highly conserved central position of the SNARE motif and by the SNARE motif's position within the SNARE complex (Fasshauer et al., 1998; Kloepper et al., 2007; Sutton et al., 1998). Also called the zero-layer residues, these arginine and glutamines of the R-SNARE, Qa-SNARE, Qb-SNARE, and Qc-SNARE form hydrogen bonds which align these SNARE proteins in relation to each other for proper SNARE complex formation (Yoon and Munson, 2018). Every SNARE complex is comprised of an R-SNARE, Qa-SNARE, Qb-SNARE, and Qc-SNARE. A more generalized classification of SNARE proteins is based on their localizations on apposing membranes – v-SNAREs (typically an R-SNARE) on vesicular membranes and t-SNAREs (typically Q-SNAREs) on target membranes (Sudhof and Rothman, 2009). Alignment of the zero-layer residues of the R-SNARE and Qa-, Qb-, and Qc-SNAREs and helical zippering completes the formation of the SNARE complex to drive membrane fusion.

Although *in vitro* experiments indicate that the physical interactions between SNARE proteins can be promiscuous, SNARE proteins *in vivo* are highly regulated and a v-SNARE interacts only with its cognate t-SNAREs to form specific SNARE complexes and to provide specificity in membrane fusion reactions (Sudhof and Rothman, 2009). In tubulovesicular transport to melanosomes, the v-SNARE has been identified as VAMP7 (Dennis et al., 2016); however, the v-SNARE on vesicles destined for melanosomes and the t-SNAREs on melanosomes are unknown.

For a v-SNARE and t-SNAREs to promote fusion, their resident membranes must be in close proximity. This is accomplished by tethering proteins, which bind apposing membranes and serve as a bridge to connect them. Tethering proteins bind membranes

and achieve specificity through their interactions with small GTPases, primarily of the Rab superfamily (Ungermann and Kummel, 2019; van der Beek et al., 2019; Yu and Hughson, 2010). A tethering protein in the endosome-to-melanosome trafficking pathway has not yet been identified, but the homotypic fusion and vacuole protein sorting (HOPS) complex is a strong candidate.

1.6.4. HOPS, VPS33A, and the *buff* mouse

HOPS is composed of 6 subunits – VPS41, VPS16, VPS33A, VPS18, VPS11, and VPS39 – organized in a seahorse shape (Balderhaar and Ungermann, 2013; Brocker et al., 2012). VPS41 and VPS39 exist on opposite ends of the complex and bind to the small GTPases and Rab adaptors, and simultaneous binding of VPS41 and VPS39 to these proteins on different membranes allows HOPS to bind and tether apposing membranes. VPS41 can bind the small GTPase ARL8B (Garg et al., 2011; Khatter et al., 2015), the RAB7 adaptor pleckstrin homology and RUN domain containing M1 (PLEKHM1) (McEwan et al., 2015), and the RAB7 effector Rab interacting lysosomal protein (RILP) (Lin et al., 2014; van der Kant et al., 2013); and VPS39 can bind the ARL8B effector SKIP (Khatter et al., 2015) and PLEKHM1 (Marwaha et al., 2017; McEwan et al., 2015). Through these interactions, HOPS is able to mediate tethering between late endosomes, lysosomes, and autophagosomes. In yeast, Vps41 and Vps39 can bind directly to Ypt7 (Brocker et al., 2012; Ho and Stroupe, 2015; Seals et al., 2000), the RAB7 ortholog; however, in mammalian systems, these interactions do not occur directly (Khatter et al., 2015). Additionally, one report suggests that yeast Vps39 acts as a guanine nucleotide exchange factor (GEF) for Ypt7 (Wurmser et al., 2000), but mammalian VPS39 does not show this activity (Peralta et al., 2010). In addition to late endosomes and lysosomes, RILP also

localizes to melanosomes, indicating that HOPS could potentially interact with melanosomes through RILP (Matsui et al., 2012; Ohbayashi et al., 2012). However, whether HOPS localizes to or mediates tethering at melanosomes is unknown.

Based on the known interactions between VPS39 or VPS41 and small GTPases and their adaptors, HOPS does not bind early endosomes; instead, a similar complex, the class C core vacuole/endosome tethering (CORVET) complex tethers early endosomes during fusion (Amaya et al., 2016; Balderhaar et al., 2013; Balderhaar and Ungermann, 2013; Chou et al., 2016; Marwaha et al., 2017; Perini et al., 2014b; van der Beek et al., 2019; Van Der Kant et al., 2015). CORVET is predicted to have a similar structure as HOPS, with which it shares 4 subunits – VPS11, VPS18, VPS33A, and VPS16 – but CORVET has VPS3 and VPS8 on opposite sides of the seahorse shape to mediate interactions with the small GTPase Rab5 on early endosomes (Lachmann et al., 2014; Peplowska et al., 2007; Perini et al., 2014a; Van Der Kant et al., 2015). Even though a role for endosome-melanosome tethering has not been described for HOPS, it is more likely that HOPS rather than CORVET is required for melanosome biogenesis because mutations in HOPS-specific but not CORVET-specific subunits have been associated with pigmentation defects in mice, *Drosophila melanogaster*, *Caenorhabditis elegans*, and zebrafish (Delahaye et al., 2014; Grant et al., 2016; Hermann et al., 2005; Huizing et al., 2001; Pulipparacharuvil et al., 2005; Sadler et al., 2005; Sevrioukov et al., 1999; Suzuki et al., 2003; Takats et al., 2014; Warner et al., 1998).

VPS33A, a subunit of both HOPS and CORVET, plays a critically important role in SNARE complex formation as a member of the Sec1/Munc18 (SM) family of proteins (Baker et al., 2013; Baker et al., 2015; Graham et al., 2013; Lobingier and Merz, 2012; Seals et al., 2000). SM proteins chaperone SNARE complex assembly, but the exact

mechanism by which this occurs may differ depending on the SM protein (Baker and Hughson, 2016). Structural data from Vps33 bound to the Qa-SNARE Vam3 and the R-SNARE Nyv1, all purified from the thermophilic fungus Chaetomium thermophilum, has led to a model where Vps33 templates SNARE complex assembly by binding to R- and Q-SNAREs and aligning them for proper formation of the four-helix bundle (Baker et al., 2015). A mutation in VPS33A has been identified in the *buff* mouse line, a mouse model of HPS characterized by hypopigmentation and bleeding diathesis, indicating that VPS33A plays a role in trafficking to LROs including melanosomes (Suzuki et al., 2003). Like HPS, the phenotype observed in mice is recessive. Intriguingly, the mice are not reported to have any major general defects in the endosomal/lysosomal system despite that fact that HOPS has a well characterized role in regulating fusion of late endosomes with lysosomes and with autophagosomes. Data from one group indicated that the *buff* mutation – VPS33A-D251E – results in increased interaction between the SM protein and SNARE proteins (Zhen and Li, 2015). However, it is unlikely that a mutation that sequesters HOPS and prevents its function would be a recessive mutation. Additionally, data from their sucrose gradient experiment indicate that HOPS is only present in the same fraction as lysosomes but not with late endosomes, which contradicts evidence that HOPS associates with both lysosomes and late endosomes (Balderhaar and Ungermann, 2013; Bowman et al., 2019; Lin et al., 2014; Marwaha et al., 2017; Pols et al., 2013a; Solinger and Spang, 2013; van der Beek et al., 2019; Wartosch et al., 2015; Zhen and Li, 2015). How VPS33A functions in melanosome biogenesis is unknown and is of major interest because it could (1) reveal more about melanosome dynamics and interactions with other organelles, and (2) identify how VPS33A confers specificity even though it functions in multiple pathways.

1.7. Molecular basis of albinism

Mutations resulting in defective melanosome biogenesis result in albinism, a rare, heterogeneous disorder characterized by hypopigmentation of the skin, hair, and eyes. The prevalence of albinism is estimated to be approximately 1:17,000 to 1:20,000 (Santiago Borrero et al., 2006; Witkop et al., 1990), although it is more common in certain populations due to founder effects. The decrease in pigmentation may vary from individual to individual, but ocular defects due to hypopigmentation of the eyes must be present for a diagnosis of albinism (Gronskov et al., 2007; Kirkwood, 2009; Marcon and Maia, 2019; Martinez-Garcia and Montoliu, 2013; Montoliu et al., 2014).

Characteristic ocular symptoms include: hypopigmentation of the iris resulting in iris transillumination; reduced pigmentation of the retinal pigment epithelium resulting in foveal hypoplasia; abnormal decussation (abnormal crossing of the optic nerve fibers); congenital nystagmus (involuntary eye movement); strabismus (misalignment of eyes); photophobia (light sensitivity); refractive errors (i.e. far-sightedness, near-sightedness, and astigmatism); and poor vision (Gronskov et al., 2007; Montoliu et al., 2014). The ocular defects are broad and severe due to a requirement for melanin synthesis in ocular melanocytes and pigmented epithelial cells during development (Levin and Stroh, 2011). The fovea is a region of the retina that is responsible for visual acuity. Therefore, foveal hypoplasia, which is the loss of the foveal pit, is the major cause of poor vision in albinism. Additionally during development, optic nerve fibers, composed of retinal ganglion cell (RGC) axons, emerge from the ventro-temporal retina and migrate towards the optic chiasm where they either cross to the contralateral brain hemisphere or continue straight to the ipsilateral brain hemisphere. This decussation, or crossing of the optic nerve fibers,

allows each brain hemisphere to receive visual cues from both eyes, which is necessary for binocular vision (Reese, 2011). During normal development, approximately 55% of the optic nerve fibers cross to the contralateral side, but this percentage is increased to 75-85% in individuals with albinism and is associated with reduced binocular vision and strabismus (Levin and Stroh, 2011). This is due to a requirement for L-DOPA, an intermediate in the melanin biosynthesis pathway, during embryological development. The presence of L-DOPA is required to coordinate the timing of RGC cell entry at the optic chiasm, which promotes ipsilateral crossing early and contralateral crossing later. The loss of L-DOPA leads to RGC cells reaching the optic chiasm later and more cells being sent to the contralateral side (Ather et al., 2019; Ilia and Jeffery, 1999; Kralj-Hans et al., 2006). These clinical criteria for the diagnosis of albinism can be tested by an ophthalmologist. While there are no treatments for albinism and most individuals with albinism are legally blind, some of the associated visual defects can be somewhat managed (Levin and Stroh, 2011). For instance, prescription corrective lenses or telescopic lenses may slightly improve vision; tinted glasses can dampen photophobia; and, while rarely performed for albinism, surgery on optical muscles may decrease nystagmus and strabismus.

Although albinism does not affect life expectancy, reduced or absent melanin makes individuals with albinism more vulnerable to the harmful effects of UVR. Individuals with albinism are at increased risk for sun damage, sunburns, and skin cancers, particularly squamous cell carcinoma and basal cell carcinoma (Marcon and Maia, 2019; Martinez-Garcia and Montoliu, 2013). Those with albinism are recommended to use sunscreen liberally, to avoid the sun, and to see a physician regularly to check for malignant lesions.

Aside from one type of albinism (ocular albinism type 1 (OA1), which is X-linked and primarily affects the eyes), all albinism is autosomal recessive and results in decreased pigmentation of the skin, hair, and eyes. Albinism can be divided into non-syndromic albinism or syndromic albinism. In non-syndromic albinism, gene mutations affect only pigmented cell types; therefore, albinism is the only systemic disorder. In syndromic albinism, additional systemic disorders are observed due to defects in non-pigmented cell types.

1.7.1. Non-syndromic albinism

The types of non-syndromic albinism identified thus far are oculocutaneous albinism types 1-8 (OCA1-OCA8) and ocular albinism type 1 (OA1) (**Table 1.2**) (Marcon and Maia, 2019; Martinez-Garcia and Montoliu, 2013; Pennamen et al., 2020b). With the exception of OCA5 and OCA7, mouse models of OCA subtypes and OA1 exist and are also hypopigmented (**Table 1.2**). OCA1, OCA2, OCA3, and OCA4 are the most common subtypes of OCA, although the prevalence of each subtype varies by region. As discussed earlier, the genes mutated in OCA1, OCA2, and OCA8 – TYR, OCA2 and DCT – have been well studied and have known roles in melanin synthesis and melanosome biogenesis (**Table 1.2**). Mutations in TYRP1 cause OCA3 and while the exact function of TYRP1 has not been unequivocally determined, TYRP1 localizes to the mature melanosome limiting membrane and influences melanin synthesis and melanosome structure; this can be seen in *brown* mice, the OCA3 mouse model, which have smaller, rounder melanosomes than their WT counterparts (Hirobe et al., 2014).The role of SLC45A2, which is mutated in OCA4, is hypothesized to be in ion transport at the melanosome (Bin et al., 2015) but this has not clearly been shown. Elucidating the structure and function of SLC45A2 is the focus

of Chapter 2. The gene mutated in OCA5, which has only been reported in 1 Pakistani family, has not been identified (Kausar et al., 2013). OCA6 has been found in 6 unrelated families and is caused by mutations in *SLC24A5*, which encodes a potassium-dependent sodium-calcium exchanger (Ginger et al., 2008; Morice-Picard et al., 2014; Wei et al., 2013). SLC24A5 does not appear to localize to melanosomes but rather has been reported to localize to the trans-Golgi network and perhaps to mitochondria, indicating that it affects melanosome biogenesis indirectly (Ginger et al., 2008; Rogasevskaia et al., 2019; Zhang et al., 2019). OCA7 has been identified in 1 Lithuanian patient and 5 unrelated individuals from the Faroe Islands (Gronskov et al., 2013). It is caused by mutations in the leucine-rich melanocyte differentiation associated (LRMDA) protein. The function of LRMDA is unknown, but it is hypothesized to play a role in melanocyte differentiation due to the decreased number of melanocytes found in adult tissues compared to fetal tissues upon knockdown of the gene in zebrafish (Gronskov et al., 2013). OCA8 has recently been described in 2 patients and is caused by mutations in DCT (Pennamen et al., 2020b).

OA1 is an X-linked form of non-syndromic albinism that affects primarily the eyes, resulting in the ocular defects seen in OCA but without severe hypopigmentation of the skin or hair (O'Donnell et al., 1976). It is caused by mutations in the G-protein-coupled receptor GPR143 (OA1) (Innamorati et al., 2006), which is expressed in all pigment-producing cells (Bassi et al., 1996; Bassi et al., 1995; Newton et al., 1996). Individuals with OA1 have macromelanosomes in both skin and eye melanocytes. However, skin pigmentation is normal in these individuals. Conversely, RPE cells have decreased pigmentation, likely because melanin is not evenly dispersed throughout the cell and is instead accumulated in a few giant melanosomes (Garner and Jay, 1980; Wong et al.,

2009). GPR143 localizes to late endosomes/lysosomes and melanosomes, primarily to the ILVs (Basrur et al., 2003; Giordano et al., 2009; Samaraweera et al., 2001; Schiaffino et al., 1996; Schiaffino et al., 2002; Schiaffino and Tacchetti, 2005). Evidence suggests that GPR143 expression prevents fusion between multivesicular bodies and lysosomes when ectopically expressed in HeLa cells (Burgoyne et al., 2013); this suggests that in pigmented cells, GPR143 may be involved in segregating maturing melanosomes from lysosomes. GPR143 also has putative roles in controlling the rate of melanosome biogenesis and controlling melanosome size (Cortese et al., 2005), inducing transcription of MITF target genes (Chen et al., 2016; Falletta et al., 2014) and regulating melanosome mobility and transport (Palmisano et al., 2008). These broad effects of GPR143 signaling are mediated by GPCR signaling.

The putative ligand-binding site for OA1 is on the lumenal side of membranes, so signaling from the melanosomal or endosomal membrane would induce downstream signaling in the cytosol to regulate melanosome biogenesis (Schiaffino and Tacchetti, 2005). One report suggests that the ligand for GPR143 is L-DOPA (Lopez et al., 2008), which should be abundant in a normal melanosome during melanin synthesis, but the conclusion is controversial (De Filippo et al., 2017).

The downstream effectors of GPR143 are an area of interest as uncovering this signal transduction pathway will reveal how GPR143 achieves its broad effects. Data indicate that GPR143 is a $G\alpha_{i/o}$-coupled receptor (Innamorati et al., 2006; Young et al., 2008). Broadly, $G\alpha$ proteins belong to one of four families: $G\alpha_{i/o}$, $G\alpha_{q/11}$, $G\alpha_{s}$, and $G\alpha_{12/13}$ (Syrovatkina et al., 2016). Each of these families is associated with different downstream signaling pathways. The $G\alpha_{i/o}$ family of proteins inhibits adenylyl cyclase activity. One

group identified guanine nucleotide binding protein, alpha inhibiting activity polypeptide 3 ($G\alpha_{i3}$) as the specific $G\alpha_i$ protein through which GPR143 signals, and RPE cells and tissue from mice with loss of *Gai3* phenocopy those of mice with loss of *Gpr143* (Young et al., 2011; Young et al., 2008). However, further work needs to be done to identify the function of $G\alpha_{i3}$ in pigmented cells.

Table 1.2: Non-syndromic Albinism

Type	Mouse Model	Protein	Function
OCA1	*albino*	TYR	Catalyzes oxidation of tyrosine or L-DOPA to dopaquinone
OCA2	*pink-eyed dilute*	OCA2	Chloride-specific anion channel
OCA3	*brown*	TYRP1	Enzyme Role in melanocytes and pigmented epithelial cells unknown
OCA4	*underwhite*	SLC45A2 (MATP, AIM-1)	Sugar-H^+ symporter? Role in melanocytes and pigmented epithelial cells unknown
OCA5	–	unknown	Unknown
OCA6	*Slc24a5*$^{-/-}$	SLC24A5 (NCKX5)	K^+-dependent Na^{2+}-Ca^{2+} exchanger Role in melanocytes unknown
OCA7	–	LRMDA	Leucine-rich melanocyte differentiation associated (LRMDA) Role in melanocytes and pigmented epithelial cells unknown
OCA8	*slaty*	DCT	Tautomerizes dopachrome to DHICA
OA1	*OA1*$^{-/-}$	GPR143 (OA1)	G-protein-coupled receptor

1.7.2. Syndromic albinism

Syndromic albinism is comprised of either HPS or Chediak-Higashi syndrome (CHS) (**Table 1.3**). HPS is a rare, autosomal recessive syndrome that affects trafficking pathways utilized by LROs, resulting in effects on multiple cell types. All subtypes of HPS

are characterized by oculocutaneous albinism and excessive bleeding and bruising due to defective trafficking to melanosomes and platelet dense granules. Some HPS subtypes have additional effects on other LROs. HPS patients have mutations in subunits of the multisubunit complexes described in Chapter 1.6.1 and 1.6.2 to regulate melanosome biogenesis – AP-3, BLOC-1, BLOC-2 and BLOC-3 (Bowman et al., 2019). Therefore, the HPS subtypes can be grouped by mutations in members of the same complex. HPS7, HPS8, HPS9, and HPS11 result from mutations in four of the eight known subunits of BLOC-1 (DTNBP1, BLOC1S3, BLOC1S6, and BLOC1S5, respectively) (**Table 1.3**) (Bowman et al., 2019; Pennamen et al., 2020a). Patients with these subtypes do not appear to exhibit consistent deficiencies other than the hypopigmentation and bleeding defects common to all HPS. Mutations in BLOC-2 subunits cause HPS3, HPS5 and HPS6. Like BLOC-1 disease, patients with BLOC-2 display only hypopigmentation and bleeding defects, although a subset of these patients also suffer from a form of inflammatory bowel disease; the physiological basis for this is not understood, but is also observed in HPS5 model mice (Itoh et al., 2016). Mutations in BLOC-3 subunits cause HPS1 and HPS4, which are severe forms of HPS and unfortunately the most common. In addition to OCA and excessive bleeding, HPS1 and HPS4 cause severe lung fibrosis and, in a minority of individuals, severe granulomatous colitis, a form of inflammatory bowel disease. The lung fibrosis is due to defective cargo trafficking to lung lamellar bodies in alveolar epithelial type 2 cells, impairing the production and/or secretion of surfactant. The cause of the granulomatous colitis is unknown. HPS2 and HPS10 are caused by mutations in the beta and delta subunits, respectively, of the heterotetrameric AP-3 complex and are also severe forms of HPS with multiple symptoms. In addition to albinism and excessive bleeding, individuals with HPS2 and HPS10 suffer from pulmonary fibrosis and recurrent

bacterial and viral infections, which are due to a requirement for AP-3 in trafficking in a number of innate and adaptive immune cell types including conventional dendritic cells, plasmacytoid dendritic cells, cytotoxic T cells, and natural killer cells. Individuals with HPS10 also have neurological symptoms (Ammann et al., 2016; Mohammed et al., 2019). CHS is a rare autosomal recessive disorder that is characterized by OCA, bleeding diathesis, immune system dysregulation, and mild neuropsychological impairment (Bowman et al., 2019; Shirazi et al., 2019). Affected cell types have enlarged lysosomes and LROs, including melanosomes, platelet dense granules, and cytolytic granules, preventing them from being secreted. CHS is caused by mutations in the lysosomal trafficking regulator (*LYST*) gene; however, the function of LYST in LRO biogenesis and regulation is unknown.

Mouse models exist for CHS and every HPS subtype (**Table 1.3**) and these mice phenocopy the human disease in all ways except for differences in how lungs are affected in those subtypes with lung fibrosis. However, additional mouse models of HPS exist with affected genes that have not yet been identified in human disease. For example, both *gunmetal* mice and *subtle gray* mice exhibit hypopigmentation and prolonged bleeding. They are caused by mutations in *Rabggta*, a gene encoding a subunit of the Rab geranylgeranyltransferase (RABGGTA), and *Slc7a11*, a gene encoding the cysteine transporter SLC7A11, respectively. Additionally, a mutation in the CORVET/HOPS subunit VPS33A has been identified in *buff* mice, a putative HPS model with hypopigmentation and bleeding defects (Suzuki et al., 2003). While studying these mouse models has improved our understanding of how BLOCs, AP3, and other putative HPS-associated proteins function in LRO biogenesis, we still do not know how VPS33A works in these pathways. I attempt to address this in Chapter 3.

Table 1.3: Syndromic Albinism				
Type	**Mouse model**	**Protein**	**Complex**	**Function**
HPS1	*pale ear*	HPS1 (BLOC3S1)	BLOC-3	RAB32/RAB38 GEF Retrograde transport from melanosomes
HPS2	*pearl*	AP-3 β3A subunit	AP-3	Adaptor protein Sorting cargo for vesicular and tubulovesicular trafficking
HPS3	*cocoa*	HPS3 (BLOC2S1)	BLOC-2	Directs tubules to or stabilizes tubules at melanosomes
HPS4	*light ear*	HPS4 (BLOC3S2)	BLOC-3	RAB32/RAB38 GEF Retrograde transport from melanosomes
HPS5	*ruby-eye 2*	HPS5 (BLOC2S2)	BLOC-2	Directs tubules to or stabilizes tubules at melanosomes
HPS6	*ruby-eye*	HPS6 (BLOC2S3)	BLOC-2	Directs tubules to or stabilizes tubules at melanosomes
HPS7	*sandy*	BLOC1S8	BLOC-1	Coordinates stabilization and elongation of growing tubules
HPS8	*reduced pigmentation*	BLOC1S3	BLOC-1	Coordinates stabilization and elongation of growing tubules
HPS9	*pallid*	BLOC1S6	BLOC-1	Coordinates stabilization and elongation of growing tubules
HPS10	*mocha*	AP-3 δ subunit	AP-3	Adaptor protein Sorting cargo for vesicular and tubulovesicular trafficking
HPS11	*muted*	BLOC1S5	BLOC-1	Coordinates stabilization and elongation of growing tubules
CHS	*beige*	LYST		Lysosomal trafficking regulator Function unknown

Row colors indicate subunits that belong to the same complex.

There is much still to be learned about the genes that have been identified in OCA, OA1, HPS, and CHS. The gene mutated in OCA5 has not been identified and it is not known how LRMDA and LYST function in melanosome biogenesis or activity. However, more genes are likely associated with albinism. Of the individuals with albinism, 27% do not have mutations in any of the known albinism genes (Pennamen et al., 2020b). While

some of this percentage may be accounted for by noncoding mutations that impact gene expression, the abundance of mouse models with a hypopigmentation phenotype and the recent identification this year of two new forms of OCA and HPS (OCA8, HPS11) (Pennamen et al., 2020a; Pennamen et al., 2020b) indicate that there are more proteins yet to be identified that are required for melanosome and LRO biogenesis in humans.

1.8. Dissertation Aims

Melanosomes are LROs within melanocytes and pigmented epithelial cells that are responsible for producing melanin for photoprotection, antioxidation, and retinal development. Defective melanosome biogenesis results in albinism, including OCA and HPS. Our studies of OCA and HPS have greatly expanded our understanding of (1) melanosome formation and function and (2) trafficking pathways to transport cargo specifically to melanosomes. However, many questions remain. SLC45A2, mutated in OCA4, has a putative role in the pH regulation of melanosomes. One report indicates that SLC45A2 localizes to and deacidifies melanosomes, but the data are inconclusive and unconvincing. It is also unknown when SLC45A2 functions and how it coordinates its actions with other ion transport proteins. Additionally, the *buff* mouse model, an HPS-like mouse model with a mutation in VPS33A, suggests that VPS33A and HOPS may play a role in trafficking to melanosomes and other LROs. However, it is unclear where, when, and how VPS33A functions in this trafficking pathway. We thus pursued the following questions:

Question 1: What is the localization and function of SLC45A2 in melanocytes? While published data indicate that SLC45A2 localizes to melanosomes, the conclusion is based on low resolution microscopy that cannot clearly differentiate between organelles, an unvalidated antibody that appears to be non-specific, and poorly controlled data. Additionally, the function of SLC45A2 in melanocytes is unclear. While experiments in zebrafish show that its expression is required for pigmentation and that treatment of zebrafish with the V-ATPase inhibitor bafilomycin A1 rescues pigmentation in the absence of *slc45a2*, its role in melanocytes and its relationship to acidification has not been characterized in a controlled cellular system. I hypothesize that SLC45A2 localizes to melanosomes where its activity as a sugar-proton symporter enhances OCA2's function to neutralize the melanosomal lumen. In chapter 2, I show through widefield and fluorescence microscopy that SLC45A2 localizes to mature melanosomes and by electron microscopy that loss of SLC45A2 results in hypopigmentation that is not as severe as loss of OCA2. Experiments done by collaborators show that expression of SLC45A2 increases pH.

Question 2: What is the phenotype of melanocytes derived from *buff* mice? Mutations in HPS-related genes have allowed us to study and understand the role of these proteins in specialized trafficking pathways used to generate LROs. In one mouse model of HPS, *buff* (*bf*) mice contain a missense mutation in *Vps33a* (D251E), encoding a subunit of both CORVET and HOPS. CORVET and HOPS function in all cells in the early endosomal and late endosomal/lysosomal systems, respectively, by binding to apposing membranes to promote SNARE complex formation and consequent fusion. The subunit

VPS33A directly binds to SNARE proteins and accelerates SNARE zippering, thereby facilitating fusion. Interestingly, the *buff* mouse is not reported to have apparent generalized endolysosomal defects, but rather selectively impairs LRO biogenesis in certain cell types such as skin melanocytes; however, how CORVET/HOPS function specifically in the biogenesis of cell-type specific LROs is unknown. Additionally, detailed studies of the function of the CORVET/HOPS in mammalian systems have been limited due to the ubiquitous requirement for these complexes in endolysosomal maturation. In chapter 3, I characterize melanosome biogenesis defects in *buff* mice and test whether they reflect a hypomorphic function of VPS33A. My data show that melanosome biogenesis and melanogenesis can proceed in cells expressing the VPS33A *buff* allele.

CHAPTER 2

SLC45A2 protein stability and regulation of melanosome pH determine melanocyte pigmentation

This chapter appeared as a peer-reviewed article titled “SLC45A2 protein stability and regulation of melanosome pH determine melanocyte pigmentation” by **Linh Le**, Iliana E. Escobar, Tina Ho, Ariel J. Lefkovith, Emily Latteri, Kirk D. Haltaufderhyde, Megan K. Dennis, Lynn Plowright, Elena V. Sviderskaya, Dorothy C. Bennett, Elena Oancea, and Michael S. Marks. *Molecular Biology of the Cell*, 2020.

2.1. Abstract

SLC45A2 encodes a putative transporter expressed primarily in pigment cells. SLC45A2 mutations cause oculocutaneous albinism type IV (OCA4) and polymorphisms are associated with pigmentation variation, but the localization, function, and regulation of SLC45A2 and its variants remain unknown. We show that SLC45A2 localizes to a cohort of mature melanosomes that only partially overlaps with those expressing the chloride channel OCA2. SLC45A2 expressed ectopically in HeLa cells localizes to lysosomes and raises lysosomal pH, suggesting that in melanocytes, SLC45A2 expression, like OCA2 expression, results in the deacidification of maturing melanosomes to support melanin synthesis. Interestingly, OCA2 overexpression compensates for loss of SLC45A2 expression in pigmentation. Analyses of SLC45A2- and OCA2-deficient mouse melanocytes show that SLC45A2 likely functions later during melanosome maturation than OCA2. Moreover, the light skin-associated SLC45A2 allelic F374 variant restores only moderate pigmentation to SLC45A2-deficient melanocytes due to rapid proteasome-dependent degradation resulting in lower protein expression levels in melanosomes than the dark skin-associated allelic variant. Our data suggest that SLC45A2 maintains melanosome neutralization initially orchestrated by transient OCA2 activity to support melanization at late stages of melanosome maturation, and that a common variant imparts reduced activity due to protein instability.

2.2. Introduction

Melanins are the main source of pigmentation in the skin, hair, and eyes of mammals and other vertebrates. In humans, melanins serve as a barrier to the harmful

effects of ultraviolet radiation and play an important role in the development and functioning of the retina (d'Ischia et al., 2015). Melanin synthesis takes place in skin and eye melanocytes and in ocular pigment epithelia within specialized organelles called melanosomes (Hearing, 2005; Marks and Seabra, 2001; Seiji et al., 1963). Heritable defects in melanin synthesis underlie the various forms of oculocutaneous albinism (OCA), characterized by impaired vision and increased susceptibility to skin and ocular cancers (Montoliu et al., 2014). To date, non-syndromic OCA has been linked to inactivating mutations in eight different genes (Montoliu et al., 2014; Pennamen et al., 2020b). Sequence variation at the loci for some of these genes has been linked to variability in skin, hair and eye color among humans (Adhikari et al., 2019a; Branicki et al., 2008; Crawford et al., 2017; Han et al., 2008; Lamason et al., 2005a; Liu et al., 2015; Martin et al., 2017; Stokowski et al., 2007). Nevertheless, the molecular function of the majority of the OCA genes has not yet been fully characterized.

OCA type 4 (OMIM #606574) represents 3-12% of total OCA patients in population studies (Gronskov et al., 2009; Lasseaux et al., 2018a; Mauri et al., 2017; Wei et al., 2010; Wei et al., 2015) and is due to mutations in the *SLC45A2* gene encoding the putative transmembrane transporter SLC45A2 (a.k.a. membrane associated transporter protein, MATP or antigen isolated from immuno-selected melanoma-1, AIM1) (Newton et al., 2001). Mutations in the homologous gene underlie pigment dilution in a number of vertebrate species, including gorilla, several breeds of dog, tigers, horses, mice, shrew, chickens, pigeons, quail, frogs, fish and perhaps cattle (Caduff et al., 2017; DeLay et al., 2018; Domyan et al., 2014; Dooley et al., 2013; Fukamachi et al., 2001; Gunnarsson et al., 2007; Mariat et al., 2003; Minvielle et al., 2009; Newton et al., 2001; Prado-Martinez et al., 2013; Rothammer et al., 2017; Tsetskhladze et al., 2012; Tsuboi et al., 2009;

Wijesena and Schmutz, 2015; Winkler et al., 2014; Xu et al., 2013), and polymorphisms at the *SLC45A2* locus are associated with skin tone differences and skin aging in several human population studies (Adhikari et al., 2019a; Branicki et al., 2008; Cerqueira et al., 2014; Fracasso et al., 2017; Han et al., 2008; Jonnalagadda et al., 2016; Law et al., 2017; Liu et al., 2015; Lopez et al., 2014; Soejima and Koda, 2007; Stokowski et al., 2007; Yuasa et al., 2006). OCA4 patients have very low levels of pigmentation and phenotypically resemble OCA2 patients who lack the melanosomal chloride channel, OCA2 (Bellono et al., 2014), suggesting that SLC45A2 plays an important role in melanogenesis (Montoliu et al., 2014). Moreover, primary melanocytes from mice carrying the inactivating *underwhite* (uw) mutation of *Slc45a2* (Du and Fisher, 2002; Newton et al., 2001) are severely hypopigmented (Costin et al., 2003), indicating a melanocyte-intrinsic defect; this would be consistent with the known restriction of SLC45A2 expression to pigment cells and a few other cell types (Baxter and Pavan, 2002; Bin et al., 2015; Harada et al., 2001; Loftus et al., 2002). However, while the 12-transmembrane domain SLC45A2 protein bears weak homology to sucrose transporters in plants and *Drosophila* (Lemoine, 2000; Meyer et al., 2011; Newton et al., 2001), its function in melanocytes is not understood.

When expressed in yeast, mouse SLC45A2 functions at the plasma membrane as an acid-dependent importer of sugars (sucrose, glucose, or fructose) into the cytosol (Bartölke et al., 2014), suggesting that if SLC45A2 localized to acidic organelles it might facilitate export of a sugar and protons from the lumen to the cytosol. Neutralization of acidic early stage melanosomes is a critical process for melanogenesis (Bellono et al., 2014; Raposo et al., 2001), as the key enzyme in melanogenesis, Tyrosinase (TYR), is minimally active at pH < 6 (Ancans et al., 2001b; Halaban et al., 2002). Consistent with a function in proton export and neutralization of acidic organelles, pigmentation of a

zebrafish *Slc45a2* mutant was rescued upon inhibition of endolysosomal and melanosomal acidification by treatment with bafilomycin A1 or by knockdown of the atp6v1 subunit of the vacuolar ATPase (Dooley et al., 2013), and knockdown of SLC45A2 in a pigmented melanoma cell line was reported to result in increased acidification of early stage melanosomes (Bin et al., 2015). However, despite limited evidence for SLC45A2 on melanosomes (Bin et al., 2015), the localization of SLC45A2 within melanocytes has not yet been firmly established and it is not clear whether the effects of *SLC45A2* mutants reflect a direct effect of SLC45A2 function on the lumenal environment of melanosomes or an indirect effect due to impaired function of other organelles during melanosome maturation, as appears to be the case for the endolysosomal transporter MFSD12 (Crawford et al., 2017). Moreover, if SLC45A2 indeed functions to neutralize melanosome pH, its function must be coordinated with that of OCA2, a major regulator of melanosomal pH (Bellono et al., 2014). While mice lacking expression of either SLC45A2 or OCA2 each have dramatic coat color dilution (Dickie, 1964b; Sweet et al., 1998), mice with hypomorphic mutations in both *Slc45a2* and *Oca2* are more severely hypopigmented than either mutant alone (Lehman et al., 2000), suggesting that the encoded proteins have distinct functions.

Differences in skin and hair pigmentation among European, Chinese, South American and South Asian human populations have been ascribed to a single genetic variant in *SLC45A2* associated with the SNP rs16891982 (c.1122G>C). This results in a missense mutation p.Leu374Phe (ClinVar ID: 194990) and is correlated with lighter skin, hair, and eyes (Adhikari et al., 2019a; Branicki et al., 2008; Cerqueira et al., 2014; Han et al., 2008; Jonnalagadda et al., 2016; Liu et al., 2015; Lopez et al., 2014; Soejima and Koda, 2007; Stokowski et al., 2007; Yuasa et al., 2006). The SLC45A2-F374 variant is

nearly fixed in light-skinned human populations (Soejima and Koda, 2007). Residue 374 lies within the 8th predicted transmembrane domain of SLC45A2 (Newton et al., 2001). When introduced into a homologous plant sucrose transporter, the amino acid corresponding to SLC45A2-F374 resulted in a 90% decrease in transporter activity without influencing the affinity for substrate (Reinders and Ward, 2015a), and slc45a2 with an introduced F374 mutation was unable to rescue pigmentation in a *slc45a2* mutant zebrafish (Tsetskhladze et al., 2012). However, the mechanism underlying the decreased activity of the SLC45A2-F374 variant is not understood.

Analyses of SLC45A2 localization and function in pigment cells have been hindered by the lack of suitable specific antibodies. Here we assess the localization and function of SLC45A2-L374 and -F374 variants in melanosome biogenesis by analyzing epitope-tagged human SLC45A2 expressed in wild-type melanocytes, *Slc45a2*-deficient melanocytes from *underwhite* mice, and HeLa cells, and by comparing the phenotypes of *underwhite* and OCA2-deficient *pink-eyed dilute* melanocytes. We show that expression of SLC45A2, like of OCA2, increases the pH of lysosomes and/or late endosomes when expressed ectopically in HeLa cells and that in melanocytes SLC45A2 localizes to melanosomes, where it likely neutralizes the melanosome lumen. We also show that OCA2 and SLC45A2 localize to distinct subsets of melanosomes and that the F374 variant accelerates SLC45A2 degradation but does not alter its localization. Our data indicate that melanosome neutralization is a critical process for the maintenance of eumelanin pigmentation that is regulated at more than one step during melanosome maturation.

2.3. Results

2.3.1. Functionality of HA-SLC45A2.

Available antibodies to SLC45A2 were not suitable in our hands for immunolocalization analyses. Therefore, we used epitope-tagging to investigate SLC45A2 localization in melanocytes. Human SLC45A2 was tagged at the N- or C-terminus with either the HA11 epitope tag or EGFP and cloned into a retroviral vector. To determine whether the tagged transgenes were functional, they were expressed by recombinant retroviral infection in *Slc45a2*-deficient melan-uw cells from *underwhite* mice (Dickie, 1964b). The *Slc45a2*^{uw} allele encodes a non-functional truncated SLC45A2 protein and an undetectable transcript (Du and Fisher, 2002; Newton et al., 2001). Consequently, *underwhite* mice (Dickie, 1964b; Lehman et al., 2000; Sweet et al., 1998) and primary melanocytes derived from them (Costin et al., 2003) are severely hypopigmented. Likewise, melan-uw cells are very pale compared to "wild-type" (WT) immortalized melanocytes (melan-Ink4a) from C57BL/6-*Ink4a*$^{-/-}$ mice (Sviderskaya et al., 2002) (**Figure 2.1a, b**). While expression of the EGFP-tagged proteins failed to consistently restore pigmentation in melan-uw cells (data not shown), expression of the N-terminally HA-tagged human SLC45A2 (HA-SLC45A2) restored partial or full pigmentation in a substantial fraction of cells by 48-72 h post-infection, whereas pigmentation was not restored by expression of a similarly tagged unrelated polytopic protein - the putative sugar-nucleotide transporter, SLC35D3, which plays no role in pigmentation (Chintala et al., 2007b) (**Figure 2.1c-g**). Additionally, quantitative analysis of melanin content in melan-uw cells stably expressing HA-SLC45A2 showed pigmentation at levels comparable to those of melan-Ink4a cells (see **Figure 2.5f**). These data indicate that HA-SLC45A2 is

fully functional in melanocytes, and therefore validate its use in defining the localization and biosynthesis of SLC45A2.

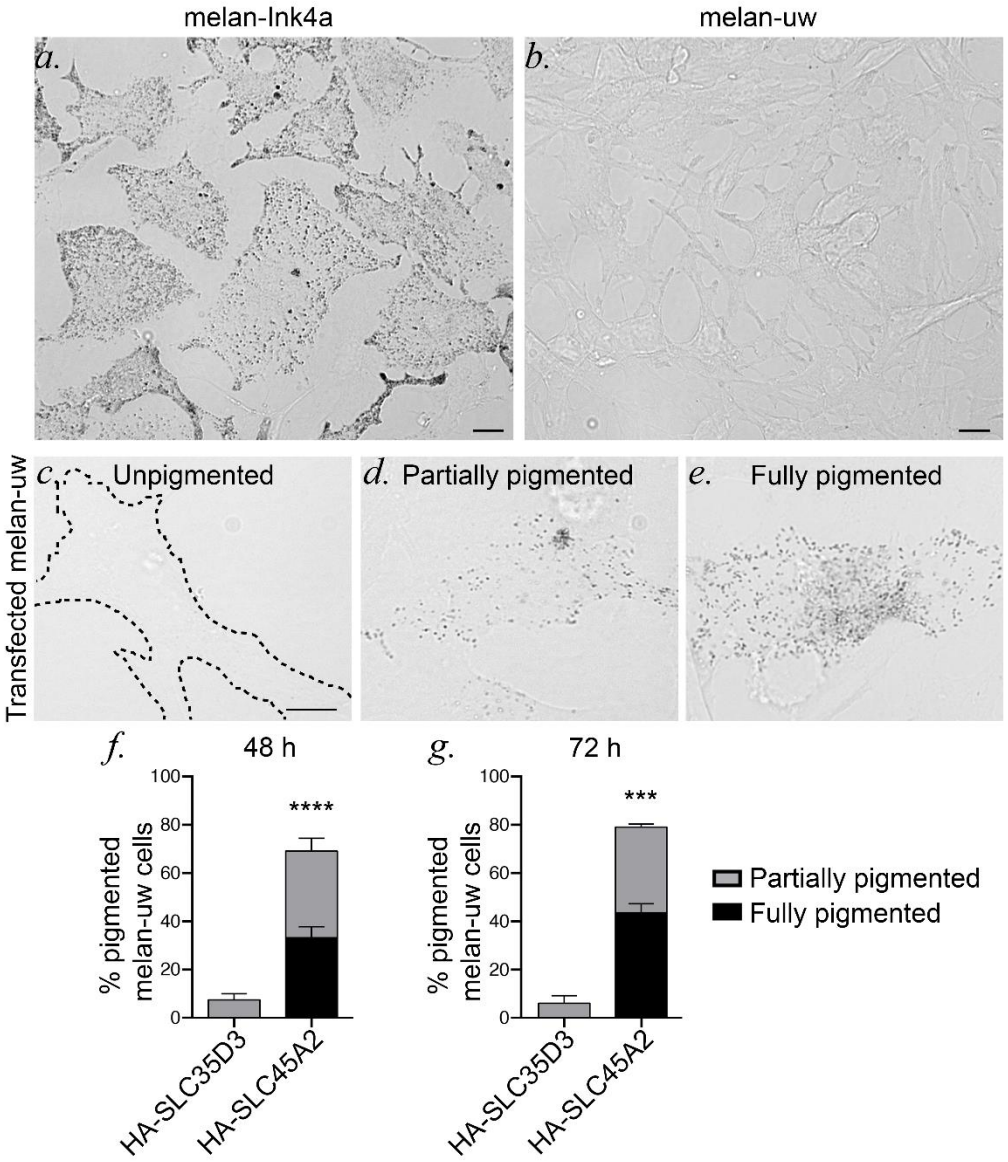

Figure 2.1: HA-SLC45A2 functionally restores pigmentation in Slc45a2-deficient underwhite melanocytes. Wide field microscopy with bright field illumination of melan-Ink4a (*a*) and melan-uw (*b*) cells to visualize pigmentation. Scale bar, 10 μm. Mouse melan-uw cells were transiently transfected with plasmids encoding human SLC45A2 with an N-terminal HA epitope (HA-SLC45A2) or with a comparably HA-tagged control polytopic protein, SLC35D3 (HA-SLC35D3). 48-72 h after transfection, HA-expressing cells were scored for their level of pigmentation. *c-e*, examples of unpigmented (*c*, like untransfected cells), partially pigmented (*d*) and fully pigmented (*e*) cells. Scale bar, 10μm. *f*, *g*, quantification of the percentage of HA-expressing cells with partial

(gray) or full (black) pigmentation at 48 (*f*) or 72 (*g*) h after transfection. Note that all cells except melan-Ink4a were treated with 200 pM cholera toxin. Data represent mean ± SEM from 3 independent experiments and the following total sample sizes: 234 (HA-SLC45A2) and 109 (HA-SLC35D3) at 48 h, 173 (HA-SLC45A2) and 108 (HA-SLC35D3) at 72 h. ***, $p < 0.001$; ****, $p<0.0001$ by unpaired two-tailed t-test.

2.3.2. HA-SLC45A2 localizes to the limiting membrane of pigmented melanosomes and is partially enriched in a membrane subdomain.

To define SLC45A2 localization in melanocytes, HA-SLC45A2 was expressed either stably from recombinant retroviruses in melan-uw cells or by transient transfection in WT melan-Ink4a melanocytes. Cells were then fixed and processed for immunofluorescence microscopy with image deconvolution (dIFM) using antibodies to the HA tag and to endogenous markers. In *Slc45a2*-deficient melan-uw cells, HA-SLC45A2 localized primarily to pigment granules (**Figure 2.2a**, **b, d**) often in a ring pattern around the granule (**Figure 2.2b**), in two to three puncta associated with the granule exterior (**Figure 2.2a**), or both (**Figure 2.2c**). The distinct patterns did not correlate with SLC45A2 expression levels. The melanosomes labeled by HA-SLC45A2 overlapped with those harboring the melanosomal enzymes Tyrosinase (TYR) and Tyrosinase-related protein-1 (TYRP1) (**Figure 2.2a**, **b, d**; overlap was 82.7 ± 1.3% with TYR and 79.2 ± 2.5% with TYRP1). By contrast, HA-SLC45A2-labeled structures overlapped poorly with LAMP2, a membrane protein of lysosomes but not melanosomes, which are distinct organelles in eumelanin-generating melanocytes (Berson et al., 2001) (**Figure 2.2c, d**; overlap was 34.4% ± 2.9% with LAMP2). Essentially identical results were observed for HA-SLC45A2 transiently expressed in melan-Ink4a cells (**Figure 2.3**), which express endogenous SLC45A2. The degree of HA-SLC45A2 labeling on punctate subdomains vs. the melanosome limiting membrane was similar in transiently transduced melan-Ink4a and

stably transduced melan-uw cells. Together, these data indicate that SLC45A2 localizes to mature melanosomes, where it is often enriched in subdomains associated with the limiting membrane.

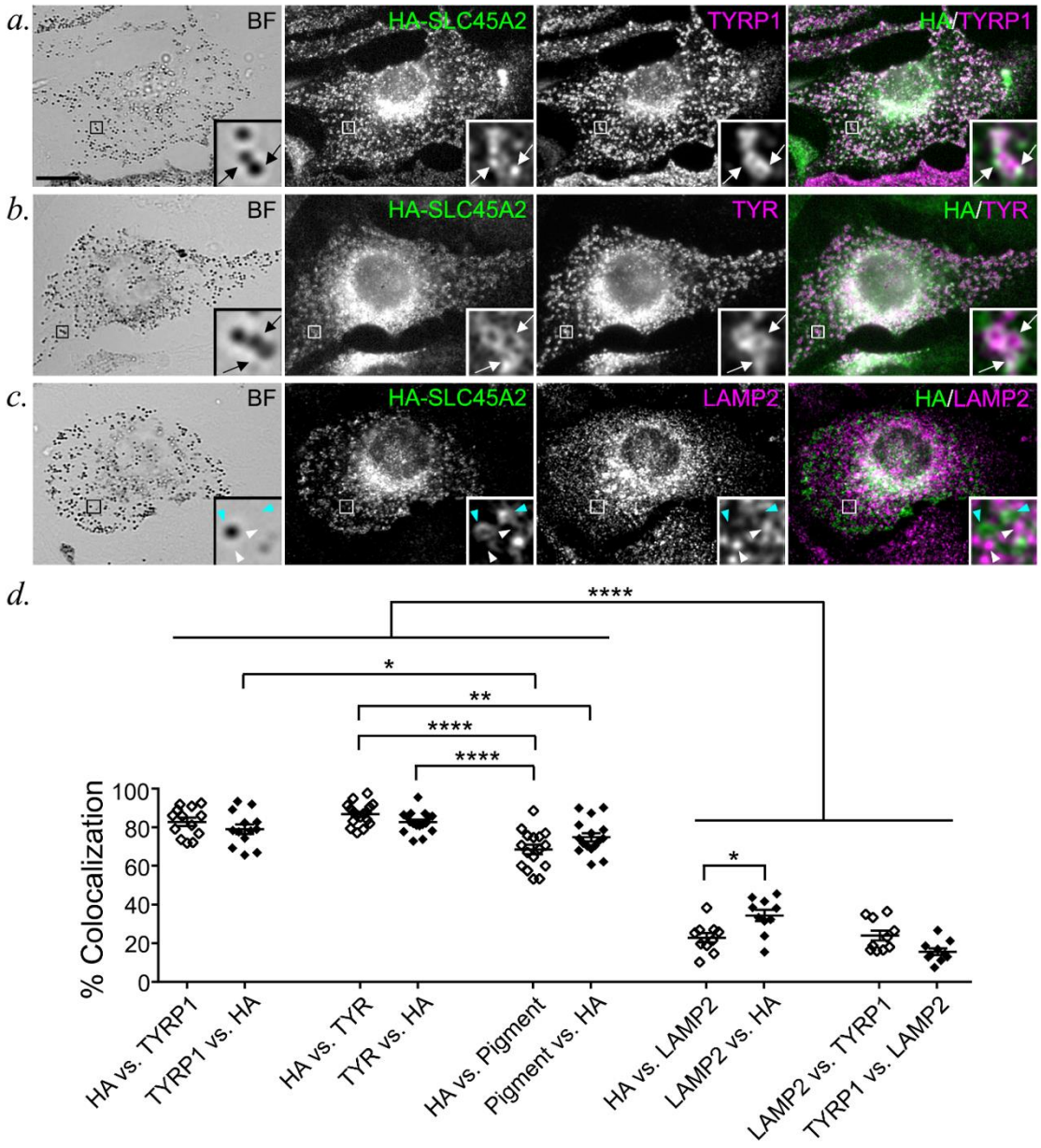

Figure 2.2: HA-SLC45A2 localizes to melanosomes when expressed in SLC45A2-deficient melan-uw melanocytes. (*a-c*) Melan-uw cells stably expressing HA-tagged SLC45A2 were fixed, labeled for HA (green) and for TYRP1 (*a*), TYR (*b*), or LAMP2 (*c*) (magenta), and analyzed by dIFM and bright field (BF) microscopy to visualize melanin. Insets of boxed regions are magnified 7.5

times. Scale bar, 10 μm. SLC45A2 that localized to TYRP1- or TYR-labeled compartments (white arrows) or SLC45A2 (cyan arrowheads) and LAMP2 (white arrowheads) on separate compartments are indicated. (*d*) The percentage of compartments with both markers in *a-c* was quantified by manual counting of at least 13 cells each from 3 separate experiments. Colocalization is represented as mean ± SEM of label 1 vs label 2, in which the number of compartments containing both label 1 and label 2 is presented as a percentage of the total number of compartments containing label 2. The % colocalization between TYRP1 and LAMP2 was quantified as a negative control. Data are from 3 independent experiments with the following total sample sizes: 13 (TYRP1 vs HA; HA vs TYRP1; LAMP2 vs HA; HA vs TYRP1; TYRP1 vs LAMP2; LAMP2 vs TYRP1) and 17 (TYR vs HA; HA vs TYR; HA vs Pigment; Pigment vs HA). Statistical significance was determined using one-way ANOVA with Tukey post hoc test for multiple comparisons; only significant differences are indicated. *, $p < 0.05$; **, $p < 0.01$; ****, $p < 0.0001$.

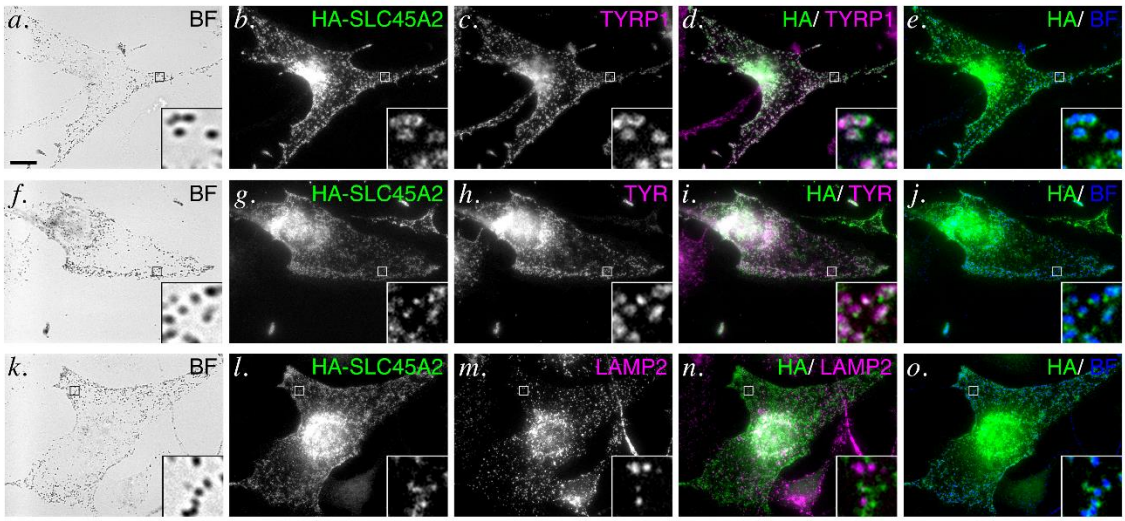

Figure 2.3: HA-SLC45A2 localizes to melanosomes upon transient transfection in WT melanocytes. Transiently transfected WT melan-Ink4a cells expressing HA-SLC45A2 were fixed, labeled for HA (green) and either TYRP1 (a-e, magenta), TYR (f-j, magenta) or LAMP2 (k-o, magenta), and analyzed by dIFM and by bright field microscopy. Shown are individual bright field (BF) or labeled panels (a-c, f-h, and k-m), merged dIFM images (d, I, n) or merged HA and bright field images (e, j, o; bright field is pseudocolored blue); boxed regions are magnified 7.5X in insets. Scale, 10 μm.

2.3.3. SLC45A2 localizes to lysosomes and regulates lysosomal pH when ectopically expressed in HeLa cells.

When expressed in non-melanocytic cells, many melanosomal proteins localize to late endosomes and lysosomes (Ambrosio et al., 2016; Bellono et al., 2016; Berson et al., 2001; Bouchard et al., 1989; Calvo et al., 1999; Piccirillo et al., 2006; Simmen et al., 1999;

Sitaram et al., 2009; Vijayasaradhi et al., 1995). Indeed, when expressed in HeLa cells and analyzed by dIFM, HA-SLC45A2 was detected on LAMP1-containing lysosomes in distinct punctate microdomains associated with the limiting membrane (**Figure 2.4a**), similar to the distribution in some melanosomes in melanocytes. This indicates that SLC45A2 localizes to lysosomes when expressed ectopically in HeLa cells and retains its ability to accumulate in a membrane subdomain.

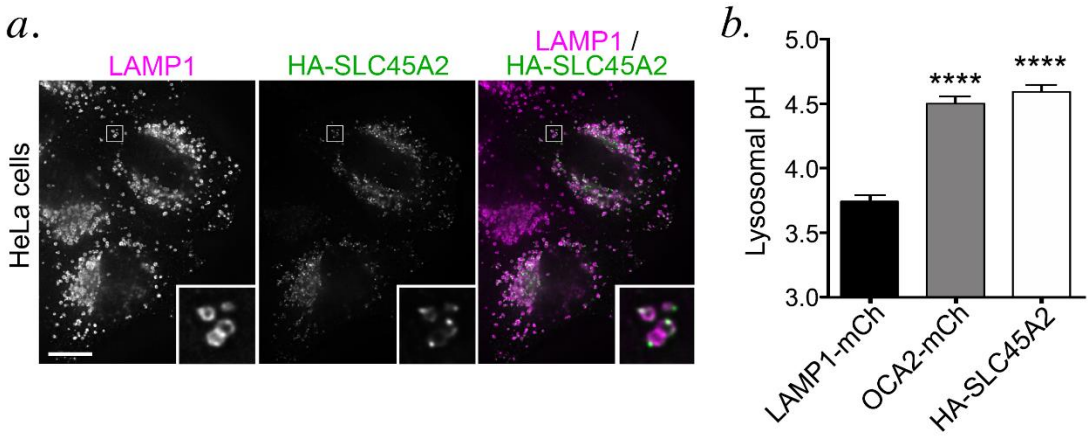

Figure 2.4: HA-SLC45A2 expressed in HeLa cells localizes to lysosomes and neutralizes lysosomal pH. *a*. HeLa cells transiently transfected with HA-SLC45A2 were fixed, labeled for HA (green) and the lysosomal protein LAMP1 (magenta), and analyzed by dIFM. Merged image is at right. Insets of boxes are magnified 5-fold. Scale bar, 10 μm. *b.* HeLa cells transiently transfected with LAMP1-mCherry alone, mCherry-OCA2, or HA-SLC45A2 and LAMP1-mCherry were incubated with Lysosensor DND-160, and analyzed by fluorescence microscopy with excitation wavelength 405. The W1/W2 emission ratio for mCherry-labeled endolysosomes was calculated and compared to that from a standard curve to define pH as described in Materials and Methods. Data represent mean ± SEM from 3 independent experiments with the following total sample sizes: 319 LAMP1-mCherry$^+$ endolysosomes, 391 OCA2-mCherry$^+$ endolysosomes, and 299 HA-SLC45A2/LAMP1-mCherry$^+$ endolysosomes. Statistical significance was determined using Welch's ANOVA with Games-Howell test for multiple comparisons; only significant differences are indicated. ****, $p < 0.0001$.

SLC45A2 was predicted to be a transmembrane transporter that influences melanosome pH (Bin et al., 2015; Newton et al., 2001). We have been unable to directly assess melanosomal pH in melanocytes using common cellular probes for lysosomal pH such as Lysotracker and Lysosensor because in our hands melanocytes fail to accumulate

these probes intracellularly. However, we previously showed that the OCA2 chloride channel expressed in HeLa cells localizes to lysosomes and neutralizes their lumenal pH, paralleling its role in neutralizing the lumenal pH of melanosomes to enhance TYR activity and melanogenesis in melanocytes (Bellono et al., 2014). We therefore tested whether SLC45A2 expression affects lysosomal acidification in HeLa cells using the pH-sensitive ratiometric dye Lysosensor DND-160. HeLa cells were transfected with either LAMP1-mCherry alone as a negative control, mCherry-OCA2 as a positive control, or LAMP1-mCherry and HA-SLC45A2 together to identify HA-SLC45A2-expressing cells by live imaging (cotransfection efficiency measured by immunostaining was >90%). Cells preincubated with Lysosensor DND-160 were imaged at two emission wavelengths, and an average emission ratio was calculated for individual mCherry-LAMP1-positive compartments (see Materials and Methods). The corresponding pH for the average emission ratio was determined using a pH curve generated in each experiment by incubation in buffers with different pH values. Our results show that the average pH of lysosomes containing HA-SLC45A2 was nearly one pH unit higher than the pH of control cells and similar to the pH of mCherry-OCA2-containing lysosomes (**Figure 2.4b**). These data indicate that, like OCA2, SLC45A2 can function to raise organellar pH, and suggest that in melanocytes SLC45A2 functions physiologically to raise melanosomal pH.

2.3.4. SLC45A2 and OCA2 function at distinct stages of melanosome maturation.

The similar function of SLC45A2 and OCA2 in neutralizing organellar pH led us to ask whether these transporters function at the same or distinct stages of melanosome maturation. We first used dIFM to compare the distribution of HA-SLC45A2 and HA-OCA2 to melanosomes labeled by the mature melanosome marker TYRP1 in transiently

transfected melan-Ink4a cells. HA-SLC45A2 and TYRP1 were largely present in the same compartments (86.58 ± 1.25% of HA-SLC45A2 in TYRP1-containing structures, and 89.17 ± 1.32% of TYRP1 in HA-SLC45A2-containing structures; **Figure 2.5a**, **e**), and the fluorescence signal intensity within positive compartments was highly correlated (**Figure 2.5c**). By contrast, although TYRP1 and OCA2 each primarily localize to subsets of pigment granules (Berson et al., 2001; Sitaram et al., 2012; Sitaram et al., 2009; Vijayasaradhi et al., 1991; Vijayasaradhi et al., 1995), they label only partially overlapping populations (58.57 ± 4.87% of HA-OCA2 in TYRP1-containing compartments, and 48.66 ± 5.32% of TYRP1 in OCA2-containing compartments; **Figure 2.5b**, **e**). Moreover, within those overlapping compartments, the fluorescence signal intensities of HA-OCA2 and TYRP1 over background correlated substantially less well than those of HA-SLC45A2 and TYRP1 (**Figure 2.5d**). These data suggest that OCA2 and SLC45A2 are enriched in melanosomes of distinct maturation stages, with SLC45A2 present in largely the same subset of mature melanosomes as TYRP1, while OCA2 occupies a partially different subset of melanosomes.

The distinct localization patterns for OCA2 and SLC45A2 suggest that they might regulate the lumenal pH and pigmentation of melanosomes at different maturation stages. We therefore tested for potential differences in melanosome pigmentation in melan-uw cells and immortalized melan-p1 melanocytes from OCA2-deficient pink-eyed dilute mice. Electron microscopy can be used to define four stages of melanosome maturation based on morphology and content of melanin pigments (Seiji et al., 1963).

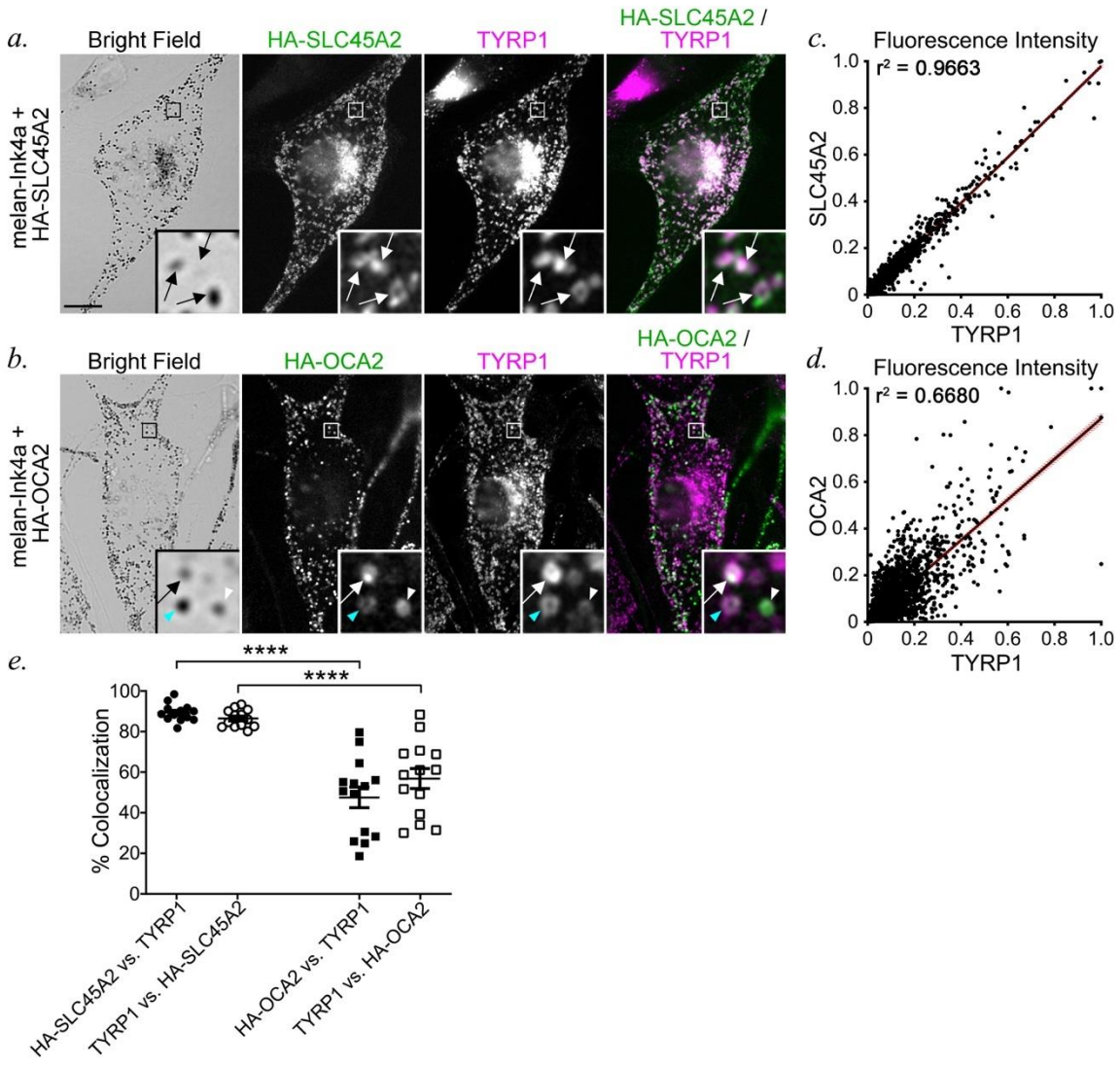

Figure 2.5: SLC45A2 and OCA2 occupy partially distinct melanosome subsets. (*a*, *b*) melan-Ink4a cells transiently expressing either HA-SLC45A2 (*a*) or HA-OCA2 (*b*) were fixed, labelled for HA (green) and TYRP1 (magenta), and analyzed by dIFM and bright field microscopy. Insets of boxed regions are magnified 7.5 times. Scale bar, 10 μm. White arrows, colocalization of HA-SLC45A2 or HA-OCA2 to TYRP1-containing compartments at comparable relative intensities; white arrowhead, compartments with high HA-OCA2 and low TYRP1; cyan arrowhead, compartments with low HA-OCA2 and high TYRP1. (*c*, *d*) Quantification of the object-based fluorescence intensity of HA-SLC45A2 versus TYRP1 (*c*) or HA-OCA2 versus TYRP1 (*d*) in 10 cells each from 3 independent experiments. Correlation coefficients (r^2) of fluorescent intensities for each pair of markers is indicated. (*e*) Manual quantification (mean ± SEM) of the % colocalization between TYRP1 and either HA-SLC45A2 or HA-OCA2 and TYRP1, shown as a percentage of total TYRP1-, SLC45A2-, or OCA2-containing compartments. Values are presented as label 1 vs label 2, in which compartments containing both label 1 and label 2 is indicated as a

percentage of total compartments containing label 2. Data are quantified from 3 independent experiments with the following total sample sizes: 13 (HA-SLC45A2) and 14 (HA-OCA2). Statistical significance was determined using Welch's ANOVA with Dunnett T3 test for multiple comparisons; only significant differences are indicated. ****, $p < 0.0001$.

Stages I and II lack pigment but are distinguished by the presence of disorganized intralumenal fibers (stage I) or well-organized fibrils in parallel intralumenal sheets (stage II). Stage III is defined by the appearance of pigment on the fibrils and stage IV by pigment throughout the organelle. Electron microscopy analyses showed that relative to either WT melan-Ink4a or "rescued" melan-uw cells stably expressing HA-SLC45A2 (melan-uw:HA-SLC45A2), both melan-uw and melan-p1 cells harbored melanosomes of similar size and number, but with more stage III melanosomes and fewer stage IV melanosomes (**Figure 2.6a-e**). However, only melan-p1 cells contained significantly more stage I/II melanosomes than the controls (**Figure 2.6e**). Moreover, although we could not quantify it, the amount of pigment on the fibrils in stage III melanosomes in melan-p1 cells consistently appeared to be lower than in melan-uw cells (**Figure 2.6**, panels **b** vs. **c**). Accordingly, quantitative melanin content assays showed that while both melan-uw and melan-p1 had dramatically lower melanin content than melan-Ink4a or melan-uw:HA-SLC45A2 cells, the melanin content of melan-p1 cells was significantly lower than that of melan-uw (**Figure 2.6f**). These data indicate that loss of SLC45A2 results in a milder phenotype than loss of OCA2. Taken together with the data showing that SLC45A2 and OCA2 are found on different subsets of melanosomes (**Figure 2.5**), the most likely scenario is that OCA2 is required at an earlier stage of melanization than SLC45A2 during melanosome maturation.

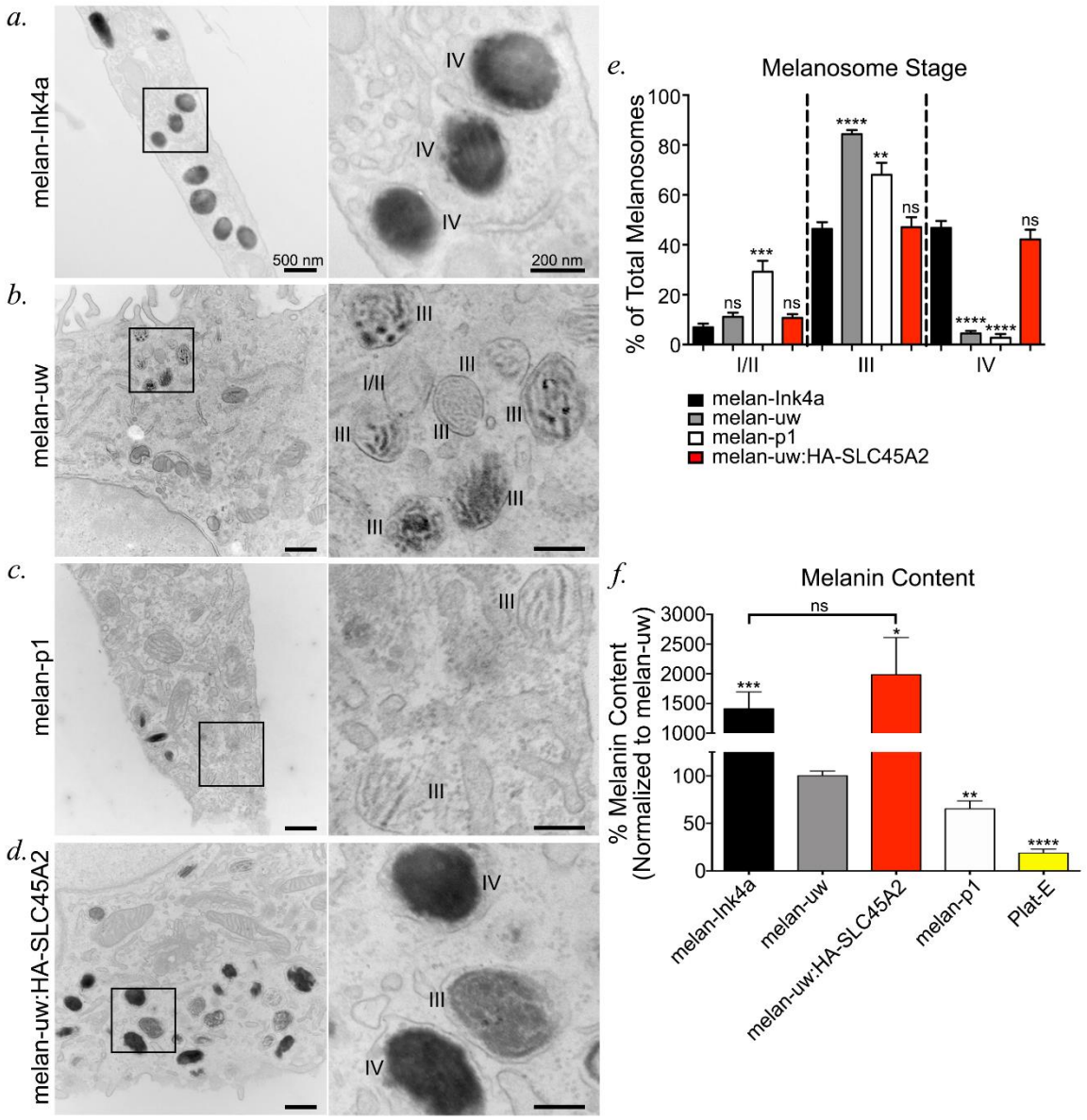

Figure 2.6: SLC45A2 is required for melanosomes to progress from stage III to stage IV. (a-d) melan-Ink4a (a), melan-uw (b), melan-p1 (c), and melan-uw cells stably expressing HA-SLC45A2 (melan-uw:HA-SLC45A2; d) were fixed and analyzed by conventional transmission electron microscopy. Insets of boxed regions on the left were magnified 4.5 times on the right. I/II, stage I/II melanosomes; III, stage III melanosomes; IV, stage IV melanosomes. Scale bars, 500 nm (left) and 200 nm (right). (e) The number of stage I/II, stage III, and stage IV melanosomes per cell was quantified for each of the cell lines and is shown as a percentage of total counted melanosomes per cell. For each stage, data represent the mean ± SEM from the following number of independent experiments, cells, and melanosomes: melan-Ink4a (2, 54, 717), melan-uw (3, 49, 1292), melan-p1 (2, 27, 626), and melan-uw:HA-SLC45A2 (3, 76, 1927). Statistical analyses were performed by Welch's ANOVA with multiple comparisons to melan-Ink4a for each stage and Dunnett T3 test for

multiple comparisons. (*f*) Melanin content in cell lysates was determined by spectrometry relative to total protein content. Plat-E cells are included as a non-pigmented cell control. The data are presented as a percentage normalized to melanin content in melan-uw samples ± SEM and represent at least 3 independent experiments performed in duplicate or triplicate. Statistical significance was determined by Welch's ANOVA with Dunnett T3 test for multiple comparisons. Except where indicated, statistical comparisons were made relative to melan-uw. Note that all cells except melan-Ink4a and Plat-E were treated with 200 pM cholera toxin. **, $p < 0.01$; ***, $p < 0.001$; ****, $p < 0.0001$; ns, no significant difference.

2.3.5. OCA2 overexpression partially compensates for loss of SLC45A2 expression.

Given that both OCA2 and SLC45A2 are capable of raising lysosomal pH when expressed in HeLa cells, we tested whether overexpression of either protein could compensate for the loss of the other. HA-SLC45A2, HA-OCA2, or HA-SLC35D3 as a negative control (see **Figure 2.1**) were transiently expressed by transfection in either *Slc45a2*-deficient melan-uw melanocytes or *Oca2*-deficient melan-p1 melanocytes, and the fraction of HA-positive cells that were pigmented after 3 days was quantified. As expected, very few melan-uw cells expressing HA-SLC35D3 were pigmented above background (19.88 ± 5.76%) whereas most HA-SLC45A2 expressing cells were pigmented (70.7 ± 5.85%; **Figure 2.7a, b, g**). Surprisingly, a large fraction of HA-OCA2-expressing melan-uw cells were also pigmented (46.37 ± 6.29%; **Figure 2.7c, g**), suggesting that OCA2 overexpression can compensate for the loss of SLC45A2. By contrast, whereas HA-OCA2 expression restored pigmentation to melan-p1 cells (93.17 ± 4.97%), HA-SLC45A2 expression was as ineffective at restoring pigmentation as the negative control HA-SLC35D3 (**Figure 2.7d-f, h**). Thus, overexpression of SLC45A2 cannot compensate for the loss of OCA2. These data are consistent with a model in which sequential function of OCA2 and then SLC45A2 is required to modulate and maintain a nearly-neutral pH in melanosomes.

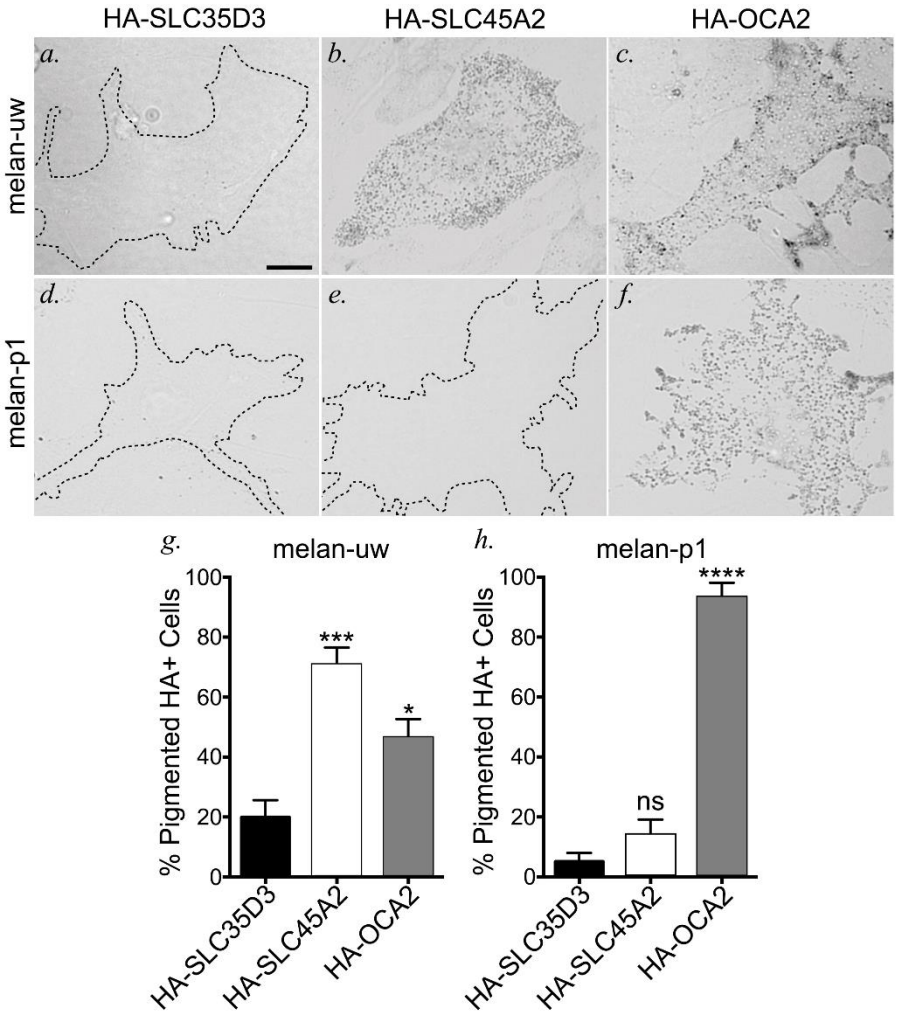

Figure 2.7: OCA2 overexpression compensates for loss of SLC45A2-dependent melanosome neutralization in melanocyte pigmentation. SLC45A2-deficient melan-uw cells or OCA2-deficient melan-p1 cells were transiently transfected with negative control HA-SLC35D3 (*a*, *d*), HA-SLC45A2 (*b*, *e*), or HA-OCA2 (*c*, *f*), and fixed and labelled for HA (not shown). Bright field microscopy was used to visualize pigmented melanosomes within HA-positive cells. Scale, 10 μm. (*g*, *h*) The number of HA-containing pigmented cells was quantified and is depicted as a mean percentage of total HA-containing (HA+) cells ± SEM. Quantification is from the following independent experiments and total sample sizes: melan-uw + HA-SLC35D3 (3, 67), melan-uw + HA-SLC45A2 (9, 320), melan-uw + HA-OCA2 (9, 308), melan-p1 + HA-SLC35D3 (3, 62), melan-p1 + HA-SLC45A2 (4, 137), melan-p1 + HA-OCA2 (4, 90). Statistical significance was determined using one-way ANOVA with Holm-Sidak's test for multiple comparisons. *, $p < 0.05$; ***, $p < 0.001$; ****, $p < 0.0001$; ns, not significant.

2.3.6. The light skin-associated SLC45A2-F374 variant protein is expressed at lower levels than the dark skin-associated SLC45A2-L374 variant.

The major human *SLC45A2* allele associated with light skin tone encodes a phenylalanine (F) instead of a leucine (L) at amino acid position 374, within the eighth transmembrane domain of the predicted 12-transmembrane domain-containing protein (**Figure 2.8a**). How does this single amino acid substitution impact pigmentation? We reasoned that the F374 variant could affect either protein folding/stability, localization to melanosomes, or transporter function within melanosomes. To begin to distinguish between these possibilities, we generated stable melan-uw cells expressing the HA-tagged dark skin-associated L374 variant (as used in **Figures 2.1-2.7**), the HA-tagged F374 variant, or HA-SLC35D3 as a control (CTRL). Bright field microscopy analysis revealed that cells expressing HA-SLC45A2-F374 were darker than control cells but lighter than cells expressing HA-SLC45A2-L374 (**Figure 2.8b**), consistent with published results (Cook et al., 2009b). The observed phenotype was confirmed by quantitative melanin content assay, in which cells expressing HA-SLC45A2-F374 harbored significantly more pigment than control cells but less than cells expressing HA-SLC45A2-L374 (**Figure 2.8c**). The lower level of pigmentation in cells expressing HA-SLC45A2-F374 did not reflect reduced SLC45A2 mRNA expression, as quantitative RT-PCR analyses showed that melan-uw cells expressing HA-SLC45A2-F374 had 1.25-fold more SLC45A2 mRNA than the wild-type HA-SLC45A2-L374-expressing cells (**Figure 2.8d**). However, immunoblotting analyses of cell lysates for the HA-tagged proteins revealed that the HA-SLC45A2-L374 stable cell line expressed two-fold more HA-SLC45A2 than cells stably expressing the HA-SLC45A2-F374 variant (**Figure 2.8e, f**). These data indicate that

the reduced pigmentation conferred by the F374 variant is reflected by a post-translational reduction in SLC45A2 protein content.

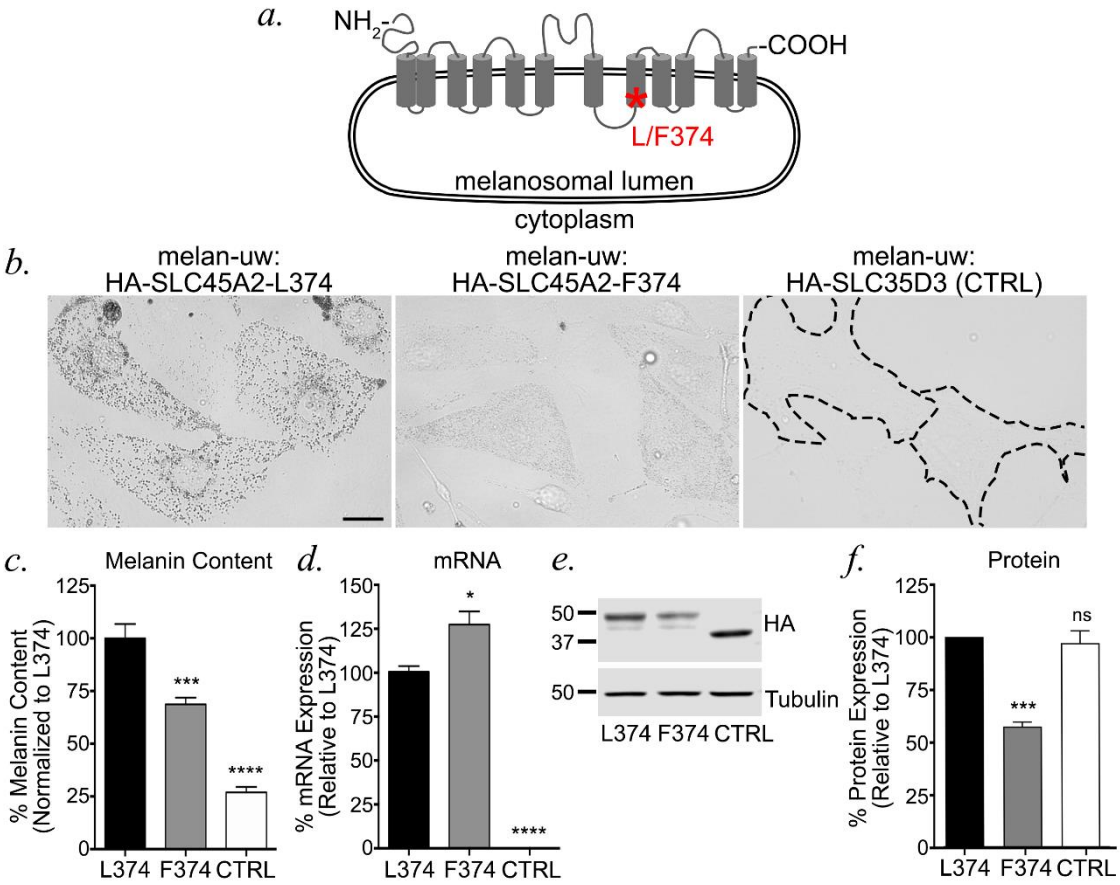

Figure 2.8: The human light skin-associated SLC45A2-F374 variant is expressed in melanosomes at lower levels than the dark variant. (*a*) Schematic diagram of human SLC45A2 primary structure, with transmembrane (gray cylinders), luminal and cytosolic domains (gray lines) indicated. An asterisk indicates the position of L/F374. (*b*) Stably transfected melan-uw cells expressing HA-SLC45A2-L374 (left), HA-SLC45A2-F374 (center), or HA-SLC35D3 as a negative control (right) were imaged by bright field microscopy to emphasize pigmentation levels. Bar, 10 μm. (*c-f*) Stably transfected melan-uw cells expressing HA-SLC45A2-L374, HA-SLC45A2-F374, or HA-SLC35D3 (CTRL) were analyzed for (*c*) melanin content by quantitative spectroscopy assay, (*d*) SLC45A2 mRNA expression by quantitative RT-PCR, or (*e*, *f*) HA protein expression by immunoblotting relative to tubulin as a loading control. A representative immunoblot is shown in *e*; quantification of HA expression normalized to tubulin levels over three experiments is shown in *f*. All values are normalized to 100% for cells expressing HA-SLC45A2-L374. Each experiment was repeated at least three times. Statistical analyses were determined by Welch's ANOVA with Dunnett T3 test for multiple comparisons (*c*, *d*) or one-way ANOVA with Dunnett's test for multiple comparisons (*f*). ns, no significant difference; *, $p < 0.05$; ***, $p < 0.001$; ****, $p < 0.0001$.

To test whether the reduced protein content of the F374 variant reflected increased protein degradation, we assessed the protein stability of each variant over time in stably transduced melan-uw cells. Cells were treated with cycloheximide (CHX) to block new protein synthesis, and the amount of HA-SLC45A2 remaining in cell lysates at different time points was assessed by immunoblotting. While the levels of both variants were substantially reduced by 32 h following CHX treatment, HA-SLC45A2-F374 was degraded at a higher rate than HA-SLC45A2-L374 (L374 half-life, 53.2 h; F374 half-life, 8.5 h) and was nearly completely eliminated by 32 h (**Figure 2.9a, c**). To determine whether the rapid decline in the HA-SLC45A2-F374 variant protein levels were dependent on proteasomal degradation, cells were treated with the proteasome inhibitor MG132 during the CHX chase. MG132 treatment nearly completely blocked the gradual disappearance of HA-SLC45A2-L374, and also blocked the rapid degradation of HA-SLC45A2-F374 at early chase times (**Figure 2.9b, c**). MG132 treatment did not, however, block the slow degradation of HA-SLC45A2-F374 at later time points (**Figure 2.9b, c**). These data indicate that normal turnover of L374 and of the labile fraction of F374 requires proteasome activity, but that degradation of F374 occurs by a proteasome-independent mechanism. To test for the role of endolysosomal degradation, cells were treated with the vacuolar ATPase inhibitor bafilomycin A1 (BafA1) during the CHX chase. BafA1 treatment caused significant cell death by 24 h, but within the first 16 h blocked degradation of both HA-SLC45A2-L374 and -F374, suggesting that degradation was largely mediated in endolysosomes (**Figure 2.10**). Importantly, dIFM analysis showed that HA-SLC45A2-F374 colocalized with TYRP1 to a similar extent as HA-SLC45A2-L374 (**Figure 2.9d, e**), indicating that the cohort of non-degraded HA-SLC45A2-F374 variant localizes properly to melanosomes where it retains some function in supporting elevated pH.

Taken together, these data suggest that the light skin-associated SLC45A2-F374 variant is less stable than the dark skin-associated SLC45A2-L374 variant due to endolysosomal proteolysis that is proteasome-dependent, resulting in lower SLC45A2 activity in melanosomes.

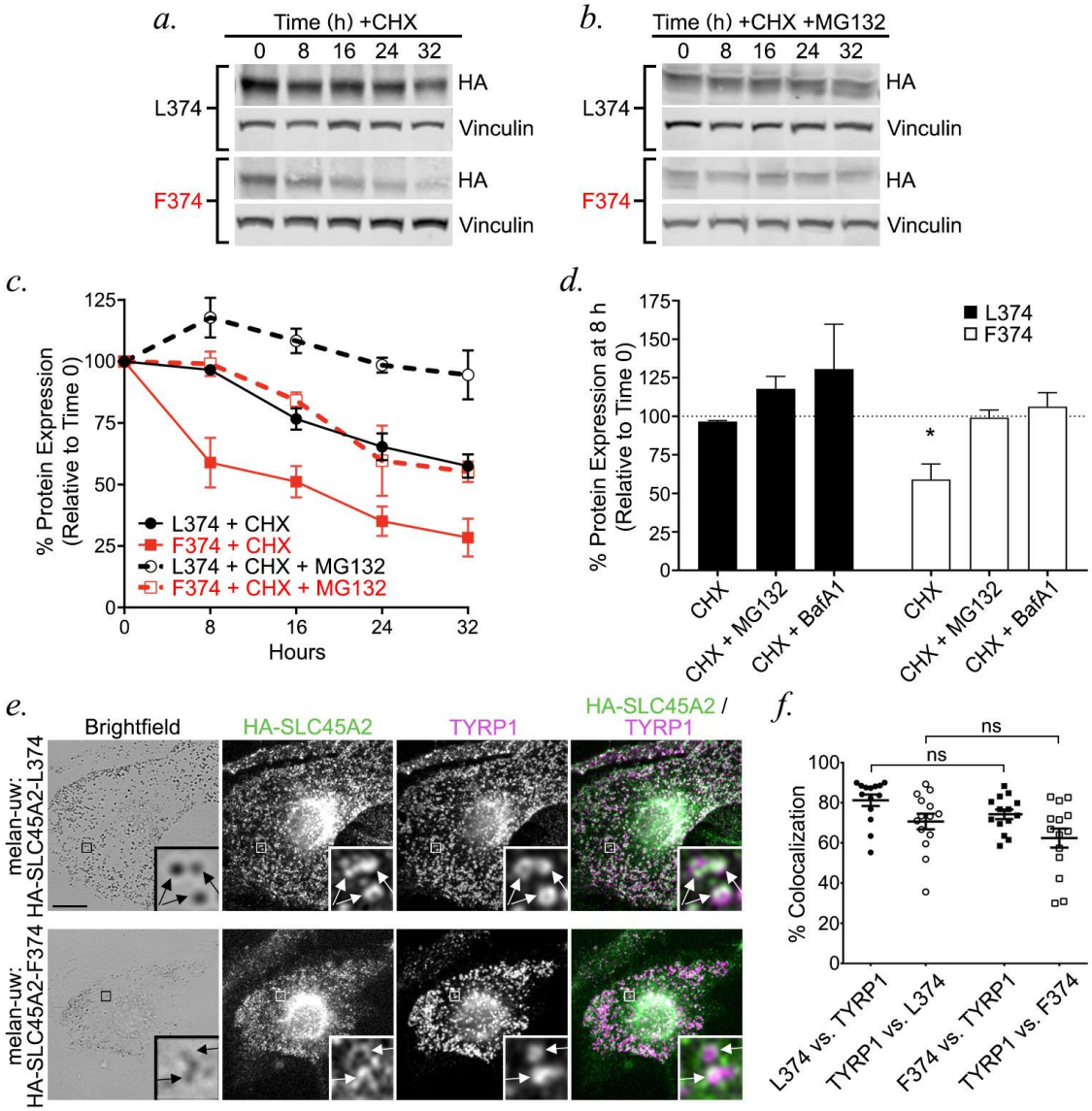

Figure 2.9: The F374 variant is less stable than the L374 variant and is degraded by a proteasome-dependent endolysosomal pathway. (*a, b*) Melan-uw cells stably expressing either HA-SLC45A2-L374 (L374; *a*, *b*, top) or -F374 (F374; *a, b,* bottom) were cultured with cycloheximide (CHX; 25 μg/ml) alone (*a*) or combined with proteasome inhibitor MG132 (25 μM; *b*) for the

indicated times in hours. At the indicated times, cells were harvested and whole cell lysates were fractionated by SDS-PAGE and analyzed by immunoblotting for HA and for vinculin as a loading control. Relevant regions of the gels are shown. (*c*) Band intensities for HA-SLC45A2 were quantified over three independent experiments, normalized to vinculin band intensities, and presented as a percentage of the signal observed at time 0 +/- SEM. (d) Band intensities for HA-SLC45A2 after treatment for 8 h with CHX alone or with MG132 or 25 nM Bafilomycin A1 (BafA1; blots are shown in Expanded View Figure EV2) were quantified over three independent experiments, normalized to vinculin band intensities, and presented as a percentage of the signal for each isoform at time 0 ± SEM. Statistical significance of values relative to those at time 0 was determined using ordinary one-way ANOVA with Dunnett post-hoc test for multiple comparisons. Only statistically significant differences are noted. (*e, f*) Melan-uw cells stably expressing either HA-SLC45A2-L374 (*e*, top) or HA-SLC45A2-F374 (*e,* bottom) were fixed, labeled for HA (green) and TYRP1 (magenta), and analyzed by dIFM and by bright field microscopy. Merged HA/TYRP1 image is at right; insets of boxed regions are magnified 7.5 times. HA-SLC45A2 and TYRP1 localizing to the same compartments are indicated with arrows. Scale, 10 μm. (*f*) The degree of TYRP1 and SLC45A2 localization to the same compartments was quantified manually from 14 cells over 2 independent experiments, and is presented as label 1 vs label 2, in which the colocalization between label 1 and label 2 is a percentage of total label 2. Quantification is from 2 independent experiments with 14 cells counted per sample. Statistical significance was determined using Kruskal-Wallis test with Dunn's post hoc test for multiple comparisons. ns, no significant difference; *, $p < 0.05$.

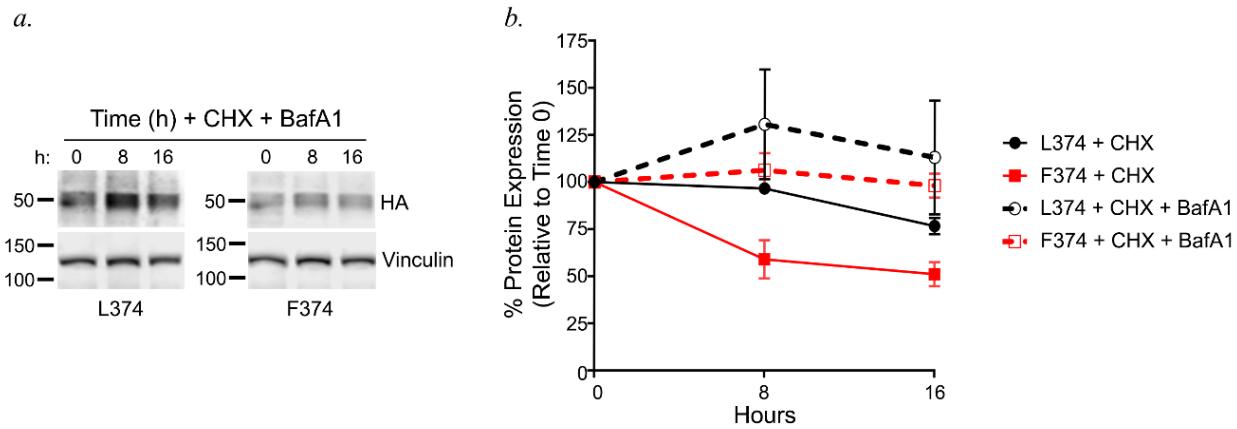

Figure 2.10: Early phase of rapid SLC45A2-F374 degradation is blocked by vATPase inhibition. (*a*) Melan-uw cells stably expressing either HA-SLC45A2-L374 (L374; *a*, left) or -F374 (F374; *a,* right) were cultured with cycloheximide and the vATPase inhibitor bafilomycin A1 (BafA1; 25 nM) for the indicated times (h). Cells were then harvested and whole cell lysates were fractionated by SDS-PAGE and analyzed by immunoblotting for HA and for vinculin as a loading control. Relevant regions of the gels from a representative experiment are shown. (*b*) Band intensities for HA-SLC45A2 were quantified over three independent experiments, normalized to vinculin band intensities, and presented as a percentage of the signal observed at time 0 +/- SEM. CHX only samples were the same as those used in the quantification in Figure 8c.

2.4. Discussion

SLC45A2 is a critical determinant of skin and eye pigmentation, but until now its localization and functional role in melanogenesis have not been clearly delineated. Using a functional epitope-tagged form of SLC45A2 expressed in immortalized SLC45A2-deficient epidermal mouse melanocytes, we show here that SLC45A2 localizes to a subset of mature melanosomes marked by TYR and TYRP1 expression, where it partially accumulates in subdomains of the organelle outer membrane. When expressed ectopically in HeLa cells, SLC45A2 localizes to subdomains of the lysosomal membrane and functions to increase lysosomal pH, supporting a previously proposed role in neutralizing melanosomes (Bin et al., 2015). Although the melanosomal chloride channel OCA2 also functions to neutralize melanosome pH (Bellono et al., 2014), SLC45A2 localizes to a partially distinct cohort of melanosomes, and SLC45A2-deficient melanocytes harbor melanosomes that are more pigmented than OCA2-deficient cells – together suggesting that SLC45A2 functions at a later melanosome maturation stage than OCA2. Accordingly, overexpression of OCA2 in SLC45A2-deficient melanocytes compensated for SLC45A2 deficiency in pigment production, whereas SLC45A2 overexpression could not compensate for OCA2 deficiency. Although it is possible that these data reflect the distinct abilities of the OCA2 channel and the SLC45A2 transporter to modulate pH on the same melanosome subsets, the localization of these two proteins to partially distinct subsets lead us to conclude that SLC45A2 functions to neutralize lumenal pH at a later stage of melanosome maturation than OCA2. We also identified the mechanism underlying the pigmentation phenotype of the light skin-associated F374 variant of SLC45A2. Although SLC45A2-F374 localizes to melanosomes like the dark skin-associated L374 variant, SLC45A2-F374 is less stable and more rapidly degraded

than -L374, resulting in reduced SLC45A2-F374 protein levels at steady state. Together, our data (1) indicate that SLC45A2 regulates melanogenesis by controlling melanosome pH in a manner that is non-redundant with OCA2 and (2) uncover the mechanism by which a common genetic variant imparts light skin color.

Our data indicate that SLC45A2 localizes to the melanosomal membrane, where we propose that it directly functions to increase lumenal pH. This is analogous to other proteins on the melanosome membrane, such as the chloride channel OCA2 and the cation channel TPC2, which also directly regulate melanosome pH through ion transport (Ambrosio et al., 2016; Bellono et al., 2014; Bellono et al., 2016; Sitaram et al., 2009), and contrasts with ion transporters/channels that may indirectly regulate melanosome pH through effects on other organelles. For example, the putative solute transporter MFSD12 negatively regulates pigmentation from lysosomes (Crawford et al., 2017) and NCKX5 encoded by *SLC24A5*, the gene deficient in OCA6, appears to positively regulate pigmentation from the trans Golgi network (Ginger et al., 2008; Rogasevskaia et al., 2019). Together, these observations suggest that melanosome pH is regulated both directly and indirectly via a complex network of putative channels/transporters. Further work is necessary to identify other regulators of melanosome pH and to understand how these proteins cooperate to fine-tune the lumenal pH of melanosomes, thereby controlling melanin synthesis.

When expressed at the plasma membrane in yeast, SLC45A2 functions as a sucrose/proton symporter that transports sucrose from the extracellular space into the cytosol in a manner that requires a proton gradient and is maximal at a slightly acidic pH (Bartölke et al., 2014). Interestingly, SLC45A2 and other SLC45 family members can transport not only the disaccharide sucrose but also the monosaccharides glucose,

fructose, and mannose (Bartölke et al., 2014). If it were to function similarly in melanocytes, SLC45A2 would expel protons and sugar molecules from the melanosome lumen into the cytosol, hence increasing melanosome pH. Whether sugars are substrates for SLC45A2 under physiological conditions in melanosomes remains to be determined, but given that lysosomal enzymes are present within maturing melanosomes (Berson et al., 2001; Diment et al., 1995b), it is possible that monosaccharides released from glycoproteins by lysosomal glycosidases in early stage melanosomes could serve as substrates for sugar/proton symporter activity. Our data show that expression of SLC45A2 in lysosomes of HeLa cells is sufficient to increase pH, indicating that its proton-dependent symporter activity is sufficient to raise lumenal pH by counteracting the activity of the vacuolar ATPase (vATPase), which pumps protons into the lumen of both melanosomes and lysosomes in an ATP-dependent manner (Bhatnagar and Ramalah, 1998; Mindell, 2012; Tabata et al., 2008). Sugar co-transport from the melanosome into the cytosol would also decrease the osmotic concentration inside the melanosome, requiring counter-ion transport to balance solute concentrations. Further investigation into the melanosomal channels, transporters, and exchangers is required to understand how the melanosome regulates not only its pH but also its osmolarity.

Unlike melanosomal proteins such as TYRP1 that are detected relatively uniformly on the melanosome membrane by IFM, SLC45A2 is sometimes detected in a punctate pattern, corresponding to specific subdomains of the melanosome membrane. The nature of these subdomains and the mechanism by which SLC45A2 assembles into them remains unclear. The punctate localization is conserved on lysosomes upon ectopic expression of SLC45A2 in non-pigmented HeLa cells, suggesting that the assembly of SLC45A2 into subdomains does not require interactions with melanocyte-specific

proteins. Some cells expressing HA-SLC45A2 displayed a mixture of punctate and ring-like SLC45A2 patterns on melanosomes. This might either reflect an artifact of overexpression or the consequence of a regulated process of aggregate assembly that may be influenced by melanosome contents or other features of melanosome maturation. The composition, regulation and function of these SLC45A2-containing structures warrants further investigation.

The high colocalization between SLC45A2 and TYRP1 suggests that SLC45A2 is co-delivered with TYRP1 to maturing melanosomes, likely via BLOC-1-dependent membrane transport (Setty et al., 2008; Setty et al., 2007). In contrast, despite similar requirements for BLOC-1 for delivery to melanosomes (Sitaram et al., 2012), there is significantly less overlap between OCA2 and TYRP1, and in structures in which they overlap their abundance is inversely related. Moreover, the relative melanin content of SLC45A2- and OCA2-deficient melanocytes is different, such that SLC45A2-deficient melanocytes harbor more mature melanosomes and slightly higher pigmentation than OCA2-deficient melanocytes. While these latter data alone could be interpreted to reflect distinct activities of OCA2 and SLC45A2 in facilitating increased melanosomal pH, together with the localization data they suggest that OCA2 functions at an earlier melanosomal maturation stage compared to SLC45A2. This would imply either that the melanosome delivery of OCA2 and TYRP1/SLC45A2 is staggered or that OCA2 is cleared soon after delivery. The latter is supported by the short half-life of OCA2 (Sitaram et al., 2009), the dependence of this half-life on melanization (Donatien and Orlow, 1995), and the accumulation of OCA2 on internal membranes in mature melanosomes (Sitaram et al., 2012). Based on these observations, we propose a model in which OCA2, SLC45A2, and TYRP1 are delivered together to maturing melanosomes – which harbor active

vATPase to acidify their lumen (Bhatnagar and Ramalah, 1998; Tabata et al., 2008). OCA2 would facilitate a rapid efflux of chloride ions, immediately reducing membrane potential and thereby slowing vATPase activity. As the melanosomes mature, OCA2 clearance from the limiting membrane coupled with continued SLC45A2 arrival would support a slow but continued melanosome neutralization mediated by SLC45A2 proton export, counteracting residual vATPase activity. If this model were true, then OCA2 overexpression, by prolonging exposure on the melanosomal membrane, would antagonize vATPase activity in a more sustained way, perhaps resulting in slow proton efflux from the melanosome through another means such as membrane recycling (Dennis et al., 2016). This model would thus explain our observation that OCA2 overexpression can compensate for SLC45A2 loss but that SLC45A2 overexpression – with its limited capacity for proton export – cannot compensate for OCA2 loss.

The SLC45A2-F374 variant is the predominant allele in Northern Europe and is strongly associated with light skin and hair and blue eyes (Branicki et al., 2008; Cook et al., 2009a; Lao et al., 2007; Lopez et al., 2014; Lucotte et al., 2010; Lucotte and Yuasa, 2013; Mukherjee et al., 2013; Sabeti et al., 2007; Soejima and Koda, 2007; Soejima et al., 2006; Yuasa et al., 2006). However, the mechanism responsible for the reduced pigmentation associated with SLC45A2-F374 was previously unclear. We show here that compared to SLC45A2-L374, expression of SLC45A2-F374 in SLC45A2-deficient melanocytes results in a more meager increase in pigmentation, despite higher levels of *SLC45A2* mRNA. Our results demonstrate that this is due to instability of the SLC45A2-F374 protein, leading to a higher rate of degradation relative to SLC45A2-L374 through a proteasome- and vATPase-dependent mechanism. Nevertheless, the remaining cohort of SLC45A2-F374 localizes appropriately to melanosomes. Thus, we propose that the

reduced pigmentation associated with the F374 allele is due to insufficient levels of SLC45A2-F374 on the melanosomal membrane to maintain optimal neutral pH for maximal TYR activity, thus resulting in decreased melanin synthesis. Whether SLC45A2-F374 is rapidly degraded following melanosomal delivery or is missorted for endolysosomal degradation remains to be determined.

In conclusion, our data significantly advance our understanding of SLC45A2 and its function on melanosomes and begin to unravel the stepwise contributions of SLC45A2 and OCA2 to lumenal pH regulation and proper melanosome maturation. We also reveal the molecular basis explaining why the SLC45A2-F374 variant is a hypomorphic allele and propose a mechanism by which this allele contributes to lighter pigmentation in humans. The regulation of melanosome pH through the coordinated function of transporters, channels, and other proteins requires further investigation.

2.5. Acknowledgements

The authors are grateful to Drs. Lynn Lamereux for generating *Slc45a2*$^{uw/uw}$*Ink4a-Arf*$^{-/-}$ mice and Lynn Plowright for technical assistance in generating melan-uw cells from these mice, to Donald Koroma for consultation on experimental details, and to Dr. Sergio Grinstein for the gift of the LAMP1-mCherry expression construct. We acknowledge funding from NIH grants R01 AR048155 (MSM), R01 AR071382 (EO and MSM), and F32 AR062476 (MKD) from the National Institute of Arthritis, Skin and Musculoskeletal Diseases, and T32 GM007229 Training Program in Cell and Molecular Biology from the National Institute of General Medical Sciences (LL and AJL), and Wellcome Trust grant 108429/Z/15/Z (EVS and DB).

2.6. Materials and Methods

2.6.1. Reagents

Unless otherwise specified, chemicals were obtained from Sigma-Aldrich (St. Louis, MO) and tissue culture reagents from Life Technologies/Thermo Fisher Scientific (Waltham, MA). Protease inhibitors were purchased from Roche Diagnostics (Rotkreuz, Switzerland), gene amplification primers from Integrated DNA Technologies (Coralville, IA), GoTaq DNA polymerase from Promega Corp. (Madison, WI), and restriction enzymes and T4 DNA ligase from New England Biolabs (Ipswich, MA).

2.6.2. Cell Culture

Immortalized melanocyte cell lines melan-p1 (OCA2 deficient) from C3H-*Oca2*^{cp}/^{25H} (pink-eyed dilute) mice (Sviderskaya et al., 1997), and "wild-type" (WT) melan-Ink4a-Arf1 (formerly called melan-Ink4a-1; referred to here as melan-Ink4a or WT) from C57BL/6J-*Ink4a-Arf*$^{-/-}$ (*Cdkn2* null) mice (Sviderskaya et al., 2002) have been described and were derived from the skins of neonatal mice. Three immortal SLC45A2 deficient melanocyte lines, melan-uw-1, -2 and -3, were similarly derived from the skins of neonatal C57BL/6J- *Ink4a-Arf*$^{-/-}$ *Slc45a2*$^{uw/uw}$ (underwhite) mice. Mice were housed and interbred by Dr Lynn Lamoreux (Texas A&M University, College Station, TX, USA), and skins were shipped on ice to London. Only the melan-uw-2 line (referred to here as melan-uw) was used here because they were more uniform in pigmentation both before and after stable expression of HA-SLC45A2. All cells were cultured at 37˚C and 10% CO_2 in RPMI 1640 medium supplemented with 10% FBS (Atlanta Biologicals) and 200 nM 12-*O*-

tetradecanoylphorbol-13-acetate (TPA). Melan-uw cells grow poorly in the absence of adenylate cyclase activators, which also stimulate the transcription of melanogenic genes. In order to properly compare them, melan-uw cells, melan-p1 cells, and all stable cell lines derived from these cells were additionally supplemented with 200 pM cholera toxin. Melan-Ink4a cell medium was not supplemented with cholera toxin, but we expect that this might contribute to underestimating the differences between Melan-Ink4a and the other cell lines due to the increased expression of melanogenic genes in the latter. Cell lines were authenticated by restoration of pigmentation upon expression of the wild-type form of their defective genes, and verified to be negative for mycoplasma every 2-3 months using the MycoAlert Mycoplasma Detection Kit (Lonza).

Retrovirus production from transiently transfected Plat-E cells(Morita et al., 2000a) and retroviral transduction of melanocyte cell lines were carried out as described previously (Meng et al., 2012a; Setty et al., 2007). Briefly, Plat-E cells were transfected with retroviral DNA constructs using Lipofectamine 2000 (Thermo Fisher), and the medium was replaced the next day. Retrovirus-containing supernatants were collected 48 h later, filtered, and added to melan-Ink4a cells or melan-uw cells in a 1:1 ratio with fresh medium. The medium was replaced the next day, and pools of stable transductants were selected 24 h later by adding 300 µg/ml hygromycin B to the medium. Stable transfectants were occasionally treated with 200 µg/ml hygromycin B for 2–3 d to maintain selective pressure for the transgene. For transient transfections, cells on glass coverslips were transfected with DNA constructs using Lipofectamine 3000 or Lipofectamine 2000 (Thermo Fisher), and the medium was replaced the next day. Cells were fixed using 4% formaldehyde/PBS 48 or 72 hours after transfection and stored at 4°C for immunolabeling and analysis.

2.6.3. DNA Constructs

We first generated a GFP-SLC45A2 (L374) fusion protein by inserting human SLC45A2 cDNA, generated by RT-PCR of RNA isolated from darkly pigmented human epidermal melanocytes, into the BamHI/XhoI sites of pcDNA4/TO (Invitrogen/Life Technologies) in frame with GFP and a Gly-Ala-Gly-Ala linker previously inserted in the AflII/HindIII sites (sequence available upon request). To generate HA-tagged SLC45A2, the insert from pcDNA4/TO-GFP-SLC45A2 was amplified by PCR adding XhoI and NotI restriction sites at the 5' and 3' ends, respectively, and subcloned into the respective sites of pCI (Promega). An N-terminal Kozak consensus start site, HA tag, and Gly-Ser linker were subsequently added by PCR using a distinct forward primer (5'-gcatatctcgagatgTACCCATACGATGTTCCAGATTACGCTggctcaggatctgggatgggtagcaac agtgggc-3') and the same reverse primer. The HA-SLC45A2 insert was subsequently subcloned as a XhoI-NotI fragment into pBMN-(XN)-IRES-hygro to generate the retroviral vector encoding HA-SLC45A2. The F374 variant was made by site-directed mutagenesis of the pBMN-(XN)-IRES-hygro-HA-SLC45A2 (L374) construct using the Clontech site-directed mutagenesis kit. All recombinant plasmids were verified by sequencing by the University of Pennsylvania Cell Center, the Nucleic Acid/Protein Research Core Facility at the Children's Hospital of Pennsylvania, or Macrogen.

The plasmid-based expression vector pCR3-OCA2-WT-HA-UTR2 and corresponding retroviral vector pBMN-OCA2-WT-HA-UTR2 encoding human OCA2 with an exofacial HA epitope were described in (Sitaram et al., 2009); pCDM8.1-HA-SLC35D3 encoding human SLC35D3 with an N-terminal HA epitope tag was described in (Meng et al., 2012a); and human LAMP1-mCherry in pCDNA3.1 was a generous gift from Sergio Grinstein (Univ. of Toronto and Hospital for Sick Children, Toronto, ON, Canada).

2.6.4. Melanin Content Quantification

Melanin quantification by spectroscopy was done essentially as described (Delevoye et al., 2009a). Briefly, melanocytes seeded on 6-cm dishes were trypsinized, pelleted, and sonicated in melanin buffer (50 mM Tris, 2 mM EDTA, and 150 mM NaCl, pH 7.4) supplemented with protease inhibitor cocktail (Roche). Insoluble material was pelleted for 15 min at 16,000 g (4°C), rinsed in ethanol/diethyl ether (1:1), and dissolved in 2 M NaOH/20% DMSO at 60°C. The optical density at 492 nm was measured to estimate melanin content and normalized to protein concentration as determined by BCA protein determination kit (Thermo Fisher). Plat-E cells, an unpigmented cell line, were used as a negative control. Statistical significance from at least 3 independent experiments was determined by Welch's ANOVA with Dunnett T3 test for multiple comparisons.

2.6.5. Antibodies

Primary antibodies used and their sources (listed in parentheses) include: mouse monoclonal antibody TA99/Mel5 to TYRP1 (American Type Culture Collection; Rockville, MD); rat monoclonal antibody 3F10 to the HA11 epitope (Sigma); mouse monoclonal antibody 16B12 to the HA11 epitope (Biolegend); mouse monoclonal antibody H4A3 to human LAMP1 (Developmental Studies Hybridoma Bank, Iowa City, IA); rabbit anti-LAMP2 (Abcam; for mouse melanocytes); rabbit anti-TYR (Pep7h, to the C-terminal 17 amino acids of human TYR (Calvo et al., 1999)); mouse monoclonal antibody to γ-Tubulin (Sigma); and rabbit antibody to vinculin (E1E9V; Cell Signaling). Species- and/or mouse isotype–specific secondary antibodies from donkey or goat and conjugated to Alexa Fluor

488 or Alexa Fluor 594 used in IFM or conjugated to Alexa Fluor 680 or Alexa Fluor 790 for immunoblots were obtained from Jackson ImmunoResearch Laboratories (West Grove, PA).

2.6.6. Bright Field Microscopy, Immunofluorescence Microscopy (IFM), and Colocalization Analyses

IFM analyses of fixed cells were done essentially as described (Dennis et al., 2016). Briefly, cells were plated on Matrigel (BD)-coated coverslips, fixed with 4% formaldehyde (VWR) in PBS, labeled with primary and secondary antibodies diluted in PBS/0.02% saponin/0.01% BSA, mounted onto slides using Prolong Gold (ThermoFisher), and analyzed on a Leica DMI-6000 microscope equipped with a 40× or 63× objective lens (Leica; 1.4 NA), a Hamamatsu Photonics ORCA-Flash4.0 sCMOS C11440-22CU digital camera, and Leica Application Suite X (LAS X) software. Images in sequential z planes (0.2 μm step size) were deconvolved with Microvolution software and further analyzed using ImageJ (http://fiji.sc/Fiji; National Institutes of Health).

Because SLC45A2 localized partially to subdomains on the melanosome membrane and thus did not fully overlap other melanosomal markers, previously used automated methods to quantify colocalization did not yield meaningful values; similarly, OCA2 localized largely to the interior of melanosomes(Sitaram et al., 2012; Sitaram et al., 2009) and was thus partially distinct from the distribution of TYRP1 or TYR cytoplasmic domain on the melanosome membrane. Therefore, quantification of the degree of overlap between two channels on individual organelles was performed manually on deconvolved, Z-projected images of cells in ImageJ. In brief, single-channel images and a merged image were synchronized using “Analyze > Tools > Synchronize Windows;” signals that were

localized to the same organelle were counted using the “Multi-Point” tool; remaining signal in single channels were counted using the “Multi-Point” tool; and the total colocalized structures was calculated as a percentage of total structures for each channel. Statistical significance was determined using one-way ANOVA with Tukey’s multiple comparisons test, Welch’s ANOVA with Dunnett T3 post hoc test, or Kruskal-Wallis test with Dunn’s multiple comparisons test where appropriate.

Scoring of pigmentation in transfected melan-uw and melan-p1 cells was done blinded. Fixed, stained coverslips were randomly assigned numbers and samples were revealed only after images were taken and scored. Statistical significance was determined using one-way ANOVA with Holm-Sidak’s test for multiple comparisons.

2.6.7. Fluorescence Intensity Analyses

Object-based fluorescence intensity was measured using ImageJ as described in https://www.unige.ch/medecine/bioimaging/files/1914/1208/6000/Quantification.pdf. Briefly, 8-bit, single-channel images were opened in ImageJ and brightness and contrast adjusted for each image. The image was duplicated and a threshold applied using “Image > Adjust > Auto Local Threshold.” To multiply binary images of the two channels of interest, we used “Process > Image Calculator > Multiply.” To redirect intensity measurements from binary image to fluorescent image, we used “Analyze > Set measurements” and pulled down the “Redirect to:” menu to choose the appropriate fluorescent image, making sure “Area” and “Integrated density” were also checked. With "binary image" clicked, we used “Analyze > Analyze Particles” to measure object intensity. This was repeated for each channel, and for each sample values were normalized to the highest integrated density

value in each channel. At least 10 cells from each of two independent experiments were analyzed.

2.6.8. Lysosomal pH Measurements

HeLa cells were transfected one day prior to imaging experiments with LAMP1-mCherry alone, mCherry-OCA2 alone, or HA-SLC45A2 and LAMP1-mCherry to identify endolysosomes, and incubated with 1 μM LysoSensor-ND160 (Thermo Fisher) for 5 min. Lysosensor was excited at 405 nm and its emission detected at 417-483 nm (W1) and 490-540 nm (W2). The ratio of LysoSensor W1/W2 emission in endolysosomes expressing LAMP1-mCherry was assigned a pH value based on a calibration curve generated prior to each experiment using solutions containing 125 mM KCl, 25 mM NaCl, 24 μM Monensin, and varying concentrations of MES to adjust the pH to 3.5, 4.5, 5, 5.5, 6.5, 7, or 7.5. The fluorescence ratio was linear from pH 5 - 7.0. Statistical significance was determined by Welch's ANOVA with Games-Howell post hoc test for multiple comparisons.

2.6.9. Electron Microscopy

Melanocytes were cultured in 10-cm dishes and fixed in situ with Karnovsky's fixative [4% paraformaldehyde (VWR Scientific, Radnor, PA), 4 mM calcium chloride, 72 mM sodium cacodylate, pH 7.4] containing 0.5% glutaraldehyde (Polysciences, Warrington, PA) for 1–2 h at room temperature. This solution was then removed and replaced with Karnovsky's fixative containing 2% glutaraldehyde, and the cells were fixed overnight at room temperature. Cells were collected by scraping using a cell scraper and centrifugation at 27 g for 5 min, resuspended in Karnovsky's fixative containing 0.5%

glutaraldehyde, and stored at 4°C until processing. After subsequent buffer washes, the samples were post-fixed in 2.0% osmium tetroxide with 1.5% $K_3Fe(CN)_6$ for 1 hour at room temperature, and then rinsed in deonized water prior to en bloc staining with 2% uranyl acetate. After dehydration through a graded ethanol series, the tissue was infiltrated and embedded in EMbed-812 (Electron Microscopy Sciences, Fort Washington, PA) at the Electron Microscopy Resource Laboratory (University of Pennsylvania). Thin sections were stained with uranyl acetate and SATO lead and examined with a JEOL 1010 electron microscope fitted with a Hamamatsu digital camera (Hamamatsu, Bridgewater, NJ) and AMT Advantage NanoSprint500 software (Advanced Microscopy Techniques, Woburn, MA).

For melanosome staging, a combined total of at least 20 cells from at least two independent experiments and over 600 melanosomes were analyzed for each cell type and the analysis was done blinded. The number of stage I/II, stage III, and stage IV melanosomes were quantified, and the percentage of melanosomes at each stage was calculated for each cell. These data were analyzed and plotted using Prism 6 (GraphPad, La Jolla, CA), and statistical significance was determined by Welch's ANOVA with multiple comparisons (samples compared to melan-Ink4a) and Dunnett T3 test for multiple comparisons.

2.6.10. Immunoblotting

Melan-uw cells stably expressing HA-SLC45A2-L374, HA-SLC45A2-F374, or HA-SLC35D3 cultured in 60 mm Petri dishes were treated with 25 µg/ml cycloheximide ± 25 µM MG-132 or ± 25 nM bafilomycin A1 and collected for immunoblot every 8 h for 32 h. For each time point the cells were rinsed in cold PBS before pelleting by centrifugation.

After collection of all time points, cell pellets were resuspended in 1X Laemmli buffer (Laemmli, 1970), lysed by sonication, and heated at 37°C for 5 minutes. Protein concentration for each sample was measured using the BCA assay (Pierce) according to the manufacturer's protocol. 20 µg protein from each sample was fractionated by SDS-PAGE on 10% polyacrylamide gels, and transferred to PVDF membranes (Immobilon-FL, Millipore). Membranes were blocked with 5% milk in TBS, incubated overnight with antibodies to HA or vinculin diluted in TBS/0.5% Tween, washed with TBS/0.5% Tween, and analyzed using Alexa Fluor 680 or 790-conjugated secondary antibodies and Odyssey imaging system (LI-COR, Lincoln, NE). For immunoblotting without drug treatments, the method was the same except that cycloheximide, MG-132, and bafilomcin A1 were not added and antibodies to tubulin were used for the loading control. Statistical significance was determined using one-way ANOVA with Dunnett's test for multiple comparisons. Protein half-lives were calculated using one phase decay.

2.6.11. Quantitative RT-PCR

Total RNA was extracted from melan-uw cells stably expressing either HA-SLC45A2, HA-SLC45A2-F374 or HA- SLC35D3 as a control using the RNeasy Plus Kit (Qiagen), and 3 µg was reverse transcribed (RT) using the SuperScript III kit (Life Technologies). The resulting cDNA was used for qPCR. Primers were designed using Primer3 (http://bioinfo.ut.ee/primer3-0.4.0/) to span an exon-exon junction to avoid amplification of any contaminating genomic DNA and were as follows: SLC45A2 (NM_016180.3) - F: CCCTGTACACTGTGCCCTTT and R: CTTCCCTCTCACGCTGTTGT. Reactions were prepared according to the manufacturer's protocol using SYBR Select Master Mix (Invitrogen/ThermoFisher Scientific) and cycled

on a Real-Time PCR System (Biorad). β-actin was used as an internal control and all reactions were run in triplicate. mRNA levels were quantified by calculating average $2^{-\Delta\Delta Ct}$ values, where Ct is the cycle number for the control and target transcript at the chosen threshold. $\Delta Ct = Ct_{target} - Ct_{\beta\text{-actin}}$ was calculated by subtracting the average Ct of β-actin from the average Ct of the target transcript. The ΔCt_{mean} was calculated for the reference sample (L374) and $\Delta\Delta Ct = \Delta Ct - \Delta Ct_{mean}$ was calculated by subtracting the ΔCt_{mean} from the ΔCt. The relative mRNA expression of samples compared to L374 samples was calculated by $2^{-\Delta\Delta Ct}$. Statistical significance was determined using Welch's ANOVA with Dunnett T3 test for multiple comparisons.

2.6.12. Statistical Analyses

Except where noted, we performed each experiment three times and sample sizes are as indicated in each figure legend. Statistical data are presented as mean ± SEM. Statistics were calculated in GraphPad Prism using ordinary unpaired Student's t test, ordinary one-way ANOVA, Welsh's ANOVA, or Kruskal-Wallis test with post hoc correction as specified. Welsh's ANOVA or Kruskal-Wallis tests were used instead of ordinary one-way ANOVA when the data displayed heteroscedasticity or did not display a normal distribution, respectively, which were determined using Graphpad Prism. Significant differences between control or experimental samples are indicated (****, $p < 0.0001$; ***, $p < 0.001$; **, $p < 0.01$; *, $p < 0.05$). Only $p < 0.05$ was considered as statistically significant.

CHAPTER 3

Characterization of melanocytes derived from the Hermansky-Pudlak syndrome mouse model *buff*

3.1. Abstract

VPS33A encodes a Sec1-Munc18 (SM) protein that is ubiquitously expressed and is a subunit of the HOPS and CORVET complexes that promote fusion between organelles in the endolysosomal and autophagosome systems. A mouse model, *buff*, with a VPS33A-D251E mutation only has apparent defects in lysosome-related organelles (LROs), suggesting that the functions of VPS33A in endolysosomal maturation and LRO biogenesis have distinct requirements. We show that, contrary to a previous report, melan-bf cells, immortalized melanocytes derived from *buff* mice, have enlarged melanosomes, a shift towards mature melanosomes, and overall hyperpigmentation at steady state. By bright field microscopy, we observe that the melanosomal marker TYRP1 largely localizes properly to melanosomes and the lysosomal marker LAMP2 properly segregates from melanosomes; however, a proportion of TYRP1 is punctate and diffuse throughout the cytoplasm, suggesting that a cohort of this protein is mistrafficked. We attempted to determine whether the VPS33A-D251E mutation was causative for these phenotypes by stably expressing human HA-VPS33A-D251E in wild-type immortalized melanocytes and knocking down endogenous VPS33A with short hairpin RNAs. Although enlarged melanosomes were observed in some cells, no significant quantitative differences in melanosome morphology or cargo localization were observed between cells expressing wild-type or *buff* mutant VPS33A. Our data show that melanosomes in *buff* melanocytes have a mild defect in melanosome biogenesis reflected by partial cargo mislocalization. Our inability to phenocopy these cells by expressing the VPS33A-D251E variant in wild-type melanocytes suggests that the mutation may not be causative for these phenotypes. Overall, we conclude that the VPS33A-D251E mutation is permissive for pigmentation and

that other genetic or environmental factors must influence pigmentation status of *buff* melanocytes.

3.2. Introduction

Melanin is a biopolymer that confers pigmentation to skin, hair, and eyes and offers photoprotection against ultraviolet radiation and folate degradation, provides antioxidant effects, and is required during retinal development (D'Alba and Shawkey, 2019; d'Ischia et al., 2015; Valejo Coelho et al., 2016). Melanin is synthesized in melanosomes, specialized lysosome-related organelles (LROs) generated in melanocytes and pigmented epithelial cells (Marks and Seabra, 2001; Seiji et al., 1961). Defects in melanosome contents or assembly result in oculocutaneous albinism, which is associated with poor vision, increased sensitivity to UV-induced DNA damage in the skin, and increased incidence of skin cancers. Oculocutaneous albinism is one feature of the Hermansky-Pudlak Syndromes (HPS), a group of genetic diseases in which melanosomes and other LROs are impaired due to defective trafficking of cargo required for maturation of these organelles (Bowman et al., 2019; Wei, 2006). HPS has been associated with pathological mutations in 11 genes, which encode ubiquitously expressed proteins in multisubunit complexes that have specialized roles in cells containing LROs (Bowman et al., 2019; Pennamen et al., 2020a). However, 27% of individuals with albinism, including syndromic forms like HPS, do not have mutations in any of the known albinism genes. Furthermore, several mouse models of HPS exist with mutations in genes that have not been identified among human HPS patients, suggesting that other genes may be critical specifically for trafficking to LROs (Bowman et al., 2019; Lasseaux et al., 2018b).

The homotypic fusion and vacuole protein sorting (HOPS) and class c core vacuole/endosome tethering (CORVET) complexes promote membrane tethering and fusion in the late endosomal/lysosomal pathway and the early endosomal pathway, respectively (Balderhaar et al., 2013; Balderhaar and Ungermann, 2013; Peplowska et al., 2007; Pols et al., 2013a; Seals et al., 2000; Solinger and Spang, 2013; van der Beek et al., 2019). Both complexes consist of a core complex of VPS11, VPS18, VPS16, and VPS33A (Peplowska et al., 2007; Seals et al., 2000). The core complex associates with either the HOPS-specific subunits VPS39 and VPS41 or the CORVET-specific subunits VPS3 and VPS8 (van der Beek et al., 2019), which exist on opposite ends of the complex and confer specificity through their interactions with small GTPases and effector proteins (Balderhaar et al., 2013; Brocker et al., 2012; Garg et al., 2011; Khatter et al., 2015; Lin et al., 2014; Marwaha et al., 2017; McEwan et al., 2015; Peplowska et al., 2007; Peralta et al., 2010; van der Kant et al., 2013). Engagement of both subunits with membrane-associated small GTPases or effector proteins brings donor and target membranes together. CORVET and HOPS promote fusion through the VPS33A subunit (Akbar et al., 2009; Gengyo-Ando et al., 2016; Lobingier and Merz, 2012; Wartosch et al., 2015). VPS33A is a Sec1/Munc18 (SM) protein that binds and aligns vSNARE and tSNAREs for SNARE complex assembly and protects SNARE complexes from premature disassembly (Baker et al., 2015; Lobingier and Merz, 2012; Lobingier et al., 2014; Seals et al., 2000). Null mutations of HOPS or CORVET subunits are lethal in higher eukaryotes, but hypomorphic alleles or conditional knockouts of HOPS or CORVET subunits are viable. Mutations in HOPS or CORVET subunits have been described to cause LRO defects, including gut granules in *Caenorhabditis elegans*, secretory lysosomes in *Tetrahymena thermophila*, and defects in pigmentation in medaka, zebrafish, *Drosophila melanogaster*,

and mice, suggesting that HOPS and/or CORVET plays a role in LRO biogenesis (Akbar et al., 2009; Delahaye et al., 2014; Hermann et al., 2005; Pulipparacharuvil et al., 2005; Sadler et al., 2005; Sevrioukov et al., 1999; Shestopal et al., 1997; Sparvoli et al., 2018; Suzuki et al., 2003; Warner et al., 1998; Yu et al., 2006). The majority of these defects have been ascribed to mutations in HOPS rather than CORVET; the exception is in *Tetrahymena thermophila* which does not have HOPS but has 8 paralogs of VPS8 that function throughout the endolysosomal pathway (Sparvoli et al., 2018). Indeed, the VPS8 paralog that is required for formation of secretory lysosomes colocalizes with the late endosomal/lysosomal marker Rab7, suggesting that this paralog functions similarly to HOPS subunits (Sparvoli et al., 2018). Together, these data indicate that HOPS rather than CORVET is likely to be involved in LRO biogenesis. However, how HOPS functions in the LRO biogenesis pathway is unclear. It may involve several levels of specificity, including HOPS-specific subunits binding to proteins on the melanosomal membrane and VPS33A binding to the SNAREs involved in melanosomal fusion.

The *buff* (*bf*) mouse model is an HPS-like mouse model that displays hypopigmentation and prolonged bleeding (Dickie, 1964a; Suzuki et al., 2003), as well as progressive neuropathy and motor defects (Chintala et al 2009). Suzuki et al. show that melanocytes cultured from the skin of *buff* mice (melan-bf (Samaraweera et al., 1999)) are hypopigmented, that choroidal and retinal pigment epithelial tissue have decreased and smaller melanosomes, and that platelets have fewer dense granules; by contrast, there is little effect on the activity of two lysosomal enzymes in the kidney (Suzuki et al., 2003). There is no reported effect on life span. A missense mutation causing an aspartic acid to glutamic acid substitution at the conserved residue 251 was identified in the *Vps33a* gene in *buff* mice. Consistent with a role for this mutation in the disease phenotype, stable

expression of the wild-type (WT) *Vps33a* gene in melan-bf cells restored normal pigmentation as assessed by low magnification bright field microscopy (Suzuki et al., 2003). The D251E mutation lies in VPS33A domain 3a, which has been shown to interact directly with vSNAREs (Graham et al., 2013). Although VPS33A-D251E is a conservative mutation, it is hypothesized that it would disrupt a hydrogen bond between Asp-251 and Ile-256 (Graham et al., 2013). Therefore, it is possible that this mutation affects VPS33A binding to vSNAREs.

A few groups have attempted to determine the mechanism underlying the *buff* phenotype (Lobingier and Merz, 2012; Zhen and Li, 2015). Expression of Vps33-D300E, the yeast analog of the *buff* mutation, had no effect on vacuole morphology or trafficking to vacuoles, and the mutant-expressing yeast cells had a wild-type phenotype by all assays tested (Lobingier and Merz, 2012). However, a more dramatic mutation, D300G, displayed partial trafficking defects to the vacuole. This suggested that this conserved residue is required for normal VPS33A function, but that a conservative mutation at this residue is not sufficient to cause a phenotype in yeast (Lobingier and Merz, 2012). Zhen et al. showed that *buff* mice have impaired autophagy, and biochemical data using cerebellar lysates and mouse embryonic fibroblasts (MEFs) derived from *buff* mice suggest that VPS33A-D251E has an increased interaction with the autophagosomal vSNARE syntaxin 17 (Zhen and Li, 2015). They also show that overexpression of VPS33A-D251E in HEK293T cells replicates these data, leading the authors to propose that an increased interaction between VPS33A and syntaxin 17 acts in a dominant negative manner to reduce the availability of VPS33A for further rounds of fusion (Zhen and Li, 2015). However, there are several weaknesses to this model, including that the data contradict published reports on HOPS localization and a dominant negative function

does not correspond to a recessive gene. Nevertheless, overall the published data suggest that *buff* mice have defects in LROs and autophagy (Suzuki et al., 2003; Zhen and Li, 2015). However, the defect in melanosome biogenesis in *buff* mice has not been well-characterized.

To analyze melanocytes and melanosomes from *buff* mice, we obtained melan-bf cells from the Spritz lab (Suzuki et al., 2003). Here, we compare the phenotype of melan-bf cells to melan-Ink4a cells, derived from "wild-type" (WT) C57BL/6J-Ink4a-Arf$^{-/-}$ mice that express WT VPS33A. We show that, despite the hypopigmentation in *buff* mice and the reported hypopigmentation of melan-bf as reported by Suzuki et al., melanosomes are enlarged in melan-bf cells with increased melanin content, indicating that the VPS33A-D251E mutation does not necessarily impede melanosome biogenesis and that other genetic or environmental factors likely influence pigmentation in melan-bf cells.

3.3. Results

3.3.1. Homozygous *Vps33a^{bf}* allele in melan-bf cells.

Melan-bf cells were generously provided by Richard Spritz, who sent sixteen numbered vials (i.e. melan-bf #1, melan-bf #2, etc) of immortalized melanocytes cultured from *buff* mice and single-cell clones derived from these cells (Dickie, 1964a; Samaraweera et al., 1999; Suzuki et al., 2003). All vials were thawed and qualitatively characterized by light microscopy (data not shown). Of the sixteen vials sent, cells from twelve survived the thaw. Of these, only cells from one vial were lightly pigmented as reported by Suzuki et al. Cells from the other 11 vials were very darkly pigmented, and

each population contained a heterogenous mixture of melanosomes that were either unusually large or comparable in size to those of WT melan-Ink4a cells (Sviderskaya et al., 2002) (see **Figure 3.2**). Unlike the even cytoplasmic distribution of melanosomes seen in WT cells, melanosomes in some cells from each of these melan-bf populations were unusually clustered in the cell periphery (see **Figure 3.2**). Among these 11 populations, two were single cell clones that contained almost all enlarged melanosomes that accumulated around the cell periphery in most individual cells.

To confirm that the melan-bf cells expressed only the *Vps33a*^{bf} allele, each population was analyzed by RT-PCR for the *Vps33a* gene using both allele-non-specific primers and primers for wild-type or D251E *Vps33a*^{bf} alleles (**Figure 3.1a**). **Figure 3.1b** shows a representative analysis of melan-bf #1 (a single cell clone) and melan-bf #2 (an uncloned population) compared to melan-Ink4a cells. While melan-Ink4a cells were homozygous for the *Vps33a*^{WT} allele, both melan-bf #1 and melan-bf #2 were homozygous for the *Vps33a*^{bf} allele. Suzuki et al. stably expressed *Vps33a*^{WT} and *Vps33a*^{bf} and selected cells with hygromycin to rescue their cells (Suzuki et al., 2003). To determine whether these melan-bf cells overexpress *Vps33a*^{bf}, we performed RT-PCR with primers for the hygromycin resistance gene and used another cell line stably expressing the hygromycin resistance gene (melan-coa:HPS3) as a positive control. Neither melan-bf #1 nor melan-bf #2 cells (nor any of the other cells tested; not shown) expressed the hygromycin resistance gene, confirming that these are untransfected melan-bf cells (**Figure 3.1b**). As a corollary experiment, cells were treated with hygromycin but, as expected given the PCR results, neither melan-Ink4a cells nor melan-bf cells were

resistant to hygromycin (data not shown). For the remaining experiments, we used melan-bf #1 cells, which we refer to as melan-bf cells.

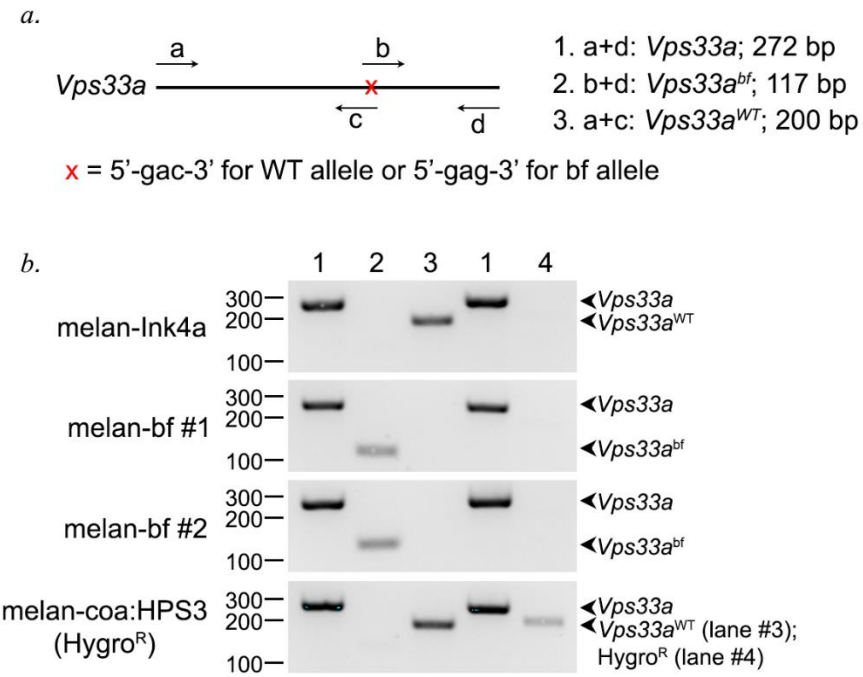

Figure 3.1: Melan-bf cells are homozygous for Vps33abf allele. (*a*) Primer design to amplify *Vps33a* in a non-allele-specific manner (primer a + primer d) or specifically *Vps33a*^{bf} (primer b + primer d) or *Vps33a*^{WT} (primer a + primer c). Sizes of expected PCR products are indicated on the figure. X marks the one-nucleotide difference between the WT and *bf* alleles, which was used to design allele-specific primers b and c. (*b*) cDNA reversed transcribed from total RNA purified from melan-Ink4a, melan-bf #1, melan-bf #2, and melan-coa:HPS3 (positive control for hygromycin resistance gene) was amplified by PCR using the primer sets described in panel a, and then analyzed by agarose gel electrophoresis. Lane #1, product using non-allele-specific primers a and d; Lane #2, product of *Vps33a*^{bf}-specific primers b and d; Lane #3, product of *Vps33a*^{WT}-specific primers a and c. Primers for the hygromycin resistance gene (lane #4) were used to assess whether cells were transfected with a construct conferring hygromycin resistance. Positions of size markers (in bp) are indicated to the left, and positions of relevant bands are indicated to the right. Data presented are representative of n=3 independent experiments.

Given that these cells did indeed express only the *Vps33a*^{bf} allele, we were surprised that they were hyperpigmented rather than hypopigmented as previously reported (Nguyen and Wei, 2004; Suzuki et al., 2003). We considered whether growth conditions

might have contributed to the different phenotypes observed; for example, we have found that AP-3-deficient melanocytes from the HPS2 and HPS10 model *pearl* and *mocha* mice generate enlarged, hyperpigmented melanosomes when grown under limiting nutrient conditions or low serum (Setty et al., 2007; Jani et al 2015), but are hypopigmented when grown in sufficient medium with high serum (Theos et al., 2005; Sitaram et al. 2012) (and M.K. Dennis, unpublished observations). To test whether a similar phenomenon occurred in melan-bf cells, cells were cultured in RPMI medium with 10% or 20% fetal bovine serum (FBS). In addition, cells were cultured with or without cholera toxin (CT), which is sometimes included in melanocyte cultures to stimulate adenylate cyclase and bypass MC1R signaling (Bennett et al., 1987). We found that CT was not required for melan-bf growth, and that cells grew as effectively in both 10% FBS and 20% FBS (data not shown). The enlarged melanosome phenotype was seen in all culture conditions; therefore, RPMI with 20% FBS without CT was chosen for all further studies because cells recovered from thaw more quickly and proliferated well under these conditions.

3.3.2. Melan-bf cells are hyperpigmented and contain enlarged, mature melanosomes.

To compare melanosome morphology in melan-bf and WT melan-Ink4a cells, we used bright field microscopy and thin section transmission electron microscopy. Melanosomes in melan-bf cells were heterogeneously sized but consistently larger than melanosomes in melan-Ink4a cells (**Figure 3.2a**). This was confirmed by electron microscopy, in which melanosomes in melan-bf cells were on average almost 3 times larger in area than melanosomes in melan-Ink4a cells (**Figure 3.2b, c**). In a majority of melan-bf cells, melanosomes were concentrated in the perinuclear area or cell periphery

whereas in melan-Ink4a, melanosomes were distributed evenly throughout the cytoplasm (**Figure 3.2a**). Consistent with this observation, melanosomes occupied less area within melan-bf cells than melanosomes in melan-Ink4a cells (**Fig 3.2d**). An increase in melanosome area and a decrease in the percent area occupied by melanosomes suggests that there are fewer melanosomes in melan-bf cells than in melan-Ink4a cells. Despite this, melan-bf cells contain more melanin than melan-Ink4a cells do (**Figure 3.2e**), indicating that these larger melanosomes are more melanized. Using electron microscopy, we are able to evaluate melanosome maturation based on morphology and melanin content (Seiji et al., 1961). Stage I and stage II melanosomes are unpigmented but stage I melanosomes contain disorganized pre-fibrils and stage II melanosomes contain organized fibrils aligned in parallel across the melanosome. Stage III melanosomes have begun to accumulate melanin, which is deposited on the fibrils; and stage IV melanosomes are filled with electron dense pigment such that the fibrils are obscured. Quantification of melanosomes by electron microscopy showed that melan-bf cells had a decrease in stage III melanosomes and a corresponding increase in stage IV melanosomes compared to melan-Ink4a cells (**Figure 3.2f**). Although the EM results were from a single experiment that needs to be repeated, together these data show that melan-bf cells are hyperpigmented compared to WT melan-Ink4a cells despite having fewer melanosomes, likely due to the increased size and maturity of the melanosomes.

We hypothesized that the enlarged melanosomes in melan-bf cells may be due to aberrant fusion. Melanocytes that are deficient in functional BLOC-3, a putative GTPase involved in the retrograde trafficking pathway from melanosomes that causes HPS when mutated, have macromelanosomes (Gardner et al., 1997; Suzuki et al., 2002) that

sometimes consist of multiple melanosomes fused together. However, by electron microscopy the melan-bf melanosomes appear as single organelles (**Figure 3.2b**).

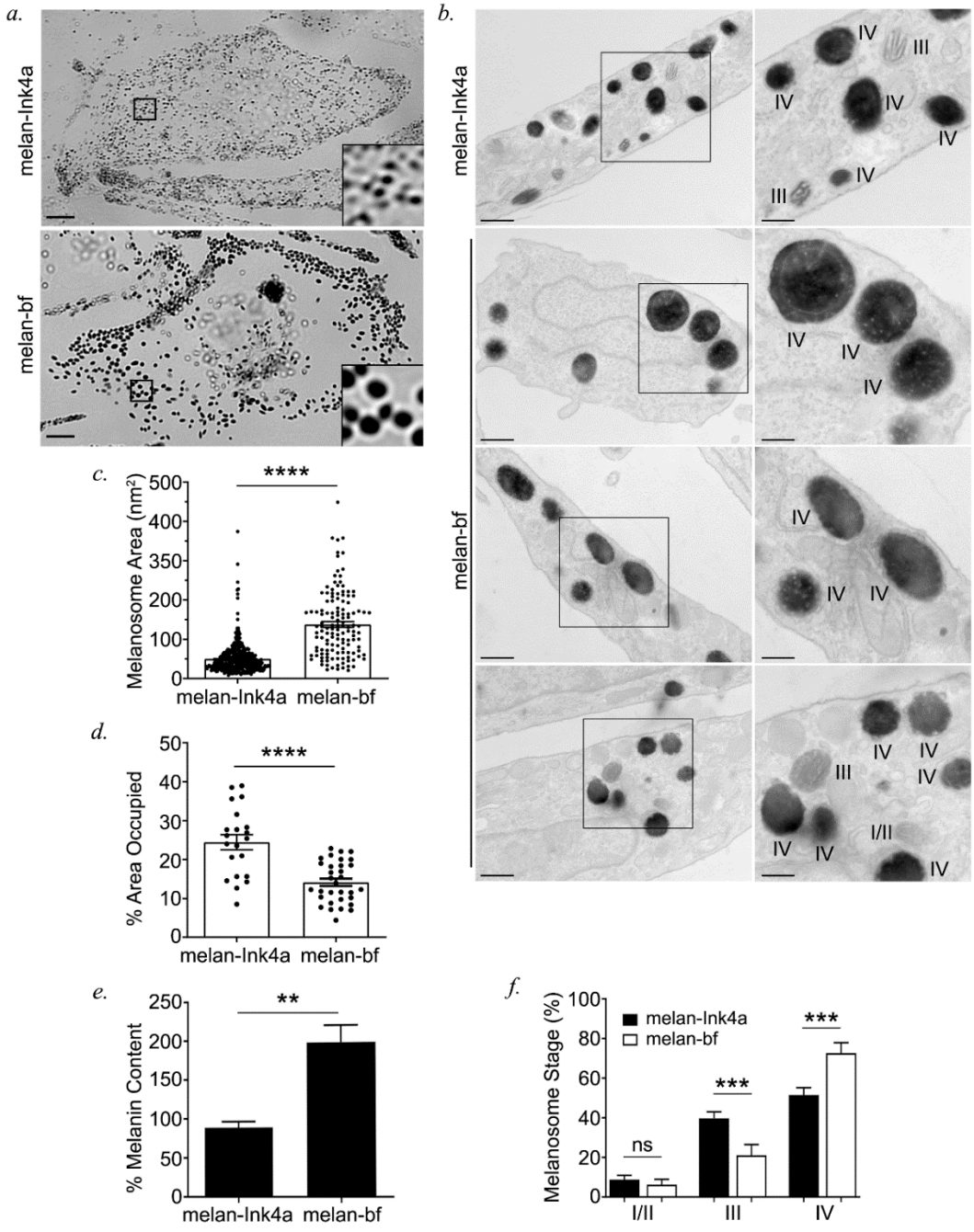

Figure 3.2: Melan-bf cells are hypopigmented and contain enlarged, mature melanosomes. (*a*) Melan-Ink4a and melan-bf cells were fixed and analyzed by bright field microscopy (*a*) or conventional transmission electron microscopy (*b*) to visualize melanosomes. In (*a*), the objective lens was 100X Plan Apo; boxed insets were magnified 5X; scale bar, 5 µm. In (*b*) insets of boxed regions were magnified 2X and shown on the right. III, stage III melanosomes; IV, stage IV melanosomes. Scale bar (left), 500 nm; scale bar (right), 250 nm. (*c*) Melanosome area was quantified from electron microscopy images and the data are represented as mean ± SEM from n=1 EM experiment. Each dot represents one melanosome analyzed; 369 melanosomes from 36 melan-Ink4a cells and 132 melanosomes from 22 melan-bf cells were analyzed. Statistical significance was determined using a two-tailed Mann-Whitney test. (*d*) The area occupied by pigment granules was determined from bright field microscopy images and the data are represented as mean ± SEM from n=3 independent experiments with each closed circle represent one cell counted with 21 total melan-Ink4a and 32 total melan-bf cells counted. Statistical significance was determined by unpaired two-tailed t-test. (*e*) Melanin content in cell lysates was determined by spectrometry relative to total protein content. The data are represented as a percentage normalized to melanin content in melan-Ink4a cells ± SEM from n=3 independent experiments. Statistical significance was determined by two-tailed Mann-Whitney test. (*f*) The number of stage I/II, stage III, and stage IV melanosomes per cell was quantified for melan-Ink4a (black bars) and melan-bf (white bars) and is shown as a percentage of total counted melanosomes per cell. For each stage, data represent the mean ± SEM from n=1 EM experiment. 369 melanosomes from 36 melan-Ink4a cells and 132 melanosomes from 22 melan-bf cells were analyzed. Statistical analyses were performed using two-tailed Mann-Whitney tests to compare melan-Ink4a and melan-bf samples for each stage. ****, $p < 0.0001$; ***, $p < 0.001$; **, $p < 0.01$; ns, no significant difference.

Additionally, although stage III melanosomes were rare, in those present we observed that fibrils were well-organized and looked similar to stage III melanosomes in melan-Ink4a cells (**Figure 3.2b**). These data suggest that melanosomes in melan-bf cells do not undergo aberrant melanosome-melanosome fusion at stages III and IV, and that if melanosome-melanosome fusion occurs at all, it is likely prior to the maturation of fibrils into organized sheets in stage II.

3.3.3. Melan-bf melanosomes have an increase in intralumenal vesicles that correlates with their increased size.

Mature melanosomes are characterized by the accumulation of intralumenal vesicles (ILVs) (Hurbain et al., 2008; Jimbow and Fitzpatrick, 1974; Sitaram and Marks, 2012; Theos et al., 2005), much like in classical multivesicular endosomes as they mature from

early to late (Gruenberg, 2020). By electron microscopy, we observed intralumenal vesicles (ILVs) in many melan-bf melanosomes (**Figure 3.2b**). Quantification of ILVs revealed that, on average, melan-bf cells contained approximately 10-fold more ILVs per melanosome than did melan-Ink4a cells (**Figure 3.3a**). ILVs serve as the site for fibril nucleation during melanosome biogenesis and thus are critical for melanosome maturation (Berson et al., 2001; Hurbain et al., 2008; Raposo et al., 2001; Theos et al., 2006b), but also may play a role in the distribution of enzymes and transporters in mature melanosomes (Sitaram and Marks, 2012; Theos et al., 2005). We wondered whether this increase in ILVs was a cause or effect of the observed phenotype in melan-bf cells and reasoned that if ILV formation was merely a downstream effect of increased melanosome size, then the number of ILVs per melanosome would correlate with melanosome area. We analyzed the correlation between number of ILVs and melanosome size and determined that the correlation was similar for both melan-Ink4a and melan-bf cells (r^2 = 0.413 and r^2 = 0.418, respectively; **Figure 3.3b**). Therefore, for both melan-Ink4a cells and melan-bf cells, approximately 41% of the variance in ILV number can be explained by the variance in melanosome area. These data suggest that, although factors in addition to melanosome size likely play a role in determining ILV number, the increase in ILV number in melan-bf cells can be partially explained by the increase in melanosome area.

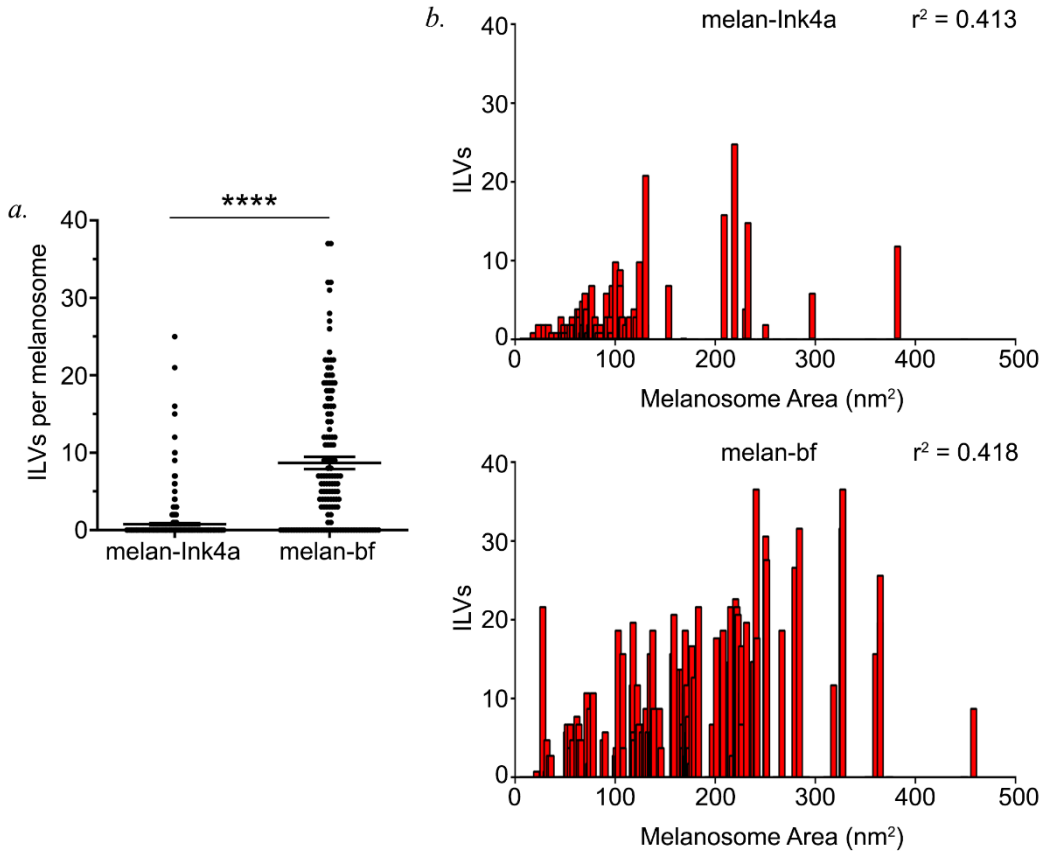

Figure 3.3: Melan-bf cells contain increased ILVs per melanosome due to increased melanosome area. (*a*) The number of ILVs per melanosome as observed by electron microscopy was quantified for melan-Ink4a and melan-bf cells. Data are shown as mean ± SEM from n=1 EM experiment and each closed circle represents one melanosome counted. 369 melanosomes from 36 melan-Ink4a cells and 132 melanosomes from 22 melan-bf cells were analyzed. Statistical analyses were performed using two-tailed Mann-Whitney test. (*b*) The number of ILVs per melanosome versus the melanosome area was graphed and the squared correlation coefficient was determined using GraphPad Prism. Top, melan-Ink4a; Bottom, melan-bf. ****, $p < 0.001$.

3.3.4. Melanosomal genes and proteins are decreased in melan-bf cells.

We wondered if a change in melanosomal gene and protein expression could be observed in melan-bf cells. An increase in melanosomal gene expression may underlie the increase in melanosome size; alternatively, a decrease in melanosomal gene expression may explain the decrease in the number of early stage melanosomes.

Preliminary data from RT-qPCR analyses indicate that mRNA levels of *Vps33a* and the melanosomal genes *Pmel*, *Tyrp1*, and *Tyr* are reduced in melan-bf cells compared to mlean-Ink4a cells (**Appendix Figure 1**). To assess protein levels, cell lysates from melan-Ink4a and melan-bf cells were analyzed by quantitative immunoblotting analyses using antibodies to VPS33A and the endogenous melanosomal proteins tyrosinase (TYR), tyrosinase-related protein 1 (TYRP1) and premelanosome protein (PMEL) (**Figure 3.4a**). The levels of VPS33A and TYRP1 in melan-bf cells were significantly reduced relative to melan-Ink4a, and the levels of TYR and the full-length PMEL P1 precursor were slightly but not significantly reduced (**Figure 3.4**). These data indicate that the VPS33A-D251E mutation causes a reduction in VPS33A gene and protein levels, supporting predictions about the mutation's effect on protein stability based on structural data (Graham et al., 2013), and that this may in turn cause reduced melanosomal gene expression and reduced TYRP1 protein expression. The significant reduction in TYRP1 protein levels and the slight but insignificant reduction in the protein levels of the other melanosomal proteins assayed could be a cause or consequence of melan-bf cells having enlarged, fewer melanosomes. Lower levels of melanosomal proteins may result in a decrease in melanosome biogenesis such that fewer melanosomes are generated but perhaps because the decrease in key melanosomal proteins is not dramatic, there are more melanosomal proteins per melanosome, resulting in increased melanin synthesis and melanosome growth. Alternatively, there may be a reduction in melanosomal proteins because there are fewer melanosomes; perhaps melanosomes become saturated with cargo and excess protein is degraded. How VPS33A controls this and whether this is direct (e.g. if VPS33A is involved in cargo trafficking) or indirect (e.g. if VPS33A function is required in a pathway upstream of MITF-mediated transcription) remains unknown.

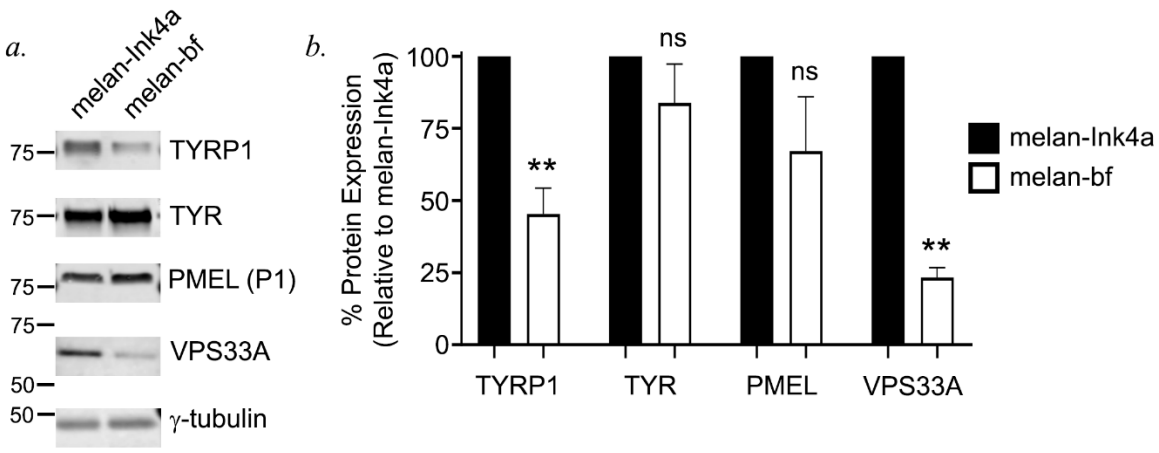

Figure 3.4: TYRP1 and VPS33A protein expression is decreased in melan-bf cells. (*a, b*) Whole cell lysates from melan-Ink4a and melan-bf cells were analyzed by immunoblotting for expression of the indicated melanosomal protein components relative to tubulin levels. A representative immunoblot (*a*) and quantification of band intensity relative to tubulin (*b*) are shown. Data are represented as mean ± SEM from n=3 independent experiments and are normalized to melan-Ink4a at 100%. Statistical analyses were determined by two-tailed Mann-Whitney test. **, $p < 0.01$; ns, no significant difference.

3.3.5. Pigment granules contain TYRP1 but a proportion of TYRP1 is present in a distinct compartment in melan-bf cells.

To assess whether melanosomal protein localization was affected in melan-bf cells, fixed cells were analyzed by bright field microscopy (BFM) and immunofluorescence microscopy with image deconvolution (dIFM) (**Figure 3.5a**). A similar percentage of pigment granules (i.e. melanosomes observed by BFM) colocalized with the melanosomal marker TYRP1 in melan-Ink4a and melan-bf cells (56% vs 62 %, respectively; **Figure 3.5b**). However, a significantly smaller fraction of the total pool of TYRP1 colocalized with pigment granules in melan-bf cells than in melan-Ink4a cells (38% in melan-bf cells vs 75% in melan-Ink4a cells; **Figure 3.5c**). Indeed, whereas in melan-Ink4a cells, the majority of TYRP1 puncta have a characteristic donut shape due to its localization to melanosomal

membranes, the majority of TYRP1 in most melan-bf cells are small puncta distributed throughout the cytosol **(Figure 3.5a**). Given our data (**Figure 3.2**) that melan-bf cells are depleted of early stage melanosomes, these data suggest that in melan-bf cells the majority of TYRP1 is mistrafficked or retained in transport intermediates. They also suggest that the reduction in TYRP1 protein in melan-bf relative to melan-Ink4a might reflect mistrafficking towards lysosomes and consequent lysosomal degradation.

Melanosomes and lysosomes both derive from the endosomal pathway and segregate as early endosomes mature to late endosomes (Raposo et al., 2001). A failure in this segregation could result in enlarged melanosomes, as observed in OA1-deficient melanocytes (Palmisano 2008; Giordano 2009). We thus asked whether these two compartments remained separate in melan-bf cells by assessing the localization of the lysosomal marker LAMP2 relative to pigment granules in melan-Ink4a and melan-bf cells (**Figure 3.5a**). LAMP2 distribution to pigment granules did not differ significantly between melan-Ink4a and melan-bf cells as a percentage of either pigment granules (24% in melan-Ink4a cells and 30% in melan-bf cells; **Figure 3.5d**) or LAMP2 (38% in melan-Ink4a cells and 36% in melan-bf cells; **Figure 3.5e**). However, while the data as a whole are not statistically significant, they do not capture appreciable cell-to-cell variation in melan-bf cells. Indeed, a substantial fraction of melan-bf cells showed an appreciable but low LAMP2 signal surrounding pigment granules (Appendix Figure 2). Nevertheless, the level of overlap between TYRP1 and LAMP2 is even lower in melan-bf cells than in melan-Ink4a (**Figure 3.5f, g**), suggesting that the LAMP2-labeled pigment granules represent a distinct maturation stage from TYRP1. It is possible that there is some degree of either LAMP2 trafficking to melanosomes or fusion between the two compartments, perhaps resulting in TYRP1 degradation. Based on these data, we conclude that TYRP1 is partially

mislocalized in melan-bf cells, that in the majority of cells the lysosomal and melanosomal pathways are well segregated, but that LAMP2 may be incorporated into melanosomes in a subset of melan-bf cells.

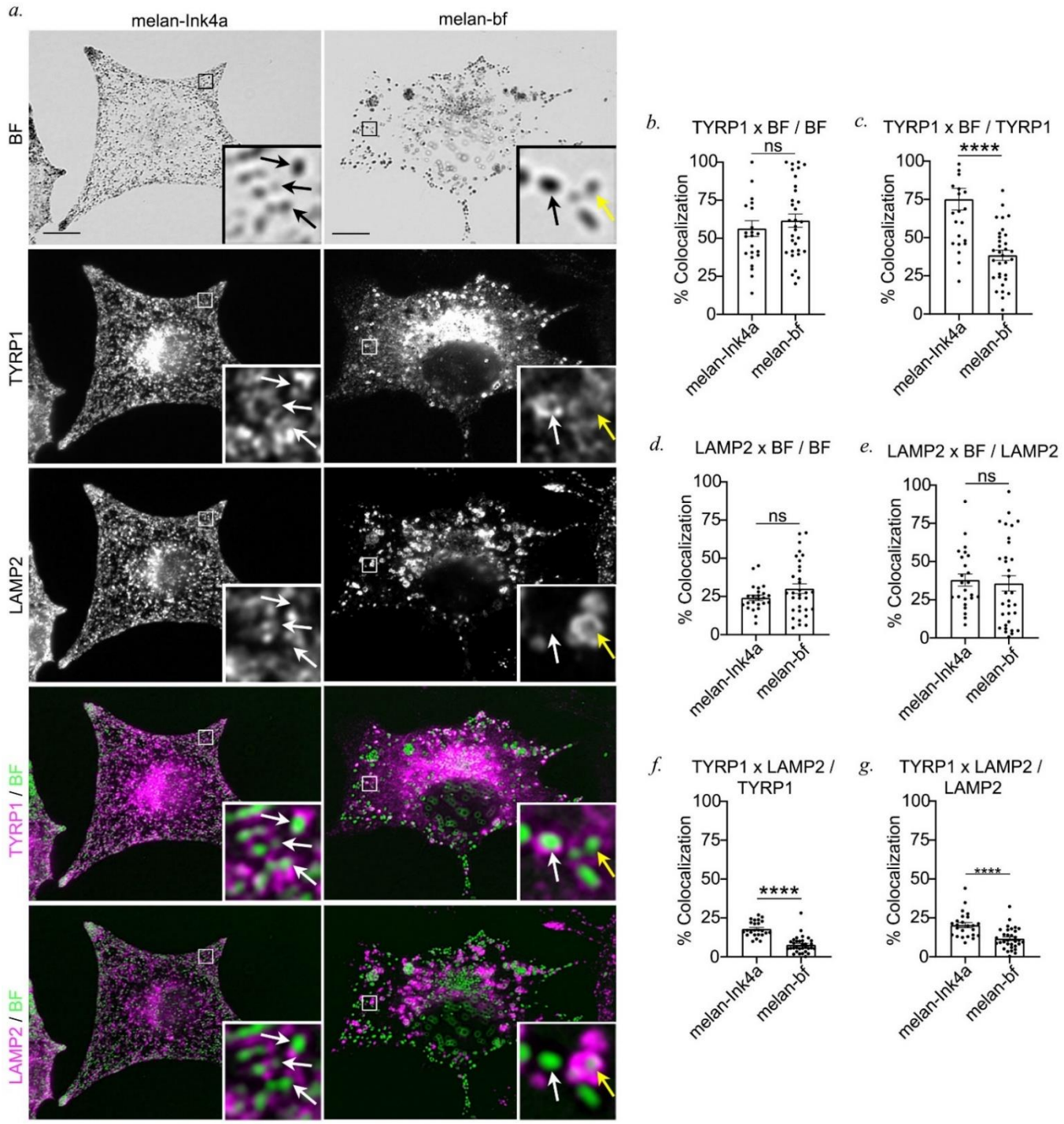

Figure 3.5: Most pigment granules contain TYRP1 but a majority of TYRP1 does not localize to pigment granules. (*a*) Melan-Ink4a and melan-bf cells were fixed, immunolabeled for TYRP1

or LAMP2 (magenta), and analyzed by dIFM and bright field (BF) microscopy to visualize pigment granules. Insets of boxed regions are magnified 7.5 times. Scale bar, 10 µm. TYRP1 (white arrows) or LAMP2 (yellow arrows) that localized to pigment granules are indicated. Imaging was done with a 63X Plan apo lens. (*b*-*e*) Quantification of the percentage of overlap between: TYRP1 and pigment granules as a percentage of pigment granules (*b*) or of TYRP1 (*c*); LAMP2 and pigment granules as a percentage of pigment granules (*d*) or of LAMP2 (*e*). Data are presented as mean ± SEM from n=3 independent experiments with each closed dot representing each cell counted, with 24 melan-Ink4a cells and 32 melan-bf cells counted. Statistical significance was determined using two-tailed Mann-Whitney test. ****, $p < 0.0001$; ns, no significant difference.

3.3.6. The endocytic pathway is normally segregated from melanosomes in melan-bf cells.

Since we observed increased LAMP2 localization to pigment granules in some melan-bf cells, we assessed whether endolysosomal/melanosomal organelle identity was altered by labeling lysosomes with fluorescently labeled endocytosed cargo. Upon endocytosis, internalized materials are trafficked through the endolysosomal pathway to lysosomes. Previous work has shown that endocytosed cargo does not appreciably access melanosomes (Fujita et al., 2001; Raposo et al., 2001). Here, we pulsed melan-Ink4a and melan-bf cells transiently expressing TYRP1-GFP with Alexa Fluor 594-labeled dextran for four hours to allow for dextran uptake. Cells were then washed and chased for 16 hours to allow dextran to accumulate in lysosomes, and then analyzed by live cell confocal fluorescence microscopy. As observed in WT melan-Ink4a cells, TYRP1-GFP and dextran were predominantly in separate compartments in melan-bf cells (**Figure 3.6a**). Some instances of colocalization and sustained contact between the two markers could be observed by video microscopy in both melan-bf and melan-Ink4a (**Figure 3.6b**), but these represented a minority of captured events (data quantification will be forthcoming), and some instances of apparent colocalization are likely due to compartments in different z

planes. By this assay, we see no appreciable differences between the segregation of the endolysosomal and melanosome biogenesis pathways in melan-Ink4a and melan-bf cells.

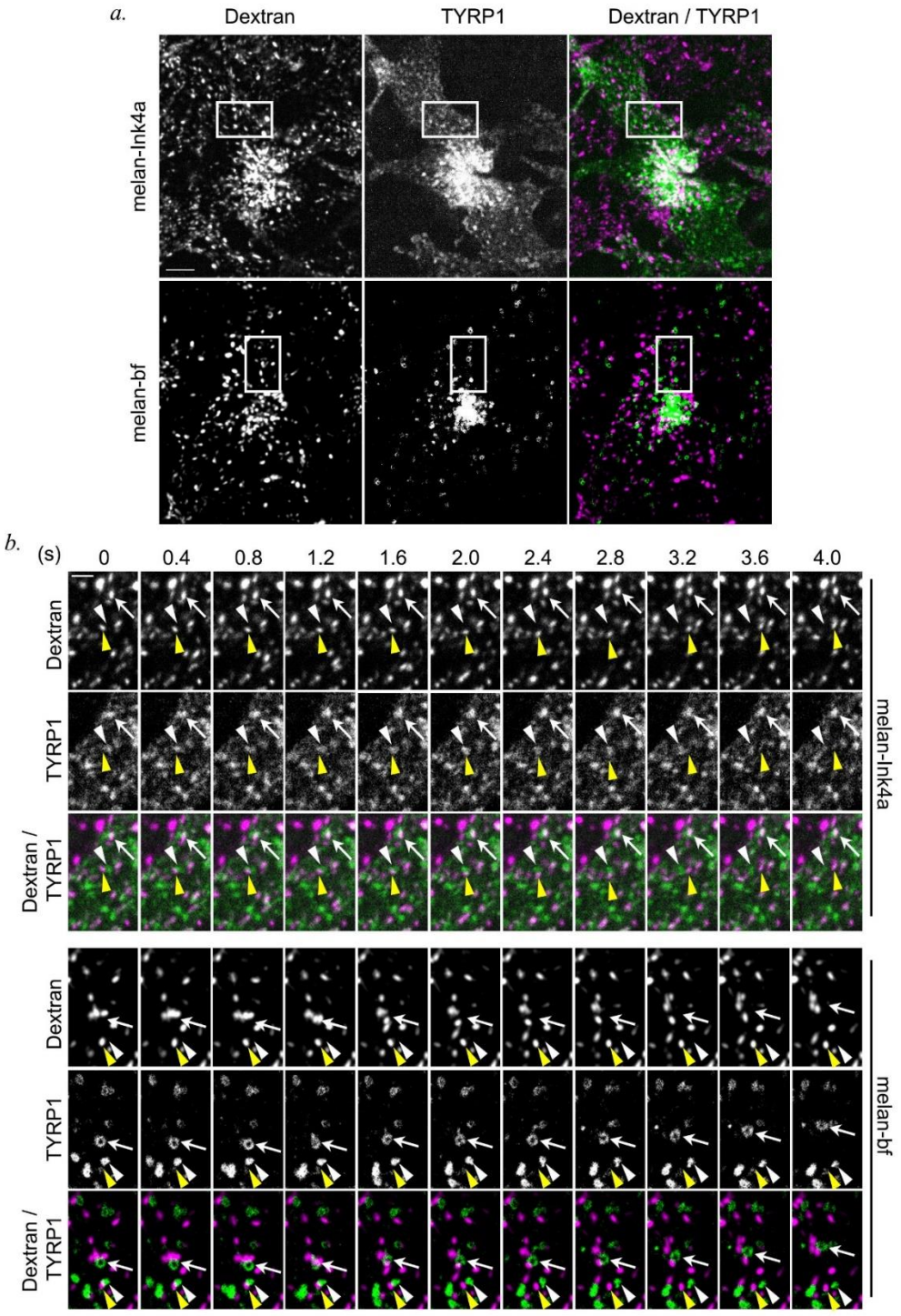

Figure 3.6: The endocytic pathway is segregated from melanosomes in melan-bf cells. (*a*, *b*) Melan-Ink4a and melan-bf cells stably expressing TYRP1-GFP were pulsed with dextran-Alexa Fluor 594 for 4 hours, chased in dextran-free medium, and analyzed 16 h later by spinning-disk confocal microscopy at 2.5 fps using a 100X Plan Apo objective lens. (*a*) Single frames of cells representative of 3 independent experiments showing dextran (left), TYRP1 (middle), or merged images (right). Scale, 5 µm. (*b*) A time-lapse series of the insets in (*a*). The inset of melan-Ink4a cells was rotated 90° counterclockwise. Note that the first frame at time = 0 s is not the same frame as the one shown in (*a*). Arrows show prolonged contact or overlap between dextran-594-labeled compartment and TYRP1-GFP-labeled compartment. White and yellow arrowheads show short contacts between TYRP1-GFP-labeled compartments and dextran-594-labeled compartments, respectively. Note that GFP and Alexafluor594 images were captured simultaneously. Scale, 2 µm.

3.3.7. Knockdown of endogenous VPS33A and overexpression of human VPS33A does not replicate the melan-bf phenotype.

Considering that the phenotype that we observe in melan-bf cells is not the same as that described by Suzuki et al. (Suzuki et al., 2003), we wanted to test whether introduction of the *Vps33a*^{D251E} mutation into WT melan-Ink4a cells would reproduce either phenotype. Initially, we attempted to knock in the *Vps33a*^{D251E} mutation into melan-Ink4a cells using a CRISPR/Cas9-D10A nickase approach (Gasiunas et al., 2012; Mali et al., 2013; Ran et al., 2013), but our attempts were unsuccessful potentially due to inefficient nucleofection in melanocytes. We then tried to knock out the endogenous *Vps33a* gene using a more standard CRISPR/Cas9 approach with paired sgRNAs (Jinek et al., 2012; Ran et al., 2013) with the intention of stably expressing WT VPS33A or VPS33A-D251E in knockout cells. However, we were unsuccessful in isolating a clone that lacked VPS33A expression, perhaps because VPS33A is necessary for viability in immortalized melanocytes. This was supported by a reduction in cell number, either due to cell death or reduced proliferation, upon infection of melan-Ink4a cells with recombinant lentiviruses expressing short hairpin RNAs (shRNAs) targeted to endogenous *Vps33a* relative to

control shRNA-expressing lentiviruses (data not shown); the reduced cell number was prevented upon expression of N-terminally HA-tagged human VPS33A, but not GFP-tagged VPS33A, prior to knockdown of endogenous mouse *Vps33a*. These data suggest that *Vps33a* is essential for viability or proliferation, and that N-terminally HA-tagged VPS33A but not GFP-tagged VPS33A functions properly within HOPS and/or CORVET complexes. Therefore, to assess functionality of VPS33A-D251E in melan-Ink4a cells, we chose the approach of stably expressing HA-tagged control or mutant VPS33A and then knocking down the endogenous *Vps33a* using shRNA-containing lentiviruses.

We hypothesized that the differences in our observed phenotype and the one published by Suzuki et al may be due to a cell adaptation over time (Suzuki et al., 2003). Therefore, we sought to assess cell phenotypes at early and late time points after shRNA knockdown. qPCR analyses in melan-Ink4a cells stably expressing HA-tagged human WT VPS33A and shRNA targeting mouse *Vps33a* or a nontarget control revealed that both shRNAs against *Vps33a* decreased endogenous mRNA levels at 4 days, 6 days, and 8 days post-selection (**Figure 3.7a**). Additionally, expression of human *VPS33A* was high relative to expression of the housekeeping gene tubulin at all time points (**Figure 3.7b**), indicating that these cells overexpress the human gene and that it is not substantially targeted by shRNAs to the mouse gene. The pattern of expression was similar at 14 days post selection with low expression of endogenous *Vps33a* in cells stably expressing *Vps33a*-specific shRNAs and high expression of human *VPS33A* in all three samples (**Appendix Figure 3a, b**). Because enlarged melanosomes are the most consistent and obvious phenotype of our melan-bf cells, we quantified melanosome size in melan-Ink4a cells, melan-bf cells, and melan-Ink4a cells expressing either human WT VPS33A or VPS33A-D251E and shRNA targeting *Vps33a* or a nontarget negative control. Analyses

of cells imaged by bright field microscopy showed that pigment granules in melan-bf cells are significantly larger than in melan-Ink4a cells (**Figure 3.7c, d**), confirming that this quantification method, while less accurate than analyses of EM images, can sufficiently differentiate melanosomes in these populations based on size. However, there was no significant difference in pigment granule size between control melan-Ink4a cells and melan-Ink4a cells expressing WT VPS33A/sh-nontarget, WT VPS33A/sh-*Vps33a*, VPS33A-D251E/sh-nontarget, or VPS33A-D251E/sh-*Vps33a* at 4 days post-selection (**Figure 3.7c, d**). Although there are no significant differences, there is a tendency for enlarged melanosomes to accumulate in cells expressing *Vps33a* shRNA relative to the nontarget control, regardless of which form of human VPS33A they express (**Figure 3.7c, d**). This suggests that knock down of the endogenous mouse VPS33A is the underlying cause, and that HA-tagged human VPS33A may be partially functionally impaired in mouse melanocytes despite 97.5% sequence identity with mouse VPS33A. At 14 days post-selection, the data are more variable but follow similar trends (**Appendix Figure 3c**). These data are thus inconclusive and do not yield firm insights into whether VPS33A-D251E expression results in enlarged melanosomes. These experiments need to be repeated but performing EM and quantifying melanosome area would be more accurate and may yield statistically significant differences.

To determine if our method of knockdown/replacement could potentially provide insights into a hypofunctional *VPS33A* mutant, we also depleted endogenous mouse *Vps33a* in cells overexpressing HA-tagged VPS33A mutants that are hypothesized, based on the structure of Vps33a from the fungus *Chaetomium thermophilum*, to disrupt VPS33A's SNARE binding function. VPS33A consists of 4 domains arranged in a classical SM fold to accommodate SNARE binding and to coordinate SNARE complex assembly

(Baker et al., 2013; Baker et al., 2015; Graham et al., 2013). The D251E mutation lies in the core helix of domain 3a, which is conserved across all SM structures and is proximal to the site of R-SNARE binding (Graham et al., 2013). vSNAREs bind along the length of domain 3a, which has a conserved hinge residue at proline 342 that is proposed to allow flexibility for open/closed conformations to facilitate vSNARE and tSNARE complex binding (Baker et al., 2013; Baker et al., 2015). VPS33A-G308 is a residue in domain 3a that is required for vSNARE binding. Mutagenesis of the yeast ortholog of that residue, G338, to E results in loss of vSNARE binding without affecting tSNARE binding and, when expressed as the only form of Vps33a in yeast, induced the formation of mutant vacuolar structures (Baker et al., 2015). Therefore, we generated a VPS33A-G308E mutant to test how destabilization of vSNARE binding impacts melanogenesis. Additionally, the hinge residue, P342 in human VPS33A, is believed to be important for binding of both vSNAREs and tSNAREs as inflexibility in that residue is predicted to cause steric hindrance and prevent SNARE binding (Baker et al., 2013; Baker et al., 2015). While the importance of this residue has not been documented in published work, we hypothesized that mutating the conserved proline at residue 342 to a tyrosine might interfere with its open/close dynamics and separately might also interfere with tSNARE binding based on structural data (Rick Baker and Fred Hughson, personal correspondence), thereby interfering with SNARE binding in two ways. We also made a P342A mutation which might affect the residue's hinge function but would not otherwise impact the tSNARE binding site.

We stably expressed human VPS33A-G308E, P342A, or P342Y in WT melan-Ink4a cells, and then transduced cells with lentiviruses expressing shRNA to endogenous *Vps33a*. Cells expressing HA-tagged VPS33A-P342Y died even in the presence of endogenous *Vps33a*, suggesting either that this mutant functions in a dominant negative

fashion to inhibit SNARE binding or that there is a mutation in the plasmid outside of the CDS that affects antibiotic selection or causes cytotoxicity. For cells expressing VPS33A-G308E and P342A and knocked down for endogenous *Vps33a*, pigment granule size does not show any consistent quantitative increase relative to those in WT melan-Ink4a cells either at 4 days or 14 days post-selection (**Figure 3.7d** and **Appendix Figure 3**). These data suggest that expression of these variants as the only VPS33A isoform in melan-Ink4a cells either does not cause a melanosome phenotype or that we have not chosen the optimal parameters to assess such a phenotype. Considering that G308 is a conserved residue and that expression of the G308E orthologue in yeast results in a vacuolar trafficking defect, we expect that the homologous mutation would impact VSP33A function in melanocytes. Therefore, in order to draw a conclusion regarding the role of VPS33A in melanosome biogenesis, we will need to assess these cells for the known VPS33A function in endosomal maturation.

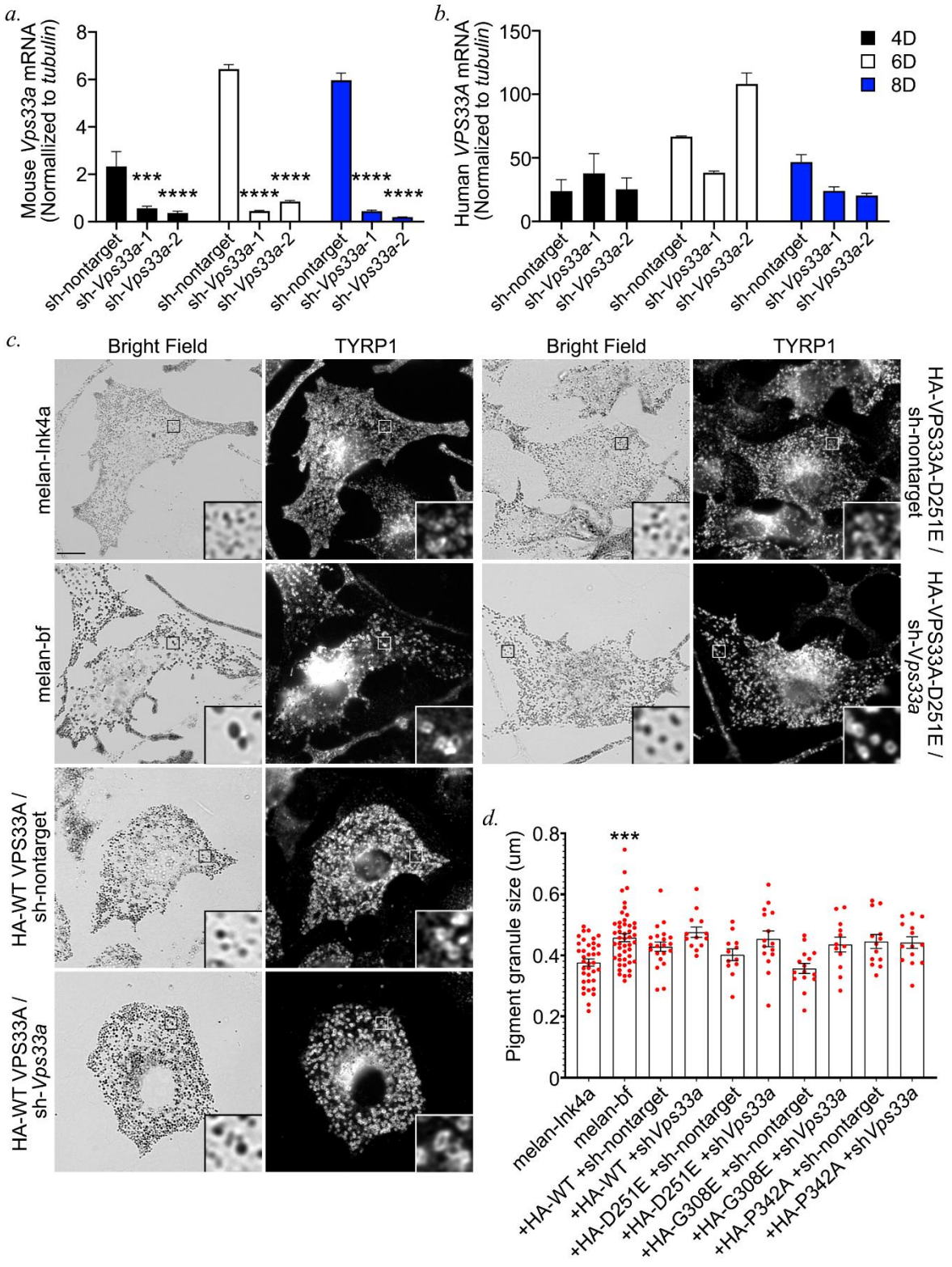

Figure 3.7: Expression of VPS33A variants in Vps33a knockdown cells does not phenocopy melan-bf cells. (*a*, *b*) Melan-Ink4a cells stably expressing HA-tagged WT VPS33A were infected with recombinant lentiviruses expressing nontarget shRNA or either of two shRNAs targeting mouse *Vps33a* and puromycin resistance. Cells were analyzed by qRT-PCR for mouse *Vps33a* mRNA expression (*a*) or human *VPS33A* mRNA expression (*b*) 4 days (black bars), 6 days (white bars), or 8 days (blue bars) post-selection with puromycin. Ct values of target genes were normalized to the Ct values of the housekeeping gene β-tubulin to determine relative expression levels. Statistical significance for values relative to sh-nontarget for each time point was determined using ordinary one-way ANOVA with Sidak's test for multiple comparisons. (*c*) Representative images of melan-Ink4a cells, melan-bf cells, or melan-Ink4a cells stably expressing HA-tagged VPS33A (WT or D251E) and nontarget shRNA or *Vps33a*-1 shRNA at 4 days post-selection. Boxed inset is magnified 5 times. Scale, 10 µm. (*d*) The average pigment granule diameter per cell in µm was quantified and is depicted as mean ± SEM with each dot representing the average pigment granule size in one cell with the following number of cell quantified: 37, melan-Ink4a; 47, melan-bf; 21, +HA-WT +sh-nontarget; 13, +HA-WT +sh*Vps33a*; 12, +HA-D251E +sh-nontarget; 15, +HA-D251E, +sh*Vps33a*; 15, +HA-G308E +sh-nontarget; 12, +HA-G308E, +sh*Vps33a*; 13, +HA-P342A +sh-nontarget; 14, +HA-P342A +sh*Vps33a*. Quantification is from n=2 independent experiments. Statistical significance was determined using one-way ANOVA with Sidak's test for multiple comparisons and comparisons were made to melan-Ink4a cells. Only statistical differences are shown. ***, $p < 0.001$; ***, $p < 0.0001$.

3.4. Discussion

Here we describe melan-bf cells with a different phenotype than what was previously published (Suzuki et al., 2003). These melan-bf cells have enlarged melanosomes with many cells having an accumulation of melanosomes around the cell periphery. We confirm that these cells express the *buff* allele of VPS33A and show that the cells have reduced mRNA and protein levels of VPS33A. Although TYRP1 protein levels are reduced in melan-bf cells, TYRP1 coats the limiting membranes of melanosomes, but the remaining TYRP1 is present in small punctate structures throughout the cytoplasm, suggesting that TYRP1 is partially missorted. Melanosomes appear to segregate normally from the endocytic pathway in melan-bf cells. We were unable to phenocopy melan-bf cells by expressing VPS33A-D251E or other variants with known or predicted SNARE-binding defects, but we hypothesize that experiments with higher resolution (EM) may yield insights into whether VPS33A-D251E causes the observed phenotypes. Overall, we find that dark pigmentation is not incompatible with the VPS33A-D251E mutation; therefore, this mutation does not interfere with an essential transport step in melanosome maturation.

We show that, although most melanosomes in melan-bf cells are marked by TYRP1, the majority of TYRP1 does not colocalize with melanosomes. TYRP1 is distributed in small, punctate structures throughout the cytoplasm by IFM in some melan-bf cells, suggesting altered trafficking. This may reflect a defect in BLOC-1-dependent protein sorting to melanosomes (Setty et al., 2007), or alternatively might be a function of melan-bf cells having fewer melanosomes than WT immortalized melanocytes as a destination for TYRP1 transport carriers. We will further investigate the BLOC-1 transport

pathway in melan-bf cells by assessing the localization of BLOC-1-dependent cargo OCA2 and VAMP7 to determine if they are distributed similarly to TYRP1. Regardless, the fact that a substantial cohort of TYRP1 still localizes to melanosomes in these cells suggests that the VPS33A-D251E mutation does not interfere with an essential step in BLOC-1-dependent transport. However, it is not known whether the other trafficking pathways to melanosomes are affected in melan-bf cells. To determine this, we will quantify localization of tyrosinase (TYR), a cargo of the AP-3-mediated vesicular pathway from endosomes, and DCT and MART-1, cargoes of the RAB6-dependent pathway from Golgi. However, based on the high level of melanization in melan-bf cells, it is likely that VPS33A does not play a critical role in these trafficking pathways. Additionally, our data suggest that the segregation of the endosomal and melanosomal pathways observed in WT melanocytes remains intact in melan-bf cells, as melan-bf and melan-Ink4a cells do not significantly differ in the degree of colocalization between TYRP1 and lysosomes marked by either the lysosomal membrane marker LAMP2 or internalized and chased fluorescent dextran. Together, our data point to a minor impairment in BLOC-1-dependent TYRP1 transport to melanosomes in melan-bf cells, but that this defect is not sufficient to impair the maturation of the reduced number of melanosomes in melan-bf cells or to impede melanization.

Vps33a appears to be essential in mouse melanocytes. We observed that knockdown of VPS33A in melan-Ink4a cells is either lethal or prevents cell proliferation. While the requirement for functional HOPS has been shown previously in mammalian (Peng et al., 2012) and invertebrate animal models (Amsterdam et al., 2004; Lindmo et al., 2006; Maldonado et al., 2006; Pulipparacharuvil et al., 2005; Sadler et al., 2005; Schonthaler et al., 2008; Sevrioukov et al., 1999; Shestopal et al., 1997), this has not been

described in cell lines. Indeed, siRNA-mediated knockdown of CORVET and HOPS subunits in HeLa cells has been used extensively to elucidate the fundamental mechanisms of these complexes in the endocytic and autophagic systems (Banach-Orlowska et al., 2018; Button et al., 2017; Jiang et al., 2014; Kvalvaag et al., 2014; Kvalvaag et al., 2013; Liang et al., 2008; Pols et al., 2013a; Pols et al., 2013b). It is possible that cell death is not observed due to the transient expression of siRNAs and the timing of experiments (72 hours post-transfection in most cases). However, shRNA-mediated knockdown of VPS16 in mouse embryonic fibroblasts (Ganley et al., 2011) and of VPS16 in human osteosarcoma cell line U2OS (Ding et al., 2019) has been described without any cell death or anti-proliferative effects reported, although it is unclear how long knockdown cells were cultured before experiments. One group generated heterogeneous pools of VPS39 knockout or VPS41 knockout HeLa cells that were used in assays 10 days after selection (Banach-Orlowska et al., 2018), potentially indicating that HeLa cells do not require HOPS to survive. However, the authors note that because single cell clones were not generated, mRNA and proteins levels of VPS39 and VPS41 were only reduced by ~50%. Finally, one group showed that, although siRNA-mediated knockdown of VPS33A and of MTOR individually did not reduce cell viability in HeLa cells, knockdown of VPS33A and MTOR together increased cell death (Button et al., 2017). Data in this report suggest that the increased death may be due to the accumulation of autophagosomes due to reduced autophagosome-lysosome fusion (Button et al., 2017). Perhaps immortalized melanocytes are more sensitive to loss of VPS33A than other cell lines due to an increased requirement for autophagy or higher basal levels of autophagy. One group has shown that loss of autophagy in melanocytes due to *Atg7* gene deletion induced cellular senescence (Zhang et al., 2015). Whether VPS33A knockdown causes cell death or

senescence in melanocytes and whether this is due to dysregulated autophagy is of interest. While it is unclear whether VPS33A functions directly in melanosome biogenesis, it is possible that it indirectly modulates melanosome biogenesis through its well-characterized role in the endolysosomal or autophagic systems. Mice with melanocyte-specific deletion of *Atg7* have a mild hypopigmentation phenotype, and knockdown of autophagy-related genes in melanocytes affects pigmentation production (Ganesan et al., 2008; Ho et al., 2011; Zhang et al., 2015), suggesting that autophagy is required for normal pigmentation. As mentioned previously, mutations in HOPS reduce autophagic flux due to its requirement for autophagosome-lysosome fusion (Jiang et al., 2014). Additionally, work from our lab has shown that knockdown of MFSD12, an ion transport protein of unknown function that is localized to lysosomes, increases pigmentation (Crawford et al., 2017), potentially due to disruption of normal lysosomal pH (Shanna Bowman, unpublished results). Therefore, mutations in VPS33A or HOPS may affect melanosome biogenesis and maturation through alterations in endolysosomal or autophagolysosomal homeostasis. The crosstalk between the endolysosomal pathway and melanosomes must be investigated further.

To determine if the *Vsp33a buff* mutation was causative for the melanosome enlargement and TYRP1 mislocalization phenotypes, we attempted to replicate the phenotype by knocking down the endogenous *Vps33a*^{WT} allele in melan-Ink4a cells stably expressing HA-tagged forms of human WT VPS33A and VPS33A-D251E. We did not observe any appreciable differences in melanosome size or TYRP1 localization in cells depleted of endogenous *Vps33a* KD cells and expressing either WT VPS33A or VPS33A-D251E. These data suggest that the *buff* allele may not be responsible for causing the

phenotypes observed in melan-bf cells. Further, expression of HA-tagged human VPS33A, including the D251E, G308E, and P342A mutant forms of VPS33A, was able to rescue the reduction in cell viability or proliferation that we observed in *Vps33a* knockdown cells, indicating that these proteins are largely functional.

Our data directly contradict published observations that melan-bf cells are hypopigmented and that the pigmentation could be rescued by expression of WT mouse VPS33A but not of VPS33A-D251E (Suzuki et al., 2003). Not only do we observe a distinct and opposite phenotype, but we were unable to correct this phenotype by expression of human WT *VPS33A.* The differences in our results cannot be explained by a different source of cells, since our studies were performed with cells obtained from the Spritz lab who published those observations. However, in our hands, 11 out of 12 vials of melan-bf cells shared with us by the Spritz lab, including at least two single cell clones, contained enlarged melanosomes. Why is there a discrepancy between the cells described by Suzuki et al and the cells that they sent to us? It is possible that the *buff* mutation causes cells to be hypopigmented at first but that these cells accumulate enlarged melanosomes over time. However, we at no time observed hypopigmentation during thawing of melan-bf cells. Moreover, our efforts to replicate the *buff* phenotype by knockdown/replacement of *Vps33a* in melan-Ink4a cells failed to show a consistent impact of VPS33A-D251E expression on pigmentation or melanosome size at either 4 or 14 days post-selection, suggesting that any phenotype observed in melan-bf cells might not reflect the *Vps33a* mutation. While it is possible that different culture conditions might underlie these differences, our culture conditions match those reported in Suzuki et al.

The question remains: why do our melan-bf cells look so different from published data? Although the Spritz lab was the first to show images of cultured melan-bf cells in published work, they were not the original group who derived the cells from *buff* mice. The melan-bf cell line was first described by Seth Orlow's group and although they did not publish images of the cells, they stated that "cultured melan-bf cells do synthesize melanin, and are nearly as dark as melan-a cells," which, like melan-Ink4a cells, are WT melanocytes derived from C57BL/6J mice (Samaraweera et al., 1999). While this description does not match the characteristics of our melan-bf cells, it suggests that the cells published by the Spritz lab acquired a hypopigmented phenotype. However, hypopigmented melanocytes better match the pigment dilution observed in *buff* mice, which have a khaki-colored coat rather than a black coat (Dickie, 1964a; Nguyen and Wei, 2004; Samaraweera et al., 1999; Suzuki et al., 2003) and have smaller melanosomes and fewer mature melanosomes observed by TEM in skin (Nguyen and Wei, 2004). The description of melan-bf cells as normally pigmented (Samaraweera et al., 1999) is difficult to judge due to lack of images and the images of hypopigmented melan-bf cells (Suzuki et al., 2003) are low magnification and low resolution; however, that the hypopigmentation can be rescued by expression of $Vps33a^{WT}$ and that melanosomes are smaller *in vivo* suggest that VPS33A-D251E mutations cause decreased pigmentation and melanosome size and that the melan-bf cells described by Suzuki et al. are the true melan-bf cell phenotype (Suzuki et al., 2003). Together, these data suggest that the melan-bf cells we obtained may have developed a secondary mutation that is dominant over the phenotype caused by VPS33A-D251E, which could explain why stable expression of WT VPS33A did not rescue the phenotype in our cells.

What could cause enlarged melanosomes? Increased melanosome size could be due to fusion between melanosomes, fusion of melanosomes with other organelles, or to increased trafficking of melanosomal cargo to maturing melanosomes. If fusion between melanosomes of stages II-IV were to occur, we would expect to see evidence by electron microscopy that the macromelanosomes would contain multiple individual melanosomes with distinct cohorts of PMEL fibrils. This was not the case, and instead we detected melanosomes in melan-bf cells that were large but proportionately normal in shape and fibril content. While it is possible that increased fusion occurs between stage I melanosomes prior to fibril formation, we did not detect any obvious enlargement of vacuolar early endosomes or multivesicular bodies in these cells. Enlarged melanosomes can be found in other models of altered pigmentation, such as in melanocytes with mutations in *Hps1* and *Hps4*, subunits of the biogenesis of lysosome-related organelles complex-3 (BLOC-3) (Dennis et al., 2016; Gardner et al., 1997; Nguyen et al., 2002; Suzuki et al., 2002), or *Gpr143* (Garner and Jay, 1980; Yoshiike et al., 1985). Although melanosomes in epidermal and choroidal melanocytes are enlarged (which may indicate differences in the requirement for BLOC-3 and downstream processes in the different melanocytes and RPE cells), high contrast EM show that these melanosomes appear to be fusion products of smaller melanosomes as the outer membrane of the melanosome is uneven and distinct ovoid regions of electron dense materials can be found within the macromelanosome (Dorothy Bennett, Elena Sviderskaya, and Ray Moss; private communications). This might reflect excessive fusion of mature melanosomes with each other and with late endosomes/lysosomes due to retention of available VAMP7, a SNARE protein involved in fusion events in the late endolysosomal and melanosomal systems (Dennis et al., 2016). However, our data indicate that our melan-bf melanosomes are a

single, enlarged organelle, suggesting that BLOC-3 mutations and melanosome-melanosome fusion are not the underlying mechanism for our melan-bf phenotype. Finally, our data suggest that increased trafficking of TYRP1 to melanosomes does not occur in our melan-bf cells since an increased proportion of TYRP1 appears to be mistrafficked. However, whether this is true of other melanosomal cargo or whether specific melanosomal transport pathways are aberrantly affected in melan-bf cells remains to be seen.

The phenotypes observed in our melan-bf cells has similarities to those of patients with ocular albinism type 1 (OA1) and OA1 mouse models (Garner and Jay, 1980; Yoshiike et al., 1985). OA1 is an X-linked form of albinism with more prominent impact in the eye and is caused by loss-of-function mutations in the G-protein-coupled receptor (GPCR) GPR143 (also known as OA1) (Innamorati et al., 2006; Schiaffino et al., 1999). GPR143 is hypothesized to regulate multiple aspects of melanosome biology, and it seems to play a critical role in the early stages of melanosome biogenesis. GPR143 expression on multivesicular bodies (MVB) appears to prevent their fusion with lysosomes (Burgoyne et al., 2013), potentially defining the MVB subset that will mature into melanosomes. Indeed, analyses of the immediate effects of GPR143 knockdown show enlarged stage II melanosomes with disorganized fibrils (Giordano et al., 2009). Stable knockdown of GPR143 results in an accumulation of enlarged stage IV melanosomes, a decrease in stage II melanosomes, and concentration of melanosomes around the cell periphery (Cortese et al., 2005; Garner and Jay, 1980; Incerti et al., 2000; Palmisano et al., 2008; Yoshiike et al., 1985), indicating that long-term GPR143 knockdown results in a different phenotype than what is seen immediately after GPR143 knockdown. EM

analyses of the enlarged melanosomes in *Gpr143* knockout (KO) mice show a dense core of melanin in the center surrounded by a halo of melanin, suggesting that these enlarged melanosomes are a result of excess growth and melanization of a single melanosome rather than fusion of multiple melanosomes, which would be expected to look disorganized in mature stages (Incerti et al., 2000). A dense core can be seen in some of our enlarged melan-bf melanosomes (**Figure 3.2b**), indicating that increased growth and not increased fusion may be the cause of increased melanosome size in our melan-bf cells. GPR143 localizes to early and late stage melanosomes, where its ligand-binding site is in the melanosomal lumen and its downstream signaling pathway is in the cytoplasm (Schiaffino et al., 1999). Data indicate that GPR143 also localizes to the lysosomal pathway (Giordano et al., 2009; Piccirillo et al., 2006), but whether GPR143 functions similarly in both pathways is unknown. The endogenous ligand for GPR143 is unknown; one group proposes that it is L-DOPA, allowing GPR143 to act as a sensor for melanin synthesis (Lopez et al., 2008), but this is highly controversial. GPR143 signaling regulates the expression of *Mitf* (Chen et al., 2016; Falletta et al., 2014), a transcription factor that controls melanosomal gene expression and regulates melanocyte biology. Additionally, GPR143 signaling might also regulate the switch between microtubule-dependent melanosome transport towards the perinuclear region and actin-dependent transport towards the cell periphery, explaining why loss of GPR143 results in exclusion of melanosomes from the perinuclear area (Palmisano et al., 2008). Because many of the characteristics of GPR143 mutant cells have also been observed in our melan-bf cells, we hypothesize that the GPR143 signaling pathway may be impacted in our melan-bf cells.

Overall, we show that melanocytes expressing point mutations in VPS33A are able to synthesize melanin and undergo melanosome maturation. These data raise questions about whether VPS33A functions directly in the melanosomal pathway. Additionally, these data suggest that a secondary mutation arose in melan-bf cells that is responsible for the phenotypes observed.

3.5. Materials and Methods

3.5.1. Reagents

Unless otherwise specified, chemicals were obtained from Sigma-Aldrich (St. Louis, MO) and tissue culture reagents from Life Technologies/Thermo Fisher Scientific (Waltham, MA). Protease inhibitors were purchased from Roche Diagnostics (Rotkreuz, Switzerland), gene amplification primers from Integrated DNA Technologies (Coralville, IA), GoTaq DNA polymerase from Promega Corp. (Madison, WI), and restriction enzymes and T4 DNA ligase from New England Biolabs (Ipswich, MA).

3.5.2. Cell culture

Immortalized melanocyte cell lines "wild-type" (WT) melan-Ink4a-Arf1$^{-/-}$ (formerly called melan-Ink4a-1; referred to here as melan-Ink4a or WT) from C57BL/6J-*Ink4a-Arf*$^{-/-}$ (*Cdkn2* null) mice (Sviderskaya et al., 2002) and melan-bf cells (Samaraweera et al., 1999) have been described and were derived from the skins of neonatal mice. Numbered vials of melan-bf cells (#1, #2, etc) were generously provided by Richard Spritz (Suzuki et al., 2003) and for figures 2-7, only melan-bf #1 cells, referred to as melan-bf, were used because they were uniform in phenotype. The immortalized melanocyte line melan-coa has been described and was derived from the skins of neonatal C57BL/10J-*Hps3*$^{coa/coa}$ mice (Suzuki et al., 2001). Melan-coa cells stably expressing HPS3 were used as a positive control for the expression of the hygromycin resistance gene. All cells were cultured at 37°C and 10% CO_2 in RPMI 1640 medium supplemented with 20% FBS (Atlanta Biologicals) and 200 nM 12-*O*-tetradecanoylphorbol-13-acetate (TPA). Melan-Ink4a and melan-coa cells are typically grown in 10% FBS but were changed to medium containing 20% FBS 2-3 days prior to an experiment in order to keep conditions consistent

between all cell lines. Cell lines were authenticated by allele-specific amplification of the *Vps33a* gene and were verified to be negative for mycoplasma every 2-3 months using the MycoAlert Mycoplasma Detection Kit (Lonza).

Retrovirus production from transiently transfected Plat-E cells (Morita et al., 2000b) and retroviral transduction of melanocyte cell lines were carried out as described previously (Meng et al., 2012b; Setty et al., 2007). Briefly, Plat-E cells were transfected with retroviral DNA constructs using Lipofectamine 2000 (Thermo Fisher), and the medium was replaced the next day. Retrovirus-containing supernatants were collected 48 h later, filtered, and added to melan-Inka4, melan-bf, or melan-coa cells in a 1:1 ratio with fresh medium and TPA. The medium was replaced the next day, and pools of stable transductants were selected 24 h later by adding 300 µg/mL hygromycin B to the medium. Stable transfectants were occasionally treated with 200 µg/mL hygromycin B for 2-3 d to maintain selective pressure for the transgene.

To produce lentivirus, HEK-293T cells were transfected with lentiviral DNA constructs using Lipofectamine 2000 (Thermo Fisher), and the medium was replaced the next day. Lentivirus-containing supernatants were collected 48 h later, filtered, and added to melan-Ink4a cells in a 1:1 ratio with fresh medium and TPA. The medium was replaced the next day, and pools of stable transductants were selected 24 h later by adding 2 µ/mL puromycin to the medium.

3.5.3. DNA constructs

The pBMN-IRES-hygro XN plasmid encoding HA-tagged human wild-type VPS33A and GFP-tagged human wild-type VPS33A were generated by subcloning the NotI-HA-VPS33A-XhoI or NotI-GFP-VPS33A-XhoI cDNA fragments from pEGFP-C3-

VPS33A into the pBMN-IRES-hygro XN vector (Setty et al., 2007). pBMN-IRES-hygro XN plasmids encoding HA-tagged or GFP-tagged VPS33A mutants D251E, G308E, P342A, and P342Y were generated by site-directed mutagenesis using the Q5 Site-Directed Mutagenesis Kit (New England Biolabs) on the WT VPS33A plasmids according to manufacturer's protocol. The pBMN-IRES-Hygro-X/N-TYRP1-EGFP encoding EGFP-tagged human TYRP1 and pBMN-hHPS3-IRES-Hygro N/X encoding human HPS3 have been described (Dennis et al., 2015).

pLKO.1-puromycin derived lentiviral vectors (Stewart et al., 2003) for small hairpin RNAs (shRNAs) against *Vps33a* and non-target shRNAs were obtained from the High-throughput Screening Core of the University of Pennsylvania. *Vps33a* #1 sense sequence: GCG ACC ACT AAA CTG ATG AAT; *Vps33a* #2 sense sequence: GCT GAT GTC AAG AAC ATC ATT; non-target sense sequence: GCG CGA TAG CGC TAA TAA TTT

All constructs were verified by sequencing by the Nucleic Acid/Protein Research Core Facility at the Children's Hospital of Pennsylvania, the Center for Applied Genomics Sequencing Core at the Children's Hospital of Pennsylvania, or by the University of Pennsylvania Cell Center.

3.5.4. Antibodies

Primary antibodies and their sources (listed in parentheses) include: mouse monoclonal antibody TA99/Mel5 to TYRP1 (American Type Culture Collection; Rockville, MD); rat anti-LAMP2 (GL2A7; Developmental Studies Hybridoma Bank); rabbit anti-PEP7h-msm to the cytoplasmic domain of TYR (Berson et al., 2000); rabbit anti-PEP13 to the C-terminus of PMEL (Berson et al., 2001); rabbit anti-TYRP1 (H-90; Santa Cruz); rabbit anti-VPS33A (16896-1-AP; ProteinTech); and mouse anti-γ-tubulin (GTU88;

Sigma). Species-specific secondary antibodies from donkey and conjugated to Alexa Fluor 488 or 594 were used for dIFM or to IRDye-790CW or IRDye-680LT for immunoblotting were obtained from Jackson ImmunoResearch Laboratories, Inc. (West Grove, PA).

3.5.5. PCR and Touchdown PCR

RNA was extracted from pelleted cells using the RNeasy Plus Mini kit (Qiagen) and DNase treatment (Invitrogen). cDNA was synthesized using 1 ug RNA per reaction with the High Capacity RNA-to-cDNA kit (Applied Biosystems) according to manufacturer's instructions and the resulting cDNA was used for PCR or Touchdown PCR (Korbie and Mattick, 2008) using 2X GoTaq Green Master Mix (Promega) and PCR products were analyzed on a 2% agarose gel containing SYBR Safe DNA Gel Stain (Invitrogen). Primers used are as follows:

Vps33a – F: 5' GTG TTC CCC GTG TTT GAT AAC C 3' and R: 5' GCG TTG AAG TTC TTG TCT CGG 3'

Vps33a (WT allele encoding D251) – F: 5' CTC ACG TAT GAA GGC CTC ATC TAT 3' and R: 5' GCG TTG AAG TTC TTG TCT CGG 3'

Vps33a (*buff* allele encoding D251E) – F: 5' GTG TTC CCC GTG TTT GAT AAC C 3' and R: 5' GTT CTG AAT GCC GTA AAT CCC C 3'

Hygromycin resistance gene – F: 5' TGG CAA ACT GTG ATG GAC GA 3' and R: 5' GGC GAC CTC GTA TTG GGA AT 3'

PCR for *Vps33a* was run as follows: 1. 95°C, 3 min; 2. 95°C, 30 sec; 3. 56°C, 30 sec; 4.72°C, 30 sec; 5. Repeat from step 2 for 35 cycles; 6. 72°C, 5 min; 7. 12°C, hold.

PCR for the hygromycin resistance gene was the same except step 3 was performed at 67°C.

Touchdown PCR for allele-specific priming was run as follows: 1. 95°C, 3 min; 2. 95°C, 30 sec; 3. 61°C, 30 sec; 4. 72°C, 30 sec; 5. Repeat from step 2 for 7 cycles @ -1°C/cycle; 6. 95°C, 30 sec; 7. 53°C, 30 sec; 8. 72°C, 30 sec; 9. Repeat from step 6 for 20 cycles; 10. 72°C, 5 min; 11. 12°C, hold.

3.5.6. Bright field microscopy (BFM), immunofluorescence microscopy (IFM), and area occupied and colocalization analyses

BFM and IFM analyses of fixed cells were done essentially as described (Dennis et al., 2016). Briefly, cells were plated on Matrigel (BD)-coated coverslips, fixed with 4% formaldehyde (VWR) in PBS, labeled for IFM with primary and secondary antibodies diluted in PBS/0.02% saponin/0.01% BSA, mounted onto slides using Prolong Gold (ThermoFisher) and anlyzed on a Leica DMI-6000 microscope equipped with a 63x or 100x objective lens (Leica; 1.4 NA), a Hamamatsu Photonics ORCA-Flash4.0 cMOS C11440-22CU digital camera, and Leica Application Suite X (LAS X) software. Images in sequential z planes (0.2 µm step size) were deconvolved using Microvolution software (Biovision Technologies) and further analyzed with ImageJ (http://fiji.sc/Fiji; National Institutes of Health).

The percent area occupied within a cell was quantified using ImageJ on wide-field bright field images. Single z planes of cells were cropped and binary images were generated using the Make Binary tool. A region of interest (ROI) excluding the nucleus and perinuclear area was drawn and the Analyze Particles function with particles from 0.1-2 µm included was used to calculate the percent area occupied.

Because TYRP1 localized to melanosomes in a donut-shape and thus did not fully overlap with pigment granules, automated counting could not be reliably used to quantify colocalization. Therefore, quantification of overlap between channels was performed manually and quantification of single channels was automated, both in ImageJ. In brief the following method for manual quantification of overlap was used: single-channel images and a merged image were synchronized using “Analyze > Tools > Synchronize Windows;” a ROI excluding the nucleus and perinuclear area was drawn around the cell; and signals that were localized to the same organelle were counted using the “Multi-Point” tool. For quantification of single channels: a thresholded image was generated using the Auto Local Threshold Tool (Bernsen method); a binary image was generated using the Make Binary tool and Watershed segmentation was performed to ensure close particles were counted separately; the same ROI used to quantify overlap was applied to the image; and the Analyze Particles tool with particles from 0.1-2 µm included was used to calculate the number of particles sin the ROI. The number of particles manually counted in the overlapped images was divided by the number of particles quantified in the single channels to calculate percent colocalization.

3.5.7. Melanin Content Assay

Melanin quantification by spectroscopy was done essentially as described (Delevoye et al., 2009b). Briefly, melanocytes seeded on 6-cm dishes were trypsinized, pelleted, and sonicated in melanin buffer (50 mM Tris, 2 mM EDTA, and 150 mM NaCl, pH 7.4) supplemented with protease inhibitor cocktail (Roche). Insoluble material was pelleted for 15 min at 16,000 g (4°C), rinsed in ethanol/diethyl ether (1:1), and dissolved in 2 MNaOH/20% DMSO at 60°C. The optical density at 492 nm was measured to estimate

melanin content and normalized to protein concentration as determined by BCA protein determination kit (Thermo Fisher). Plat-E cells, an unpigmented cell line, were used as a negative control and normalized values from Plat-E cells were subtracted from experimental samples. Data were normalized to melan-Ink4a cells. Statistical significance was determined by two-tailed Mann-Whitney test.

3.5.8. Electron microscopy

Melanocytes were cultured in 10-cm dishes and fixed in situ with Karnovsky's fixative [4% paraformaldehyde (VWR Scientific, Radnor, PA), 4 mM calcium chloride, 72 mM sodium cacodylate, pH 7.4] containing 0.5% glutaraldehyde (Polysciences, Warrington, PA) for 1–2 h at room temperature. This solution was then removed and replaced with Karnovsky's fixative containing 2% glutaraldehyde, and the cells were fixed overnight at room temperature. Cells were collected by scraping using a cell scraper and centrifugation at 27 x g for 5 min, resuspended in Karnovsky's fixative containing 0.5% glutaraldehyde, and stored at 4°C until processing. After subsequent buffer washes, the samples were post-fixed in 2.0% osmium tetroxide with 1.5% $K_3Fe(CN)_6$ for 1 hour at room temperature, and then rinsed in deonized water prior to en bloc staining with 2% uranyl acetate. After dehydration through a graded ethanol series, the tissue was infiltrated and embedded in EMbed-812 (Electron Microscopy Sciences, Fort Washington, PA) at the Electron Microscopy Resource Laboratory (University of Pennsylvania). Thin sections were stained with uranyl acetate and SATO lead and examined with a JEOL 1010 electron microscope fitted with a Hamamatsu digital camera (Hamamatsu, Bridgewater, NJ) and

AMT Advantage NanoSprint500 software (Advanced Microscopy Techniques, Woburn, MA).

For melanosome area measurement, an ROI was drawn around each melanosome and the "Measure" tool was used in ImageJ. Images were calibrated using the scale bar in each EM image and the area measurements were reported in nm^2. Data were graphed using Prism 8 and statistical significance was determined by two-tailed Mann-Whitney test.

For melanosome staging, melanosomes were analyzed for each cell line, the number of stage I/II, stage III, and stage IV melanosomes were quantified, and the percentage of melanosomes at each stage was calculated for each cell. These data were analyzed and plotted using Prism 8 (GraphPad, La Jolla, CA), and statistical significance was determined by two-tailed Mann-Whitney test**.**

For ILV quantification, the number of ILVs per melanosome was manually counted. Data were graphed using Prism 8 and statistical significance was determined by two-tailed Mann-Whitney test. The number of ILVs per melanosome was cross-referenced with melanosome area to generate an XY graph and the correlation between the two variables was calculated using Prism 8 to determine r^2.

3.5.9. Immunoblotting

Melan-Ink4a cells and melan-bf cells were cultured in 60mm or 100 mm dishes and collected for immunoblot. Cells were rinsed in cold PBS before pelleting by centrifugation. Cell pellets were resuspended in 1X Laemmli buffer (Laemmli, 1970), lysed by sonication, and heated at 95°C for 5 minutes. Protein concentration for each sample was measured using the BCA assay (Pierce) according to the manufacturer's protocol. 40

µg protein from each sample was fractionated by SDS-PAGE on 10% polyacrylamide gels, and transferred to PVDF membranes (Immobilon-FL, Millipore). Membranes were blocked with 5% milk in TBS, incubated overnight with primary antibodies diluted in TBS/0.5% Tween, washed with TBS/0.5% Tween, and analyzed using Alexa Fluor 680 or 790-conjugated secondary antibodies and Odyssey imaging system (LI-COR, Lincoln, NE). Band intensities were quantified in ImageJ. The background for each blot was subtracted from the signal and normalized to background-subtracted loading control (tubulin). Statistical significance was determined using two-tailed Mann-Whitney test.

3.5.10. RT-qPCR

Total RNA was extracted from cells using the RNeasy Plus Mini Kit (Qiagen) and was DNase treated (Invitrogen). Reverse transcriptase reactions were performed with 1 µg of RNA using the High Capacity RNA-to-cDNA kit (Applied Biosystems) and the resulting cDNA was used for qPCR. Results were quantified using real-time PCR with SYBR Green Dye on an Applied Biosystems 7900HT Fast Real-Time PCR System (ThermoFisher Scientific). Primers were designed using Primer3 (http://bioinfo.ut.ee/primer3-0.4.0/) to span an exon-exon junction to avoid amplification of contaminating genomic DNA, and were as follows:

Vps33a (NM_029929.3): F: 5' – GTT CGA GGA GCG ACA CAA CG – 3' and R: 5' – AAT TGA GGT GTG GTT GGC GA – 3'

VPS33A (NM_022916.6): F: 5' GCA GCA TTC GAG GAA AGA CA – 3' and R: 5' – GTG GGG CAA CTG GGA AA CAA – 3'

Tyr (NM_011661.5): F: 5' – CCT CCT GGC AGA TCA TTT GT - 3' and R: 5' GGC AAA TCC TTC CAG TGT GT - 3'

Tyrp1 (NM_031202.3): F: 5' – AAG TTC AAT GGC CAG GTC AG -3' and R: 5' TCA GTG AGG AGA GGC TGG TT -3'

Pmel (NM_021882.4): F:5' - GCA CCC AAC TTG TTG TTC CT - 3' and R: 5' – GTG CTA CCA TGT GGC ATT TG - 3'

Tubb4b (NM_146116.2): F: 5' – CGC ATC AAC GTG TAC TAC AAC G - 3' and R: 5' – ACA ACG TCC AAC ACC GAG TC – 3'

Tubulin (*Tubb4b*) was used as an internal control and all reactions were run in triplicate. mRNA levels were quantified by calculating average $2^{-\Delta\Delta Ct}$ values, where Ct is the cycle number for the control and target transcript at the chosen threshold. $\Delta Ct = Ct_{target} - Ct_{tubulin}$ was calculated by subtracting the average Ct of tubulin from the average Ct of the target transcript. The ΔCt_{mean} was calculated for the reference sample (melan-Ink4a; or sh-nontarget) and $\Delta\Delta Ct = \Delta Ct - \Delta Ct_{mean}$ was calculated by subtracting the ΔCt_{mean} from the ΔCt. The relative mRNA expression of samples compared to the reference samples was calculated by $2^{-\Delta\Delta Ct}$.

3.5.11. Dextran Pulse-Chase and Live Cell Fluorescence Imaging

Melan-Ink4a and melan-bf cells were plated onto 35mm glass-bottom dishes and supernatant containing TYRP1-GFP-expressing retroviruses was added in a 1:1 ratio with fresh medium the next day. 24 h later, cells were rinsed 2X with dPBS and cells were incubated with 250 µg/mL dextran-594 (D22913; Thermo Fisher) diluted in serum-free medium for 4 hours at 37°C in 10% CO_2. After the 4 h pulse, cells were gently washed 3X with sterile dPBS and incubated in melanocyte medium overnight (~16 h) for live imaging the next day. Before imaging, the medium was switched to Lebovitz's CO_2-independent

medium without phenol red (Invitrogen) supplemented with 10% FBS and imaging was performed in an environmental chamber set to 37°C with 10% CO2. Confocal fluorescence images were acquired using a DMI8 inverted microscope (Leica Biosystems) equipped with a spinning disc system (VisiScope CSU-W1), a 100X TIRF objective (1.47 NA), and a Hamamatsu Photonics ORCA-Flash 4.0 sCMOS digital camera with W-VIEW GEMINI Image splitting optics for the simultaneous acquisition of dual wavelengths. Single plane images of 488 nm and 594 nm channels were simultaneously captured every 400 ms for 30 s. Images were processed and analyzed using Image J.

3.5.12. Statistical analyses

Statistical data are presented as mean ± SEM. Statistics were calculated in GraphPad Prism 8 using: unpaired two-tailed t test or one-way ANOVA with Sidak's post hoc test for multiple comparisons for normally distributed data; two-tailed Mann-Whitney test for data not normally distributed; or Welch's ANOVA with Dunnett's T3 test for data displaying heteroscedasticity. Normality and heteroscedasticity were determined in GraphPad Prism. Significant differences between samples are indicated (****, $p < 0.0001$; ***, $p < 0.001$; **, $p < 0.01$; *, $p < 0.05$). Only $p < 0.05$ was considered statistically significant.

CHAPTER 4: DISCUSSION

4.1. Data Summary

Melanin is required for protection from UVR and oxidative damage and its synthesis is necessary during development for the normal formation of the visual system. Loss of normal melanin production results in albinism. Mouse models of albinism have been critical for studying the roles of genes involved in albinism, including most known genes for which mutations have been identified in human patients with albinism and a few additional genes that have not. Therefore, further investigation of mouse models of albinism may yield insights into the basic cellular biology underlying melanogenesis and may identify genes that can be included in albinism gene panels. We have been investigating two mouse models of albinism – the *underwhite* mouse model of human OCA type 4, which has a mutation in *Slc45a2*, and the *buff* mouse, which has a mutation in *Vps33a* – to understand how the proteins encoded by these genes are involved in melanosome biogenesis and maturation. The work presented in this dissertation (1) defined a role for SLC45A2 on melanosomes to regulate pH and (2) characterized alterations in the melanosomal and endolysosomal pathways in *buff* melanocytes.

In Chapter 2, we found that the putative sugar/proton symporter SLC45A2 localizes to melanosomes, where it is required for the progression of melanosomes from stage III to stage IV. We show that in a heterologous system, SLC45A2 increases the pH of lysosomes to which it localizes, indicating that it likely retains its putative sugar/proton transport activity at melanosomes to transport protons and sugars from the melanosomal lumen to the cytosol. We show that SLC45A2 exists on a subset of melanosomes that only partially overlaps with the subset harboring the chloride channel OCA2, which based

on our data we hypothesize to be due to SLC45A2's stability on maturing melanosomes as opposed to OCA2's short half-life. We show that OCA2 can compensate for loss of SLC45A2 but that SLC45A2 cannot compensate for loss of OCA2, likely reflecting differences in the magnitude of ion transport between a channel protein and a transporter protein. Based on these results, our model is that, whereas OCA2 is required to slow or inhibit V-ATPase activity, SLC45A2 is required for the gradual expulsion of protons from the melanosomal lumen to raise melanosomal pH (**Figure 4.1**). Furthermore, we show that a common SLC45A2 variant associated with decreased skin, hair, and eye pigmentation results in decreased protein expression due to increased protein degradation. It remains to be seen whether the variant protein functions properly; however, a study showed that a mutation analogous to L374F in the SLC45A2 ortholog OsSUT1 resulted in decreased sucrose transport but no change in substrate affinity (Reinders and Ward, 2015b). Our data reveal that the observed decrease in pigmentation in cells expressing SLC45A2-F374 correlates with a decrease in total SLC45A2 protein, suggesting that lower SLC45A2 levels on melanosomes leads to reduced proton export and reduced neutralization of the melanosomal lumen. Our findings indicate that SLC45A2 is a melanosomal protein involved in pH regulation and required for melanosome maturation.

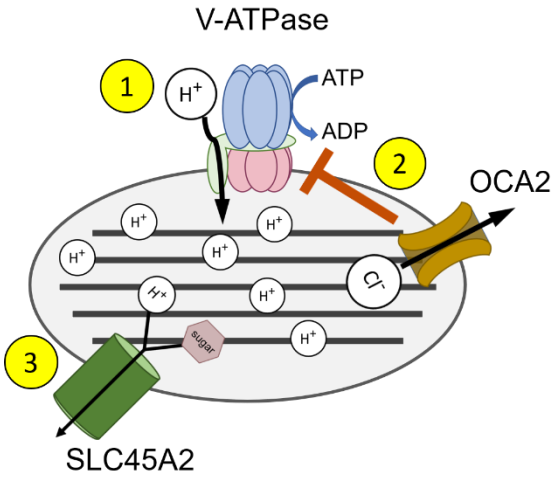

Figure 4.1. Model of SLC45A2 function in melanosome pH regulation. (1) V-ATPase promotes melanosome acidification by pumping protons into the lumen. (2) OCA2 activity slows or stops V-ATPase activity to reduce acidification by exporting chloride ions and thus altering membrane potential. (3) SLC45A2 actively deacidifies the melanosome by transporting protons out of the lumen.

In Chapter 3, we characterized melan-bf cells, immortalized melanocytes derived from the *buff* mouse model. We show that, despite a mutation in VPS33A, melanogenesis was able to occur but that melanosomes were reduced in number and larger compared to those in WT melanocytes. Furthermore, we show that these cells have reduced expression of VPS33A and the melanosomal protein TYRP1, and that although melanosomes still harbor TYRP1 as in WT cells, a significant proportion of TYRP1 is aberrantly distributed in punctate structures throughout the cytoplasm in melan-bf cells. We attempted to determine if the VPS33A-D251E mutation in melan-bf cells caused this phenotype, but although our results were inconclusive and we will need to perform additional experiments and assess cells at longer time points, the preliminary data suggest that the mutation is not responsible for the phenotype. Overall, we show that melan-bf cells are hyperpigmented despite having VPS33A-D251E mutation and have a phenotype

similar to that of melanocytes and RPE cells from $Oa1^{-/-}$ mice, the mouse model of OA1, indicating that melanogenesis can proceed even in the presence of the *buff* mutation.

Our studies of mouse models of albinism have raised questions about ion regulation and the potential role of VPS33A during melanosome biogenesis. The purpose of this chapter is to discuss open questions and future directions pertaining to these topics.

4.2. Future Directions

4.2.1. Is there a functional role for SLC45A2 punctate structures?

Our data show that SLC45A2 can form discrete puncta on the melanosomal membrane, and that this "microdomain" distribution is even more consistent and pronounced at the lysosomal membrane when SLC45A2 is expressed in non-pigmented cells. Membrane microdomains containing ion transporters have been described, particularly as a mechanism for calcium signaling (Filadi and Pozzan, 2015). Whether these SLC45A2 puncta form a functional microdomain are unclear but is an intriguing question that we would like to test.

Ideally, we would like to directly determine the relationship between puncta formation and transporter activity. One method to test this was used to analyze the puncta formation and activity of stromal interacting molecule 1 (STIM1), a calcium sensor and calcium channel activator at the endoplasmic reticulum (Wu et al., 2006). By total internal reflection fluorescence (TIRF) microscopy of GFP-labeled STIM1 and whole-cell patch clamp recordings to measure calcium entry by the STIM1-activated Ca^{2+} release–activated Ca^{2+} (CRAC) channel, it was determined that STIM1 puncta formation always immediately preceded calcium transfer (Wu et al., 2006). However, this is not a feasible experiment in our system for two reasons: (1) SLC45A2 is on melanosomes and, although

patch-clamping has been successfully performed on purified, manipulated melanosomes (Bellono et al., 2014; Bellono et al., 2016), purification of melanosomes may alter SLC45A2 puncta dynamics and function; and (2) conventional patch clamping to measure transporter activity is difficult due a 10,000- to 100,000-fold-lower transport capacity of transporters compared to ion channels (Grewer et al., 2013). Therefore, we will instead use a combination of imaging and biochemical techniques to determine the functional role, if any, for SLC45A2 puncta.

To visualize the dynamics of SLC45A2 at the melanosomal membrane, we will generate fluorescent protein-tagged SLC45A2, express the construct in mouse melanocytes, and use live confocal microscopy to assess SLC45A2 puncta formation. Our analyses of fixed melanocytes indicate that HA-tagged SLC45A2 can be found either in punctate or diffuse forms at the melanosomal membrane. By using live, time-lapse microscopy, we will be able to determine whether SLC45A2 transitions from a diffuse distribution to a punctate localization and vice versa or whether these two forms are distinct and static. A model in which SLC45A2 is redistributed from a diffuse to a punctate localization may suggest that it switches between active and inactive forms, which has been described for STIM1 (Wu et al., 2006). Furthermore, we would supplement the live imaging data with immunogold-labeled EM to identify whether SLC45A2 localizes to melanosomal membrane regions that are adjacent to other structures. For example, does SLC45A2 localize to regions near tubular membranes? This may suggest a role for SLC45A2 function at sites of transport. Alternatively, does SLC45A2 localize to regions adjacent to other organelles? This may suggest that SLC45A2 is part of a microdomain involved in inter-organelle communication. While these experiments will not inform us whether these punctate structures are required for SLC45A2 function, we plan to

supplement these live imaging experiments with proteomics analyses to identify SLC45A2 interacting partners and subsequent knockdown and overexpression experiments to determine if SLC45A2 interacting partners are necessary for puncta formation and function.

SLC45A2 contains a large central cytoplasmic loop between the sixth and seventh transmembrane domains (**Figure 4.2**), which, in related sucrose transporters (e.g. the glucose transporter (GLUT) family), has a regulatory role via direct interactions with other proteins (Jung, 1998; Schulze et al., 2000; Weinglass and Kaback, 2000). To identify SLC45A2 interaction partners, we will express HA-tagged SLC45A2 in melan-uw cells, use an antibody to the HA epitope tag to immunoprecipitate SLC45A2 and any associated proteins, and perform tandem mass spectrometry analysis with gene ontology enrichment analyses to identify bound proteins and their associated pathways. To differentiate between proteins that interact with diffuse SLC45A2 and those that interact with punctate SLC45A2, we will also perform this experiment using HA-tagged SLC45A2 expressed in HeLa cells, in which we observe almost all SLC45A2 in puncta. As a negative control, we will use HA-tagged SLC35D3, which is unrelated to SLC45A2 (Chintala et al., 2007a). Using this unbiased approach, we hope to identify novel interacting partners of SLC45A2.

Potential candidate proteins are scaffolding proteins with known roles in organizing microdomains. For example, ankyrins, proteins that link integral membrane proteins with the cytoskeleton (Bennett and Healy, 2009; Nilsson and Bennett, 2009), and 14-3-3 proteins, adaptor proteins that mediate protein-protein interactions through their ability to bind multiple partner proteins (Jin et al., 2004; Pozuelo Rubio et al., 2004), have both been found in microdomains or as part of multiprotein signaling complexes. Indeed, a member of the 14-3-3 protein family, 14-3-3-γ, was shown to indirectly interact with SLC45A2 and

its plant ortholog OsSUT1 and to negatively regulate their function and localization in yeast or in *Xenopus laevis* oocytes (Vitavska et al., 2018). Further testing of such an interaction between mammalian SLC45A2 and 14-3-3 family members in mammalian melanocytes warrants investigation. Additionally, 14-3-3 family members interact with most proteins via recognition of phosphoserine and phosphothreonine motifs (Muslin et al., 1996; Sluchanko, 2018); therefore, one mechanism to regulate SLC45A2 puncta formation may be through phosphorylation, but this has not yet been explored.

To test if candidate proteins identified by mass spectrometry analyses are involved in SLC45A2 puncta formation, we will knock down or overexpress these proteins in melan-uw cells stably expressing fluorescently-tagged SLC45A2 and assess SLC45A2 localization and dynamics by IFM. We predict that knockdown of proteins involved in SLC45A2 puncta formation will result in diffuse SLC45A2 localization while overexpression will increase puncta formation. We will also assess cells for melanin content to determine if loss of puncta results in a change in melanogenesis, an indirect readout for SLC45A2 function. Overall, these proposed studies will identify SLC45A2 binding partners and will determine if SLC45A2 puncta serve a functional role.

4.2.2. How does SLC45A2 traffic to melanosomes?

Our data show that SLC45A2 localizes to melanosomes in pigmented cells and to late endosomes/lysosomes when expressed in non-pigmented cells – a common feature of melanosomal constituents (Ambrosio et al., 2016; Bellono et al., 2016; Berson et al., 2001; Bouchard et al., 1989; Calvo et al., 1999; Piccirillo et al., 2006; Simmen et al., 1999; Sitaram et al., 2009; Vijayasaradhi et al., 1995). However, how SLC45A2 is transported to melanosomes is unknown. As discussed in Chapter 1, melanosomal proteins are

transported to melanosomes either directly from Golgi by RAB6 vesicles or via endosomal intermediates using AP-3-mediated vesicular or AP-1- and AP-3-mediated tubulovesicular transport pathways (Bowman et al., 2019). To test whether SLC45A2 requires RAB6 or AP-1, we will knock down RAB6 or AP-1 subunits in melan-uw cells, express HA-tagged SLC45A2, and assess protein localization by immunofluorescence microscopy of fixed cells. To test whether SLC45A2 requires AP-3, we will express HA-tagged SLC45A2 in melan-pearl cells, which are immortalized melanocytes derived from mice with loss-of-function mutations in the β subunit of AP-3. AP-1 and AP-3 are obligate multisubunit complexes; therefore, loss of one subunit results in increased degradation of the remaining subunits and loss of complex formation. We will assess localization of HA-tagged SLC45A2 in these cells. Performing these experiments will determine which pathway SLC45A2 uses to traffic to melanosomes.

If SLC45A2 is mislocalized in either the AP-1 knockdown or AP-3 knockout cells, we can further investigate how SLC45A2 engages either of these pathways. AP-1 and AP-3 facilitate cargo sorting at endosomes by recognizing and binding linear sequences on the cytoplasmic domains of transmembrane proteins. The best characterized binding signals conform to a conserved acidic dileucine motif (D/E]XXXL[L/I]) or a tyrosine-based motif (YXXΦ), where X represents any amino acid and Φ represents a bulky hydrophobic amino acid. Similar signals in TYR, TYRP1, and OCA2 direct these proteins to melanosomes in pigmented cells (Calvo et al., 1999; Simmen et al., 1999; Sitaram et al., 2012; Theos et al., 2005; Vijayasaradhi et al., 1995). SLC45A2 contains three putative tyrosine-based motifs in its cytoplasmic domains (**Figure 4.2**). Preliminary experiments suggest that the Y268 tyrosine motif is required for proper localization to melanosomes (Ariel J. Lefkovith, unpublished data); however, the other tyrosine-based motifs in

SLC45A2 have not been investigated. We hypothesize that SLC45A2 engages AP-1 and/or AP-3 to traffic to melanosomes and that this interaction is mediated by tyrosine-based motifs in the SLC45A2 sequence.

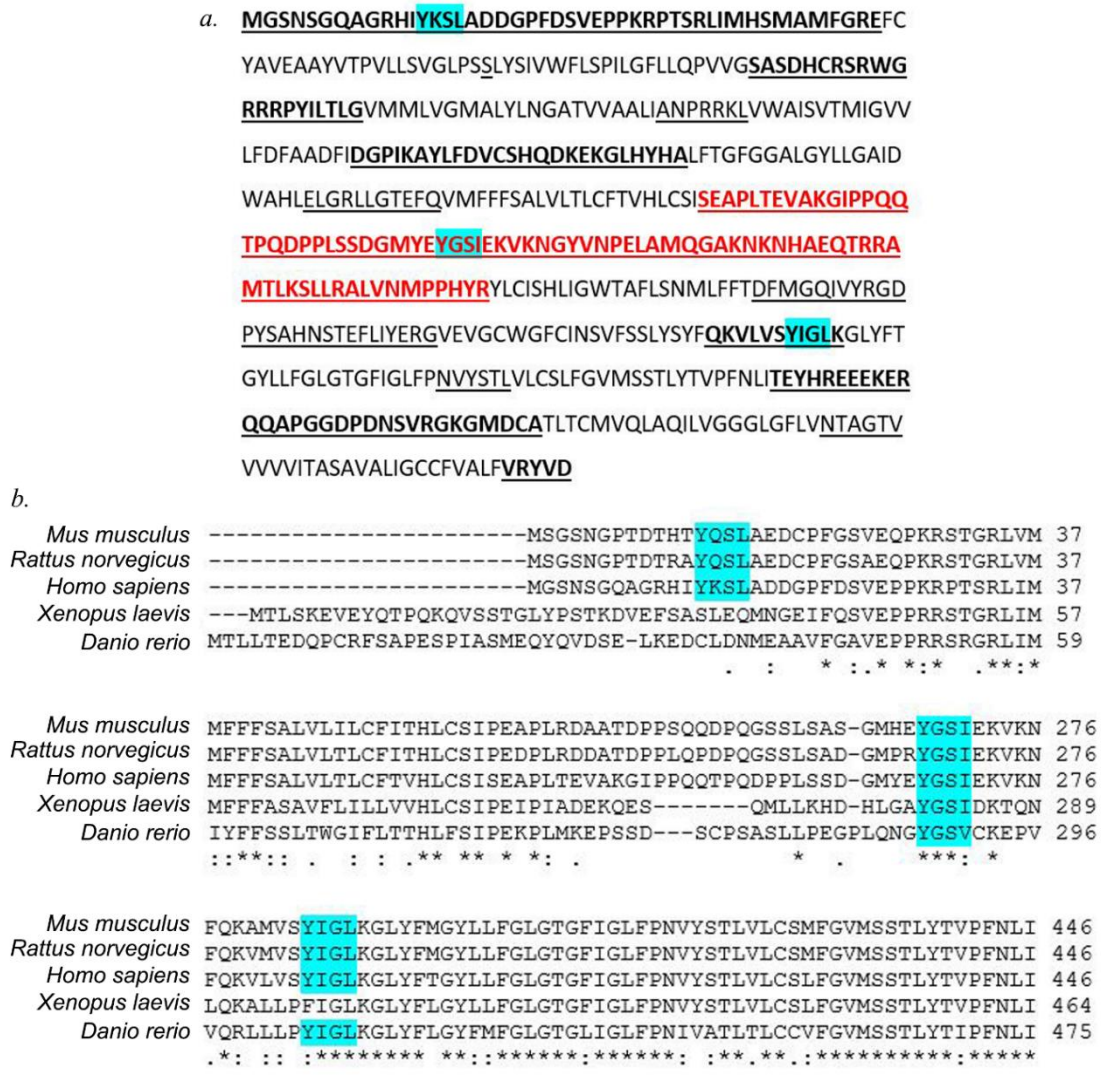

Figure 4.2: Annotated human SLC45A2 amino acid sequence and aligned sequence. (*a*) Human SLC45A2 is a 530 amino acid protein with 12 transmembrane domains. Underlined and bold, cytoplasmic topological domains. Underlined, lumenal topological domains. No underline, transmembrane domains. Red text, large cytoplasmic loop between sixth and seventh transmembrane domains. Cyan highlight, putative tyrosine-based motifs. Only sorting motifs in cytoplasmic domains are shown. (*b*) Mouse, rat, human, *Xenopus*, and zebrafish SLC45A2 amino acid sequences surrounding the human tyrosine-based motif are aligned. The tyrosine-based

motifs identified in the human SLC45A2 sequence and the conserved site in other species are highlighted in cyan. Note that the tyrosine-based motif at human Y268 is well conserved among all five species, the tyrosine-based motif at human Y394 is conserved in mice, rats, human, and zebrafish, and the tyrosine-based motif at human Y13 is conserved in mice, rats, and humans. Amino acid sequence was performed on SLC45A2 orthologs using Basic Local Alignment Search Tool (BLAST) (UniProt, 2019). The UniProt identifiers are as follows: Q9UMX9 (*Homo sapiens*); P58355 (*Mus musculus*); D3ZR99 (*Rattus norvegicus*); A0A1L8I2M1 (*Xenopus laevis*); and A8WG95 (*Danio rerio*).

To test whether SLC45A2 interacts with AP-1 and/or AP-3, we will perform either a yeast 2-hybrid assay, a glutathione S-transferase (GST) pulldown assay using GST fusion proteins followed by immunoblotting, or both, as previously described (Ohno et al., 1998; Ohno et al., 1995; Starcevic and Dell'Angelica, 2004; Stephens and Banting, 1998). AP-1 and AP-3 are heterotetrameric complexes consisting of β1, μ1, σ1, and γ subunits for AP-1 and β3, μ3, σ3, and δ subunits for AP-3 (Robinson and Bonifacino, 2001). The μ subunits of AP-1 and AP-3 mediate binding to tyrosine-based motifs (Ohno et al., 1998; Ohno et al., 1995). Therefore, we can use a yeast 2-hybrid assay and generate constructs with the GAL4 binding domain fused to SLC45A2 cytoplasmic loops containing each tyrosine-based motif and use previously published constructs with the GAL4 activation domain fused to μ1 of AP-1 or μ3 of-AP-3 (Ohno et al., 1996). These fusion proteins will be co-expressed in yeast without endogenous GAL4 activity; an interaction between a protein fused to the GAL4 binding domain and a protein fused to the GAL4 activation domain will result in GAL4 activity, which can be assessed by growth of His3-negative yeast expressing Gal4-His3 on agar plates lacking histidine. The GAL4 binding domain fused to the cytoplasmic tail of TGN38, which contains a tyrosine-based motif that is recognized by both μ1 and μ3 subunits (Ohno et al., 1998; Ohno et al., 1995; Stephens and Banting, 1998), will be used as a positive control. As a negative control, we will use a GAL4 binding domain fused to the cytoplasmic tail of OCA2, which is recognized by AP-1

and AP-3 through their γ/σ1 and δ/σ3 subunits, respectively (Sitaram et al., 2012). To validate these data, we will perform a GST pulldown assay using melanocyte cell lysates incubated with GST fusion proteins containing the SLC45A2 cytoplasmic domains with tyrosine-based motifs. Interactions with AP-1 or AP-3 will be assessed by immunoblotting with antibodies to their respective μ subunits.

To test whether an interaction between SLC45A2 and AP-1 and/or AP-3 requires any of the three tyrosine-based motifs in the cytoplasmic domains of SLC45A2, we will generate GST-tagged constructs with mutations in tyrosine-based motifs shown to bind AP-1 or AP-3 in the previous set of experiments. If all three tyrosine-based motifs were shown to bind, then constructs will be generated in which one, two, or three of the tyrosine-based motifs are combinatorially mutated. We will then repeat the GST pulldown experiment and assess AP-1 and AP-3 binding by immunoblotting.

It is possible that we will not observe interactions between SLC45A2 cytoplasmic domains and AP-1 or AP-3 by either yeast two-hybrid or GST pulldown. Preliminary yeast two-hybrid and GST pulldown assays using the Y268 tyrosine motif within the context of the cytoplasmic loop between the 6th and 7th transmembrane domains (red in **Figure 4.2a**) failed to demonstrate an interaction (Hayley A. Hanby and Alexa Jaume, unpublished data). However, this may be due to folding requirements that are not met when using short fragments. If this is the case, we will mutagenize the tyrosine residue in each tyrosine-based motif and express each HA-tagged mutant SLC45A2 construct in melan-uw cells to assess their effects on localization and pigmentation rescue. We will also perform proximity ligation assays in cells expressing WT and mutant forms of HA-SLC45A2 using antibodies to HA and AP-1 or AP-3 subunits. These assays will determine if WT SLC45A2 is in close proximity to AP-1 and/or AP-3 and if mutation of any of the tyrosine-based motifs

antagonizes this localization. While these experiments do not inform us whether there are direct interactions between the tyrosine-based motifs and AP-1 or AP-3, they do reveal whether these motifs are required for sorting and we would expect these results to be similar to those of WT SLC45A2 expressed in cells with loss of AP-1 or AP-3. Of note, experiments performed with a Y268A mutated tyrosine-based motif indicate that SLC45A2 is largely mislocalized in these cells (Ho, 2015); however, cells regain partial pigment, which could be due to partial localization of SLC45A2 to melanosomes by the other tyrosine-based motifs. We will repeat this experiment with mutations in the other tyrosine-based motifs and quantify localization to melanosomes. Overall, these experiments will determine if AP-1 and/or AP-3 bind SLC45A2 (or are at least required for SLC45A2 localization) and whether and which tyrosine-based motifs are required for any of these interactions.

4.2.3. What is the role of sugar in the melanosome?

SLC45A2 is predicted to transport protons down their electrochemical gradient from the lumen to the cytosol. When expressed in yeast, mouse SLC45A2 functioned as a proton-dependent sugar transporter; it facilitated import of the disaccharide sucrose, and putatively the monossacharides glucose, mannose, and fructose, from the extracellular medium to the cytoplasm only when the growth medium was acidified (Bartolke et al., 2014). This implies that in the physiological context, SLC45A2 would export a proton with a sugar molecule from the melanosome lumen to the cytosol. The source of such sugar substrates in melanosomes and whether sugar export is required for melanosome biogenesis or merely a byproduct of proton export has not been defined. Nothing has been published about the presence or role of sugars within the melanosome except as

components of glycoproteins. However, this topic has been discussed in the context of lysosomes. Within lysosomes, mature glycoproteins can be catabolized into peptides and monosaccharides, primarily by hydrolases such as cathepsins and glycosidases, which are then transported into the cytosol for recycling (Winchester, 2005). All known resident melanosomal proteins are integral membrane proteins (or in the case of PMEL, fragments of integral membrane proteins) that are heavily glycosylated. Additionally, melanosomes contain a cohort of lysosomal hydrolases, including cathepsins B and L (Diment et al., 1995a) and D (G. Raposo and M. S. Marks, unpublished). Thus, catabolism of melanosomal glycoproteins by these hydrolases and glycosidases might be a major source of sugar molecules within the melanosome.

To test whether export of these sugar molecules by SLC45A2 is required for proper melanosome maturation, the residues required to bind and transport sugar must first be identified and then can be mutated to determine if proton transport and sugar transport can be uncoupled in SLC45A2. The rice sucrose transporter OsSUT1 is an ortholog of SLC45A2 and has been used to study the effects of SLC45A2 mutations and variants at conserved sites. The arginine residue at position 188 (R188) in OsSUT1 is located in the fourth transmembrane domain and is required for sugar transport; mutation of this residue to a lysine (R188K) results in loss of sugar transport and a proton leak (Sun et al., 2012; Sun and Ward, 2012). However, in experimental conditions, this proton leak was blocked when sucrose was added to the system, putatively because sucrose can still bind the transporter but cannot induce a conformational change to trigger export. Therefore, it is unclear if a proton leak actually occurs in vivo. In SLC45A2 the orthologous residue is a lysine at position 164 (K164). We propose mutating this residue to investigate if it is needed for sucrose but not proton transport. Sucrose uptake can be assessed by

expressing WT or mutant SLC45A2 in the yeast strain HOD55-4B, which is incapable of sucrose uptake due to lack of yeast sucrose transporters; thus these yeast cells cannot grow on sucrose-containing minimal medium agar plates without the ectopic expression of a functional sucrose transproter (Bartolke et al., 2014). When expressed in yeast, at least a fraction of SLC45A2 localizes to the plasma membrane from where it facilitates sucrose import into the cell, allowing HOD55-4B cell growth (Bartolke et al., 2014). To test whether this mutant can transport protons, we will express it in HeLa cells and measure endolysosomal pH with LysoSensor. A SLC45A2 mutant that can transport protons without co-transporting sugars will be expressed in melan-uw cells and analyzed by BFM and IFM to visualize pigmentation and SLC45A2 localization; EM for melanosome size and maturation, and melanin content assay for melanization. In particular, we will be looking for evidence of melanosome swelling due to osmotic stress. These tests will determine if sugar export is required for proper melanosome maturation.

4.2.4. How to further investigate the differences between SLC45A2 localization and OCA2 localization on melanosomes?

Our IFM analyses indicate that SLC45A2 and OCA2 localize to different populations of melanosomes at steady state and that SLC45A2 localization correlates well with the mature melanosome markers TYR and TYRP1 whereas OCA2 localization is less correlated with TYRP1. We also show that SLC45A2 is a relatively stable protein with a half-life of 53 hours while OCA2 is short-lived with a half-life of <4 hours (Sitaram et al., 2009). Furthermore, data indicate that a cohort of OCA2 localizes to intralumenal membranes/vesicles (ILVs) (Sitaram et al., 2012) and that OCA2 interacts closely with melanin (Donatien and Orlow, 1995). These data suggest that, while SLC45A2 is long-

lived on the melanosome, OCA2 is only transiently expressed at the limiting membrane and becomes rapidly internalized and buried by melanin or degraded. However, the mechanism by which OCA2 becomes internalized and the functional consequences for pH regulation are unclear.

The major pathway for sorting into ILVs in maturing endosomes is by the recognition of ubiquitylated cargo by endosomal sorting complexes required for transport (ESCRT)-0, -I, -II, and -III (Gruenberg, 2020). ESCRT complexes exist in the cytoplasm and are recruited to endosomal membranes by the interaction between ESCRT-0 and phosphatidylinositol 3-phosphate (PtdIns3P). ESCRT-0 binds both ubiquitylated cargo and PtdIns3P and recruits ESCRT-1, which recruits ESCRT-II. ESCRT-II nucleates ESCRT-III formation and oligomerization; ESCRT-III filaments drive membrane deformation to form ILVs (Gruenberg, 2020). Cargo sorting to ILVs can also occur in the absence of direct ubiquitylation of a particular cargo; instead, cargo can interact with a ubiquitylated protein that is recognized by ESCRT-0 (Hislop et al., 2004). Furthermore, there are examples of ESCRT-dependent, ubiquitin-independent cargo sorting, in which integral membrane cargo are sorted into ILVs through their direct interactions with ESCRT subunits themselves (Yamashita et al., 2008) or with ESCRT-associated proteins (Dores et al., 2012; Dores et al., 2016).

To determine if OCA2 is transported to ILVs via an ESCRT-dependent pathway, we will knock down the ESCRT-III subunit charged MVB protein 4 (CHMP4). CHMP4 is expressed in 3 isoforms (CHMP4A, CHMP4B, and CHMP4C). RNA-seq data show that CHMP4A and CHMP4B are expressed in human melanocytes whereas CHMP4C is only expressed at low levels (Reemann et al., 2014). To validate that this is applicable to melan-p1 cells, we will perform RT-PCR. We will then knock down the expressed isoforms using

short hairpin RNAs (shRNAs), express HA-tagged OCA2, and assess localization by IFM and IEM. The results from this experiment will indicate whether internalization of OCA2 is mediated through an ESCRT-dependent or -independent pathway. However, if the data indicate an ESCRT-dependent pathway, they do not inform us whether this occurs through a ubiquitylation-dependent pathway.

To determine if OCA2 requires direct or indirect ubiquitylation for entry into ILVs, we will generate a construct where OCA2 is fused to the catalytic domain of the deubiquitinating peptidase domain of Herpes Virus UL36 (OCAC2-DUb); thus, OCA2 will be resistant to ubiquitylation and may also render associated proteins resistant to ubiquitylation. Previous studies have generated cargo-DUb fusion constructs to test ubiquitylation requirements for ESCRT-mediated ILV formation (Sette et al., 2013; Stringer and Piper, 2011). We will assess the localization of WT OCA2 and OCA2-DUb by IFM and IEM. As a negative control, we will generate and analyze constructs in which OCA2 is fused to a catalytically inactive deubiquitinating peptidase domain. This experiment will determine if ubiquitylation is required for OCA2 sorting into ILVs.

While the ESCRT-dependent pathway is the canonical pathway for sorting into ILVs, some cargo are sorted into ILVs in an ESCRT-independent pathway. For example, PMEL, which requires localization to ILVs for proper processing and fibrillization, is sorted into ILVs by an ESCRT-independent, CD63- and apolipoprotein E-dependent mechanism that is dependent on PMEL's lumenal domain (Theos et al., 2006b; van Niel et al., 2015; van Niel et al., 2011). If our initial experiments indicate that OCA2 uses an ESCRT-independent pathway for sorting into ILVs, we can determine if CD63 is required for OCA2 sorting into ILVs. To test if OCA2 internalization is dependent on CD63, we will knock down CD63 in melan-p1 cells, express HA-tagged OCA2, and assess protein localization

by IFM and IEM. This experiment will determine if OCA2 sorting into ILVs is dependent on CD63.

After identifying the mechanism of OCA2 sorting into ILVs, we will inhibit its invagination onto ILVs and investigate how this affects pigmentation. We show that OCA2 overexpression can rescue loss of SLC45A2 expression. If this is due to increased localization of OCA2 at the melanosomal membrane, preventing OCA2 internalization in melan-uw cells should result in a similar effect. Additionally, we can perform IFM to determine whether restricting OCA2 to the melanosomal limiting membrane results in increased colocalization of OCA2 with the mature melanosomal marker TYRP1 and perform cycloheximide pulse-chase and immunoblotting, wherein we block protein synthesis and observe protein levels at various time points, to determine whether this results in increased protein half-life. Overall, these experiments will yield insights into the mechanism by which OCA2 is sorted into ILVs and whether OCA2 internalization can partially explain some of the differences between OCA2 and SLC45A2 localization and half-life, and how OCA2 overexpression can compensate for loss of SLC45A2 activity.

4.2.5. How to measure melanosomal pH?

Our data show that expression of HA-tagged SLC45A2 in HeLa cells results in increased pH at the late endosomes/lysosomes to which they localize. However, we have been unable to measure the pH of melanosomes. Lysotracker and Lysosensor are widely used fluorescent reagents to label acidic organelles and to measure their pH, respectively, in many cell types. They are membrane-permeable weak bases that are uncharged at neutral pH and thus diffuse into organelles, where in acidic organelles they become protonated and trapped; Lysosensor fluorescence can be measured after excitation at two

wavelengths, and the ratio of fluorescence is dependent on pH. However, in our hands (and confirmed by collaborators), Lysosensor and Lysotracker do not reproducibly accumulate well within organelles in melanocytes. The mechanism underlying this is unclear.

An alternative method to specifically measure melanosomal pH has been developed and termed MELOPS (melanosome-localized pH sensor). MELOPS consists of the pH-sensitive fluorescent protein, mNectarine, fused to a lumenal loop of OCA2-V443I (Ambrosio et al., 2016), an inactive variant of OCA2 (Bellono et al 2014). mNectarine is a dsRed derivative with a pKa of 6.9 and a linear increase in fluorescence intensity from pH 6-7.5 (Johnson et al., 2009). mNectarine was originally generated to be used for cytoplasmic pH measurements, where the average pH ranges between ~6.8 – 7.4, which is much higher than the average pH of acidic organelles ranging from ~4.5 – 6.0. Although one study has successfully used MELOPS to estimate melanosomal pH (Ambrosio et al., 2016), when we measured MELOPS fluorescence in melan-Ink4a and melan-uw cells and in HeLa cells expressing HA-OCA2 or HA-SLC45A2, the results indicated that the melan-Ink4a cells were lower than expected and contradicted our previous measurements using Lysosensor (data in Appendix). Based on our data, we conclude that mNectarine is not an optimal fluorescent protein for measuring melanosomal pH.

We propose generating a novel MELOPS variant to more accurately monitor melanosomal pH within the range expected for acidic early stage and more neutral late stage melanosomes. We propose to replace the mNectarine fluorophore with one that was optimized for and extensively tested in lumenal compartments. One candidate is the fluorescent construct pH-Lemon, a ratiometric pH sensor generated by the fusion of the

pH-stable fluorescent protein mTurquoise2 and the pH-sensitive fluorescent protein enhanced yellow fluorescent protein (EYFP) (Burgstaller et al., 2019). mTurquoise2 can act as a fluorescence resonance energy transfer (FRET) donor, and the close proximity of the two fluorescent proteins yields high FRET signals at neutral to basic pH. Therefore, pH-Lemon is a ratiometric pH sensor that can be excited at 430 nm and analyzed at emission wavelengths 475 and 525 nm, and the ratio of donor (mTurquoise) fluorescence to FRET (EYFP) fluorescence can be correlated to pH based on a standard curve. Data indicate when this reporter is fused to the lumenal domain of either the LC3B to visualize pH changes during autophagosome maturation or to a glycophosphatidylinositol anchor to measure pH in the endocytic pathway, it can dynamically and reversibly shift fluorescence intensities in response to changes in pH with a range from ~pH 4 – 10 (Burgstaller et al., 2019). Therefore, we will replace mNectarine in the lumenal loop of OCA2-V443I with pH-Lemon and repeat the previously described flow cytometry in HeLa cells expressing this modified MELOPS construct to test if it serves as a better melanosomal pH sensor. If so, we will use this construct to measure pH in melan-Ink4a cells, melan-uw cells, melan-uw cells stably expressing HA-tagged SLC45A2, melan-p1 cells, and melan-p1 cells stably expressing HA-tagged OCA2. We will also measure melanosomal pH in melan-uw cells overexpressing HA-OCA2 and melan-p1 cells expressing HA-SLC45A2. Overall, generation of this construct or a similar optimized MELOPS construct and performing these experiments will allow us to determine the pH of melanosomes in these WT, mutant, rescue, and overexpressing cell lines. A reliable MELOPS construct can also be used to measure melanosomal pH in melanocytes from other models of albinism (e.g. other OCA subtypes and HPS) to generate novel hypotheses regarding the etiology of those disorders and the fates of transporters,

channels, and ion pumps in these cells. Additionally, measuring melanosomal pH will be useful to determine whether ion transport proteins localized on nonmelanosomal organelles affect pigmentation through indirect modulation of melanosomal pH.

4.2.6. How do other ion transport proteins regulate melanosome pH and melanogenesis?

Ion transport and its regulation of melanogenesis is an important topic of study. While the main goal in Chapter 2 was to determine the localization and role of SLC45A2 in melanocytes and to investigate how SLC45A2 and OCA2 coordinate to regulate melanosomal pH, other ion transport proteins have been identified as modulators of melanogenesis. What we currently know about other ion transport proteins aside from SLC45A2 and OCA2 will be discussed in this subsection. The ion transport proteins that have been studied in melanocytes or that result in a pigmentation phenotype when mutated are TPC2, SLC24A5, MFSD12, ClC-7, and TRPM1.

Two-pore channel 2 (TPC2) is a cation channel that localizes to melanosomes in pigmented cells (Ambrosio et al., 2016; Bellono et al., 2016). TPC2 is a gated channel activated by phosphatidylinositol 3,5-bisphosphate [PtdIns(3,5)P_2] that is Na^{2+}-selective (Bellono et al., 2016; Wang et al., 2012). Previous data had suggested that TPC2 was activated by the second messenger nicotinic acid adenine dinucleotide phosphate (NAADP) and was Ca^{2+}-selective (Calcraft et al., 2009), but direct measurements of TPC2 by patch clamp analysis showed that it does not respond to NAADP and that it is 100 times more selective for Na^{2+} than Ca^{2+} (Bellono et al., 2016; Wang et al., 2012). TPC2 was originally linked to a role in pigmentation by a genome-wide association study (GWAS) in which TPC2 variants were associated with blonde versus brown hair color in humans

(Sulem et al., 2008), and another study confirmed that the variants identified were causative for a decrease in pigmentation and that this was due to TPC2 gain-of-function (Chao et al., 2017). Patch clamp experiments show that TPC2 activity increases membrane potential (Bellono et al., 2016). Knockdown or knockout of TPC2 in mouse melanocytes results in increased lumenal pH, melanin content, and melanosome size, while TPC2 overexpression results in decreased pH and decreased melanin content (Ambrosio et al., 2016; Bellono et al., 2016). The model of TPC2 function at the melanosome is that it increases membrane potential by driving Na^{2+} efflux, and that this enhances V-ATPase activity and promotes melanosomal acidification. Indeed, overexpression of TPC2 antagonized the increased pigmentation observed when OCA2 was overexpressed (Bellono et al., 2016), indicating that the activities of these two ion transport proteins counteract each other. Whether TPC2 and OCA2 co-exist on the same melanosome or whether they are delivered and function sequentially is unknown. One possibility is that TPC2 localizes to immature melanosomes and OCA2 localizes to maturing melanosomes. Alternatively, TPC2 may function at a later stage to slow or halt melanogenesis in mature melanosomes.

The *SLC24A5* gene encodes the potassium-dependent sodium-calcium exchanger 5 (NCKX5) protein, which is expressed in pigmented cell types and localizes primarily to the *trans*-Golgi network (TGN) and/or to mitochondria but not to melanosomes (Ginger et al., 2008; Rogasevskaia et al., 2019; Wilson et al., 2013; Zhang et al., 2019). NCKX5 is a Na^{2+}/Ca^{2+} antiporter that is dependent on an outward Na^{2+} gradient and an inward K^{+} gradient for the inward transport of Ca^{2+} (where inward is from the cytoplasm towards the organelle lumen, and outward is from the organelle lumen towards the cytoplasm) (Altimimi and Schnetkamp, 2007; Szerencsei et al., 2016). Mutations in

NCKX5 result in OCA6 (Morice-Picard et al., 2014; Wei et al., 2013) and allelic variants are associated with pigmentation variation in multiple populations (Cook et al., 2009b; Crawford et al., 2017; Ginger et al., 2008; Lamason et al., 2005b). *Slc24a5*$^{-/-}$ mice have smaller melanosomes and reduced pigmentation (Vogel et al., 2008) and knockdown of *Slc24a5* in mouse and human melanocytes results in decreased melanin content (Ginger et al., 2008; Wilson et al., 2013; Zhang et al., 2019), decreased melanosomal protein expression (Ginger et al., 2008), reduced MC1R mRNA levels (Wilson et al., 2013), and reduced melanosomal Ca^{2+} content (Zhang et al., 2019). It is unclear how NCKX5 exerts its influence on melanogenesis from either the TGN or mitochondria, but several hypotheses exist. The TGN is a site of Ca^{2+} storage and regulated Ca^{2+} release allows it to act as a powerful second messenger (Dolman and Tepikin, 2006); it is possible that Ca^{2+} functions as a second messenger to control melanogenesis, although this might not function at the level of controlling melanosomal gene expression (Wilson et al., 2013). Therefore, NCKX5-mediated Ca^{2+} import may be required for replenishing Ca2+ stores for repeated rounds of signaling (Ginger et al., 2008). Zhang et al. report that NCKX5 on mitochondria are responsible for Ca^{2+} transport into melanosomes (Zhang et al., 2019), which is known to have a large store of Ca^{2+} and other divalent cations (Bush and Simon, 2007); however, how a Ca^{2+} importer on mitochondria would mediate this has not been described and a role for Ca^{2+} within melanosomes has not been identified.

Major facilitator superfamily domain containing 12 (MFSD12) belongs to a large family of ion transport proteins which have diverse substrates. *MFSD12* was first identified as a gene associated with pigmentation variation by GWAS of populations in Africa (Crawford et al., 2017) and this has been validated in other studies (Adhikari et al., 2019b; Lona-Durazo et al., 2019). *Mfsd12*$^{-/-}$ mice have gray coat color compared to their agouti

WT littermates and analysis of hairs from these mice indicate that *Mfsd12*$^{-/-}$ mice have defects in pheomelanin synthesis but not eumelanin synthesis (Crawford et al., 2017). In darkly pigmented melanocytes, MFSD12 localizes to lysosomes, but its substrates and mechanism of action there are unknown. Knockdown of *Mfsd12* in such cells results in increased melanosome and melanin content as assessed by BFM and spectroscopy (Crawford et al., 2017). Together these data suggest that MFSD12 positively regulates pheomelanin synthesis and negatively regulates eumelanin synthesis from its localization at lysosomes, indicating that lysosomal crosstalk to melanosomes is an important regulator of melanogenesis.

Chloride channel 7 (ClC-7), encoded by *CLCN7*, is a Cl^-/H^+ antiporter that in non-pigmented cells localizes to lysosomes (Graves et al., 2008; Lange et al., 2006); its localization in pigmented cell types has not been identified. ClC-7 forms a molecular complex with OSTM1, and mice with loss of function mutations in either protein have a grey rather than agouti coat color like *Mfsd12*$^{-/-}$ mice (Chalhoub et al., 2003; Lange et al., 2006). ClC-7 imports chloride into the lysosomal lumen via driving protons down their electrochemical gradient into the cytosol in a 2:1 $Cl^-:H^+$ ratio (Graves et al., 2008). Knockdown of *Clcn7* results in decreased of H^+-driven chloride uptake and reduces lysosomal acidification (Graves et al., 2008). This is likely due to the requirement for an anion flow parallel to V-ATPase to neutralize the lumenal positive membrane potential, allowing further V-ATPase activity (Carraro-Lacroix et al., 2009; Wagner et al., 2004). Whether ClC-7 plays a similar role in melanocytes depends on where and when CLC7 is expressed and the ion concentrations within the organelle it resides. Based on the coat color phenotype of *Clcn7*$^{-/-}$ mice, it is possible that ClC-7 may play a role in pheomelanogenesis and may coordinate this process with MFSD12.

Transient receptor potential cation channel, subfamily M, member 1 (TRPM1, a.k.a. melastatin) is a Ca^{2+} channel that localizes primarily to unidentified intracellular compartments (not melanosomes) and to the plasma membrane in melanocytes (Oancea et al., 2009; Xu et al., 2001). Increased *TRPM1* mRNA in human melanocytes correlates with increased melanin content (Oancea et al., 2009), suggesting a role for TRPM1 in modulating some part of melanogenesis. However, more work needs to be done to determine the cellular localization of TRPM1 and the role of Ca^{2+} in melanin synthesis or stabilization.

4.2.7. How to investigate VPS33A functions in the melanosomal pathway?

Our data in Chapter 3 showed that immortalized melan-bf melanocytes were able to generate high levels of melanin despite bearing the VPS33A-D251E mutation. However, our investigation into VPS33A mechanisms was complicated by reports of differing phenotypes of melan-bf cells, difficulties recreating the phenotype in melan-Ink4a cells, and concerns that the melan-bf cells we received had acquired a different mutation that caused the hyperpigmentation phenotype that we observed. There are several possible explanations why these melan-bf cells have a different phenotype than the ones published (Suzuki et al., 2003). (1) The melan-bf cells that we received may have acquired new mutations in culture, in which case we can rederive new melan-bf cells from *buff* mice. (2) The hyperpigmentation phenotype may be due to a compensatory adaptation to the VPS33A-D251E mutation, in which case newly derived melan-bf cells will phenocopy the published melan-bf cells initially but will eventually develop our observed phenotype. (3) *Buff* mice may have a second mutation that causes the hyperpigmentation phenotype to develop over time and would look similar to possibility 2. It would be difficult to distinguish

between possibilities 2 and 3 using cells derived from *buff* mice; rather, we would have to express the VPS33A-D251E mutation in WT melan-Ink4a cells to investigate its effect on melanosome biogenesis. Therefore, to distinguish between possibilities 1 and 2 and to avoid complications from possibility 3, we will optimize the human VPS33A (WT or D251E) stable expression/endogenous *Vps33a* knockdown model in melan-Ink4a to analyze the effects of VPS33A-D251E expression. As a control to validate this method, we will also knock down endogenous *Vps33a* in melan-Ink4a cells stably expressing human VPS33A-G308E, which results in a sorting defect when the conserved residue is mutated in the yeast ortholog Vps33 (Baker et al., 2015). Based on the data published about this mutation in yeast, we hypothesize that the G308E mutation will cause defects in the endolysosomal pathway. To assess problems in the endolysosomal pathway, we will perform a dextran pulse-chase over a short time course to observe dextran co-localization with markers of early endosomes, late endosomes, and lysosomes. This will allow us to optimize and validate the conditions of this method.

Published data show that melan-bf cells are hypopigmented with small melanosomes and able to be rescued by expression of WT VPS33A (Suzuki et al., 2003), indicating that VPS33A-D251E is causative for the hypopigmentation phenotype. Therefore, we expect that expression of VPS33A-D251E results in smaller melanosomes, and if enlarged melanosomes are due to a compensatory mechanism, they will arise later. This is not something we observed in our preliminary experiments using this method; however, brightfield microscopy might not be the optimal method to assess these cells due to the preexisting melanosomes in the cell. Therefore, we will perform EM of cells at early time points and later time points to quantify any changes in melanosome area and maturation.

Upon determining which time points yield relevant melanosome or endolysosomal phenotypes, we will then perform similar experiments to those done in Chapter 3, including: BFM and IFM to visualize pigment granules and the localization of melanosomal and lysosomal markers; EM to assess melanosome size and maturation; and a dextran pulse-chase time course experiment to characterize the endocytic pathway. Since VPS33A is involved in membrane fusion, the IFM experiments to assess the localization of TYR (vesicular pathway cargo), TYRP1 or OCA2 (tubulovesicular pathway cargo), and MART-1 or DCT (RAB6 pathway cargo) will inform us if there are overt defects in any of the three trafficking pathways to melanosomes. If the results from this experiment suggest that the tubulovesicular pathway is altered, we can generate WT VPS33A and VPS33A-D251E tagged with fluorescent proteins to visualize by live confocal microscopy whether these proteins associate with tubules or affect tubule number, length, or stability. As explained above, the dextran pulse-chase time course will allow us to assess the effects of the VPS33A-D251E mutation on the endolysosomal pathway.

We will also express the HA-tagged WT and mutant VPS33A proteins in WT melan-Ink4a cells and immunoprecipitate associated proteins using an antibody to the HA epitope. We will blot for HOPS and CORVET subunits to determine whether VPS33A-D251E alters complex formation. The tSNAREs that mediate fusion at the melanosomal membrane are unknown; however, we can assess whether WT VPS33A interacts with the melanosomal vSNARE VAMP7 and whether this is altered with VPS33A-D251E.

Overall, these experiments will determine whether VPS33A has a role in trafficking in the melanosomal pathway and whether the VPS33A-D251E mutation affects the melanosomal or endolysosomal trafficking pathway.

4.2.8. How to assess GPR143 pathway in melan-bf cells?

In Chapter 3, we show that the melan-bf cells received from the Spritz lab have a phenotype strikingly similar to that of melanocytes from *Oa1*$^{-/-}$ mice. Melan-bf cells contain enlarged, mature melanosomes, and, in many of the cells, melanosomes were restricted to the cell periphery. We will first determine if there is a change in GPR143 and/or $G\alpha_{i3}$ mRNA and protein levels in melan-bf cells relative to melan-Ink4a cells by qPCR and immunoblotting. If levels of these proteins are not altered, we will test if these components are functionally impaired in melan-bf cells by stably expressing WT GPR143 or its downstream signaling partner $G\alpha_{i3}$ and visualizing cells by BFM to determine whether cells are rescued. Data in *Oa1*$^{-/-}$ melanocytes show that transient expression of WT GPR143 is sufficient to rescue the peripheral melanosome phenotype by 24 hours but stable expression of the protein is required for rescue of melanosome size (Palmisano et al., 2008). If neither WT GPR143 nor $G\alpha_{i3}$ rescue the phenotype, it is possible that downstream mediators of the GPR143 pathway, which have not been described, are mutated in melan-bf cells. One downstream effect of GPR143 overexpression is increased *MITF* mRNA and protein expression (Chen et al., 2016). Therefore, to determine if this pathway is functional, we will assess *MITF* levels in cells with and without expression of WT GPR143 or $G\alpha_{i3}$. We predict that overexpression of either GPR143 or $G\alpha_{i3}$ would increase *MITF* mRNA levels if the downstream signaling pathway is intact but that there would be no change in *MITF* if the downstream pathway is mutated. As a control, we will repeat this experiment in melan-Ink4a cells. If the downstream signaling pathway is functional in melan-bf cells, then we expect that overexpression of GPR143 or $G\alpha_{i3}$ would be able to rescue our observed phenotype if either GPR143 or $G\alpha_{i3}$ are mutated. However,

if the downstream pathway is mutated, we would expect that overexpression of GPR143 or $G\alpha_{i3}$ would not be sufficient to rescue the phenotypes in melan-bf cells and we would not be able to perform a rescue experiment without a knowledge of the proteins involved downstream of GPR143. Overall, these experiments will determine if the GPR143 pathway is functional in melan-bf cells and whether expression of WT GPR143 or $G\alpha_{i3}$ can rescue the hyperpigmentation and localization phenotypes we observe in melan-bf cells.

4.3. Concluding remarks

Over 230 mouse models with pigmentation phenotypes exist; yet only a fraction of the genes that are mutated in those mouse models have a defined role in melanogenesis. Here, we investigate two mouse models of albinism – the OCA4 mouse model *underwhite*, which has a mutation in *Slc45a2*, and the HPS model *buff*, which has a mutation in *Vps33a*. We identify a direct role for SLC45A2 in the pH regulation of melanosomes and characterize the phenotype of melan-bf cells.

Our study of SLC45A2 shows that it is important not only to study ion transport channels that modulate melanogenesis but also to study them in the context of other ion transport channels to determine how multiple proteins coordinate melanosome pH at different stages of maturation. It will be of interest to determine to what stage melanosomes TPC2 localizes and how ion transport proteins on other organelles regulate melanogenesis. Additionally, given the excitement over the emerging field of studying inter-organelle contacts, we are interested to identify whether ion transport channels on lysosomes, TGN, or mitochondria are part of contact sites between their resident organelles and melanosomes, and whether ion transport proteins mediate their effects

through regulation of inter-organelle communication. Alternatively, ion transport proteins on non-melanosomal organelles may indirectly regulate melanogenesis through modulation of signaling cascades. It will be exciting to discover more about the crosstalk between signaling pathways and between organelles within pigmented cells to learn about how these cells regulate melanogenesis.

The role of VPS33A in melanogenesis has been more elusive due to its critical role in the endolysosomal pathway. However, our studies show that despite the VPS33A-D251E mutation, melanocytes can become pigmented. Whether this is due to compensatory effects or additional mutations is unclear, but we believe this mutation warrants further careful study.

Overall, our studies highlight the importance of studying mouse models of albinism as a way to determine the cellular basis of pigmentation. Additionally, studying gene variants associated with pigmentation differences identified by GWAS provides insight into whether the proteins encoded by these genes are functional and how variants affect melanogenesis. In addition to having a better understanding about the regional differences in pigmentation in modern-day humans, identifying functional variants provides insight into the evolution of human diversity.

APPENDIX

Appendix A: VPS33A

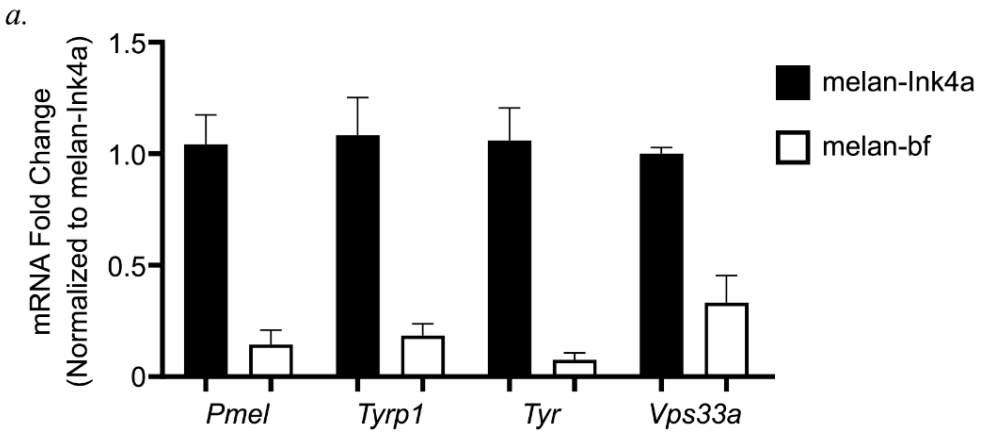

Appendix Figure 1: Decreased expression of melanosomal genes and Vps33a in melan-bf cells. (*a*) RNA from melan-Ink4a and melan-bf cells was reverse transcribed and assessed by qPCR to quantify relative expression of *Vps33a* and the melanosomal genes *Pmel*, *Tyrp1*, and *Tyr*. Data were normalized to the housekeeping gene *Tubb4b* and are shown as fold change relative to mRNA levels in melan-Ink4a. Data shown are from n=2 experiments each done in triplicate.

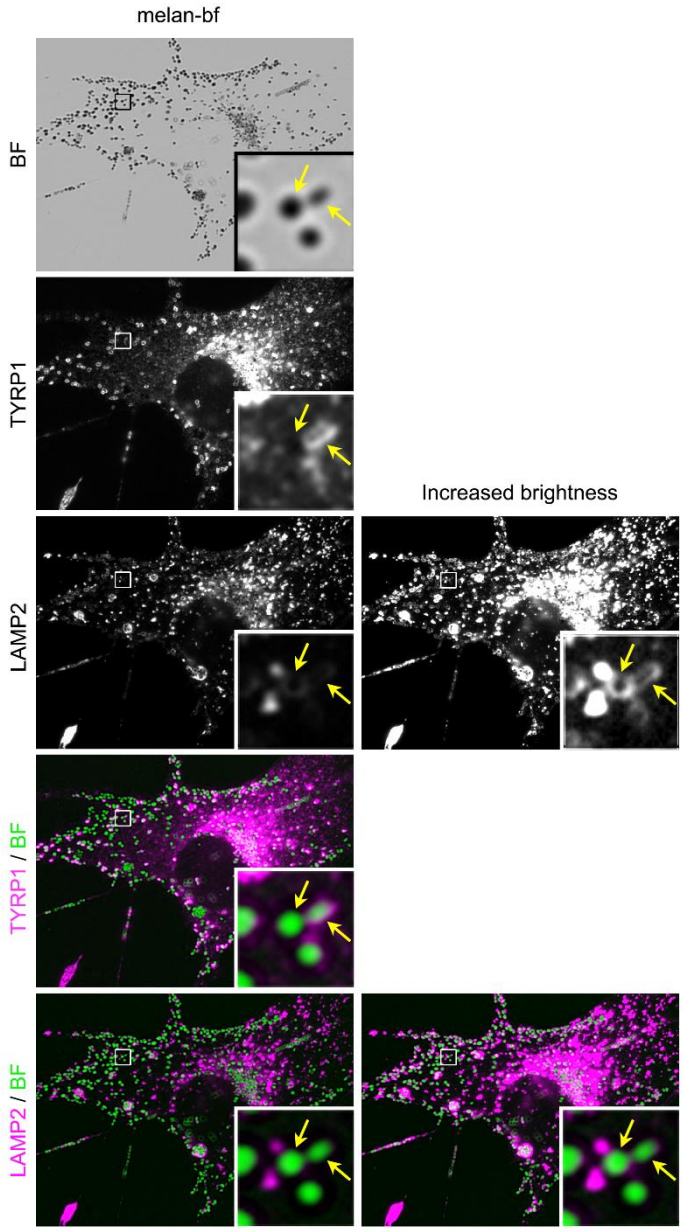

Appendix Figure 2: Low levels of LAMP2 colocalize to pigment granules. Melan-bf cells were fixed, immunolabeled for TYRP1 or LAMP2 (magenta), and analyzed by dIFM and bright field (BF) microscopy to visualize pigment granules (pseudocolored green in merged images). Images on the right have were adjusted in Adobe Photoshop to increase brightness so that low levels of LAMP2 could be seen. Insets of boxed regions are magnified 7.5 times. Scale bar, 10 µm. LAMP2 (yellow arrows) that localized to pigment granules are indicated. Imaging was done with a 63X Plan apo lens.

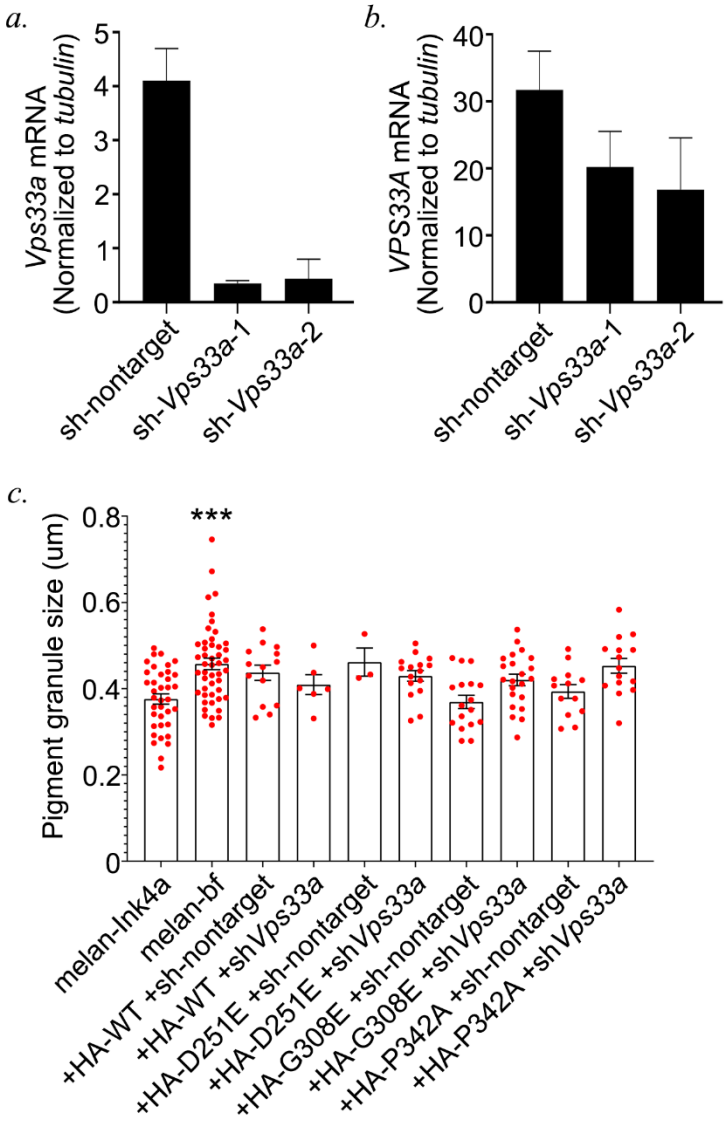

Appendix Figure 3: Overexpression of human VPS33A and knockdown of endogenous Vps33a does not phenocopy melan-bf cells at 14 days post-selection. (*a*, *b*) Melan-Ink4a cells stably expressing human *WT VPS33A* were infected with lentivirus expressing non-target shRNA or shRNAs against *Vps33a* and were analyzed by qRT-PCR for mRNA levels of mouse *Vps33a* (*a*) or human *VPS33A* (*b*) 14 days post-selection. Ct values of target genes were normalized to the Ct values of the housekeeping gene tubulin to determine relative expression levels. Data are from n=1 experiment. (*c*) The average pigment granule size per cell in μm was quantified and is depicted as mean ± SEM with each dot representing the average pigment granule size in one cell. Quantification is from n=1 experiment, except for melan-Ink4a and melan-bf which are from n=2 experiments and are the same data and statistical analyses as graphed in Figure 3.7d.

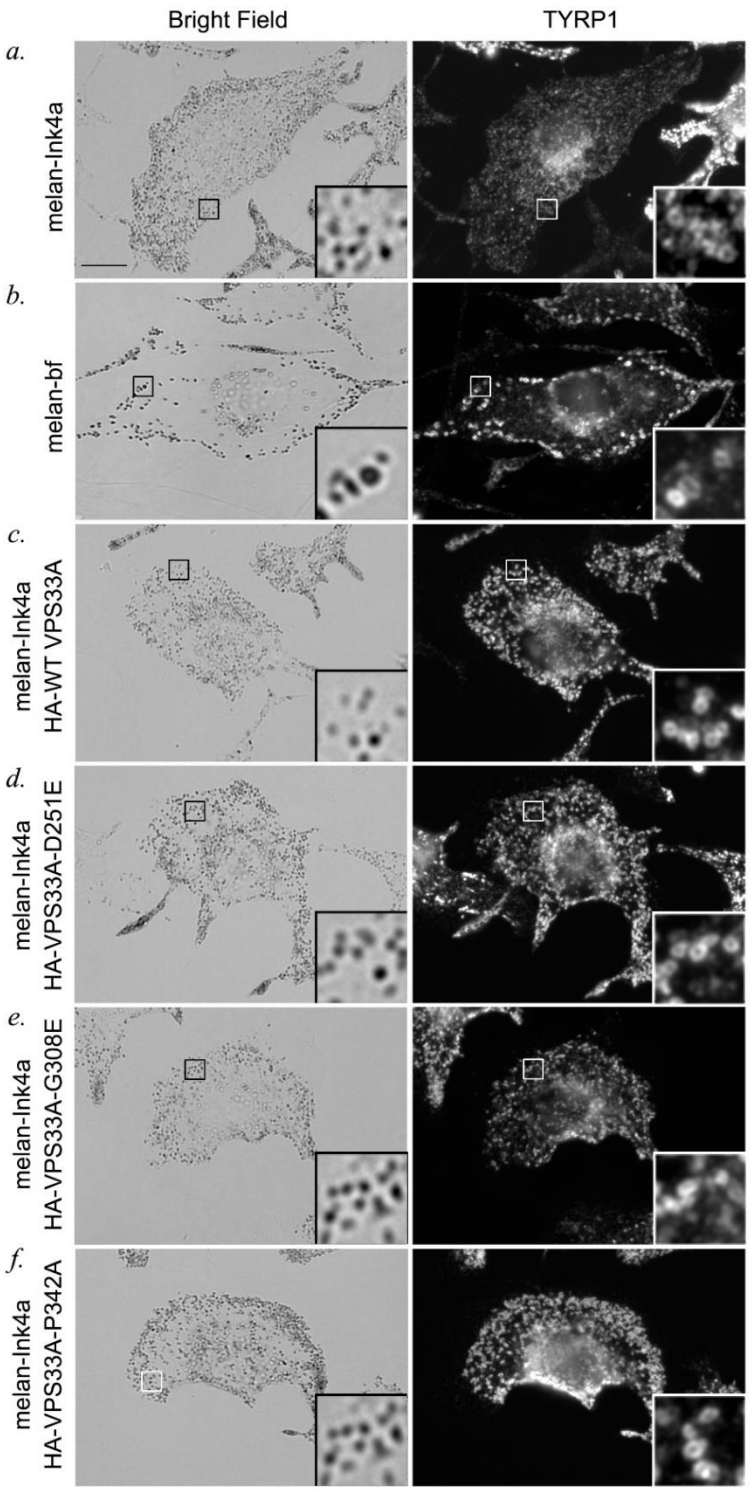

Appendix Figure 4: Overexpression of human WT VPS33A or variants does not phenocopy melan-bf cells. (*a-f*) Melan-Ink4a cells (*a*), melan-bf cells (*b*), or melan-Ink4a cells stably

expressing HA-tagged human WT or variant VPS33A (*c-f*) were fixed, stained with an antibody to TYRP1, and analyzed by BFM (left) and IFM (right). Images are representative of n=1 experiment.

Appendix B: MELOPS

To measure melanosomal pH using MELOPS, we subcloned MELOPS into a retroviral vector, generated retrovirus, and infected melan-Ink4a cells and melan-uw cells as a pilot experiment to test the construct. We were concerned that the presence of melanin in melan-Ink4a cells might decrease fluorescence intensity independent of pH by masking or quenching the fluorophore; therefore, we treated both melan-Ink4a and melan-uw cells with phenylthiourea, which inhibits TYR function by binding to copper ions at its active site (Chang, 2009), until cells were depigmented. We validated MELOPS localization to TYRP1-GFP-positive melanosomes by live confocal microscopy (**Appendix Figure 5**). We measured fluorescence intensity by flow cytometry and generated a standard curve by incubating cells in buffers at pH 5, 6, 7, and 8 with the ionophores nigericin and monensin (**Appendix Figure 6a** in PTU-treated melan-Ink4a cells; note that incubation in pH 5 buffer resulted in cell death). However, the fluorescence intensity of melan-Ink4a cells (not treated with ionophores) was lower than expected at ~ pH 5.5 – 5.8 (**Appendix Figure 6b, c**). This estimated pH is consistent with the reported pH of MNT-1 cells, a melanoma line, measured by MELOPS (Ambrosio et al., 2016), but both are low considering that melan-Ink4a and MNT-1 cells are well pigmented and thus should contain melansoomes closer to near-neutral pH. Additionally, we observed that the fluorescence intensity from untreated melan-uw cells was much higher than that of melan-Ink4a cells (**Appendix Figure 6b, d**), which contradicts our model of SLC45A2 function and the pH requirement for melanin synthesis. Together, those data suggest that MELOPS

fluorescence may be influenced by something other than pH in the melanosomal lumen (considering that the standard curves generated in the presence of ionophore are reasonable but that measurements of untreated cells yield unexpected results), so it may not be an optimal fluorophore for melanosome pH measurements.

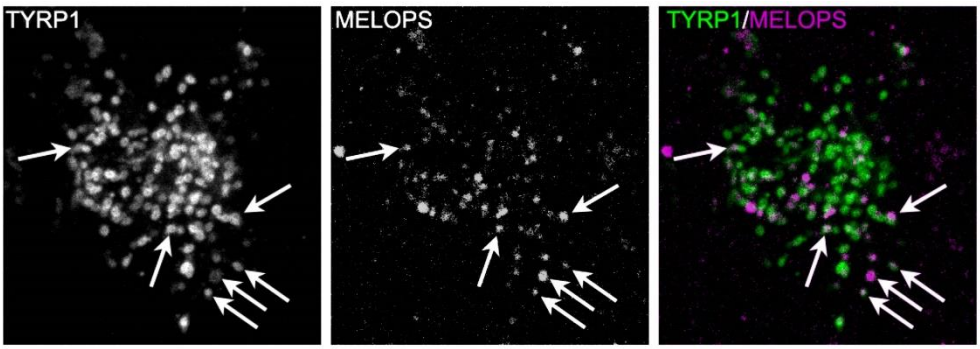

Appendix Figure 5: MELOPS localizes to TYRP1-containing melanosomes. Melan-Ink4a cells were infected with retroviruses to express MELOPS and TYRP1-GFP. 2 days post-infection, cells were imaged by live confocal microscopy in pH 8 buffer with ionophores. Arrows, examples of TYRP1-GFP and MELOPS overlap.

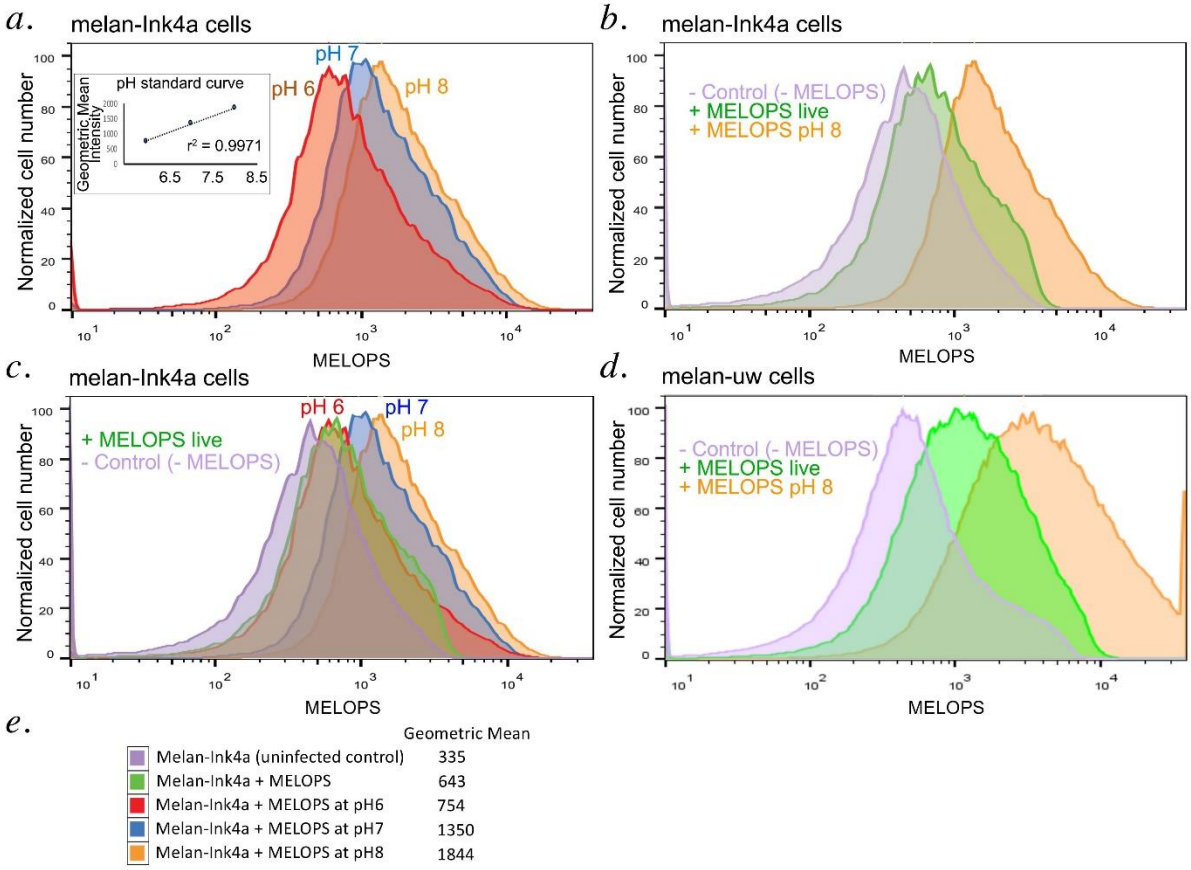

Appendix Figure 6: MELOPS indicates a low melanosome pH. Melan-Ink4a (a-c) or melan-uw (d) cells were pre-treated for over two months with 300 µM PTU and were uninfected or infected with retrovirus encoding MELOPS. Cells were analyzed 2 days later by flow cytometry. MELOPS fluorescence intensity from live cells (gated using forward and side scatter) is shown by histogram. (*a, c*) To define a pH standard curve for MELOPS fluorescence, cells were collected, washed with PBS, and resuspended in isotonic buffers at pH 6, 7, and 8. Nigericin and monensin (10 µM each) were added to each sample at room temperature, and samples were analyzed 5 min later. Geometric means of intensity are shown in panel *e*. (*b*, *d*) Live cells not expressing (- Control) or expressing MELOPS (+ MELOPS live) were analyzed directly in medium with no ionophores. For melan-Ink4a, geometric means of intensity are shown in panel *e* relative to pH controls. The calculated pH of melan-Ink4a melanosomes was ~ 5.8.

To validate our data from melanocytes, we repeated the experiment in HeLa cells, were we have shown that ectopically expressed OCA2 or SLC45A2 localizes to lysosomes and increases lysosomal pH. HeLa cells were transfected with LAMP1-GFP alone,

MELOPS alone, or LAMP1-GFP and MELOPS with or without HA-SLC45A2 or HA-OCA2, and then analyzed – with or without treatment with ionophores and defined pH buffers – by flow cytometry for GFP and for mNectarine in MELOPS. Using cells expressing GFP-LAMP1 + MELOPS and treated with ionophores at varying pH, we were able to obtain a standard curve for MELOPS for pH 6 – 8 (**Appendix Figure 7**; Appendix Figure 7a shows the gates used to define LAMP1-GFP+ cells and Appendix Figure 7b shows the corresponding MELOPS signal in these cells).

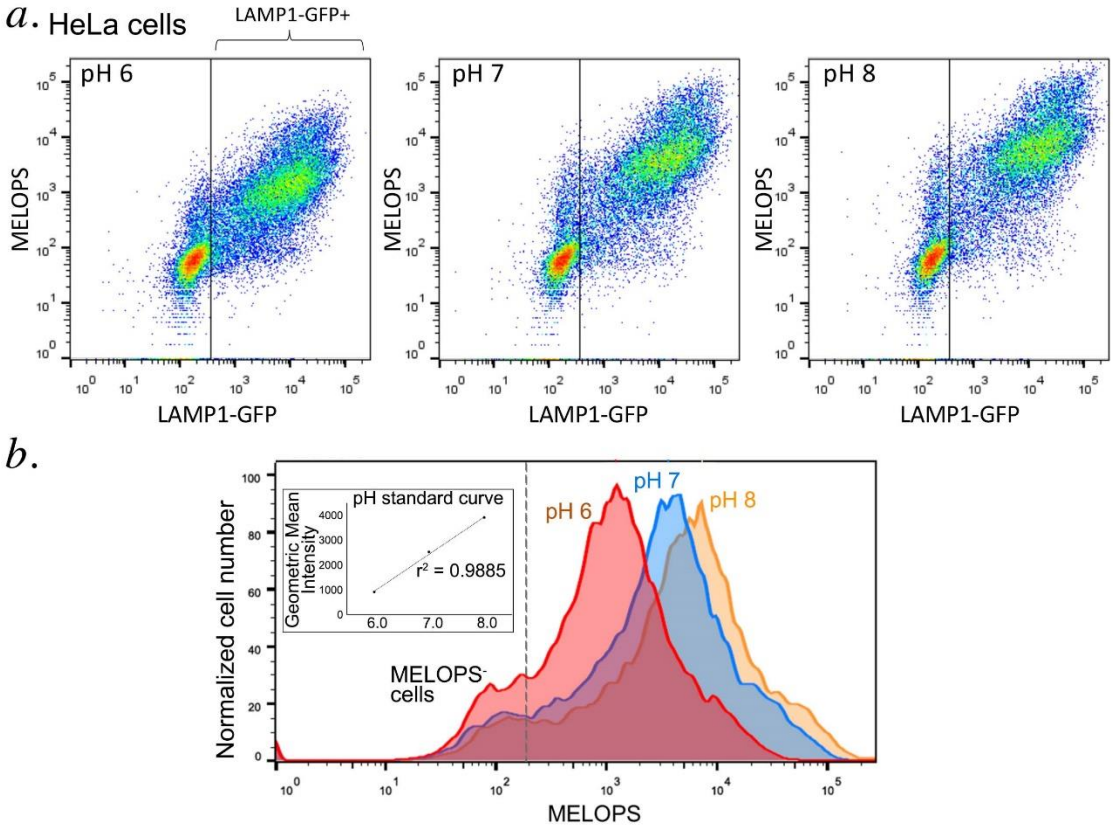

Appendix Figure 7: pH curve in LAMP1-GFP/MELOPS-expressing HeLa cells. HeLa cells were transfected with MELOPS and LAMP1-GFP and analyzed by flow cytometry 2 days later. For the pH standard, cells were collected, washed with PBS,a nd resuspended in buffers at pH 6, 7, and 8. Nigericin and monensin (10 µM each) were added to each sample for 5 min at room temperature before analysis. (*a*) 2D plot of LAMP1-GFP vs MELOPS signal for live cells gated using forward and side scatter. (*b*) Histogram of MELOPS fluorescence of the GFP+ gate (shown in *a*) and calculated standard curve of fluorescence (geometric mean intensity) vs. pH.

We then generated a histogram of the MELOPS fluorescence intensity of LAMP1-GFP+ of HeLa cells expressing LAMP1-GFP and MELOPS; LAMP1-GFP, MELOPS, and HA-OCA2; and LAMP1-GFP, MELOPS, and HA-SLC45A2 (**Appendix Figure 8a**). We observed two populations of MELOPS-expressing cells (**Appendix Figure 8a, b**) and excluded the population of with higher MELOPS expression from our analyses because we reasoned that these cells likely overexpressed MELOPS, resulting in cell surface expression due to competition for sorting machinery (Marks et al., 1996). From this histogram, we see that HeLa cells with MELOPS alone have the highest fluorescence intensity and the peaks gradually shift left with expression of HA-OCA2 and HA-SLC45A2 (**Appendix Figure 8c**), correlating with decreased pH in the MELOPS+ compartments of these cells and contradicting work from our lab and others that show that OCA2 (Bellono et al., 2014) or SLC45A2 can increase pH. Therefore, we show that, although MELOPS responds predictably to ionophore treatment and buffers of increasing pH, the mNectarine fluorophore is being influenced by other lumenal factors, making it a poor sensor of lumenal pH.

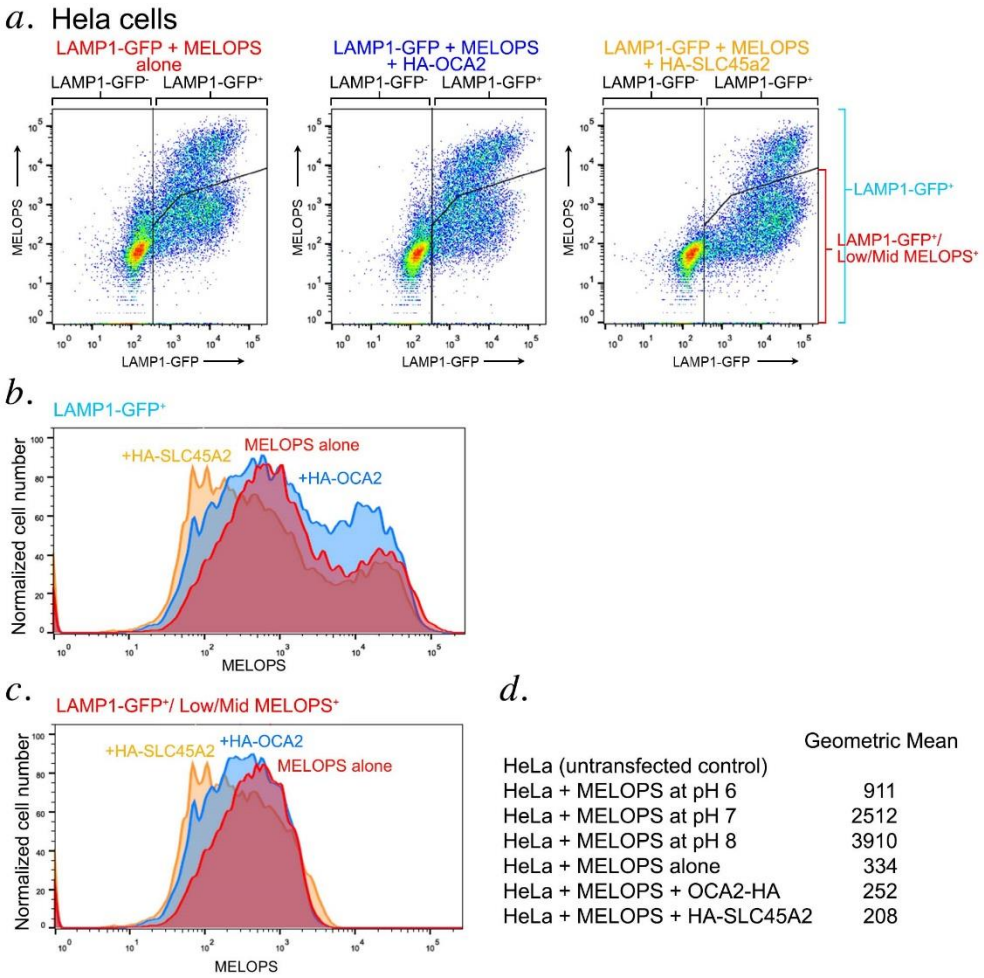

d.

	Geometric Mean
HeLa (untransfected control)	
HeLa + MELOPS at pH 6	911
HeLa + MELOPS at pH 7	2512
HeLa + MELOPS at pH 8	3910
HeLa + MELOPS alone	334
HeLa + MELOPS + OCA2-HA	252
HeLa + MELOPS + HA-SLC45A2	208

Appendix Figure 8: MELOPS measurements of HA-OCA2 and HA-SLC45A2 effects on late-endosomal/lysosomal pH in HeLa cells. HeLa cells were co-transfected with LAMP1-GFP and MELOPS with either an empty vector, HA-OCA2, or HA-SLC45A2, and analyzed by flow cytometry 2 days post-transfection. (*a*) 2D plot comparing LAMP1-GFP and MELOPS expression in live cells gated on forward and side scatter. LAMP1-GFP+ and LAMP1-GFP- gates are indicated for histogram analyses in *b*. Also shown is the gate used to exclude the population of exceedingly high MELOPS expressers. (*b*, *c*) Histogram analyses of total LAMP1-GFP+ population (*b*) or Low/Mid MELOPS+ population (*c*). (*d*) Geometric means of pH standards (from Figure 4.5) and experimental samples in the LAMP1+/Low-Mid MELOPS+ gate shown in panel *c*.

BIBLIOGRAPHY

Abdul-Hay, S.O., Sahara, T., McBride, M., Kang, D., and Leissring, M.A. (2012). Identification of BACE2 as an avid ss-amyloid-degrading protease. Mol Neurodegener *7*, 46.

Adema, G.J., de Boer, A.J., Vogel, A.M., Loenen, W.A., and Figdor, C.G. (1994). Molecular characterization of the melanocyte lineage-specific antigen gp100. J Biol Chem *269*, 20126-20133.

Adhikari, K., Mendoza-Revilla, J., Sohail, A., Fuentes-Guajardo, M., Lampert, J., Chacon-Duque, J.C., Hurtado, M., Villegas, V., Granja, V., Acuna-Alonzo, V.*, et al.* (2019a). A GWAS in Latin Americans highlights the convergent evolution of lighter skin pigmentation in Eurasia. Nat Commun *10*, 358.

Adhikari, K., Mendoza-Revilla, J., Sohail, A., Fuentes-Guajardo, M., Lampert, J., Chacon-Duque, J.C., Hurtado, M., Villegas, V., Granja, V., Acuna-Alonzo, V.*, et al.* (2019b). A GWAS in Latin Americans highlights the convergent evolution of lighter skin pigmentation in Eurasia. Nat Commun *10*, 358.

Agbai, O.N., Buster, K., Sanchez, M., Hernandez, C., Kundu, R.V., Chiu, M., Roberts, W.E., Draelos, Z.D., Bhushan, R., Taylor, S.C.*, et al.* (2014). Skin cancer and photoprotection in people of color: a review and recommendations for physicians and the public. J Am Acad Dermatol *70*, 748-762.

Akbar, M.A., Ray, S., and Kramer, H. (2009). The SM Protein Car/Vps33A Regulates SNARE-mediated Trafficking to Lysosomes and Lysosome-related Organelles. Molecular Biology of the Cell *20*, 1705-1714.

Aksan, I., and Goding, C.R. (1998). Targeting the microphthalmia basic helix-loop-helix-leucine zipper transcription factor to a subset of E-box elements in vitro and in vivo. Mol Cell Biol *18*, 6930-6938.

Alberts, B., Johnson, A., Lewis, J., Raff, M., Roberts, K., and Walter, P. (2002). Carrier Proteins and Active Membrane Transport. In Molecular Biology of the Cell (New York: Garland Science).

Alsaif, H.S., Al-Owain, M., Barrios-Llerena, M.E., Gosadi, G., Binamer, Y., Devadason, D., Ravenscroft, J., Suri, M., and Alkuraya, F.S. (2019). Homozygous Loss-of-Function Mutations in AP1B1, Encoding Beta-1 Subunit of Adaptor-Related Protein Complex 1, Cause MEDNIK-like Syndrome. Am J Hum Genet *105*, 1016-1022.

Altimimi, H.F., and Schnetkamp, P.P. (2007). Na+/Ca2+-K+ exchangers (NCKX): functional properties and physiological roles. Channels (Austin) *1*, 62-69.

Amaya, C., Militello, R.D., Calligaris, S.D., and Colombo, M.I. (2016). Rab24 interacts with the Rab7/Rab interacting lysosomal protein complex to regulate endosomal degradation. Traffic *17*, 1181-1196.

Ambrosio, A.L., Boyle, J.A., Aradi, A.E., Christian, K.A., and Di Pietro, S.M. (2016). TPC2 controls pigmentation by regulating melanosome pH and size. Proc Natl Acad Sci U S A *113*, 5622-5627.

Ammann, S., Schulz, A., Krageloh-Mann, I., Dieckmann, N.M., Niethammer, K., Fuchs, S., Eckl, K.M., Plank, R., Werner, R., Altmuller, J.*, et al.* (2016). Mutations in AP3D1 associated with immunodeficiency and seizures define a new type of Hermansky-Pudlak syndrome. Blood *127*, 997-1006.

Amsterdam, A., Nissen, R.M., Sun, Z., Swindell, E.C., Farrington, S., and Hopkins, N. (2004). Identification of 315 genes essential for early zebrafish development. Proc Natl Acad Sci U S A *101*, 12792-12797.
Ancans, J., Hoogduijn, M.J., and Thody, A.J. (2001a). Melanosomal pH, pink locus protein and their roles in melanogenesis. J Invest Dermatol *117*, 158-159.
Ancans, J., and Thody, A.J. (2000). Activation of melanogenesis by vacuolar type H(+)-ATPase inhibitors in amelanotic, tyrosinase positive human and mouse melanoma cells. FEBS Lett *478*, 57-60.
Ancans, J., Tobin, D.J., Hoogduijn, M.J., Smit, N.P., Wakamatsu, K., and Thody, A.J. (2001b). Melanosomal pH controls rate of melanogenesis, eumelanin/phaeomelanin ratio and melanosome maturation in melanocytes and melanoma cells. Exp Cell Res *268*, 26-35.
Ando, H., Niki, Y., Ito, M., Akiyama, K., Matsui, M.S., Yarosh, D.B., and Ichihashi, M. (2012). Melanosomes are transferred from melanocytes to keratinocytes through the processes of packaging, release, uptake, and dispersion. J Invest Dermatol *132*, 1222-1229.
Ando, H., Niki, Y., Yoshida, M., Ito, M., Akiyama, K., Kim, J.H., Yoon, T.J., Matsui, M.S., Yarosh, D.B., and Ichihashi, M. (2011). Involvement of pigment globules containing multiple melanosomes in the transfer of melanosomes from melanocytes to keratinocytes. Cell Logist *1*, 12-20.
Armas, L.A., Dowell, S., Akhter, M., Duthuluru, S., Huerter, C., Hollis, B.W., Lund, R., and Heaney, R.P. (2007). Ultraviolet-B radiation increases serum 25-hydroxyvitamin D levels: the effect of UVB dose and skin color. J Am Acad Dermatol *57*, 588-593.
Aspengren, S., Hedberg, D., and Wallin, M. (2006). Studies of pigment transfer between Xenopus laevis melanophores and fibroblasts in vitro and in vivo. Pigment Cell Res *19*, 136-145.
Ather, S., Proudlock, F.A., Welton, T., Morgan, P.S., Sheth, V., Gottlob, I., and Dineen, R.A. (2019). Aberrant visual pathway development in albinism: From retina to cortex. Hum Brain Mapp *40*, 777-788.
Bahadoran, P., Aberdam, E., Mantoux, F., Busca, R., Bille, K., Yalman, N., de Saint-Basile, G., Casaroli-Marano, R., Ortonne, J.P., and Ballotti, R. (2001). Rab27a: A key to melanosome transport in human melanocytes. J Cell Biol *152*, 843-850.
Baker, R.W., and Hughson, F.M. (2016). Chaperoning SNARE assembly and disassembly. Nat Rev Mol Cell Biol *17*, 465-479.
Baker, R.W., Jeffrey, P.D., and Hughson, F.M. (2013). Crystal Structures of the Sec1/Munc18 (SM) Protein Vps33, Alone and Bound to the Homotypic Fusion and Vacuolar Protein Sorting (HOPS) Subunit Vps16*. PLoS ONE *8*, 28-30.
Baker, R.W., Jeffrey, P.D., Zick, M., Phillips, B.P., Wickner, W.T., and Hughson, F.M. (2015). A direct role for the Sec1/Munc18-family protein Vps33 as a template for SNARE assembly. Science *349*, 1111-1114.
Balderhaar, H.J.k., Lachmann, J., Yavavli, E., Brocker, C., Lurick, A., and Ungermann, C. (2013). The CORVET complex promotes tethering and fusion of Rab5/Vps21-positive membranes. Proceedings of the National Academy of Sciences *110*, 3823-3828.
Balderhaar, H.J.k., and Ungermann, C. (2013). CORVET and HOPS tethering complexes - coordinators of endosome and lysosome fusion. Journal of Cell Science *126*, 1307-1316.
Banach-Orlowska, M., Jastrzebski, K., Cendrowski, J., Maksymowicz, M., Wojciechowska, K., Korostynski, M., Moreau, D., Gruenberg, J., and Miaczynska, M.

(2018). The topology of the lymphotoxin beta receptor that accumulates upon endolysosomal dysfunction dictates the NF-kappaB signaling outcome. J Cell Sci *131*.
Barnicot, N.A., and Birbeck, M.S. (1958). The Electron Microscopy of Human Melanocytes and Melanin Granules. In The Biology of Hair Growth, W. Montagna, and R.A. Ellis, eds. (Academic Press), pp. 239-253.
Bartolke, R., Heinisch, J.J., Wieczorek, H., and Vitavska, O. (2014). Proton-associated sucrose transport of mammalian solute carrier family 45: an analysis in Saccharomyces cerevisiae. Biochem J *464*, 193-201.
Bartölke, R., Heinisch, J.J., Wieczorek, H., and Vitavska, O. (2014). Proton-associated sucrose transport of mammalian solute carrier family 45: an analysis in Saccharomyces cerevisiae. Biochem J *464*, 193-201.
Basrur, V., Yang, F., Kushimoto, T., Higashimoto, Y., Yasumoto, K., Valencia, J., Muller, J., Vieira, W.D., Watabe, H., Shabanowitz, J.*, et al.* (2003). Proteomic analysis of early melanosomes: identification of novel melanosomal proteins. J Proteome Res *2*, 69-79.
Bassi, M.T., Incerti, B., Easty, D.J., Sviderskaya, E.V., and Ballabio, A. (1996). Cloning of the murine homolog of the ocular albinism type 1 (OA1) gene: sequence, genomic structure, and expression analysis in pigment cells. Genome Res *6*, 880-885.
Bassi, M.T., Schiaffino, M.V., Renieri, A., De Nigris, F., Galli, L., Bruttini, M., Gebbia, M., Bergen, A.A., Lewis, R.A., and Ballabio, A. (1995). Cloning of the gene for ocular albinism type 1 from the distal short arm of the X chromosome. Nat Genet *10*, 13-19.
Bastiaens, M.T., ter Huurne, J.A., Kielich, C., Gruis, N.A., Westendorp, R.G., Vermeer, B.J., Bavinck, J.N., and Leiden Skin Cancer Study, T. (2001). Melanocortin-1 receptor gene variants determine the risk of nonmelanoma skin cancer independently of fair skin and red hair. Am J Hum Genet *68*, 884-894.
Baxter, L.L., and Pavan, W.J. (2002). The oculocutaneous albinism type IV gene Matp is a new marker of pigment cell precursors during mouse embryonic development. Mech Dev *116*, 209-212.
Bellono, N.W., Escobar, I.E., Lefkovith, A.J., Marks, M.S., and Oancea, E. (2014). An intracellular anion channel critical for pigmentation. eLife *3*, e04543-e04543.
Bellono, N.W., Escobar, I.E., and Oancea, E. (2016). A melanosomal two-pore sodium channel regulates pigmentation. Sci Rep *6*, 26570.
Benito-Martinez, S., Zhu, Y., Jani, R.A., Harper, D.C., Marks, M.S., and Delevoye, C. (2020). Research Techniques Made Simple: Cell Biology Methods for the Analysis of Pigmentation. J Invest Dermatol *140*, 257-268 e258.
Bennett, D.C., Cooper, P.J., and Hart, I.R. (1987). A line of non-tumorigenic mouse melanocytes, syngeneic with the B16 melanoma and requiring a tumour promoter for growth. Int J Cancer *39*, 414-418.
Bennett, D.C., and Lamoreux, M.L. (2003). The color loci of mice--a genetic century. Pigment Cell Res *16*, 333-344.
Bennett, V., and Healy, J. (2009). Membrane domains based on ankyrin and spectrin associated with cell-cell interactions. Cold Spring Harb Perspect Biol *1*, a003012.
Bentley, N.J., Eisen, T., and Goding, C.R. (1994). Melanocyte-specific expression of the human tyrosinase promoter: activation by the microphthalmia gene product and role of the initiator. Mol Cell Biol *14*, 7996-8006.
Berson, J.F., Frank, D.W., Calvo, P.A., Bieler, B.M., and Marks, M.S. (2000). A common temperature-sensitive allelic form of human tyrosinase is retained in the endoplasmic reticulum at the nonpermissive temperature. J Biol Chem *275*, 12281-12289.

Berson, J.F., Harper, D.C., Tenza, D., Raposo, G., and Marks, M.S. (2001). Pmel17 initiates premelanosome morphogenesis within multivesicular bodies. Mol Biol Cell *12*, 3451-3464.
Berson, J.F., Theos, A.C., Harper, D.C., Tenza, D., Raposo, G., and Marks, M.S. (2003). Proprotein convertase cleavage liberates a fibrillogenic fragment of a resident glycoprotein to initiate melanosome biogenesis. J Cell Biol *161*, 521-533.
Bertolotto, C., Bille, K., Ortonne, J.P., and Ballotti, R. (1996). Regulation of tyrosinase gene expression by cAMP in B16 melanoma cells involves two CATGTG motifs surrounding the TATA box: implication of the microphthalmia gene product. J Cell Biol *134*, 747-755.
Bhatnagar, V., Anjaiah, S., Puri, N., Darshanam, B.N., and Ramaiah, A. (1993). pH of melanosomes of B 16 murine melanoma is acidic: its physiological importance in the regulation of melanin biosynthesis. Arch Biochem Biophys *307*, 183-192.
Bhatnagar, V., and Ramalah, A. (1998). Characterization of Mg2+-ATPase activity in isolated B16 murine melanoma melanosomes. Mol Cell Biochem *189*, 99-106.
Bin, B.H., Bhin, J., Yang, S.H., Shin, M., Nam, Y.J., Choi, D.H., Shin, D.W., Lee, A.Y., Hwang, D., Cho, E.G.*, et al.* (2015). Membrane-Associated Transporter Protein (MATP) Regulates Melanosomal pH and Influences Tyrosinase Activity. PLoS One *10*, e0129273.
Birbeck, M.S.C., Mercer, E.H., and Barnicot, N.A. (1956). The structure and formation of pigment granules in human hair. Experimental Cell Research *10*, 505-514.
Blagoveshchenskaya, A.D., Hewitt, E.W., and Cutler, D.F. (1999). Di-leucine signals mediate targeting of tyrosinase and synaptotagmin to synaptic-like microvesicles within PC12 cells. Mol Biol Cell *10*, 3979-3990.
Boissy, R.E., Sakai, C., Zhao, H., Kobayashi, T., and Hearing, V.J. (1998). Human tyrosinase related protein-1 (TRP-1) does not function as a DHICA oxidase activity in contrast to murine TRP-1. Exp Dermatol *7*, 198-204.
Boissy, R.E., Zhao, H., Oetting, W.S., Austin, L.M., Wildenberg, S.C., Boissy, Y.L., Zhao, Y., Sturm, R.A., Hearing, V.J., King, R.A.*, et al.* (1996). Mutation in and lack of expression of tyrosinase-related protein-1 (TRP-1) in melanocytes from an individual with brown oculocutaneous albinism: a new subtype of albinism classified as "OCA3". Am J Hum Genet *58*, 1145-1156.
Bouchard, B., Fuller, B.B., Vijayasaradhi, S., and Houghton, A.N. (1989). Induction of pigmentation in mouse fibroblasts by expression of human tyrosinase cDNA. J Exp Med *169*, 2029-2042.
Bowman, S.L., Bi-Karchin, J., Le, L., and Marks, M.S. (2019). The road to lysosome-related organelles: Insights from Hermansky-Pudlak syndrome and other rare diseases. Traffic *20*, 404-435.
Branda, R.F., and Eaton, J.W. (1978). Skin color and nutrient photolysis: an evolutionary hypothesis. Science *201*, 625-626.
Branicki, W., Brudnik, U., Draus-Barini, J., Kupiec, T., ., and Wojas-Pelc, A. (2008). Association of the SLC45A2 gene with physiological human hair colour variation. J Hum Genet *53*, 966-971.
Brilliant, M.H. (2001). The mouse p (pink-eyed dilution) and human P genes, oculocutaneous albinism type 2 (OCA2), and melanosomal pH. Pigment Cell Res *14*, 86-93.
Brocker, C., Kuhlee, A., Gatsogiannis, C., Balderhaar, H.J., Honscher, C., Engelbrecht-Vandre, S., Ungermann, C., and Raunser, S. (2012). Molecular architecture of the

multisubunit homotypic fusion and vacuole protein sorting (HOPS) tethering complex. Proc Natl Acad Sci U S A *109*, 1991-1996.
Bultema, J.J., Ambrosio, A.L., Burek, C.L., and Di Pietro, S.M. (2012). BLOC-2, AP-3, and AP-1 proteins function in concert with Rab38 and Rab32 proteins to mediate protein trafficking to lysosome-related organelles. Journal of Biological Chemistry.
Burgoyne, T., Jolly, R., Martin-Martin, B., Seabra, M.C., Piccirillo, R., Schiaffino, M.V., and Futter, C.E. (2013). Expression of OA1 limits the fusion of a subset of MVBs with lysosomes - a mechanism potentially involved in the initial biogenesis of melanosomes. J Cell Sci *126*, 5143-5152.
Burgstaller, S., Bischof, H., Gensch, T., Stryeck, S., Gottschalk, B., Ramadani-Muja, J., Eroglu, E., Rost, R., Balfanz, S., Baumann, A.*, et al.* (2019). pH-Lemon, a Fluorescent Protein-Based pH Reporter for Acidic Compartments. ACS Sens *4*, 883-891.
Bush, W.D., and Simon, J.D. (2007). Quantification of Ca(2+) binding to melanin supports the hypothesis that melanosomes serve a functional role in regulating calcium homeostasis. Pigment Cell Res *20*, 134-139.
Bustamante, J., Bredeston, L., Malanga, G., and Mordoh, J. (1993). Role of melanin as a scavenger of active oxygen species. Pigment Cell Res *6*, 348-353.
Button, R.W., Roberts, S.L., Willis, T.L., Hanemann, C.O., and Luo, S. (2017). Accumulation of autophagosomes confers cytotoxicity. J Biol Chem *292*, 13599-13614.
Caduff, M., Bauer, A., Jagannathan, V., and Leeb, T. (2017). A single base deletion in the SLC45A2 gene in a Bullmastiff with oculocutaneous albinism. Anim Genet *48*, 619-621.
Calcraft, P.J., Ruas, M., Pan, Z., Cheng, X., Arredouani, A., Hao, X., Tang, J., Rietdorf, K., Teboul, L., Chuang, K.T.*, et al.* (2009). NAADP mobilizes calcium from acidic organelles through two-pore channels. Nature *459*, 596-600.
Calvo, P.A., Frank, D.W., Bieler, B.M., Berson, J.F., and Marks, M.S. (1999). A cytoplasmic sequence in human tyrosinase defines a second class of di-leucine-based sorting signals for late endosomal and lysosomal delivery. J Biol Chem *274*, 12780-12789.
Carraro-Lacroix, L.R., Lessa, L.M., Fernandez, R., and Malnic, G. (2009). Physiological implications of the regulation of vacuolar H+-ATPase by chloride ions. Braz J Med Biol Res *42*, 155-163.
Cerdan, D., Redziniak, G., Bourgeois, C.A., Monsigny, M., and Kieda, C. (1992). C32 human melanoma cell endogenous lectins: characterization and implication in vesicle-mediated melanin transfer to keratinocytes. Exp Cell Res *203*, 164-173.
Cerqueira, C.C., Hunemeier, T., Gomez-Valdes, J., Ramallo, V., Volasko-Krause, C.D., Barbosa, A.A., Vargas-Pinilla, P., Dornelles, R.C., Longo, D., Rothhammer, F.*, et al.* (2014). Implications of the admixture process in skin color molecular assessment. PLoS One *9*, e96886.
Cesarini, J.P. (1988). Photo-induced events in the human melanocytic system: photoaggression and photoprotection. Pigment Cell Res *1*, 223-233.
Chakraborty, A.K., Funasaka, Y., Slominski, A., Ermak, G., Hwang, J., Pawelek, J.M., and Ichihashi, M. (1996). Production and release of proopiomelanocortin (POMC) derived peptides by human melanocytes and keratinocytes in culture: regulation by ultraviolet B. Biochimica et Biophysica Acta (BBA) - Molecular Cell Research *1313*, 130-138.
Chalhoub, N., Benachenhou, N., Rajapurohitam, V., Pata, M., Ferron, M., Frattini, A., Villa, A., and Vacher, J. (2003). Grey-lethal mutation induces severe malignant autosomal recessive osteopetrosis in mouse and human. Nat Med *9*, 399-406.

Chang, T.S. (2009). An updated review of tyrosinase inhibitors. Int J Mol Sci *10*, 2440-2475.
Chao, Y.K., Schludi, V., Chen, C.C., Butz, E., Nguyen, O.N.P., Muller, M., Kruger, J., Kammerbauer, C., Ben-Johny, M., Vollmar, A.M.*, et al.* (2017). TPC2 polymorphisms associated with a hair pigmentation phenotype in humans result in gain of channel function by independent mechanisms. Proc Natl Acad Sci U S A *114*, E8595-E8602.
Chaplin, G. (2004). Geographic distribution of environmental factors influencing human skin coloration. Am J Phys Anthropol *125*, 292-302.
Chedekel, M.R., Agin, P.P., and Sayre, R.M. (1980). Photochemistry of Pheomelanin: Action Spectrum for Superoxide Production. Photochemistry and Photobiology *31*, 553-555.
Chedekel, M.R., Smith, S.K., Post, P.W., Pokora, A., and Vessell, D.L. (1978). Photodestruction of pheomelanin: role of oxygen. Proc Natl Acad Sci U S A *75*, 5395-5399.
Chen, T., Wang, H., Liu, Y., Zhao, B., Zhao, Y., Fan, R., Wang, P., and Dong, C. (2016). Ocular Albinism Type 1 Regulates Melanogenesis in Mouse Melanocytes. Int J Mol Sci *17*.
Cheng, J., Moss, S.C., and Eisner, M. (1994a). X-ray characterization of melanins--II. Pigment Cell Res *7*, 263-273.
Cheng, J., Moss, S.C., Eisner, M., and Zschack, P. (1994b). X-ray characterization of melanins--I. Pigment Cell Res *7*, 255-262.
Chhajlani, V., and Wikberg, J.E.S. (1992). Molecular cloning and expression of the human melanocyte stimulating hormone receptor cDNA. FEBS Letters *309*, 417-420.
Chiaverini, C., Beuret, L., Flori, E., Busca, R., Abbe, P., Bille, K., Bahadoran, P., Ortonne, J.P., Bertolotto, C., and Ballotti, R. (2008). Microphthalmia-associated transcription factor regulates RAB27A gene expression and controls melanosome transport. J Biol Chem *283*, 12635-12642.
Chintala, S., Li, W., Lamoreux, M.L., Ito, S., Wakamatsu, K., Sviderskaya, E.V., Bennett, D.C., Park, Y.M., Gahl, W.A., Huizing, M.*, et al.* (2005). Slc7a11 gene controls production of pheomelanin pigment and proliferation of cultured cells. Proc Natl Acad Sci U S A *102*, 10964-10969.
Chintala, S., Tan, J., Gautam, R., Rusiniak, M.E., Guo, X., Li, W., Gahl, W.A., Huizing, M., Spritz, R.A., Hutton, S.*, et al.* (2007a). The Slc35d3 gene, encoding an orphan nucleotide sugar transporter, regulates platelet-dense granules. Blood *109*, 1533-1540.
Chintala, S., Tan, J., Gautam, R., Rusiniak, M.E., Guo, X., Li, W., Gahl, W.A., Huizing, M., Spritz, R.A., Hutton, S.*, et al.* (2007b). The Slc35d3 gene, encoding an orphan nucleotide sugar transporter, regulates platelet dense granules. Blood *109*, 1533-1540.
Chou, H.-T., Dukovski, D., Chambers, M.G., Reinisch, K.M., and Walz, T. (2016). CATCHR, HOPS and CORVET tethering complexes share a similar architecture. Nature Structural & Molecular Biology *23*, 761-763.
Clancy, C.M., and Simon, J.D. (2001). Ultrastructural organization of eumelanin from Sepia officinalis measured by atomic force microscopy. Biochemistry *40*, 13353-13360.
Cohen, J., and Szabo, G. (1968). Study of pigment donation in vitro. Exp Cell Res *50*, 418-433.
Cook, A.L., Chen, W., Thurber, A.E., Smit, D.J., Smith, A.G., Bladen, T.G., Brown, D.L., Duffy, D.L., Pastorino, L., Bianchi-Scarra, G.*, et al.* (2009a). Analysis of cultured human

melanocytes based on polymorphisms within the SLC45A2/MATP, SLC24A5/NCKX5, and OCA2/P loci. J Invest Dermatol *129*, 392-405.
Cook, A.L., Chen, W., Thurber, A.E., Smit, D.J., Smith, A.G., Bladen, T.G., Brown, D.L., Duffy, D.L., Pastorino, L., Bianchi-Scarra, G.*, et al.* (2009b). Analysis of cultured human melanocytes based on polymorphisms within the SLC45A2/MATP, SLC24A5/NCKX5, and OCA2/P loci. J Invest Dermatol *129*, 392-405.
Cooksey, C.J., Garratt, P.J., Land, E.J., Pavel, S., Ramsden, C.A., Riley, P.A., and Smit, N.P. (1997). Evidence of the indirect formation of the catecholic intermediate substrate responsible for the autoactivation kinetics of tyrosinase. J Biol Chem *272*, 26226-26235.
Cortese, K., Giordano, F., Surace, E.M., Venturi, C., Ballabio, A., Tacchetti, C., and Marigo, V. (2005). The ocular albinism type 1 (OA1) gene controls melanosome maturation and size. Invest Ophthalmol Vis Sci *46*, 4358-4364.
Costin, G.E., Valencia, J.C., Vieira, W.D., Lamoreux, M.L., and Hearing, V.J. (2003). Tyrosinase processing and intracellular trafficking is disrupted in mouse primary melanocytes carrying the underwhite (uw) mutation. A model for oculocutaneous albinism (OCA) type 4. J Cell Sci *116*, 3203-3212.
Cotter, K., Stransky, L., McGuire, C., and Forgac, M. (2015). Recent Insights into the Structure, Regulation, and Function of the V-ATPases. Trends Biochem Sci *40*, 611-622.
Crawford, N.G., Kelly, D.E., Hansen, M.E.B., Beltrame, M.H., Fan, S., Bowman, S.L., Jewett, E., Ranciaro, A., Thompson, S., Lo, Y.*, et al.* (2017). Loci associated with skin pigmentation identified in African populations. Science *358*.
Cruickshank, C.N., and Harcourt, S.A. (1964). Pigment Donation in Vitro. J Invest Dermatol *42*, 183-184.
Cui, R., Widlund, H.R., Feige, E., Lin, J.Y., Wilensky, D.L., Igras, V.E., D'Orazio, J., Fung, C.Y., Schanbacher, C.F., Granter, S.R.*, et al.* (2007). Central role of p53 in the suntan response and pathologic hyperpigmentation. Cell *128*, 853-864.
D'Alba, L., and Shawkey, M.D. (2019). Melanosomes: Biogenesis, Properties, and Evolution of an Ancient Organelle. Physiol Rev *99*, 1-19.
d'Ischia, M., Wakamatsu, K., Cicoira, F., Di Mauro, E., Garcia-Borron, J.C., Commo, S., Galvan, I., Ghanem, G., Kenzo, K., Meredith, P.*, et al.* (2015). Melanins and melanogenesis: from pigment cells to human health and technological applications. Pigment Cell Melanoma Res *28*, 520-544.
De Filippo, E., Manga, P., and Schiedel, A.C. (2017). Author Response: Comment on "Identification of Novel G Protein-Coupled Receptor 143 Ligands as Pharmacologic Tools for Investigating X-Linked Ocular Albinism". Invest Ophthalmol Vis Sci *58*, 4735-4736.
De Luca, M., Siegrist, W., Bondanza, S., Mathor, M., Cancedda, R., and Eberle, A.N. (1993). Alpha melanocyte stimulating hormone (alpha MSH) stimulates normal human melanocyte growth by binding to high-affinity receptors. J Cell Sci *105 (Pt 4)*, 1079-1084.
Delahaye, J.L., Foster, O.K., Vine, A., Saxton, D.S., Curtin, T.P., Somhegyi, H., Salesky, R., and Hermann, G.J. (2014). Caenorhabditis elegans HOPS and CCZ-1 mediate trafficking to lysosome-related organelles independently of RAB-7 and SAND-1. Mol Biol Cell *25*, 1073-1096.
Delamere, N.A. (2005). Ciliary Body and Ciliary Epithelium. Adv Organ Biol *10*, 127-148.
DeLay, B.D., Corkins, M.E., Hanania, H.L., Salanga, M., Deng, J.M., Sudou, N., Taira, M., Horb, M.E., and Miller, R.K. (2018). Tissue-Specific Gene Inactivation in Xenopus laevis: Knockout of lhx1 in the Kidney with CRISPR/Cas9. Genetics *208*, 673-686.

Delevoye, C., Heiligenstein, X., Ripoll, L., Gilles-Marsens, F., Dennis, M.K., Linares, R.A., Derman, L., Gokhale, A., Morel, E., Faundez, V., *et al.* (2016). BLOC-1 Brings Together the Actin and Microtubule Cytoskeletons to Generate Recycling Endosomes. Curr Biol *26*, 1-13.
Delevoye, C., Hurbain, I., Tenza, D., Sibarita, J.B., Uzan-Gafsou, S., Ohno, H., Geerts, W.J., Verkleij, A.J., Salamero, J., Marks, M.S., *et al.* (2009a). AP-1 and KIF13A coordinate endosomal sorting and positioning during melanosome biogenesis. J Cell Biol *187*, 247-264.
Delevoye, C., Hurbain, I., Tenza, D., Sibarita, J.B., Uzan-Gafsou, S., Ohno, H., Geerts, W.J.C., Verkleij, A.J., Salamero, J., Marks, M.S., *et al.* (2009b). AP-1 and KIF13A coordinate endosomal sorting and positioning during melanosome biogenesis. Journal of Cell Biology *187*, 247-264.
Dennis, M.K., Delevoye, C., Acosta-Ruiz, A., Hurbain, I., Romao, M., Hesketh, G.G., Goff, P.S., Sviderskaya, E.V., Bennett, D.C., Luzio, J.P., *et al.* (2016). BLOC-1 and BLOC-3 regulate VAMP7 cycling to and from melanosomes via distinct tubular transport carriers. Journal of Cell Biology *214*, 293-308.
Dennis, M.K., Mantegazza, A.R., Snir, O.L., Tenza, D., Acosta-Ruiz, A., Delevoye, C., Zorger, R., Sitaram, A., de Jesus-Rojas, W., Ravichandran, K., *et al.* (2015). BLOC-2 targets recycling endosomal tubules to melanosomes for cargo delivery. Journal of Cell Biology *209*, 563-577.
Di Pietro, S.M., Falcon-Perez, J.M., Tenza, D., Setty, S.R., Marks, M.S., Raposo, G., and Dell'Angelica, E.C. (2006). BLOC-1 interacts with BLOC-2 and the AP-3 complex to facilitate protein trafficking on endosomes. Mol Biol Cell *17*, 4027-4038.
Diaz, P., Gimeno, Y., Carro, P., Gonzalez, S., Schilardi, P.L., Benitez, G., Salvarezza, R.C., and Creus, A.H. (2005). Electrochemical self-assembly of melanin films on gold. Langmuir *21*, 5924-5930.
Dickie, M.M. (1964a). Buff. Mouse News Lett *30*, 30.
Dickie, M.M. (1964b). Underwhite. Mouse News Lett *30*, 30.
Diffey, B.L. (2002). What is light? Photodermatol Photoimmunol Photomed *18*, 68-74.
Diment, S., Eidelman, M., Rodriguez, G.M., and Orlow, S.J. (1995a). Lysosomal hydrolases are present in melanosomes and are elevated in melanizing cells. J Biol Chem *270*, 4213-4215.
Diment, S., Eidelman, M., Rodriguez, G.M., and Orlow, S.J. (1995b). Lysosomal hydrolases are present in melanosomes and are elevated in melanizing cells. J Biol Chem *270*, 4213-4215.
Ding, X., Jiang, X., Tian, R., Zhao, P., Li, L., Wang, X., Chen, S., Zhu, Y., Mei, M., Bao, S., *et al.* (2019). RAB2 regulates the formation of autophagosome and autolysosome in mammalian cells. Autophagy *15*, 1774-1786.
Dolman, N.J., and Tepikin, A.V. (2006). Calcium gradients and the Golgi. Cell Calcium *40*, 505-512.
Domyan, E.T., Guernsey, M.W., Kronenberg, Z., Krishnan, S., Boissy, R.E., Vickrey, A.I., Rodgers, C., Cassidy, P., Leachman, S.A., Fondon, J.W., 3rd, *et al.* (2014). Epistatic and combinatorial effects of pigmentary gene mutations in the domestic pigeon. Curr Biol *24*, 459-464.
Donatien, P.D., Hunt, G., Pieron, C., Lunec, J., Taieb, A., and Thody, A.J. (1992). The expression of functional MSH receptors on cultured human melanocytes. Arch Dermatol Res *284*, 424-426.

Donatien, P.D., and Orlow, S.J. (1995). Interaction of melanosomal proteins with melanin. Eur J Biochem *232*, 159-164.
Dooley, C.M., Schwarz, H., Mueller, K.P., Mongera, A., Konantz, M., Neuhauss, S.C., Nusslein-Volhard, C., and Geisler, R. (2013). Slc45a2 and V-ATPase are regulators of melanosomal pH homeostasis in zebrafish, providing a mechanism for human pigment evolution and disease. Pigment Cell Melanoma Res *26*, 205-217.
Dores, M.R., Chen, B., Lin, H., Soh, U.J., Paing, M.M., Montagne, W.A., Meerloo, T., and Trejo, J. (2012). ALIX binds a YPX(3)L motif of the GPCR PAR1 and mediates ubiquitin-independent ESCRT-III/MVB sorting. J Cell Biol *197*, 407-419.
Dores, M.R., Grimsey, N.J., Mendez, F., and Trejo, J. (2016). ALIX Regulates the Ubiquitin-Independent Lysosomal Sorting of the P2Y1 Purinergic Receptor via a YPX3L Motif. PLoS One *11*, e0157587.
Du, J., and Fisher, D.E. (2002). Identification of Aim-1 as the underwhite mouse mutant and its transcriptional regulation by MITF. J Biol Chem *277*, 402-406.
Duffy, D.L., Box, N.F., Chen, W., Palmer, J.S., Montgomery, G.W., James, M.R., Hayward, N.K., Martin, N.G., and Sturm, R.A. (2004). Interactive effects of MC1R and OCA2 on melanoma risk phenotypes. Hum Mol Genet *13*, 447-461.
Eagle, R.C., Jr. (1988). Iris pigmentation and pigmented lesions: an ultrastructural study. Trans Am Ophthalmol Soc *86*, 581-687.
Enechukwu, N., Cockburn, M., Ogun, G., Ezejiofor, O.I., George, A., and Ogunbiyi, A. (2019). Higher vitamin D levels in Nigerian albinos compared with pigmented controls. Int J Dermatol *58*, 1148-1152.
Evans, W.C., and Raper, H.S. (1937). The accumulation of l-3:4-dihydroxyphenylalanine in the tyrosinase-tyrosine reaction. Biochem J *31*, 2162-2170.
Falletta, P., Bagnato, P., Bono, M., Monticone, M., Schiaffino, M.V., Bennett, D.C., Goding, C.R., Tacchetti, C., and Valetti, C. (2014). Melanosome-autonomous regulation of size and number: The OA1 receptor sustains PMEL expression. Pigment Cell and Melanoma Research *27*, 565-579.
Fang, D., and Setaluri, V. (1999). Role of microphthalmia transcription factor in regulation of melanocyte differentiation marker TRP-1. Biochem Biophys Res Commun *256*, 657-663.
Fasshauer, D., Sutton, R.B., Brunger, A.T., and Jahn, R. (1998). Conserved structural features of the synaptic fusion complex: SNARE proteins reclassified as Q- and R-SNAREs. Proc Natl Acad Sci U S A *95*, 15781-15786.
Filadi, R., and Pozzan, T. (2015). Generation and functions of second messengers microdomains. Cell Calcium *58*, 405-414.
Fowler, D.M., Koulov, A.V., Alory-Jost, C., Marks, M.S., Balch, W.E., and Kelly, J.W. (2006). Functional amyloid formation within mammalian tissue. PLoS Biol *4*, e6.
Fracasso, N.C.A., de Andrade, E.S., Wiezel, C.E.V., Andrade, C.C.F., Zanao, L.R., da Silva, M.S., Marano, L.A., Donadi, E.A., E, C.C., Simoes, A.L.*, et al.* (2017). Haplotypes from the SLC45A2 gene are associated with the presence of freckles and eye, hair and skin pigmentation in Brazil. Leg Med (Tokyo) *25*, 43-51.
Frandberg, P.A., Doufexis, M., Kapas, S., and Chhajlani, V. (1998). Human pigmentation phenotype: a point mutation generates nonfunctional MSH receptor. Biochem Biophys Res Commun *245*, 490-492.

Fujita, H., Sasano, E., Yasunaga, K., Furuta, K., Yokota, S., Wada, I., and Himeno, M. (2001). Evidence for distinct membrane traffic pathways to melanosomes and lysosomes in melanocytes. J Investig Dermatol Symp Proc *6*, 19-24.
Fukamachi, S., Shimada, A., and Shima, A. (2001). Mutations in the gene encoding B, a novel transporter protein, reduce melanin content in medaka. Nature Genet *28*, 381-385.
Fuller, B.B., Spaulding, D.T., and Smith, D.R. (2001). Regulation of the catalytic activity of preexisting tyrosinase in black and Caucasian human melanocyte cell cultures. Exp Cell Res *262*, 197-208.
Furumura, M., Solano, F., Matsunaga, N., Sakai, C., Spritz, R.A., and Hearing, V.J. (1998). Metal ligand-binding specificities of the tyrosinase-related proteins. Biochem Biophys Res Commun *242*, 579-585.
Gallas, J.M., Littrell, K.C., Seifert, S., Zajac, G.W., and Thiyagarajan, P. (1999). Solution structure of copper ion-induced molecular aggregates of tyrosine melanin. Biophys J *77*, 1135-1142.
Ganesan, A.K., Ho, H., Bodemann, B., Petersen, S., Aruri, J., Koshy, S., Richardson, Z., Le, L.Q., Krasieva, T., Roth, M.G.*, et al.* (2008). Genome-wide siRNA-based functional genomics of pigmentation identifies novel genes and pathways that impact melanogenesis in human cells. PLoS Genet *4*, e1000298.
Ganley, I.G., Wong, P.M., Gammoh, N., and Jiang, X. (2011). Distinct autophagosomal-lysosomal fusion mechanism revealed by thapsigargin-induced autophagy arrest. Mol Cell *42*, 731-743.
Garcia-Borron, J.C., Abdel-Malek, Z., and Jiménez-Cervantes, C. (2014). MC1R, the cAMP pathway and the response to solar UV: Extending the horizon beyond pigmentation. Pigment Cell & Melanoma Research *27*, 699-720.
Gardner, J.M., Wildenberg, S.C., Keiper, N.M., Novak, E.K., Rusiniak, M.E., Swank, R.T., Puri, N., Finger, J.N., Hagiwara, N., Lehman, A.L.*, et al.* (1997). The mouse pale ear (ep) mutation is the homologue of human Hermansky-Pudlak syndrome. Proc Natl Acad Sci U S A *94*, 9238-9243.
Garg, S., Sharma, M., Ung, C., Tuli, A., Barral, D.C., Hava, D.L., Veerapen, N., Besra, G.S., Hacohen, N., and Brenner, M.B. (2011). Lysosomal trafficking, antigen presentation, and microbial killing are controlled by the Arf-like GTPase Arl8b. Immunity *35*, 182-193.
Garner, A., and Jay, B.S. (1980). Macromelanosomes in X-linked ocular albinism. Histopathology *4*, 243-254.
Gasiunas, G., Barrangou, R., Horvath, P., and Siksnys, V. (2012). Cas9-crRNA ribonucleoprotein complex mediates specific DNA cleavage for adaptive immunity in bacteria. Proc Natl Acad Sci U S A *109*, E2579-2586.
Gengyo-Ando, K., Kage-Nakadai, E., Yoshina, S., Otori, M., Kagawa-Nagamura, Y., Nakai, J., and Mitani, S. (2016). Distinct roles of the two VPS33 proteins in the endolysosomal system in Caenorhabditis elegans. Traffic *17*, 1197-1213.
Getting, W.S., and King, R.A. (1994). Molecular Basis of Oculocutaneous Albinism. Journal of Investigative Dermatology *103*, S131-S136.
Ginger, R.S., Askew, S.E., Ogborne, R.M., Wilson, S., Ferdinando, D., Dadd, T., Smith, A.M., Kazi, S., Szerencsei, R.T., Winkfein, R.J.*, et al.* (2008). SLC24A5 encodes a trans-Golgi network protein with potassium-dependent sodium-calcium exchange activity that regulates human epidermal melanogenesis. J Biol Chem *283*, 5486-5495.
Giordano, F., Bonetti, C., Surace, E.M., Marigo, V., and Raposo, G.a. (2009). The ocular albinism type 1 (OA1) G-protein-coupled receptor functions with MART-1 at early stages

of melanogenesis to control melanosome identity and composition. Human Molecular Genetics *18*, 4530-4545.
Gloster, H.M., Jr., and Neal, K. (2006). Skin cancer in skin of color. J Am Acad Dermatol *55*, 741-760; quiz 761-744.
Graham, S.C., Wartosch, L., Gray, S.R., Scourfield, E.J., Deane, J.E., Luzio, J.P., and Owen, D.J. (2013). Structural basis of Vps33A recruitment to the human HOPS complex by Vps16. Proceedings of the National Academy of Sciences of the United States of America *110*, 13345-13350.
Grant, P., Maga, T., Loshakov, A., Singhal, R., Wali, A., Nwankwo, J., Baron, K., and Johnson, D. (2016). An Eye on Trafficking Genes: Identification of Four Eye Color Mutations in Drosophila. G3 (Bethesda) *6*, 3185-3196.
Graves, A.R., Curran, P.K., Smith, C.L., and Mindell, J.A. (2008). The Cl-/H+ antiporter ClC-7 is the primary chloride permeation pathway in lysosomes. Nature *453*, 788-792.
Grewer, C., Gameiro, A., Mager, T., and Fendler, K. (2013). Electrophysiological characterization of membrane transport proteins. Annu Rev Biophys *42*, 95-120.
Gronskov, K., Dooley, C.M., Ostergaard, E., Kelsh, R.N., Hansen, L., Levesque, M.P., Vilhelmsen, K., Mollgard, K., Stemple, D.L., and Rosenberg, T. (2013). Mutations in c10orf11, a melanocyte-differentiation gene, cause autosomal-recessive albinism. Am J Hum Genet *92*, 415-421.
Gronskov, K., Ek, J., and Brondum-Nielsen, K. (2007). Oculocutaneous albinism. Orphanet J Rare Dis *2*, 43.
Gronskov, K., Ek, J., Sand, A., Scheller, R., Bygum, A., Brixen, K., Brondum-Nielsen, K., and Rosenberg, T. (2009). Birth prevalence and mutation spectrum in danish patients with autosomal recessive albinism. Invest Ophthalmol Vis Sci *50*, 1058-1064.
Gruenberg, J. (2020). Life in the lumen: The multivesicular endosome. Traffic *21*, 76-93.
Gudbjartsson, D.F., Sulem, P., Stacey, S.N., Goldstein, A.M., Rafnar, T., Sigurgeirsson, B., Benediktsdottir, K.R., Thorisdottir, K., Ragnarsson, R., Sveinsdottir, S.G.*, et al.* (2008). ASIP and TYR pigmentation variants associate with cutaneous melanoma and basal cell carcinoma. Nat Genet *40*, 886-891.
Gunnarsson, U., Hellström, A.R., Tixier-Boichard, M., Minvielle, F., Bed'hom, B., Ito, S., Jensen, P., Rattink, A., Vereijken, A., and Andersson, L. (2007). Mutations in Slc45a2 cause plumage color variation in chicken and Japanese quail. Genetics *175*, 867-877.
Guyonneau, L., Murisier, F., Rossier, A., Moulin, A., and Beermann, F. (2004). Melanocytes and pigmentation are affected in dopachrome tautomerase knockout mice. Mol Cell Biol *24*, 3396-3403.
Halaban, R., and Moellmann, G. (1990). Murine and human b locus pigmentation genes encode a glycoprotein (gp75) with catalase activity. Proc Natl Acad Sci U S A *87*, 4809-4813.
Halaban, R., Patton, R.S., Cheng, E., Svedine, S., Trombetta, E.S., Wahl, M.L., Ariyan, S., and Hebert, D.N. (2002). Abnormal acidification of melanoma cells induces tyrosinase retention in the early secretory pathway. J Biol Chem *277*, 14821-14828.
Haltaufderhyde, K.D., and Oancea, E. (2014). Genome-wide transcriptome analysis of human epidermal melanocytes. Genomics *104*, 482-489.
Han, J., Kraft, P., Nan, H., Guo, Q., Chen, C., Qureshi, A., Hankinson, S.E., Hu, F.B., Duffy, D.L., Zhao, Z.Z.*, et al.* (2008). A genome-wide association study identifies novel alleles associated with hair color and skin pigmentation. PLoS Genet *4*, e1000074.

Harada, M., Li, Y.F., El-Gamil, M., Rosenberg, S.A., and Robbins, P.F. (2001). Use of an in vitro immunoselected tumor line to identify shared melanoma antigens recognized by HLA-A*0201-restricted T cells. Cancer Res *61*, 1089-1094.
Harris, S.S., and Dawson-Hughes, B. (1998). Seasonal changes in plasma 25-hydroxyvitamin D concentrations of young American black and white women. Am J Clin Nutr *67*, 1232-1236.
Hartwig, C., Zlatic, S.A., Wallin, M., Vrailas-Mortimer, A., Fahrni, C.J., and Faundez, V. (2019). Trafficking mechanisms of P-type ATPase copper transporters. Curr Opin Cell Biol *59*, 24-33.
Hearing, V.J. (2005). Biogenesis of pigment granules: a sensitive way to regulate melanocyte function. J Dermatol Sci *37*, 3-14.
Hee, J.S., Mitchell, S.M., Liu, X., and Leonhardt, R.M. (2017). Melanosomal formation of PMEL core amyloid is driven by aromatic residues. Sci Rep *7*, 44064.
Hellström, A.R., Watt, B., Fard, S.S., Tenza, D., Mannström, P., Narfström, K., Ekesten, B., Ito, S., Wakamatsu, K., Larsson, J.*, et al.* (2011). Inactivation of PMEL alters melanosome shape but has only a subtle effect on visible pigmentation. PLoS Genetics *7*.
Helsing, P., Nymoen, D.A., Rootwelt, H., Vardal, M., Akslen, L.A., Molven, A., and Andresen, P.A. (2012). MC1R, ASIP, TYR, and TYRP1 gene variants in a population-based series of multiple primary melanomas. Genes Chromosomes Cancer *51*, 654-661.
Hemesath, T.J., Price, E.R., Takemoto, C., Badalian, T., and Fisher, D.E. (1998). MAP kinase links the transcription factor Microphthalmia to c-Kit signalling in melanocytes. Nature *391*, 298-301.
Hermann, G.J., Schroeder, L.K., Hieb, C.A., Kershner, A.M., Rabbitts, B.M., Fonarev, P., Grant, B.D., and Priess, J.R. (2005). Genetic analysis of lysosomal trafficking in Caenorhabditis elegans. Mol Biol Cell *16*, 3273-3288.
Herraiz, C., Garcia-Borron, J.C., Jiménez-Cervantes, C., and Olivares, C. (2017). MC1R signaling. Intracellular partners and pathophysiological implications. Biochimica et Biophysica Acta (BBA) - Molecular Basis of Disease.
Herraiz, C., Jimenez-Cervantes, C., Zanna, P., and Garcia-Borron, J.C. (2009). Melanocortin 1 receptor mutations impact differentially on signalling to the cAMP and the ERK mitogen-activated protein kinase pathways. FEBS Lett *583*, 3269-3274.
Hider, J.L., Gittelman, R.M., Shah, T., Edwards, M., Rosenbloom, A., Akey, J.M., and Parra, E.J. (2013). Exploring signatures of positive selection in pigmentation candidate genes in populations of East Asian ancestry. BMC Evol Biol *13*, 150.
Hirobe, T., Ito, S., Wakamatsu, K., Kawa, Y., and Abe, H. (2014). The mouse brown (b/Tyrp1(b)) allele does not affect pheomelanin synthesis in mice. Zoolog Sci *31*, 53-63.
Hislop, J.N., Marley, A., and Von Zastrow, M. (2004). Role of mammalian vacuolar protein-sorting proteins in endocytic trafficking of a non-ubiquitinated G protein-coupled receptor to lysosomes. J Biol Chem *279*, 22522-22531.
Ho, H., Kapadia, R., Al-Tahan, S., Ahmad, S., and Ganesan, A.K. (2011). WIPI1 coordinates melanogenic gene transcription and melanosome formation via TORC1 inhibition. J Biol Chem *286*, 12509-12523.
Ho, R., and Stroupe, C. (2015). The HOPS/class C Vps complex tethers membranes by binding to one Rab GTPase in each apposed membrane. Molecular biology of the cell *26*, 2655-2663.

Ho, T. (2015). Regulation of functional amyloid formation and pigmentation during melanosome biogenesis. In Cell and Molecular Biology (ProQuest: University of Pennsylvania).
Hoek, K.S., Schlegel, N.C., Eichhoff, O.M., Widmer, D.S., Praetorius, C., Einarsson, S.O., Valgeirsdottir, S., Bergsteinsdottir, K., Schepsky, A., Dummer, R.*, et al.* (2008). Novel MITF targets identified using a two-step DNA microarray strategy. Pigment Cell Melanoma Res *21*, 665-676.
Holloway, Z.G., Velayos-Baeza, A., Howell, G.J., Levecque, C., Ponnambalam, S., Sztul, E., and Monaco, A.P. (2013). Trafficking of the Menkes copper transporter ATP7A is regulated by clathrin-, AP-2-, AP-1-, and Rab22-dependent steps. Mol Biol Cell *24*, 1735-1748, S1731-1738.
Hu, D.N., Savage, H.E., and Roberts, J.E. (2002). Uveal melanocytes, ocular pigment epithelium, and Muller cells in culture: in vitro toxicology. Int J Toxicol *21*, 465-472.
Hu, D.N., Simon, J.D., and Sarna, T. (2008). Role of ocular melanin in ophthalmic physiology and pathology. Photochem Photobiol *84*, 639-644.
Huizing, M., Didier, A., Walenta, J., Anikster, Y., Gahl, W.A., and Krämer, H. (2001). Molecular cloning and characterization of human VPS18, VPS 11, VPS16, and VPS33. Gene *264*, 241-247.
Hume, A.N., Collinson, L.M., Rapak, A., Gomes, A.Q., Hopkins, C.R., and Seabra, M.C. (2001). Rab27a regulates the peripheral distribution of melanosomes in melanocytes. J Cell Biol *152*, 795-808.
Hurbain, I., Geerts, W.J.C., Boudier, T., Marco, S., Verkleij, A.J., Marks, M.S., and Raposo, G. (2008). Electron tomography of early melanosomes: implications for melanogenesis and the generation of fibrillar amyloid sheets. Proceedings of the National Academy of Sciences of the United States of America *105*, 19726-19731.
Ilia, M., and Jeffery, G. (1999). Retinal mitosis is regulated by dopa, a melanin precursor that may influence the time at which cells exit the cell cycle: analysis of patterns of cell production in pigmented and albino retinae. J Comp Neurol *405*, 394-405.
Incerti, B., Cortese, K., Pizzigoni, A., Surace, E.M., Varani, S., Coppola, M., Jeffery, G., Seeliger, M., Jaissle, G., Bennett, D.C.*, et al.* (2000). Oa1 knock-out: new insights on the pathogenesis of ocular albinism type 1. Hum Mol Genet *9*, 2781-2788.
Innamorati, G., Piccirillo, R., Bagnato, P., Palmisano, I., and Schiaffino, M.V. (2006). The melanosomal/lysosomal protein OA1 has properties of a G protein-coupled receptor. Pigment Cell Res *19*, 125-135.
Iozumi, K., Hoganson, G.E., Pennella, R., Everett, M.A., and Fuller, B.B. (1993). Role of tyrosinase as the determinant of pigmentation in cultured human melanocytes. J Invest Dermatol *100*, 806-811.
Istrate, M., Vlaicu, B., Poenaru, M., Hasbei-Popa, M., Salavat, M.C., and Iliescu, D.A. (2020). Photoprotection role of melanin in the human retinal pigment epithelium. Imaging techniques for retinal melanin. Rom J Ophthalmol *64*, 100-104.
Ito, S., and Wakamatsu, K. (2003). Quantitative analysis of eumelanin and pheomelanin in humans, mice, and other animals: a comparative review. Pigment Cell Res *16*, 523-531.
Ito, S., and Wakamatsu, K. (2008). Chemistry of mixed melanogenesis--pivotal roles of dopaquinone. Photochem Photobiol *84*, 582-592.

Itoh, Y., Nagaoka, Y., Katakura, Y., Kawahara, H., and Takemori, H. (2016). Simple chronic colitis model using hypopigmented mice with a Hermansky-Pudlak syndrome 5 gene mutation. Pigment Cell Melanoma Res *29*, 578-582.
Izagirre, N., Garcia, I., Junquera, C., de la Rua, C., and Alonso, S. (2006). A scan for signatures of positive selection in candidate loci for skin pigmentation in humans. Mol Biol Evol *23*, 1697-1706.
Jablonski, N.G. (2012). The evolution of human skin colouration and its relevance to health in the modern world. J R Coll Physicians Edinb *42*, 58-63.
Jablonski, N.G., and Chaplin, G. (2000). The evolution of human skin coloration. J Hum Evol *39*, 57-106.
Jablonski, N.G., and Chaplin, G. (2010). Colloquium paper: human skin pigmentation as an adaptation to UV radiation. Proc Natl Acad Sci U S A *107 Suppl 2*, 8962-8968.
Jablonski, N.G., and Chaplin, G. (2017). The colours of humanity: the evolution of pigmentation in the human lineage. Philos Trans R Soc Lond B Biol Sci *372*.
Jablonski, N.G., and Chaplin, G. (2018). The roles of vitamin D and cutaneous vitamin D production in human evolution and health. Int J Paleopathol *23*, 54-59.
Jiang, P., Nishimura, T., Sakamaki, Y., Itakura, E., Hatta, T., Natsume, T., and Mizushima, N. (2014). The HOPS complex mediates autophagosome-lysosome fusion through interaction with syntaxin 17. Molecular Biology of the Cell *25*, 1327-1337.
Jiang, S., Liu, X.M., Dai, X., Zhou, Q., Lei, T.C., Beermann, F., Wakamatsu, K., and Xu, S.Z. (2010). Regulation of DHICA-mediated antioxidation by dopachrome tautomerase: implication for skin photoprotection against UVA radiation. Free Radic Biol Med *48*, 1144-1151.
Jimbow, K., and Fitzpatrick, T.B. (1974). Characterization of a new melanosomal structural component--the vesiculoglobular body--by conventional transmission, high-voltage, and scanning electron microscopy. J Ultrastruct Res *48*, 269-283.
Jimenez-Cervantes, C., Garcia-Borron, J.C., Valverde, P., Solano, F., and Lozano, J.A. (1993). Tyrosinase isoenzymes in mammalian melanocytes. 1. Biochemical characterization of two melanosomal tyrosinases from B16 mouse melanoma. Eur J Biochem *217*, 549-556.
Jimenez-Cervantes, C., Solano, F., Kobayashi, T., Urabe, K., Hearing, V.J., Lozano, J.A., and Garcia-Borron, J.C. (1994). A new enzymatic function in the melanogenic pathway. The 5,6-dihydroxyindole-2-carboxylic acid oxidase activity of tyrosinase-related protein-1 (TRP1). J Biol Chem *269*, 17993-18000.
Jimenez, M., Tsukamoto, K., and Hearing, V.J. (1991). Tyrosinases from two different loci are expressed by normal and by transformed melanocytes. J Biol Chem *266*, 1147-1156.
Jin, J., Smith, F.D., Stark, C., Wells, C.D., Fawcett, J.P., Kulkarni, S., Metalnikov, P., O'Donnell, P., Taylor, P., Taylor, L.*, et al.* (2004). Proteomic, functional, and domain-based analysis of in vivo 14-3-3 binding proteins involved in cytoskeletal regulation and cellular organization. Curr Biol *14*, 1436-1450.
Jinek, M., Chylinski, K., Fonfara, I., Hauer, M., Doudna, J.A., and Charpentier, E. (2012). A programmable dual-RNA-guided DNA endonuclease in adaptive bacterial immunity. Science *337*, 816-821.
Johnson, D.E., Ai, H.W., Wong, P., Young, J.D., Campbell, R.E., and Casey, J.R. (2009). Red fluorescent protein pH biosensor to detect concentrative nucleoside transport. J Biol Chem *284*, 20499-20511.

Johnson, R., and Jackson, I.J. (1992). Light is a dominant mouse mutation resulting in premature cell death. Nat Genet *1*, 226-229.
Jonnalagadda, M., Norton, H., Ozarkar, S., Kulkarni, S., and Ashma, R. (2016). Association of genetic variants with skin pigmentation phenotype among populations of west Maharashtra, India. Am J Hum Biol *28*, 610-618.
Jung, C.Y. (1998). Proteins that interact with facilitative glucose transporters: implication for function. Exp Physiol *83*, 267-273.
Kadekaro, A.L., Chen, J., Yang, J., Chen, S., Jameson, J., Swope, V.B., Cheng, T., Kadakia, M., and Abdel-Malek, Z. (2012). Alpha-melanocyte-stimulating hormone suppresses oxidative stress through a p53-mediated signaling pathway in human melanocytes. Mol Cancer Res *10*, 778-786.
Kaidbey, K.H., Agin, P.P., Sayre, R.M., and Kligman, A.M. (1979). Photoprotection by melanin--a comparison of black and Caucasian skin. J Am Acad Dermatol *1*, 249-260.
Kausar, T., Bhatti, M.A., Ali, M., Shaikh, R.S., and Ahmed, Z.M. (2013). OCA5, a novel locus for non-syndromic oculocutaneous albinism, maps to chromosome 4q24. Clin Genet *84*, 91-93.
Kaxiras, E., Tsolakidis, A., Zonios, G., and Meng, S. (2006). Structural model of eumelanin. Phys Rev Lett *97*, 218102.
Kayatz, P., Thumann, G., Luther, T.T., Jordan, J.F., Bartz-Schmidt, K.U., Esser, P.J., and Schraermeyer, U. (2001). Oxidation causes melanin fluorescence. Invest Ophthalmol Vis Sci *42*, 241-246.
Khatter, D., Raina, V.B., Dwivedi, D., Sindhwani, A., Bahl, S., and Sharma, M. (2015). The small GTPase Arl8b regulates assembly of the mammalian HOPS complex on lysosomes. Journal of Cell Science *128*, 1746-1761.
Kikuchi, A., Shimizu, H., and Nishikawa, T. (1996). Expression and ultrastructural localization of HMB-45 antigen. Br J Dermatol *135*, 400-405.
Kirkwood, B.J. (2009). Albinism and its implications with vision. Insight *34*, 13-16.
Kloepper, T.H., Kienle, C.N., and Fasshauer, D. (2007). An elaborate classification of SNARE proteins sheds light on the conservation of the eukaryotic endomembrane system. Mol Biol Cell *18*, 3463-3471.
Kobayashi, N., Nakagawa, A., Muramatsu, T., Yamashina, Y., Shirai, T., Hashimoto, M.W., Ishigaki, Y., Ohnishi, T., and Mori, T. (1998a). Supranuclear melanin caps reduce ultraviolet induced DNA photoproducts in human epidermis. J Invest Dermatol *110*, 806-810.
Kobayashi, T., Imokawa, G., Bennett, D.C., and Hearing, V.J. (1998b). Tyrosinase stabilization by Tyrp1 (the brown locus protein). J Biol Chem *273*, 31801-31805.
Kobayashi, T., Urabe, K., Winder, A., Jiménez-Cervantes, C., Imokawa, G., Brewington, T., Solano, F., García-Borrón, J.C., and Hearing, V.J. (1994). Tyrosinase related protein 1 (TRP1) functions as a DHICA oxidase in melanin biosynthesis. The EMBO Journal *13*, 5818-5825.
Koch, S.L., Tridico, S.R., Bernard, B.A., Shriver, M.D., and Jablonski, N.G. (2020). The biology of human hair: A multidisciplinary review. Am J Hum Biol *32*, e23316.
Korbie, D.J., and Mattick, J.S. (2008). Touchdown PCR for increased specificity and sensitivity in PCR amplification. Nat Protoc *3*, 1452-1456.
Kralj-Hans, I., Tibber, M., Jeffery, G., and Mobbs, P. (2006). Differential effect of dopamine on mitosis in early postnatal albino and pigmented rat retinae. J Neurobiol *66*, 47-55.

Kushimoto, T., Basrur, V., Valencia, J., Matsunaga, J., Vieira, W.D., Ferrans, V.J., Muller, J., Appella, E., and Hearing, V.J. (2001). A model for melanosome biogenesis based on the purification and analysis of early melanosomes. Proc Natl Acad Sci U S A *98*, 10698-10703.
Kvalvaag, A.S., Pust, S., and Sandvig, K. (2014). Vps11, a subunit of the tethering complexes HOPS and CORVET, is involved in regulation of glycolipid degradation and retrograde toxin transport. Commun Integr Biol *7*, e28129.
Kvalvaag, A.S., Pust, S., Sundet, K.I., Engedal, N., Simm, R., and Sandvig, K. (2013). The ERM proteins ezrin and moesin regulate retrograde Shiga toxin transport. Traffic *14*, 839-852.
Kwon, B.S., Halaban, R., Kim, G.S., Usack, L., Pomerantz, S., and Haq, A.K. (1987). A melanocyte-specific complementary DNA clone whose expression is inducible by melanotropin and isobutylmethyl xanthine. Mol Biol Med *4*, 339-355.
Lachmann, J., Glaubke, E., Moore, P.S., and Ungermann, C. (2014). The Vps39-like TRAP1 is an effector of Rab5 and likely the missing Vps3 subunit of human CORVET. Cell Logist *4*, e970840.
Laemmli, U.K. (1970). Cleavage of structural proteins during the assembly of the head of bacteriophage T4. Nature *227*, 680-685.
Lai, X., Wichers, H.J., Soler-Lopez, M., and Dijkstra, B.W. (2017). Structure of Human Tyrosinase Related Protein 1 Reveals a Binuclear Zinc Active Site Important for Melanogenesis. Angew Chem Int Ed Engl *56*, 9812-9815.
Lamason, R.L., Mohideen, M.-A.P.K., Mest, J.R., Wong, A.C., Norton, H.L., Aros, M.C., Jurynec, M.J., Mao, X., Humphreville, V.R., Humbert, J.E*., et al.* (2005a). SLC24A5, a putative cation exchanger, affects pigmentation in zebrafish and humans. Science *310*, 1782-1786.
Lamason, R.L., Mohideen, M.A., Mest, J.R., Wong, A.C., Norton, H.L., Aros, M.C., Jurynec, M.J., Mao, X., Humphreville, V.R., Humbert, J.E*., et al.* (2005b). SLC24A5, a putative cation exchanger, affects pigmentation in zebrafish and humans. Science *310*, 1782-1786.
Lange, P.F., Wartosch, L., Jentsch, T.J., and Fuhrmann, J.C. (2006). ClC-7 requires Ostm1 as a beta-subunit to support bone resorption and lysosomal function. Nature *440*, 220-223.
Lao, O., de Gruijter, J.M., van Duijn, K., Navarro, A., and Kayser, M. (2007). Signatures of positive selection in genes associated with human skin pigmentation as revealed from analyses of single nucleotide polymorphisms. Ann Hum Genet *71*, 354-369.
Lasseaux, E., Plaisant, C., Michaud, V., Pennamen, P., Trimouille, A., Gaston, L., Monferme, S., Lacombe, D., Rooryck, C., Morice-Picard, F*., et al.* (2018a). Molecular characterization of a series of 990 index patients with albinism. Pigment Cell Melanoma Res *31*, 466-474.
Lasseaux, E., Plaisant, C., Michaud, V., Pennamen, P., Trimouille, A., Gaston, L., Monferme, S., Lacombe, D., Rooryck, C., Morice-Picard, F*., et al.* (2018b). Molecular characterization of a series of 990 index patients with albinism. Pigment Cell Melanoma Res *31*, 466-474.
Law, M.H., Medland, S.E., Zhu, G., Yazar, S., Vinuela, A., Wallace, L., Shekar, S.N., Duffy, D.L., Bataille, V., Glass, D*., et al.* (2017). Genome-wide association shows that pigmentation genes play a role in skin aging. J Invest Dermatol *137*, 1887-1894.

Lee, H.H., Nemecek, D., Schindler, C., Smith, W.J., Ghirlando, R., Steven, A.C., Bonifacino, J.S., and Hurley, J.H. (2012). Assembly and architecture of biogenesis of lysosome-related organelles complex-1 (BLOC-1). J Biol Chem *287*, 5882-5890.
Lehman, A.L., Silvers, W.K., Puri, N., Wakamatsu, K., Ito, S., and Brilliant, M.H. (2000). The underwhite (uw) locus acts autonomously and reduces the production of melanin via a unique pathway. J Invest Dermatol *115*, 601-606.
Lemoine, R. (2000). Sucrose transporters in plants: update on function and structure. Biochim Biophys Acta *1465*, 246-262.
Leonhardt, R.M., Vigneron, N., Hee, J.S., Graham, M., and Cresswell, P. (2013). Critical residues in the PMEL/Pmel17 N-terminus direct the hierarchical assembly of melanosomal fibrils. Mol Biol Cell *24*, 964-981.
Lerner, A.B., Fitzpatrick, T.B., Calkins, E., and Summerson, W.H. (1949). Mammalian tyrosinase; preparation and properties. J Biol Chem *178*, 185-195.
Levin, A.V., and Stroh, E. (2011). Albinism for the busy clinician. J AAPOS *15*, 59-66.
Liang, C., Lee, J.S., Inn, K.S., Gack, M.U., Li, Q., Roberts, E.A., Vergne, I., Deretic, V., Feng, P., Akazawa, C.*, et al.* (2008). Beclin1-binding UVRAG targets the class C Vps complex to coordinate autophagosome maturation and endocytic trafficking. Nat Cell Biol *10*, 776-787.
Lin-Moshier, Y., Keebler, M.V., Hooper, R., Boulware, M.J., Liu, X., Churamani, D., Abood, M.E., Walseth, T.F., Brailoiu, E., Patel, S.*, et al.* (2014). The Two-pore channel (TPC) interactome unmasks isoform-specific roles for TPCs in endolysosomal morphology and cell pigmentation. Proc Natl Acad Sci U S A *111*, 13087-13092.
Lin, J.Y., and Fisher, D.E. (2007). Melanocyte biology and skin pigmentation. Nature *445*, 843-850.
Lin, W., Qureshi, A.A., Kraft, P., Nan, H., Guo, Q., Hu, F.B., Jensen, M.K., and Han, J. (2011). ASIP genetic variants and the number of non-melanoma skin cancers. Cancer Causes Control *22*, 495-501.
Lin, X., Yang, T., Wang, S., Wang, Z., Yun, Y., Sun, L., Zhou, Y., Xu, X., Akazawa, C., Hong, W.*, et al.* (2014). RILP interacts with HOPS complex via VPS41 subunit to regulate endocytic trafficking. Scientific reports *4*, 7282-7282.
Lindmo, K., Simonsen, A., Brech, A., Finley, K., Rusten, T.E., and Stenmark, H. (2006). A dual function for Deep orange in programmed autophagy in the Drosophila melanogaster fat body. Exp Cell Res *312*, 2018-2027.
Lips, P. (2006). Vitamin D physiology. Prog Biophys Mol Biol *92*, 4-8.
Liu, F., Visser, M., Duffy, D.L., Hysi, P.G., Jacobs, L.C., Lao, O., Zhong, K., Walsh, S., Chaitanya, L., Wollstein, A.*, et al.* (2015). Genetics of skin color variation in Europeans: genome-wide association studies with functional follow-up. Hum Genet *134*, 823-835.
Liu, Y., and Simon, J.D. (2003a). The effect of preparation procedures on the morphology of melanin from the ink sac of Sepia officinalis. Pigment Cell Res *16*, 72-80.
Liu, Y., and Simon, J.D. (2003b). Isolation and biophysical studies of natural eumelanins: applications of imaging technologies and ultrafast spectroscopy. Pigment Cell Res *16*, 606-618.
Lobingier, B.T., and Merz, A.J. (2012). Sec1/Munc18 protein Vps33 binds to SNARE domains and the quaternary SNARE complex. Molecular Biology of the Cell *23*, 4611-4622.

Lobingier, B.T., Nickerson, D.P., Lo, S.Y., and Merz, A.J. (2014). SM proteins Sly1 and Vps33 co-assemble with Sec17 and SNARE complexes to oppose SNARE disassembly by Sec18. eLife *3*, e02272-e02272.
Loftus, S.K., Larson, D.M., Baxter, L.L., Antonellis, A., Chen, Y.A., Wu, X.S., Jiang, Y., Bittner, M., Hammer, J.A., III, and Pavan, W.J. (2002). Mutation of melanosome protein RAB38 in chocolate mice. Proc Natl Acad Sci USA *99*, 4471-4476.
Lona-Durazo, F., Hernandez-Pacheco, N., Fan, S., Zhang, T., Choi, J., Kovacs, M.A., Loftus, S.K., Le, P., Edwards, M., Fortes-Lima, C.A.*, et al.* (2019). Meta-analysis of GWA studies provides new insights on the genetic architecture of skin pigmentation in recently admixed populations. BMC Genet *20*, 59.
Lopez, S., Garcia, O., Yurrebaso, I., Flores, C., Acosta-Herrera, M., Chen, H., Gardeazabal, J., Careaga, J.M., Boyano, M.D., Sanchez, A.*, et al.* (2014). The interplay between natural selection and susceptibility to melanoma on allele 374F of SLC45A2 gene in a South European population. PLoS One *9*, e104367.
Lopez, V.M., Decatur, C.L., Stamer, W.D., Lynch, R.M., and McKay, B.S. (2008). L-DOPA is an endogenous ligand for OA1. PLoS Biol *6*, e236.
Lucock, M. (2000). Folic acid: nutritional biochemistry, molecular biology, and role in disease processes. Mol Genet Metab *71*, 121-138.
Lucock, M., Beckett, E., Martin, C., Jones, P., Furst, J., Yates, Z., Jablonski, N.G., Chaplin, G., and Veysey, M. (2017). UV-associated decline in systemic folate: implications for human nutrigenetics, health, and evolutionary processes. Am J Hum Biol *29*.
Lucock, M., Jones, P., Martin, C., Yates, Z., Veysey, M., Furst, J., and Beckett, E. (2018a). Photobiology of vitamins. Nutr Rev *76*, 512-525.
Lucock, M., Thota, R., Garg, M., Martin, C., Jones, P., Furst, J., Yates, Z., Jablonski, N.G., Chaplin, G., Veysey, M.*, et al.* (2018b). Vitamin D and folate: A reciprocal environmental association based on seasonality and genetic disposition. Am J Hum Biol *30*, e23166.
Lucotte, G., Mercier, G., Dieterlen, F., and Yuasa, I. (2010). A decreasing gradient of 374F allele frequencies in the skin pigmentation gene SLC45A2, from the north of West Europe to North Africa. Biochem Genet *48*, 26-33.
Lucotte, G., and Yuasa, I. (2013). Near fixation of 374l allele frequencies of the skin pigmentation gene SLC45A2 in Africa. Biochem Genet *51*, 655-665.
Luo, D., Chen, H., and Jimbow, K. (1994). Cotransfection of genes encoding human tyrosinase and tyrosinase-related protein-1 prevents melanocyte death and enhances melanin pigmentation and gene expression of Lamp-1. Exp Cell Res *213*, 231-241.
Maccioni, L., Rachakonda, P.S., Scherer, D., Bermejo, J.L., Planelles, D., Requena, C., Hemminki, K., Nagore, E., and Kumar, R. (2013). Variants at chromosome 20 (ASIP locus) and melanoma risk. Int J Cancer *132*, 42-54.
Maldonado, E., Hernandez, F., Lozano, C., Castro, M.E., and Navarro, R.E. (2006). The zebrafish mutant vps18 as a model for vesicle-traffic related hypopigmentation diseases. Pigment Cell Res *19*, 315-326.
Mali, P., Aach, J., Stranges, P.B., Esvelt, K.M., Moosburner, M., Kosuri, S., Yang, L., and Church, G.M. (2013). CAS9 transcriptional activators for target specificity screening and paired nickases for cooperative genome engineering. Nat Biotechnol *31*, 833-838.
Manga, P., and Orlow, S.J. (1999). The pink-eyed dilution gene and the molecular pathogenesis of tyrosinase-positive albinism (OCA2). J Dermatol *26*, 738-747.
Marcon, C.R., and Maia, M. (2019). Albinism: epidemiology, genetics, cutaneous characterization, psychosocial factors. An Bras Dermatol *94*, 503-520.

Maresh, G.A., Marken, J.S., Neubauer, M., Aruffo, A., Hellstrom, I., Hellstrom, K.E., and Marquardt, H. (1994a). Cloning and expression of the gene for the melanoma-associated ME20 antigen. DNA Cell Biol *13*, 87-95.
Maresh, G.A., Wang, W.C., Beam, K.S., Malacko, A.R., Hellstrom, I., Hellstrom, K.E., and Marquardt, H. (1994b). Differential processing and secretion of the melanoma-associated ME20 antigen. Arch Biochem Biophys *311*, 95-102.
Mariat, D., Taourit, S., and Guérin, G. (2003). A mutation in the MATP gene causes the cream coat colour in the horse. Genet Sel Evol *35*, 119-133.
Marks, M.S., and Seabra, M.C. (2001). The melanosome: membrane dynamics in black and white. Nature Reviews Molecular Cell Biology *2*, 738-748.
Marks, M.S., Woodruff, L., Ohno, H., and Bonifacino, J.S. (1996). Protein targeting by tyrosine- and di-leucine-based signals: evidence for distinct saturable components. J Cell Biol *135*, 341-354.
Martin, A.R., Lin, M., Granka, J.M., Myrick, J.W., Liu, X., Sockell, A., Atkinson, E.G., Werely, C.J., Moller, M., Sandhu, M.S.*, et al.* (2017). An Unexpectedly Complex Architecture for Skin Pigmentation in Africans. Cell *171*, 1340-1353 e1314.
Martinez-Garcia, M., and Montoliu, L. (2013). Albinism in Europe. J Dermatol *40*, 319-324.
Marwaha, R., Arya, S.B., Jagga, D., Kaur, H., Tuli, A., and Sharma, M. (2017). The Rab7 effector PLE KHM1 binds Arl8b to promote cargo traffic to lysosomes. Journal of Cell Biology *216*, 1051-1070.
Mason, H.S. (1948). The chemistry of melanin; mechanism of the oxidation of dihydroxyphenylalanine by tyrosinase. J Biol Chem *172*, 83-99.
Matsui, T., Ohbayashi, N., and Fukuda, M. (2012). The Rab interacting lysosomal protein (RILP) homology domain functions as a novel effector domain for small GTPase Rab36: Rab36 regulates retrograde melanosome transport in melanocytes. J Biol Chem *287*, 28619-28631.
Mauri, L., Manfredini, E., Del Longo, A., Veniani, E., Scarcello, M., Terrana, R., Radaelli, A.E., Calo, D., Mingoia, G., Rossetti, A.*, et al.* (2017). Clinical evaluation and molecular screening of a large consecutive series of albino patients. J Hum Genet *62*, 277-290.
McCall, K.A., Huang, C., and Fierke, C.A. (2000). Function and mechanism of zinc metalloenzymes. J Nutr *130*, 1437S-1446S.
McEvoy, B., Beleza, S., and Shriver, M.D. (2006). The genetic architecture of normal variation in human pigmentation: an evolutionary perspective and model. Hum Mol Genet *15 Spec No 2*, R176-181.
McEwan, D.G., Popovic, D., Gubas, A., Terawaki, S., Suzuki, H., Stadel, D., Coxon, F.P., MirandadeStegmann, D., Bhogaraju, S., Maddi, K.*, et al.* (2015). PLEKHM1 regulates autophagosome-lysosome fusion through HOPS complex and LC3/GABARAP proteins. Molecular Cell *57*, 39-54.
McNeill, M.S., Paulsen, J., Bonde, G., Burnight, E., Hsu, M.Y., and Cornell, R.A. (2007). Cell death of melanophores in zebrafish trpm7 mutant embryos depends on melanin synthesis. J Invest Dermatol *127*, 2020-2030.
Meng, R., Wang, Y., Yao, Y., Zhang, Z., Harper, D.C., Heijnen, H.F.G., Sitaram, A., Li, W., Raposo, G., Weiss, M.J.*, et al.* (2012a). SLC35D3 delivery from megakaryocyte early endosomes is required for platelet dense granule biogenesis and differentially defective in Hermansky-Pudlak syndrome models. Blood *120*, 404-414.
Meng, R., Wang, Y., Yao, Y., Zhang, Z., Harper, D.C., Heijnen, H.F.G., Sitaram, A., Li, W., Raposo, G., Weiss, M.J.*, et al.* (2012b). SLC35D3 delivery from megakaryocyte early

endosomes is required for platelet dense granule biogenesis and is differentially defective in Hermansky-Pudlak syndrome models. Blood *120*, 404-414.
Meng, S., and Kaxiras, E. (2008a). Mechanisms for ultrafast nonradiative relaxation in electronically excited eumelanin constituents. Biophys J *95*, 4396-4402.
Meng, S., and Kaxiras, E. (2008b). Theoretical models of eumelanin protomolecules and their optical properties. Biophys J *94*, 2095-2105.
Meyer, H., Vitavska, O., and Wieczorek, H. (2011). Identification of an animal sucrose transporter. J Cell Sci *124*, 1984-1991.
Miller, M.W., Duhl, D.M., Vrieling, H., Cordes, S.P., Ollmann, M.M., Winkes, B.M., and Barsh, G.S. (1993). Cloning of the mouse agouti gene predicts a secreted protein ubiquitously expressed in mice carrying the lethal yellow mutation. Genes Dev *7*, 454-467.
Mindell, J.A. (2012). Lysosomal acidification mechanisms. Annu Rev Physiol *74*, 69-86.
Minvielle, F., Cecchi, T., Passamonti, P., Gourichon, D., and Renieri, C. (2009). Plumage colour mutations and melanins in the feathers of the Japanese quail: a first comparison. Anim Genet *40*, 971-974.
Mohammed, M., Al-Hashmi, N., Al-Rashdi, S., Al-Sukaiti, N., Al-Adawi, K., Al-Riyami, M., and Al-Maawali, A. (2019). Biallelic mutations in AP3D1 cause Hermansky-Pudlak syndrome type 10 associated with immunodeficiency and seizure disorder. Eur J Med Genet *62*, 103583.
Mondal, S., Thampi, A., and Puranik, M. (2018). Kinetics of Melanin Polymerization during Enzymatic and Nonenzymatic Oxidation. J Phys Chem B *122*, 2047-2063.
Monteilh-Zoller, M.K., Hermosura, M.C., Nadler, M.J., Scharenberg, A.M., Penner, R., and Fleig, A. (2003). TRPM7 provides an ion channel mechanism for cellular entry of trace metal ions. J Gen Physiol *121*, 49-60.
Montoliu, L., Gronskov, K., Wei, A.H., Martinez-Garcia, M., Fernandez, A., Arveiler, B., Morice-Picard, F., Riazuddin, S., Suzuki, T., Ahmed, Z.M.*, et al.* (2014). Increasing the complexity: new genes and new types of albinism. Pigment Cell Melanoma Res *27*, 11-18.
Morice-Picard, F., Lasseaux, E., Francois, S., Simon, D., Rooryck, C., Bieth, E., Colin, E., Bonneau, D., Journel, H., Walraedt, S.*, et al.* (2014). SLC24A5 mutations are associated with non-syndromic oculocutaneous albinism. J Invest Dermatol *134*, 568-571.
Morita, S., Kojima, T., and Kitamura, T. (2000a). Plat-E: an efficient and stable system for transient packaging of retroviruses. Gene Ther *7*, 1063-1066.
Morita, S., Kojima, T., and Kitamura, T. (2000b). Plat-E: an efficient and stable system for transient packaging of retroviruses. Gene Ther *7*, 1063-1066.
Mottaz, J.H., and Zelickson, A.S. (1967). Melanin transfer: a possible phagocytic process. J Invest Dermatol *49*, 605-610.
Mountjoy, K.G., Robbins, L.S., Mortrud, M.T., and Cone, R.D. (1992). The cloning of a family of genes that encode the melanocortin receptors. Science *257*, 1248-1251.
Mukherjee, M., Mukerjee, S., Sarkar-Roy, N., Ghosh, T., Kalpana, D., and Sharma, A.K. (2013). Polymorphisms of four pigmentation genes (SLC45A2, SLC24A5, MC1R and TYRP1) among eleven endogamous populations of India. J Genet *92*, 135-139.
Muller-Rover, S., Handjiski, B., van der Veen, C., Eichmuller, S., Foitzik, K., McKay, I.A., Stenn, K.S., and Paus, R. (2001). A comprehensive guide for the accurate classification of murine hair follicles in distinct hair cycle stages. J Invest Dermatol *117*, 3-15.
Muslin, A.J., Tanner, J.W., Allen, P.M., and Shaw, A.S. (1996). Interaction of 14-3-3 with signaling proteins is mediated by the recognition of phosphoserine. Cell *84*, 889-897.

Myles, S., Somel, M., Tang, K., Kelso, J., and Stoneking, M. (2007). Identifying genes underlying skin pigmentation differences among human populations. Hum Genet *120*, 613-621.
Nakamura, M., Tobin, D.J., Richards-Smith, B., Sundberg, J.P., and Paus, R. (2002). Mutant laboratory mice with abnormalities in pigmentation: annotated tables. Journal of Dermatological Science *28*, 1-33.
Narayanan, D.L., Saladi, R.N., and Fox, J.L. (2010). Ultraviolet radiation and skin cancer. Int J Dermatol *49*, 978-986.
Newton, J.M., Cohen-Barak, O., Hagiwara, N., Gardner, J.M., Davisson, M.T., King, R.A., and Brilliant, M.H. (2001). Mutations in the human orthologue of the mouse underwhite gene (uw) underlie a new form of oculocutaneous albinism, OCA4. Am J Hum Genet *69*, 981-988.
Newton, J.M., Orlow, S.J., and Barsh, G.S. (1996). Isolation and characterization of a mouse homolog of the X-linked ocular albinism (OA1) gene. Genomics *37*, 219-225.
Newton, R.A., Smit, S.E., Barnes, C.C., Pedley, J., Parsons, P.G., and Sturm, R.A. (2005). Activation of the cAMP pathway by variant human MC1R alleles expressed in HEK and in melanoma cells. Peptides *26*, 1818-1824.
Nguyen, T., Novak, E.K., Kermani, M., Fluhr, J., Peters, L.L., Swank, R.T., and Wei, M.L. (2002). Melanosome morphologies in murine models of hermansky-pudlak syndrome reflect blocks in organelle development. J Invest Dermatol *119*, 1156-1164.
Nguyen, T., and Wei, M.L. (2004). Characterization of Melanosomes in Murine Hermansky-Pudlak Syndrome: Mechanisms of Hypopigmentation. Journal of Investigative Dermatology *122*, 452-460.
Nickla, D.L., and Wallman, J. (2010). The multifunctional choroid. Prog Retin Eye Res *29*, 144-168.
Nilsson, K.R., Jr., and Bennett, V. (2009). Ankyrin-based patterning of membrane microdomains: new insights into a novel class of cardiovascular diseases. J Cardiovasc Pharmacol *54*, 106-115.
Nishimura, E.K. (2011). Melanocyte stem cells: a melanocyte reservoir in hair follicles for hair and skin pigmentation. Pigment Cell Melanoma Res *24*, 401-410.
Norman, A.W. (2008). From vitamin D to hormone D: fundamentals of the vitamin D endocrine system essential for good health. Am J Clin Nutr *88*, 491S-499S.
Norton, H.L., Kittles, R.A., Parra, E., McKeigue, P., Mao, X., Cheng, K., Canfield, V.A., Bradley, D.G., McEvoy, B., and Shriver, M.D. (2007). Genetic evidence for the convergent evolution of light skin in Europeans and East Asians. Mol Biol Evol *24*, 710-722.
O'Donnell, F.E., Jr., Hambrick, G.W., Jr., Green, W.R., Iliff, W.J., and Stone, D.L. (1976). X-linked ocular albinism. An oculocutaneous macromelanosomal disorder. Arch Ophthalmol *94*, 1883-1892.
Oancea, E., Vriens, J., Brauchi, S., Jun, J., Splawski, I., and Clapham, D.E. (2009). TRPM1 forms ion channels associated with melanin content in melanocytes. Sci Signal *2*, ra21.
Oetting, W.S., and King, R.A. (1994a). Analysis of tyrosinase mutations associated with tyrosinase-related oculocutaneous albinism (OCA1). Pigment Cell Res *7*, 285-290.
Oetting, W.S., and King, R.A. (1994b). Molecular basis of oculocutaneous albinism. J Invest Dermatol *103*, 131S-136S.

Off, M.K., Steindal, A.E., Porojnicu, A.C., Juzeniene, A., Vorobey, A., Johnsson, A., and Moan, J. (2005). Ultraviolet photodegradation of folic acid. J Photochem Photobiol B *80*, 47-55.
Ohbayashi, N., and Fukuda, M. (2018). SNARE dynamics during melanosome maturation. Biochem Soc Trans *46*, 911-917.
Ohbayashi, N., Maruta, Y., Ishida, M., and Fukuda, M. (2012). Melanoregulin regulates retrograde melanosome transport through interaction with the RILP-p150Glued complex in melanocytes. J Cell Sci *125*, 1508-1518.
Ohishi, Y., Kinoshita, R., Marubashi, S., Ishida, M., and Fukuda, M. (2019). The BLOC-3 subunit HPS4 is required for activation of Rab32/38 GTPases in melanogenesis, but its Rab9 activity is dispensable for melanogenesis. J Biol Chem *294*, 6912-6922.
Ohno, H., Aguilar, R.C., Yeh, D., Taura, D., Saito, T., and Bonifacino, J.S. (1998). The medium subunits of adaptor complexes recognize distinct but overlapping sets of tyrosine-based sorting signals. J Biol Chem *273*, 25915-25921.
Ohno, H., Fournier, M.C., Poy, G., and Bonifacino, J.S. (1996). Structural determinants of interaction of tyrosine-based sorting signals with the adaptor medium chains. J Biol Chem *271*, 29009-29015.
Ohno, H., Stewart, J., Fournier, M.C., Bosshart, H., Rhee, I., Miyatake, S., Saito, T., Gallusser, A., Kirchhausen, T., and Bonifacino, J.S. (1995). Interaction of tyrosine-based sorting signals with clathrin-associated proteins. Science *269*, 1872-1875.
Oikawa, A., Saeki, H., Akiyama, T., and Matsumoto, J. (1987). Electron microscopic evidence for stimulation of melanosomal maturation by lysosomotropic agents and monensin in cultured B16 mouse melanoma cells. Pigment Cell Res *1*, 44-50.
Okazaki, K., Uzuka, M., Morikawa, F., Toda, K., and Seiji, M. (1976). Transfer mechanism of melanosomes in epidermal cell culture. J Invest Dermatol *67*, 541-547.
Olivares, C., and Solano, F. (2009). New insights into the active site structure and catalytic mechanism of tyrosinase and its related proteins. Pigment Cell Melanoma Res *22*, 750-760.
Opdecamp, K., Nakayama, A., Nguyen, M.T., Hodgkinson, C.A., Pavan, W.J., and Arnheiter, H. (1997). Melanocyte development in vivo and in neural crest cell cultures: crucial dependence on the Mitf basic-helix-loop-helix-zipper transcription factor. Development *124*, 2377-2386.
Orlow, S.J., Zhou, B.K., Chakraborty, A.K., Drucker, M., Pifko-Hirst, S., and Pawelek, J.M. (1994). High-molecular-weight forms of tyrosinase and the tyrosinase-related proteins: evidence for a melanogenic complex. J Invest Dermatol *103*, 196-201.
Palmisano, I., Bagnato, P., Palmigiano, A., Innamorati, G., Rotondo, G., Altimare, D., Venturi, C., Sviderskaya, E.V., Piccirillo, R., Coppola, M.*, et al.* (2008). The ocular albinism type 1 protein, an intracellular G protein-coupled receptor, regulates melanosome transport in pigment cells. Hum Mol Genet *17*, 3487-3501.
Park, A.M., Khan, S., and Rawnsley, J. (2018). Hair Biology: Growth and Pigmentation. Facial Plast Surg Clin North Am *26*, 415-424.
Patwardhan, A., Bardin, S., Miserey-Lenkei, S., Larue, L., Goud, B., Raposo, G., and Delevoye, C. (2017). Routing of the RAB6 secretory pathway towards the lysosome related organelle of melanocytes. Nat Commun *8*, 15835.
Paus, R., Burgoa, I., Platt, C.I., Griffiths, T., Poblet, E., and Izeta, A. (2016). Biology of the eyelash hair follicle: an enigma in plain sight. Br J Dermatol *174*, 741-752.

Peng, C., Ye, J., Yan, S., Kong, S., Shen, Y., Li, C., Li, Q., Zheng, Y., Deng, K., Xu, T., *et al.* (2012). Ablation of vacuole protein sorting 18 (Vps18) gene leads to neurodegeneration and impaired neuronal migration by disrupting multiple vesicle transport pathways to lysosomes. J Biol Chem *287*, 32861-32873.
Pennamen, P., Le, L., Tingaud-Sequeira, A., Fiore, M., Bauters, A., Van Duong Beatrice, N., Coste, V., Bordet, J.C., Plaisant, C., Diallo, M., *et al.* (2020a). BLOC1S5 pathogenic variants cause a new type of Hermansky-Pudlak syndrome. Genet Med.
Pennamen, P., Tingaud-Sequeira, A., Gazova, I., Keighren, M., McKie, L., Marlin, S., Halem, S.G., Kaplan, J., Delevoye, C., Lacombe, D., *et al.* (2020b). Dopachrome tautomerase variants in patients with oculocutaneous albinism.
Peplowska, K., Markgraf, D.F., Ostrowicz, C.W., Bange, G., and Ungermann, C. (2007). The CORVET tethering complex interacts with the yeast Rab5 homolog Vps21 and is involved in endo-lysosomal biogenesis. Dev Cell *12*, 739-750.
Peralta, E.R., Martin, B.C., and Edinger, A.L. (2010). Differential effects of TBC1D15 and mammalian Vps39 on Rab7 activation state, lysosomal morphology, and growth factor dependence. J Biol Chem *285*, 16814-16821.
Perini, E.D., Schaefer, R., Stoter, M., Kalaidzidis, Y., and Zerial, M. (2014a). Mammalian CORVET is required for fusion and conversion of distinct early endosome subpopulations. Traffic *15*, 1366-1389.
Perini, E.D., Schaefer, R., Stöter, M., Kalaidzidis, Y., and Zerial, M. (2014b). Mammalian CORVET is required for fusion and conversion of distinct early endosome subpopulations. Traffic *15*, 1366-1389.
Peters, S., Lamah, T., Kokkinou, D., Bartz-Schmidt, K.U., and Schraermeyer, U. (2006). Melanin protects choroidal blood vessels against light toxicity. Z Naturforsch C J Biosci *61*, 427-433.
Piccirillo, R., Palmisano, I., Innamorati, G., Bagnato, P., Altimare, D., and Schiaffino, M.V. (2006). An unconventional dileucine-based motif and a novel cytosolic motif are required for the lysosomal and melanosomal targeting of OA1. J Cell Sci *119*, 2003-2014.
Pols, M.S., Ten Brink, C., Gosavi, P., Oorschot, V., and Klumperman, J. (2013a). The HOPS Proteins hVps41 and hVps39 Are Required for Homotypic and Heterotypic Late Endosome Fusion. Traffic *14*, 219-232.
Pols, M.S., van Meel, E., Oorschot, V., ten Brink, C., Fukuda, M., Swetha, M.G., Mayor, S., and Klumperman, J. (2013b). hVps41 and VAMP7 function in direct TGN to late endosome transport of lysosomal membrane proteins. Nature Communications *4*, 1361-1361.
Pozuelo Rubio, M., Geraghty, K.M., Wong, B.H., Wood, N.T., Campbell, D.G., Morrice, N., and Mackintosh, C. (2004). 14-3-3-affinity purification of over 200 human phosphoproteins reveals new links to regulation of cellular metabolism, proliferation and trafficking. Biochem J *379*, 395-408.
Prado-Martinez, J., Hernando-Herraez, I., Lorente-Galdos, B., Dabad, M., Ramirez, O., Baeza-Delgado, C., Morcillo-Suarez, C., Alkan, C., Hormozdiari, F., Raineri, E., *et al.* (2013). The genome sequencing of an albino Western lowland gorilla reveals inbreeding in the wild. BMC Genomics *14*, 363.
Prota, G. (1995). The chemistry of melanins and melanogenesis. Fortschr Chem Org Naturst *64*, 93-148.

Pulipparacharuvil, S., Akbar, M.A., Ray, S., Sevrioukov, E.A., Haberman, A.S., Rohrer, J., and Kramer, H. (2005). Drosophila Vps16A is required for trafficking to lysosomes and biogenesis of pigment granules. J Cell Sci *118*, 3663-3673.
Puri, N., Gardner, J.M., and Brilliant, M.H. (2000). Aberrant pH of melanosomes in pink-eyed dilution (p) mutant melanocytes. J Invest Dermatol *115*, 607-613.
Quast, T., Wehner, S., Kirfel, G., Jaeger, K., De Luca, M., and Herzog, V. (2003). sAPP as a regulator of dendrite motility and melanin release in epidermal melanocytes and melanoma cells. FASEB J *17*, 1739-1741.
Quillen, E.E., Norton, H.L., Parra, E.J., Lona-Durazo, F., Ang, K.C., Illiescu, F.M., Pearson, L.N., Shriver, M.D., Lasisi, T., Gokcumen, O.*, et al.* (2019). Shades of complexity: New perspectives on the evolution and genetic architecture of human skin. Am J Phys Anthropol *168 Suppl 67*, 4-26.
Rad, H.H., Yamashita, T., Jin, H.Y., Hirosaki, K., Wakamatsu, K., Ito, S., and Jimbow, K. (2004). Tyrosinase-related proteins suppress tyrosinase-mediated cell death of melanocytes and melanoma cells. Exp Cell Res *298*, 317-328.
Raimondi, S., Sera, F., Gandini, S., Iodice, S., Caini, S., Maisonneuve, P., and Fargnoli, M.C. (2008). MC1R variants, melanoma and red hair color phenotype: a meta-analysis. Int J Cancer *122*, 2753-2760.
Ramsden, C.A., and Riley, P.A. (2014). Tyrosinase: the four oxidation states of the active site and their relevance to enzymatic activation, oxidation and inactivation. Bioorg Med Chem *22*, 2388-2395.
Ran, F.A., Hsu, P.D., Wright, J., Agarwala, V., Scott, D.A., and Zhang, F. (2013). Genome engineering using the CRISPR-Cas9 system. Nat Protoc *8*, 2281-2308.
Raper, H.S. (1926). The Tyrosinase-Tyrosine Reaction: Production of l-3.4-Dihydroxyphenylalanine from Tyrosine. Biochem J *20*, 735-742.
Raper, H.S. (1927). The Tyrosinase-tyrosine Reaction: Production from Tyrosine of 5: 6-Dihydroxyindole and 5: 6-Dihydroxyindole-2-carboxylic Acid-the Precursors of Melanin. Biochem J *21*, 89-96.
Raper, H.S., and Speakman, H.B. (1926). The Tyrosinase-Tyrosine Reaction: Note on the Identity of Tyrosinase from Different Sources. Biochem J *20*, 69-72.
Raper, H.S., and Wormall, A. (1923). The Tyrosinase-Tyrosine Reaction. Biochem J *17*, 454-469.
Raposo, G., and Marks, M.S. (2002). The dark side of lysosome-related organelles: specialization of the endocytic pathway for melanosome biogenesis. Traffic *3*, 237-248.
Raposo, G., and Marks, M.S. (2007). Melanosomes — dark organelles enlighten endosomal membrane transport. Nature Reviews Molecular Cell Biology *8*, 786-797.
Raposo, G., Marks, M.S., and Cutler, D.F. (2007). Lysosome-Related Organelles: Driving post-Golgi compartments into specialisation. Curr Opin Cell Biol *19*, 394-401.
Raposo, G., Tenza, D., Murphy, D.M., Berson, J.F., and Marks, M.S. (2001). Distinct protein sorting and localization to premelanosomes, melanosomes, and lysosomes in pigmented melanocytic cells. J Cell Biol *152*, 809-824.
Reemann, P., Reimann, E., Ilmjarv, S., Porosaar, O., Silm, H., Jaks, V., Vasar, E., Kingo, K., and Koks, S. (2014). Melanocytes in the skin--comparative whole transcriptome analysis of main skin cell types. PLoS One *9*, e115717.
Rees, J.L. (2003). Genetics of hair and skin color. Annu Rev Genet *37*, 67-90.
Reese, B.E. (2011). Development of the retina and optic pathway. Vision Res *51*, 613-632.

Reinders, A., and Ward, J.M. (2015a). Investigating polymorphisms in membrane-associated transporter protein SLC45A2, using sucrose transporters as a model. Mol Med Rep *12*, 1393-1398.
Reinders, A., and Ward, J.M. (2015b). Investigating polymorphisms in membrane-associated transporter protein SLC45A2, using sucrose transporters as a model. Mol Med Rep *12*, 1393-1398.
Ringholm, A., Klovins, J., Rudzish, R., Phillips, S., Rees, J.L., and Schioth, H.B. (2004). Pharmacological characterization of loss of function mutations of the human melanocortin 1 receptor that are associated with red hair. J Invest Dermatol *123*, 917-923.
Robbins, L.S., Nadeau, L.S., Johnson, K.R., Kelly, M.A., Roselli-Rehfuss, L., Baack, E., Mountjoy, K.G., and Cone, R.D. (1993). Pigmentation phenotypes of variant extension locus alleles result from point mutations that alter MSH receptor function. Cell *72*, 827-834.
Roberts, D.F., and Kahlon, D.P. (1976). Environmental correlations of skin colour. Ann Hum Biol *3*, 11-22.
Robila, V., Ostankovitch, M., Altrich-Vanlith, M.L., Theos, A.C., Drover, S., Marks, M.S., Restifo, N., and Engelhard, V.H. (2008). MHC class II presentation of gp100 epitopes in melanoma cells requires the function of conventional endosomes and is influenced by melanosomes. J Immunol *181*, 7843-7852.
Robinson, M.S., and Bonifacino, J.S. (2001). Adaptor-related proteins. Curr Opin Cell Biol *13*, 444-453.
Rochin, L., Hurbain, I., Serneels, L., Fort, C., Watt, B., Leblanc, P., Marks, M.S., De Strooper, B., Raposo, G., and van Niel, G. (2013). BACE2 processes PMEL to form the melanosome amyloid matrix in pigment cells. Proc Natl Acad Sci U S A *110*, 10658-10663.
Rogasevskaia, T.P., Szerencsei, R.T., Jalloul, A.H., Visser, F., Winkfein, R.J., and Schnetkamp, P.P.M. (2019). Cellular localization of the K(+) -dependent Na(+) -Ca(2+) exchanger NCKX5 and the role of the cytoplasmic loop in its distribution in pigmented cells. Pigment Cell Melanoma Res *32*, 55-67.
Rothammer, S., Kunz, E., Seichter, D., Krebs, S., Wassertheurer, M., Fries, R., Brem, G., and Medugorac, I. (2017). Detection of two non-synonymous SNPs in SLC45A2 on BTA20 as candidate causal mutations for oculocutaneous albinism in Braunvieh cattle. Genet Sel Evol *49*, 73.
Rousseau, K., Kauser, S., Pritchard, L.E., Warhurst, A., Oliver, R.L., Slominski, A., Wei, E.T., Thody, A.J., Tobin, D.J., and White, A. (2007). Proopiomelanocortin (POMC), the ACTH/melanocortin precursor, is secreted by human epidermal keratinocytes and melanocytes and stimulates melanogenesis. FASEB J *21*, 1844-1856.
Sabeti, P.C., Varilly, P., Fry, B., Lohmueller, J., Hostetter, E., Cotsapas, C., Xie, X., Byrne, E.H., McCarroll, S.A., Gaudet, R.*, et al.* (2007). Genome-wide detection and characterization of positive selection in human populations. Nature *449*, 913-918.
Sadler, K.C., Amsterdam, A., Soroka, C., Boyer, J., and Hopkins, N. (2005). A genetic screen in zebrafish identifies the mutants vps18, nf2 and foie gras as models of liver disease. Development *132*, 3561-3572.
Saeki, H., and Oikawa, A. (1983). Stimulation of tyrosinase activity of cultured melanoma cells by lysosomotropic agents. J Cell Physiol *116*, 93-97.
Saeki, H., and Oikawa, A. (1985). Stimulation by ionophores of tyrosinase activity of mouse melanoma cells in culture. J Invest Dermatol *85*, 423-425.

Samaraweera, P., Donatien, P.D., Qazi, S., Kobayashi, T., Hearing, V.J., Panthier, J.J., and Orlow, S.J. (1999). Identification and characterization of a melanocyte-specific novel 65-kDa peripheral membrane protein. Eur J Biochem *266*, 924-934.
Samaraweera, P., Shen, B., Newton, J.M., Barsh, G.S., and Orlow, S.J. (2001). The mouse ocular albinism 1 gene product is an endolysosomal protein. Exp Eye Res *72*, 319-329.
Sanchez-Laorden, B.L., Herraiz, C., Valencia, J.C., Hearing, V.J., Jimenez-Cervantes, C., and Garcia-Borron, J.C. (2009). Aberrant trafficking of human melanocortin 1 receptor variants associated with red hair and skin cancer: Steady-state retention of mutant forms in the proximal golgi. J Cell Physiol *220*, 640-654.
Sanchez-Laorden, B.L., Sanchez-Mas, J., Martinez-Alonso, E., Martinez-Menarguez, J.A., Garcia-Borron, J.C., and Jimenez-Cervantes, C. (2006). Dimerization of the human melanocortin 1 receptor: functional consequences and dominant-negative effects. J Invest Dermatol *126*, 172-181.
Sanchez-Mas, J., Hahmann, C., Gerritsen, I., Garcia-Borron, J.C., and Jimenez-Cervantes, C. (2004). Agonist-independent, high constitutive activity of the human melanocortin 1 receptor. Pigment Cell Res *17*, 386-395.
Santiago Borrero, P.J., Rodriguez-Perez, Y., Renta, J.Y., Izquierdo, N.J., Del Fierro, L., Munoz, D., Molina, N.L., Ramirez, S., Pagan-Mercado, G., Ortiz, I.*, et al.* (2006). Genetic testing for oculocutaneous albinism type 1 and 2 and Hermansky-Pudlak syndrome type 1 and 3 mutations in Puerto Rico. J Invest Dermatol *126*, 85-90.
Schauer, E., Trautinger, F., Kock, A., Schwarz, A., Bhardwaj, R., Simon, M., Ansel, J.C., Schwarz, T., and Luger, T.A. (1994). Proopiomelanocortin-derived peptides are synthesized and released by human keratinocytes. J Clin Invest *93*, 2258-2262.
Scherer, D., and Kumar, R. (2010). Genetics of pigmentation in skin cancer--a review. Mutat Res *705*, 141-153.
Schiaffino, M.V., Baschirotto, C., Pellegrini, G., Montalti, S., Tacchetti, C., De Luca, M., and Ballabio, A. (1996). The ocular albinism type 1 gene product is a membrane glycoprotein localized to melanosomes. Proc Natl Acad Sci U S A *93*, 9055-9060.
Schiaffino, M.V., d'Addio, M., Alloni, A., Baschirotto, C., Valetti, C., Cortese, K., Puri, C., Bassi, M.T., Colla, C., De Luca, M.*, et al.* (1999). Ocular albinism: evidence for a defect in an intracellular signal transduction system. Nat Genet *23*, 108-112.
Schiaffino, M.V., Dellambra, E., Cortese, K., Baschirotto, C., Bondanza, S., Clementi, M., Nucci, P., Ballabio, A., Tacchetti, C., and De Luca, M. (2002). Effective retrovirus-mediated gene transfer in normal and mutant human melanocytes. Hum Gene Ther *13*, 947-957.
Schiaffino, M.V., and Tacchetti, C. (2005). The ocular albinism type 1 (OA1) protein and the evidence for an intracellular signal transduction system involved in melanosome biogenesis. Pigment Cell Res *18*, 227-233.
Schioth, H.B., Phillips, S.R., Rudzish, R., Birch-Machin, M.A., Wikberg, J.E., and Rees, J.L. (1999). Loss of function mutations of the human melanocortin 1 receptor are common and are associated with red hair. Biochem Biophys Res Commun *260*, 488-491.
Schneider, M.R., Schmidt-Ullrich, R., and Paus, R. (2009). The hair follicle as a dynamic miniorgan. Curr Biol *19*, R132-142.
Schonthaler, H.B., Fleisch, V.C., Biehlmaier, O., Makhankov, Y., Rinner, O., Bahadori, R., Geisler, R., Schwarz, H., Neuhauss, S.C., and Dahm, R. (2008). The zebrafish mutant

lbk/vam6 resembles human multisystemic disorders caused by aberrant trafficking of endosomal vesicles. Development *135*, 387-399.
Schraermeyer, U., and Heimann, K. (1999). Current understanding on the role of retinal pigment epithelium and its pigmentation. Pigment Cell Res *12*, 219-236.
Schraermeyer, U., Peters, S., Thumann, G., Kociok, N., and Heimann, K. (1999). Melanin granules of retinal pigment epithelium are connected with the lysosomal degradation pathway. Exp Eye Res *68*, 237-245.
Schulze, W., Weise, A., Frommer, W.B., and Ward, J.M. (2000). Function of the cytosolic N-terminus of sucrose transporter AtSUT2 in substrate affinity. FEBS Letters *485*, 189-194.
Scott, G., Leopardi, S., Printup, S., and Madden, B.C. (2002). Filopodia are conduits for melanosome transfer to keratinocytes. J Cell Sci *115*, 1441-1451.
Seals, D.F., Eitzen, G., Margolis, N., Wickner, W.T., and Price, A. (2000). A Ypt/Rab effector complex containing the Sec1 homolog Vps33p is required for homotypic vacuole fusion. Proc Natl Acad Sci U S A *97*, 9402-9407.
Seiberg, M., Paine, C., Sharlow, E., Andrade-Gordon, P., Costanzo, M., Eisinger, M., and Shapiro, S.S. (2000). The protease-activated receptor 2 regulates pigmentation via keratinocyte-melanocyte interactions. Exp Cell Res *254*, 25-32.
Seiji, M., Fitzpatrick, T.B., and Birbeck, M.S. (1961). The melanosome: a distinctive subcellular particle of mammalian melanocytes and the site of melanogenesis. J Invest Dermatol *36*, 243-252.
Seiji, M., Fitzpatrick, T.B., Simpson, R.T., and Birbeck, M.S. (1963). Chemical composition and terminology of specialized organelles (melanosomes and melanin granules) in mammalian melanocytes. Nature *197*, 1082-1084.
Sette, P., Nagashima, K., Piper, R.C., and Bouamr, F. (2013). Ubiquitin conjugation to Gag is essential for ESCRT-mediated HIV-1 budding. Retrovirology *10*, 79.
Setty, S.R., Tenza, D., Sviderskaya, E.V., Bennett, D.C., Raposo, G., and Marks, M.S. (2008). Cell-specific ATP7A transport sustains copper-dependent tyrosinase activity in melanosomes. Nature *454*, 1142-1146.
Setty, S.R.G., Tenza, D., Truschel, S.T., Chou, E., Sviderskaya, E.V., Theos, A.C., Lamoreaux, M.L., Di Pietro, S.M., Starcevic, M., Bennett, D.C.*, et al.* (2007). BLOC-1 Is Required for Cargo-specific Sorting from Vacuolar Early Endosomes toward Lysosome-related Organelles - Correction Fig 7. Molecular biology of the cell *18*, 768-780.
Sevrioukov, E.A., He, J.P., Moghrabi, N., Sunio, A., and Kramer, H. (1999). A role for the deep orange and carnation eye color genes in lysosomal delivery in Drosophila. Mol Cell *4*, 479-486.
Shestopal, S.A., Makunin, I.V., Belyaeva, E.S., Ashburner, M., and Zhimulev, I.F. (1997). Molecular characterization of the deep orange (dor) gene of Drosophila melanogaster. Mol Gen Genet *253*, 642-648.
Shirazi, T.N., Snow, J., Ham, L., Raglan, G.B., Wiggs, E.A., Summers, A.C., Toro, C., and Introne, W.J. (2019). The neuropsychological phenotype of Chediak-Higashi disease. Orphanet J Rare Dis *14*, 101.
Simmen, T., Schmidt, A., Hunziker, W., and Beermann, F. (1999). The tyrosinase tail mediates sorting to the lysosomal compartment in MDCK cells via a di-leucine and a tyrosine-based signal. J Cell Sci *112 (Pt 1)*, 45-53.

Singh, S.K., Kurfurst, R., Nizard, C., Schnebert, S., Perrier, E., and Tobin, D.J. (2010). Melanin transfer in human skin cells is mediated by filopodia--a model for homotypic and heterotypic lysosome-related organelle transfer. FASEB J *24*, 3756-3769.
Sitaram, A., Dennis, M.K., Chaudhuri, R., De Jesus-Rojas, W., Tenza, D., Setty, S.R.G., Wood, C.S., Sviderskaya, E.V., Bennett, D.C., Raposo, G.*, et al.* (2012). Differential recognition of a dileucine-based sorting signal by AP-1 and AP-3 reveals a requirement for both BLOC-1 and AP-3 in delivery of OCA2 to melanosomes. Molecular biology of the cell *23*, 3178-3192.
Sitaram, A., and Marks, M.S. (2012). Mechanisms of protein delivery to melanosomes in pigment cells. Physiology (Bethesda, Md) *27*, 85-99.
Sitaram, A., Piccirillo, R., Palmisano, I., Harper, D.C., Dell'Angelica, E.C., Schiaffino, M.V., and Marks, M.S. (2009). Localization to Mature Melanosomes by Virtue of Cytoplasmic Dileucine Motifs Is Required for Human OCA2 Function. Molecular Biology of the Cell *20*, 1464-1477.
Slominski, A., Tobin, D.J., Shibahara, S., and Wortsman, J. (2004). Melanin pigmentation in mammalian skin and its hormonal regulation. Physiol Rev *84*, 1155-1228.
Sluchanko, N.N. (2018). Association of Multiple Phosphorylated Proteins with the 14-3-3 Regulatory Hubs: Problems and Perspectives. J Mol Biol *430*, 20-26.
Soejima, M., and Koda, Y. (2007). Population differences of two coding SNPs in pigmentation-related genes SLC24A5 and SLC45A2. Int J Legal Med *121*, 36-39.
Soejima, M., Tachida, H., Ishida, T., Sano, A., and Koda, Y. (2006). Evidence for recent positive selection at the human AIM1 locus in a European population. Mol Biol Evol *23*, 179-188.
Solano, F. (2018). On the Metal Cofactor in the Tyrosinase Family. Int J Mol Sci *19*.
Solano, F., Jimenez-Cervantes, C., Martinez-Liarte, J.H., Garcia-Borron, J.C., Jara, J.R., and Lozano, J.A. (1996). Molecular mechanism for catalysis by a new zinc-enzyme, dopachrome tautomerase. Biochem J *313 (Pt 2)*, 447-453.
Solinger, J.A., and Spang, A. (2013). Tethering complexes in the endocytic pathway: CORVET and HOPS. FEBS Journal *280*, 2743-2757.
Sparvoli, D., Richardson, E., Osakada, H., Lan, X., Iwamoto, M., Bowman, G.R., Kontur, C., Bourland, W.A., Lynn, D.H., Pritchard, J.K.*, et al.* (2018). Remodeling the Specificity of an Endosomal CORVET Tether Underlies Formation of Regulated Secretory Vesicles in the Ciliate Tetrahymena thermophila. Curr Biol *28*, 697-710 e613.
Starcevic, M., and Dell'Angelica, E.C. (2004). Identification of snapin and three novel proteins (BLOS1, BLOS2, and BLOS3/reduced pigmentation) as subunits of biogenesis of lysosome-related organelles complex-1 (BLOC-1). J Biol Chem *279*, 28393-28401.
Steingrimsson, E., Copeland, N.G., and Jenkins, N.A. (2006). Mouse coat color mutations: from fancy mice to functional genomics. Dev Dyn *235*, 2401-2411.
Stenmark, H. (2009). Rab GTPases as coordinators of vesicle traffic. Nat Rev Mol Cell Biol *10*, 513-525.
Stenn, K.S., and Paus, R. (2001). Controls of hair follicle cycling. Physiol Rev *81*, 449-494.
Stephens, D.J., and Banting, G. (1998). Specificity of interaction between adaptor-complex medium chains and the tyrosine-based sorting motifs of TGN38 and lgp120. Biochem J *335 (Pt 3)*, 567-572.

Stewart, S.A., Dykxhoorn, D.M., Palliser, D., Mizuno, H., Yu, E.Y., An, D.S., Sabatini, D.M., Chen, I.S., Hahn, W.C., Sharp, P.A., *et al.* (2003). Lentivirus-delivered stable gene silencing by RNAi in primary cells. RNA *9*, 493-501.
Stokowski, R.P., Pant, P.V., Dadd, T., Fereday, A., Hinds, D.A., Jarman, C., Filsell, W., Ginger, R.S., Green, M.R., van der Ouderaa, F.J., *et al.* (2007). A genomewide association study of skin pigmentation in a South Asian population. Am J Hum Genet *81*, 1119-1132.
Stringer, D.K., and Piper, R.C. (2011). A single ubiquitin is sufficient for cargo protein entry into MVBs in the absence of ESCRT ubiquitination. J Cell Biol *192*, 229-242.
Sudhof, T.C., and Rothman, J.E. (2009). Membrane fusion: grappling with SNARE and SM proteins. Science *323*, 474-477.
Sulem, P., Gudbjartsson, D.F., Stacey, S.N., Helgason, A., Rafnar, T., Jakobsdottir, M., Steinberg, S., Gudjonsson, S.A., Palsson, A., Thorleifsson, G., *et al.* (2008). Two newly identified genetic determinants of pigmentation in Europeans. Nat Genet *40*, 835-837.
Sun, Y., Lin, Z., Reinders, A., and Ward, J.M. (2012). Functionally important amino acids in rice sucrose transporter OsSUT1. Biochemistry *51*, 3284-3291.
Sun, Y., and Ward, J.M. (2012). Arg188 in rice sucrose transporter OsSUT1 is crucial for substrate transport. BMC Biochem *13*, 26.
Sutton, R.B., Fasshauer, D., Jahn, R., and Brunger, A.T. (1998). Crystal structure of a SNARE complex involved in synaptic exocytosis at 2.4 A resolution. Nature *395*, 347-353.
Suzuki, I., Tada, A., Ollmann, M.M., Barsh, G.S., Im, S., Lamoreux, M.L., Hearing, V.J., Nordlund, J.J., and Abdel-Malek, Z.A. (1997). Agouti signaling protein inhibits melanogenesis and the response of human melanocytes to alpha-melanotropin. J Invest Dermatol *108*, 838-842.
Suzuki, T., Li, W., Zhang, Q., Karim, A., Novak, E.K., Sviderskaya, E.V., Hill, S.P., Bennett, D.C., Levin, A.V., Nieuwenhuis, H.K., *et al.* (2002). Hermansky-Pudlak syndrome is caused by mutations in HPS4, the human homolog of the mouse light-ear gene. Nat Genet *30*, 321-324.
Suzuki, T., Li, W., Zhang, Q., Novak, E.K., Sviderskaya, E.V., Wilson, A., Bennett, D.C., Roe, B.A., Swank, R.T., and Spritz, R.A. (2001). The gene mutated in cocoa mice, carrying a defect of organelle biogenesis, is a homologue of the human hermansky-pudlak syndrome-3 gene. Genomics *78*, 30-37.
Suzuki, T., Oiso, N., Gautam, R., Novak, E.K., Panthier, J.-J., Suprabha, P.G., Vida, T., Swank, R.T., and Spritz, R.A. (2003). The mouse organellar biogenesis mutant buff results from a mutation in Vps33a, a homologue of yeast vps33 and Drosophila carnation. Proceedings of the National Academy of Sciences *100*, 1146-1150.
Sviderskaya, E.V., Bennett, D.C., Ho, L., Bailin, T., Lee, S.T., and Spritz, R.A. (1997). Complementation of hypopigmentation in p-mutant (pink-eyed dilution) mouse melanocytes by normal human P cDNA, and defective complementation by OCA2 mutant sequences. J Invest Dermatol *108*, 30-34.
Sviderskaya, E.V., Hill, S.P., Evans-Whipp, T.J., Chin, L., Orlow, S.J., Easty, D.J., Cheong, S.C., Beach, D., DePinho, R.A., and Bennett, D.C. (2002). p16(Ink4a) in melanocyte senescence and differentiation. J Natl Cancer Inst *94*, 446-454.
Sweet, H.O., Brilliant, M.H., Cook, S.A., Johnson, K.R., and Davisson, M.T. (1998). A new allelic series for the underwhite gene on mouse chromosome15. J Heredity *89*, 546-551.
Swift, J.A. (1964). Transfer of Melanin Granules from Melanocytes to the Cortical Cells of Human Hair. Nature *203*, 976-977.

Swope, V., Alexander, C., Starner, R., Schwemberger, S., Babcock, G., and Abdel-Malek, Z.A. (2014). Significance of the melanocortin 1 receptor in the DNA damage response of human melanocytes to ultraviolet radiation. Pigment Cell Melanoma Res *27*, 601-610.
Syrovatkina, V., Alegre, K.O., Dey, R., and Huang, X.Y. (2016). Regulation, Signaling, and Physiological Functions of G-Proteins. J Mol Biol *428*, 3850-3868.
Szerencsei, R.T., Ginger, R.S., Green, M.R., and Schnetkamp, P.P. (2016). Identification and Characterization of K(+)-Dependent Na(+)-Ca(2+) Exchange Transport in Pigmented MEB4 Cells Mediated by NCKX4. Biochemistry *55*, 2704-2712.
Tabata, H., Kawamura, N., Sun-Wada, G.H., and Wada, Y. (2008). Vacuolar-type H(+)-ATPase with the a3 isoform is the proton pump on premature melanosomes. Cell Tissue Res *332*, 447-460.
Takats, S., Pircs, K., Nagy, P., Varga, A., Karpati, M., Hegedus, K., Kramer, H., Kovacs, A.L., Sass, M., and Juhasz, G. (2014). Interaction of the HOPS complex with Syntaxin 17 mediates autophagosome clearance in Drosophila. Mol Biol Cell *25*, 1338-1354.
Tarafder, A.K., Bolasco, G., Correia, M.S., Pereira, F.J.C., Iannone, L., Hume, A.N., Kirkpatrick, N., Picardo, M., Torrisi, M.R., Rodrigues, I.P.*, et al.* (2014). Rab11b mediates melanin transfer between donor melanocytes and acceptor keratinocytes via coupled exo/endocytosis. J Invest Dermatol *134*, 1056-1066.
Thathachari, Y.T., and Blois, M.S. (1969). Physical studies on melanins. II. X-ray diffraction. Biophys J *9*, 77-89.
Theos, A.C., Berson, J.F., Theos, S.C., Herman, K.E., Harper, D.C., Tenza, D., Sviderskaya, E.V., Lamoreaux, M.L., Bennett, D.C., Raposo, G.*, et al.* (2006a). Dual Loss of ER Export and Endocytic Signals with Altered Melanosome Morphology in the silver Mutation of Pmel17. Molecular biology of the cell *17*, 3598-3612.
Theos, A.C., Tenza, D., Martina, J.A., Hurbain, I., Peden, A.A., Sviderskaya, E.V., Stewart, A., Robinson, M.S., Bennett, D.C., Cutler, D.F.*, et al.* (2005). Functions of adaptor protein (AP)-3 and AP-1 in tyrosinase sorting from endosomes to melanosomes. Mol Biol Cell *16*, 5356-5372.
Theos, A.C., Truschel, S.T., Tenza, D., Hurbain, I., Harper, D.C., Berson, J.F., Thomas, P.C., Raposo, G., and Marks, M.S. (2006b). A lumenal domain-dependent pathway for sorting to intralumenal vesicles of multivesicular endosomes involved in organelle morphogenesis. Developmental Cell *10*, 343-354.
Thompson, A., Land, E.J., Chedekel, M.R., Subbarao, K.V., and Truscott, T.G. (1985). A pulse radiolysis investigation of the oxidation of the melanin precursors 3,4-dihydroxyphenylalanine (dopa) and the cysteinyldopas. Biochim Biophys Acta *843*, 49-57.
Tomita, Y., Takeda, A., Matsunaga, J., Okinaga, S., Shibahara, S., and Tagami, H. (1992). Molecular bases of tyrosinase-negative oculocutaneous albinism: a single base insertion or a missense point mutation in the tyrosinase gene. Pigment Cell Res *Suppl 2*, 96-100.
Toyofuku, K., Valencia, J.C., Kushimoto, T., Costin, G.E., Virador, V.M., Vieira, W.D., Ferrans, V.J., and Hearing, V.J. (2002). The etiology of oculocutaneous albinism (OCA) type II: the pink protein modulates the processing and transport of tyrosinase. Pigment Cell Res *15*, 217-224.
Tsetskhladze, Z.R., Canfield, V.A., Ang, K.C., Wentzel, S.M., Reid, K.P., Berg, A.S., Johnson, S.L., Kawakami, K., and Cheng, K.C. (2012). Functional assessment of human coding mutations affecting skin pigmentation using zebrafish. PLoS One *7*, e47398.

Tsuboi, K., Hayashi, Y., Jogahara, T., Ogura, G., Murata, Y., and Oda, S. (2009). Oculocutaneous albinism in Suncus murinus: establishment of a strain and identification of its responsible gene. Exp Anim *58*, 31-40.
Tsukamoto, K., Jackson, I.J., Urabe, K., Montague, P.M., and Hearing, V.J. (1992). A second tyrosinase-related protein, TRP-2, is a melanogenic enzyme termed DOPAchrome tautomerase. EMBO J *11*, 519-526.
Ungermann, C., and Kummel, D. (2019). Structure of membrane tethers and their role in fusion. Traffic *20*, 479-490.
UniProt, C. (2019). UniProt: a worldwide hub of protein knowledge. Nucleic Acids Res *47*, D506-D515.
Valejo Coelho, M.M., Matos, T.R., and Apetato, M. (2016). The dark side of the light: mechanisms of photocarcinogenesis. Clin Dermatol *34*, 563-570.
Valverde, P., Healy, E., Jackson, I., Rees, J.L., and Thody, A.J. (1995). Variants of the melanocyte-stimulating hormone receptor gene are associated with red hair and fair skin in humans. Nat Genet *11*, 328-330.
Van Den Bossche, K., Naeyaert, J.M., and Lambert, J. (2006). The quest for the mechanism of melanin transfer. Traffic *7*, 769-778.
van der Beek, J., Jonker, C., van der Welle, R., Liv, N., and Klumperman, J. (2019). CORVET, CHEVI and HOPS - multisubunit tethers of the endo-lysosomal system in health and disease. J Cell Sci *132*.
van der Kant, R., Fish, A., Janssen, L., Janssen, H., Krom, S., Ho, N., Brummelkamp, T., Carette, J., Rocha, N., and Neefjes, J. (2013). Late endosomal transport and tethering are coupled processes controlled by RILP and the cholesterol sensor ORP1L. Journal of Cell Science *126*, 3462-3474.
Van Der Kant, R., Jonker, C.T.H., Wijdeven, R.H., Bakker, J., Janssen, L., Klumperman, J., and Neefjes, J. (2015). Characterization of the mammalian CORVET and HOPS complexes and their modular restructuring for endosome specificity. Journal of Biological Chemistry *290*, 30280-30290.
van Niel, G., Bergam, P., Di Cicco, A., Hurbain, I., Lo Cicero, A., Dingli, F., Palmulli, R., Fort, C., Potier, M.C., Schurgers, L.J.*, et al.* (2015). Apolipoprotein E Regulates Amyloid Formation within Endosomes of Pigment Cells. Cell Rep *13*, 43-51.
van Niel, G., Charrin, S., Simoes, S., Romao, M., Rochin, L., Saftig, P., Marks, M.S., Rubinstein, E., and Raposo, G. (2011). The Tetraspanin CD63 Regulates ESCRT-Independent and -Dependent Endosomal Sorting during Melanogenesis. Developmental Cell *21*, 708-721.
Vandamme, N., and Berx, G. (2019). From neural crest cells to melanocytes: cellular plasticity during development and beyond. Cell Mol Life Sci *76*, 1919-1934.
Vijayasaradhi, S., Doskoch, P.M., and Houghton, A.N. (1991). Biosynthesis and intracellular movement of the melanosomal membrane glycoprotein gp75, the human b (brown) locus product. Exp Cell Res *196*, 233-240.
Vijayasaradhi, S., Xu, Y., Bouchard, B., and Houghton, A.N. (1995). Intracellular sorting and targeting of melanosomal membrane proteins: identification of signals for sorting of the human brown locus protein, gp75. J Cell Biol *130*, 807-820.
Virador, V.M., Muller, J., Wu, X., Abdel-Malek, Z.A., Yu, Z.X., Ferrans, V.J., Kobayashi, N., Wakamatsu, K., Ito, S., Hammer, J.A.*, et al.* (2002). Influence of alpha-melanocyte-stimulating hormone and ultraviolet radiation on the transfer of melanosomes to keratinocytes. FASEB J *16*, 105-107.

Vitavska, O., Bartolke, R., Tabke, K., Heinisch, J.J., and Wieczorek, H. (2018). Interaction of mammalian and plant H(+)/sucrose transporters with 14-3-3 proteins. Biochem J *475*, 3239-3254.
Vogel, P., Read, R.W., Vance, R.B., Platt, K.A., Troughton, K., and Rice, D.S. (2008). Ocular albinism and hypopigmentation defects in Slc24a5-/- mice. Vet Pathol *45*, 264-279.
Wagner, C.A., Finberg, K.E., Breton, S., Marshansky, V., Brown, D., and Geibel, J.P. (2004). Renal vacuolar H+-ATPase. Physiol Rev *84*, 1263-1314.
Wakamatsu, K., Hu, D.N., McCormick, S.A., and Ito, S. (2008). Characterization of melanin in human iridal and choroidal melanocytes from eyes with various colored irides. Pigment Cell Melanoma Res *21*, 97-105.
Wakamatsu, K., and Ito, S. (2002). Advanced chemical methods in melanin determination. Pigment Cell Res *15*, 174-183.
Wakamatsu, K., Kavanagh, R., Kadekaro, A.L., Terzieva, S., Sturm, R.A., Leachman, S., Abdel-Malek, Z., and Ito, S. (2006). Diversity of pigmentation in cultured human melanocytes is due to differences in the type as well as quantity of melanin. Pigment Cell Research *19*, 154-162.
Wang, X., Zhang, X., Dong, X.P., Samie, M., Li, X., Cheng, X., Goschka, A., Shen, D., Zhou, Y., Harlow, J.*, et al.* (2012). TPC proteins are phosphoinositide- activated sodium-selective ion channels in endosomes and lysosomes. Cell *151*, 372-383.
Warner, T.S., Sinclair, D.A., Fitzpatrick, K.A., Singh, M., Devlin, R.H., and Honda, B.M. (1998). The light gene of Drosophila melanogaster encodes a homologue of VPS41, a yeast gene involved in cellular-protein trafficking. Genome *41*, 236-243.
Wartosch, L., G??nesdogan, U., Graham, S.C., and Luzio, J.P. (2015). Recruitment of VPS33A to HOPS by VPS16 Is Required for Lysosome Fusion with Endosomes and Autophagosomes. Traffic *16*, 727-742.
Wasmeier, C., Romao, M., Plowright, L., Bennett, D.C., Raposo, G., and Seabra, M.C. (2006). Rab38 and Rab32 control post-Golgi trafficking of melanogenic enzymes. J Cell Biol *175*, 271-281.
Wei, A., Wang, Y., Long, Y., Wang, Y., Guo, X., Zhou, Z., Zhu, W., Liu, J., Bian, X., Lian, S.*, et al.* (2010). A comprehensive analysis reveals mutational spectra and common alleles in Chinese patients with oculocutaneous albinism. J Invest Dermatol *130*, 716-724.
Wei, A.H., Zang, D., J., Zhang, Z., Yang, X.M., and Li, W. (2015). Prenatal genotyping of four common oculocutaneous albinism genes in 51 Chinese families. J Genet Genomics *42*, 279-286.
Wei, A.H., Zang, D.J., Zhang, Z., Liu, X.Z., He, X., Yang, L., Wang, Y., Zhou, Z.Y., Zhang, M.R., Dai, L.L.*, et al.* (2013). Exome sequencing identifies SLC24A5 as a candidate gene for nonsyndromic oculocutaneous albinism. J Invest Dermatol *133*, 1834-1840.
Wei, M.L. (2006). Hermansky-Pudlak syndrome: A disease of protein trafficking and organelle function. Pigment Cell Research *19*, 19-42.
Weiner, L., Fu, W., Chirico, W.J., and Brissette, J.L. (2014). Skin as a living coloring book: how epithelial cells create patterns of pigmentation. Pigment Cell Melanoma Res *27*, 1014-1031.
Weinert, S., Jabs, S., Hohensee, S., Chan, W.L., Kornak, U., and Jentsch, T.J. (2014). Transport activity and presence of ClC-7/Ostm1 complex account for different cellular functions. EMBO Rep *15*, 784-791.

Weinglass, A.B., and Kaback, H.R. (2000). The central cytoplasmic loop of the major facilitator superfamily of transport proteins governs efficient membrane insertion. Proc Natl Acad Sci U S A *97*, 8938-8943.
Weiter, J.J., Delori, F.C., Wing, G.L., and Fitch, K.A. (1986). Retinal pigment epithelial lipofuscin and melanin and choroidal melanin in human eyes. Invest Ophthalmol Vis Sci *27*, 145-152.
Wijesena, H.R., and Schmutz, S.M. (2015). A Missense Mutation in SLC45A2 Is Associated with Albinism in Several Small Long Haired Dog Breeds. J Hered *106*, 285-288.
Wilkerson, C.L., Syed, N.A., Fisher, M.R., Robinson, N.L., Wallow, I.H., and Albert, D.M. (1996). Melanocytes and iris color. Light microscopic findings. Arch Ophthalmol *114*, 437-442.
Williams, J.D., Jacobson, E.L., Kim, H., Kim, M., and Jacobson, M.K. (2012). Folate in skin cancer prevention. Subcell Biochem *56*, 181-197.
Williams, P.F., Olsen, C.M., Hayward, N.K., and Whiteman, D.C. (2011). Melanocortin 1 receptor and risk of cutaneous melanoma: a meta-analysis and estimates of population burden. Int J Cancer *129*, 1730-1740.
Williams, R.J.P. (1987). The biochemistry of zinc. Polyhedron *6*, 61-69.
Wilson, S., Ginger, R.S., Dadd, T., Gunn, D., Lim, F.L., Sawicka, M., Sandel, M., Schnetkamp, P.P., and Green, M.R. (2013). NCKX5, a natural regulator of human skin colour variation, regulates the expression of key pigment genes MC1R and alpha-MSH and alters cholesterol homeostasis in normal human melanocytes. Adv Exp Med Biol *961*, 95-107.
Wilson, S.M., Yip, R., Swing, D.A., O'Sullivan, T.N., Zhang, Y., Novak, E.K., Swank, R.T., Russell, L.B., Copeland, N.G., and Jenkins, N.A. (2000). A mutation in Rab27a causes the vesicle transport defects observed in ashen mice. Proc Natl Acad Sci U S A *97*, 7933-7938.
Winchester, B. (2005). Lysosomal metabolism of glycoproteins. Glycobiology *15*, 1R-15R.
Winkler, P.A., Gornik, K.R., Ramsey, D.T., Dubielzig, R.R., Venta, P.J., Petersen-Jones, S.M., and Bartoe, J.T. (2014). A partial gene deletion of SLC45A2 causes oculocutaneous albinism in Doberman pinscher dogs. PLoS One *9*, e92127.
Witkop, C.J., Nunez Babcock, M., Rao, G.H., Gaudier, F., Summers, C.G., Shanahan, F., Harmon, K.R., Townsend, D., Sedano, H.O., King, R.A.*, et al.* (1990). Albinism and Hermansky-Pudlak syndrome in Puerto Rico. Bol Asoc Med P R *82*, 333-339.
Wolf Horrell, E.M., Boulanger, M.C., and D'Orazio, J.A. (2016a). Melanocortin 1 receptor: Structure, function, and regulation.
Wolf Horrell, E.M., Boulanger, M.C., and D'Orazio, J.A. (2016b). Melanocortin 1 Receptor: Structure, Function, and Regulation. Front Genet *7*, 95.
Wong, L., O'Donnell, F.E., and Richard Green, W. (2009). Giant pigment granules in the retinal pigment epithelium of a fetus with X-linked ocular albinism. Ophthalmic Paediatrics and Genetics *2*, 47-65.
Wu, M.M., Buchanan, J., Luik, R.M., and Lewis, R.S. (2006). Ca2+ store depletion causes STIM1 to accumulate in ER regions closely associated with the plasma membrane. J Cell Biol *174*, 803-813.
Wu, X., and Hammer, J.A. (2014). Melanosome transfer: it is best to give and receive. Curr Opin Cell Biol *29*, 1-7.

Wu, X.S., Masedunskas, A., Weigert, R., Copeland, N.G., Jenkins, N.A., and Hammer, J.A. (2012). Melanoregulin regulates a shedding mechanism that drives melanosome transfer from melanocytes to keratinocytes. Proc Natl Acad Sci U S A *109*, E2101-2109.
Wurmser, A.E., Sato, T.K., and Emr, S.D. (2000). New component of the vacuolar class C-Vps complex couples nucleotide exchange on the Ypt7 GTPase to SNARE-dependent docking and fusion. J Cell Biol *151*, 551-562.
Xu, H., Delling, M., Li, L., Dong, X., and Clapham, D.E. (2007). Activating mutation in a mucolipin transient receptor potential channel leads to melanocyte loss in varitint-waddler mice. Proc Natl Acad Sci U S A *104*, 18321-18326.
Xu, X., Dong, G.X., Hu, X.S., Miao, L., Zhang, X.L., Zhang, D.L., Yang, H.D., Zhang, T.Y., Zou, Z.T., Zhang, T.T.*, et al.* (2013). The genetic basis of white tigers. Curr Biol *23*, 1031-1035.
Xu, X.Z., Moebius, F., Gill, D.L., and Montell, C. (2001). Regulation of melastatin, a TRP-related protein, through interaction with a cytoplasmic isoform. Proc Natl Acad Sci U S A *98*, 10692-10697.
Yamashita, Y., Kojima, K., Tsukahara, T., Agawa, H., Yamada, K., Amano, Y., Kurotori, N., Tanaka, N., Sugamura, K., and Takeshita, T. (2008). Ubiquitin-independent binding of Hrs mediates endosomal sorting of the interleukin-2 receptor beta-chain. J Cell Sci *121*, 1727-1738.
Yasumoto, K., Mahalingam, H., Suzuki, H., Yoshizawa, M., and Yokoyama, K. (1995). Transcriptional activation of the melanocyte-specific genes by the human homolog of the mouse Microphthalmia protein. J Biochem *118*, 874-881.
Yasumoto, K., Yokoyama, K., Shibata, K., Tomita, Y., and Shibahara, S. (1994). Microphthalmia-associated transcription factor as a regulator for melanocyte-specific transcription of the human tyrosinase gene. Mol Cell Biol *14*, 8058-8070.
Yi, L., and Kaler, S.G. (2015). Direct interactions of adaptor protein complexes 1 and 2 with the copper transporter ATP7A mediate its anterograde and retrograde trafficking. Hum Mol Genet *24*, 2411-2425.
Yoon, T.Y., and Munson, M. (2018). SNARE complex assembly and disassembly. Curr Biol *28*, R397-R401.
Yoshiike, T., Manabe, M., Hayakawa, M., and Ogawa, H. (1985). Macromelanosomes in X-linked ocular albinism (XLOA). Acta Derm Venereol *65*, 66-69.
Young, A., Jiang, M., Wang, Y., Ahmedli, N.B., Ramirez, J., Reese, B.E., Birnbaumer, L., and Farber, D.B. (2011). Specific interaction of Galphai3 with the Oa1 G-protein coupled receptor controls the size and density of melanosomes in retinal pigment epithelium. PLoS One *6*, e24376.
Young, A., Powelson, E.B., Whitney, I.E., Raven, M.A., Nusinowitz, S., Jiang, M., Birnbaumer, L., Reese, B.E., and Farber, D.B. (2008). Involvement of OA1, an intracellular GPCR, and G alpha i3, its binding protein, in melanosomal biogenesis and optic pathway formation. Invest Ophthalmol Vis Sci *49*, 3245-3252.
Young, A.R., Morgan, K.A., Ho, T.W., Ojimba, N., Harrison, G.I., Lawrence, K.P., Jakharia-Shah, N., Wulf, H.C., Cruickshank, J.K., and Philipsen, P.A. (2020). Melanin has a Small Inhibitory Effect on Cutaneous Vitamin D Synthesis: A Comparison of Extreme Phenotypes. J Invest Dermatol *140*, 1418-1426 e1411.
Yu, I.M., and Hughson, F.M. (2010). Tethering factors as organizers of intracellular vesicular traffic. Annu Rev Cell Dev Biol *26*, 137-156.

Yu, J.F., Fukamachi, S., Mitani, H., Hori, H., and Kanamori, A. (2006). Reduced expression of vps11 causes less pigmentation in medaka, Oryzias latipes. Pigment Cell Res *19*, 628-634.
Yuasa, I., Umetsu, K., Harihara, S., Kido, A., Miyoshi, A., Saitou, N., Dashnyam, B., Jin, F., Lucotte, G., Chattopadhyay, P.K.*, et al.* (2006). Distribution of the F374 allele of the SLC45A2 (MATP) gene and founder-haplotype analysis. Ann Hum Genet *70*, 802-811.
Zajac, G.W., Gallas, J.M., Cheng, J., Eisner, M., Moss, S.C., and Alvarado-Swaisgood, A.E. (1994). The fundamental unit of synthetic melanin: a verification by tunneling microscopy of X-ray scattering results. Biochim Biophys Acta *1199*, 271-278.
Zhang, C.F., Gruber, F., Ni, C., Mildner, M., Koenig, U., Karner, S., Barresi, C., Rossiter, H., Narzt, M.S., Nagelreiter, I.M.*, et al.* (2015). Suppression of autophagy dysregulates the antioxidant response and causes premature senescence of melanocytes. J Invest Dermatol *135*, 1348-1357.
Zhang, Z., Gong, J., Sviderskaya, E.V., Wei, A., and Li, W. (2019). Mitochondrial NCKX5 regulates melanosomal biogenesis and pigment production. J Cell Sci *132*.
Zhen, Y., and Li, W. (2015). Impairment of autophagosome-lysosome fusion in the buff mutant mice with the VPS33AD251E mutation. Autophagy *11*, 1608-1622.